VOLUME 122 NUMBER 1

THE ASTROPHYSICAL JOURNAL

AN INTERNATIONAL REVIEW OF SPECTROSCOPY AND ASTRONOMICAL PHYSICS

JULY 1955

ON THE INSTABILITY OF SUPERPOSED FLUIDS IN A GRAVITATIONAL FIELD
David Layzer 1

OBSERVABLE TESTS ON THE NATURE OF THE COSMOLOGICAL RED SHIFT
E. N. Milford 13

ON STELLAR STATISTICS
Alladi Ramakrishnan 24

A TABLE OF THE RADIATIVE OPACITIES OF A NUMBER OF GAS MIXTURES
Geoffrey Keller and Roland E. Meyerott 32

STELLAR PULSATION AS A LIMIT-CYCLE PHENOMENON
Wesley S. Kinman 43

WAVE FUNCTIONS, SPIN-ORBIT, AND SPIN-SPIN PARAMETERS FOR THE $1s^2 2p$ ISOELECTRONIC SEQUENCE
Russell Sitler 52

VIBRATIONAL TRANSITION PROBABILITIES OF DIATOMIC MOLECULES: COLLECTED RESULTS. III. N_2, NO, O_2, O_2^+, OH, CO, CO^+
W. R. Jarmain, P. A. Fraser, and R. W. Nicholls 55

THE SPECTRUM OF NGC 7027
L. H. Aller, I. S. Bowen, and R. Minkowski 62

STUDIES OF RV TAURI STARS. I. U MONOCEROTIS
Helmut A. Abt 72

PASCHEN AND BALMER SERIES IN SPECTRA OF CHI OPHIUCHI AND P CYGNI
E. Margaret Burbidge and G. R. Burbidge 89

THE BETA CANIS MAJORIS STARS GAMMA PEGASI, DELTA CETI, AND 53 CANIS MAJORIS
D. H. McNamara 95

A MICROPHOTOMETRIC STUDY OF THE SPECTRUM OF SIGMA SCORPII
Su-Shu Huang and Otto Struve 103

THE RADIAL VELOCITY OF SIGMA SCORPII
O. Struve, D. H. McNamara, and V. Zebergs 122

THE VELOCITY CURVE OF 12 DD LACERTAE
Otto Struve and Velta Zebergs 134

THE RADIO POSITION OF THE GALACTIC NUCLEUS
J. D. Kraus and R. C. Ko 139

SOME EVIDENCE FOR A REGIONAL VARIATION IN THE LAW OF INTERSTELLAR REDDENING
H. L. Johnson and W. W. Morgan 142

COLOR-MAGNITUDE ARRAY FOR STARS IN THE GLOBULAR CLUSTER M13
Archibald Sharpless 146

THE GLOBULAR CLUSTER, M13
H. C. Arp and H. L. Johnson 171

CLASSIFICATION OF LATE M-TYPE STARS FROM LOW-DISPERSION SPECTRA IN THE NEAR INFRARED
D. M. Cameron and J. J. Nassau 177

MAGNITUDES AND COLORS OF BRIGHT F STARS
Peter Abt 182

PHOTOMETRIC AND SPECTROSCOPIC STUDIES OF EARLY-TYPE STARS BETWEEN GALACTIC LONGITUDE $l = 330°$ AND $l = 55°$
W. A. Hiltner and Beatrice Mayo 185

COMET OUTBURSTS
Charles Whipple 190

NOTES

Identification of the λ3442 Interstellar Line
Andrew McKellar and E. H. Richardson 196

A Note on the Galactic Microwave Spectrum
A. E. Lilley 197

The Spectrum of Nova Sagittarii 1954.1
Helmut A. Abt 199

Note on the Mass of M92
M. Schwarzschild and S. Bernstein 200

On the Annual Motions of Stars with Constant Opacity
John Negaard 202

East-West Motions in the Aurora
R. C. Bless, C. W. Gartlein, and D. E. Harris 205

Systematic Asteroidal Motions
A. R. Miller 206

ERRATA 208

THE UNIVERSITY OF CHICAGO PRESS
CHICAGO, ILLINOIS, U.S.A.

July 1955 Vol. 122, No. 1

THE ASTROPHYSICAL JOURNAL

AN INTERNATIONAL REVIEW OF SPECTROSCOPY AND ASTRONOMICAL PHYSICS

Founded in 1895 by George E. Hale and James E. Keeler

Published in Collaboration with the American Astronomical Society

S. CHANDRASEKHAR
Managing Editor

GERARD P. KUIPER
Associate Editor

Yerkes Observatory of the University of Chicago

EDITORIAL BOARD

LEO GOLDBERG (1955-59)
The Observatory of the University of Michigan

H. W. BABCOCK (1953-57)
Mount Wilson Observatory of the Carnegie Institution of Washington

MARTIN SCHWARZSCHILD (1954-58)
Princeton University Observatory

G. HERZBERG (1952-56)
National Research Council, Ottawa

C. D. SHANE (1952-55)
Lick Observatory, University of California

The Astrophysical Journal is published bimonthly by the University of Chicago at the University of Chicago Press, 5750 Ellis Avenue, Chicago 37, Illinois, during January, March, May, July, September, and November. ¶Two volumes are published per year, one beginning with the January issue and the other beginning with the July issue. On all orders from the United States and its possessions the subscription price is $7.50 per volume or $15.00 per year; the price of single copies is $3.50. ¶On all orders from Canada the subscription price is $8.00 per volume or $16.00 per year; the price of single copies is $3.65. On all orders from all other countries the subscription price is $8.25 per volume or $16.50 per year; the price of single copies is $3.75. (Orders for service of less than a volume will be charged at the single-copy rate.) ¶Subscriptions are payable in advance. Please make all remittances payable to The University of Chicago Press, in United States currency or its equivalent by postal or express money orders or bank drafts. (Exception: members of The American Astronomical Society must send their subscriptions and remittances to the Treasurer of the Society.)

The following is an authorized agent:

For the British Commonwealth, except North America and Australasia: The Cambridge University Press, Bentley House, 200 Euston Road, London, N.W. 1, England. Prices of yearly subscriptions and of single copies may be had on application.

Claims for missing numbers should be made within the month following the regular month of publication. The publishers expect to supply missing numbers free only when losses have been sustained in transit, and when the reserve stock will permit.

Business correspondence should be addressed to The University of Chicago Press, Chicago 37, Illinois.

Communications for the editors and manuscripts should be addressed to: S. Chandrasekhar, Editor of THE ASTROPHYSICAL JOURNAL, Yerkes Observatory, Williams Bay, Wisconsin.

Line drawings and photographs should be made by the author, and all marginal notes such as co-ordinates, wave lengths, etc., should be included in the cuts. It will not be possible to set up such material in type.

One copy of the corrected galley proof should be returned as soon as possible to the editor, Yerkes Observatory, Williams Bay, Wisconsin. Authors should take notice that the manuscript will not be sent to them with the proof.

The cable address is "Observatory, Williamsbay, Wisconsin."

The articles in this journal are indexed in the *International Index to Periodicals*, New York, N.Y.

Applications for permission to quote from this journal should be addressed to The University of Chicago Press, and will be freely granted.

Microfilms of complete journal volumes are available to regular subscribers only and may be obtained at the end of the year. Orders and inquiries should be addressed to University Microfilms, 313 North First Street, Ann Arbor, Michigan.

Notice to subscribers: If you change your address, please notify us and your local postmaster immediately.

Entered as second-class matter, July 31, 1940, at the Post-Office at Chicago, Ill., under the Act of March 3, 1879.
Acceptance for mailing at special rate of postage provided for in United States Postal Act of October 3, 1917, Section 1103, amended February 28, 1925.
Copyright 1955 by the University of Chicago.

[PRINTED IN U.S.A.]

THE ASTROPHYSICAL JOURNAL

AN INTERNATIONAL REVIEW OF SPECTROSCOPY AND ASTRONOMICAL PHYSICS

VOLUME 122 JULY 1955 NUMBER 1

ON THE INSTABILITY OF SUPERPOSED FLUIDS IN A GRAVITATIONAL FIELD*

DAVID LAYZER

Harvard College Observatory

Received January 3, 1955

ABSTRACT

In this paper an approximate analytic solution is obtained for the following problem: A perfect, incompressible fluid occupies the upper half of a vertical tube, being supported against gravity by a rigid diaphragm. The lower half of the tube is empty. At time t_0 the diaphragm is removed, and an infinitesimal disturbance of a simple kind is impressed on the free surface of the fluid. The problem is to describe the subsequent flow, on the assumption that the fluid at sufficiently great heights above the free surface is permanently at rest. The initial disturbance is so chosen that the fluid rises in the center of the tube and runs down at the sides. The range of validity of the approximate solution obtained is discussed. It is shown that the vertex height ζ increases exponentially, in agreement with the linearized theory, until $\zeta \approx 0.2\ \lambda/2\beta_1$, where λ is the diameter of the tube and β_1 is the first zero of the Bessel function $J_1(r)$. When $\zeta \gtrsim 1.5\ \lambda/2\ \beta_1$, it increases at a nearly constant rate. The method of solution described is applied to an analogous problem involving two-dimensional flow between parallel plane walls and also to spatially periodic flows.

I. INTRODUCTION

The study of small oscillations at the interface between superposed fluids in a gravitational field was initiated by Stokes (see Lamb 1932). In the simplest case both fluids are inviscid and incompressible and extend to infinity on either side of the interface. If the mean level of the interface is the plane $y = 0$, and the gravitational potential is $-gy$, the equation of the interface is

$$\eta(x, t) = \int_{-\infty}^{\infty} A_k(t)\ e^{ikx} dk \qquad (A_{-k} = A_k^*), \quad (1)$$

where

$$A_k(t) = A_k e^{\sigma(k)t}, \qquad \sigma = \left[g k \frac{\rho_2 - \rho_1}{\rho_2 + \rho_1} \right]^{1/2}. \quad (2)$$

* Most of the new work described herein was done during the month of July, 1952, at the Forrestal Research Center of Princeton University; the rest has been generously supported by the Air Force Cambridge Research Center, Geophysics Research Directorate, through Contract AF 19(604)-146 with Harvard University.

The subscripts 1 and 2 refer to the lower and upper fluids, respectively. The initial condition,

$$\eta(x, 0) = \int_{-\infty}^{\infty} A_k e^{ikx} dk, \tag{3}$$

determines the coefficients A_k.

When $\rho_1 > \rho_2$, the frequency σ/i is real, and the interface oscillates periodically. When $\rho_1 < \rho_2$, however, σ itself is real, and small disturbances of the interface grow exponentially. The instability tends to bring the heavy fluid to the bottom and the light fluid to the top.

In the hydrodynamic equations the constant g need not represent a true gravitational acceleration; it can equally well represent an "inertial" acceleration (see Taylor 1950). For example, if two incompressible fluids occupy a tube fitted with a moving piston and no gravitational field is present, the hydrodynamic equations in a frame of reference moving with the piston are identical with those for superposed fluids at rest in a gravitational field that is equal in magnitude and opposite in sign to the acceleration of the piston. A more interesting example is that of a liquid separated from a gas by a rigid diaphragm. If the pressure of the gas exceeds the pressure of the liquid, the interface will be unstable when the diaphragm is taken away. Evidence for this kind of instability appears in photographs of underwater explosions (Cole 1948).

Spitzer (1954; see also Frieman 1954) has suggested that something analogous to an underwater explosion may occur when an O star or a B star is formed in a medium of neutral hydrogen. The ionizing radiation from the star produces a spherical volume of gas in which the pressure and temperature are much higher than in the surrounding medium. As the hot gas expands, it becomes less dense than its surroundings. One would therefore expect the interface between the regions of neutral and ionized hydrogen to become unstable—provided that the star is formed sufficiently rapidly.

The early work of Stokes has been generalized in several ways:

a) *Viscosity and interfacial tension.*—Stokes himself discussed the influence of viscosity and surface tension on the oscillations at the free surface of a liquid (Lamb 1932). Harrison (1908) worked out an approximate theory of oscillations at the interface between superposed viscous liquids, taking into account the effects of interfacial tension. Pennington (1952), Chandrasekhar (1955), and Hide (1955) have extended Harrison's results. Viscosity and interfacial tension both exert a stabilizing influence on the interface. When $\rho_1 < \rho_2$, a critical wave length exists, whose value depends on the viscosity and the interfacial tension. The interface is unstable against disturbances whose wave lengths exceed the critical frequency, but stable against disturbances of shorter wave length.

b) *Compressibility.*—Wheeler, Carter, Frieman, and Pennington (1952) have modified Stokes's theory to include the effects of compressibility when the Mach number is not too large.

c) *Boundary conditions.*—The formulae that have been obtained for two-dimensional flow can be extended in a straightforward way to axially symmetric flow. But the problem of small oscillations (or instability) at a spherical interface presents some new features. It has recently been solved by Chandrasekhar (1955).

The investigations mentioned so far all proceed from a set of approximate hydrodynamic equations from which the nonlinear terms have been omitted. Consequently, they apply only to the initial development of an unstable interface. Now in astronomical applications the subsequent development is also of interest. In the present paper we shall derive an approximate analytic solution of the exact, nonlinear equations for an especially simple problem, which may be formulated in the following terms:

Let an incompressible, inviscid fluid occupy the region above the plane $z = 0$ inside a right circular cylinder centered on the z-axis. The rest of the cylinder is empty; but the

fluid is supported against gravity by a diaphragm. At time t_0 the diaphragm is taken away, and a small disturbance of a simple kind is impressed on the free surface. We assume that the fluid at very great heights above the interface is permanently at rest. The problem is to describe the ensuing flow.

For the initial conditions that we shall use, the fluid rises near the center of the tube and descends near the sides (see Fig. 1). After enough time has elapsed, the flow takes on a quasi-steady aspect: the vertex (i.e., the highest point of the interface) rises at a constant rate, and in a frame of reference moving with the vertex the flow is identical with the steady flow around a solid of revolution in the absence of a gravitational field—except that the descending fluid, having traveled only a finite distance, will not fill the space between the solid and the walls of the tube.

Davies and Taylor (1950) have given an approximate theory of the steady state. For the speed of the vertex they find

$$V = 0.464\,(gR)^{1/2}\,, \tag{4}$$

where R is the radius of the tube.

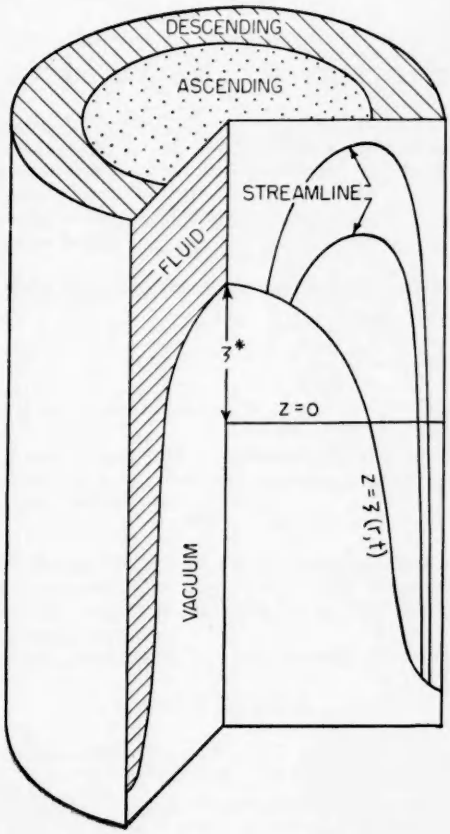

FIG. 1.—Illustrating the case of axially symmetric flow treated in Section II, 1

The theory of Davies and Taylor holds for $t \gg t_0$. The linear theory holds for $t \approx t_0$. One can bridge the gap between the two in a rough sort of way by using the linear theory until the predicted vertex speed attains the value (4) and then switching to the steady-state theory. As it happens (see Fig. 2), this simple approximation, which was originally suggested by Fermi, is never in error by more than about 25 per cent. For many purposes this accuracy will suffice. However, the more precise theory described later may be of some interest in its own right, because very few nonsteady flows with a free boundary have been successfully treated analytically, even in an approximate way.

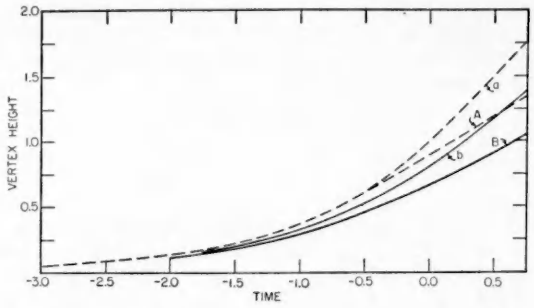

FIG. 2.—Vertex height as a function of time, in the dimensionless units defined by equations (5) and (52). *A*, Fermi's approximation for two-dimensional flow. *B*, Fermi's approximation for tubular flow. *a*, Present approximation for two-dimensional flow. *b*, Present approximation for tubular flow.

II. APPROXIMATE SOLUTIONS

1. TUBULAR FLOW

We shall find it convenient to adopt the units of length and time defined by the equations

$$\frac{R}{\beta_1} = 1\,, \qquad g = 1\,, \tag{5}$$

where R is the radius of the tube, g is the acceleration of gravity, and $\beta_1 (= 3.83\ldots)$ is the first zero of the Bessel function $J_1(r)$.

Since the fluid is inviscid and is initially at rest, the motion is permanently irrotational. The velocity field can therefore be derived from a scalar velocity potential

$$\boldsymbol{q} = -\nabla\phi\,. \tag{6}$$

Since the fluid is also incompressible, the velocity field is solenoidal, so that ϕ must satisfy Laplace's equation,

$$\nabla^2\phi = 0\,. \tag{7}$$

We seek an axially symmetric solution $\phi(z, r, t)$ of Laplace's equation that satisfies the boundary conditions,

$$\phi_r(z, \beta_1, t) = 0 \tag{8}$$[1]

(no radial flow at the walls) and

$$\phi_z(\infty, r, t) = 0 \tag{9}$$

[1] Here and in what follows we shall use subscripts to indicate partial derivatives. Thus $\phi_r \equiv \partial\phi/\partial r$, etc.

(vanishing vertical flow at large positive values of z). In addition, ϕ must satisfy Bernoulli's equation,

$$\phi_t - \tfrac{1}{2}(\phi_z^2 + \phi_r^2) - z = \alpha(t) \tag{10}$$

on the free surface. Here α is an arbitrary function.

The simplest nonconstant function that satisfies equations (7)–(9) is

$$\phi = F(t)\, e^{-z} J_0(r), \tag{11}$$

where $J_0(r)$ is the Bessel function of order zero. The function $F(t)$ must be chosen in such a way that equation (10) is satisfied as nearly as possible on the free surface.

Now the equations of motion for a fluid particle are

$$\dot{z} = -\phi_z = F(t)\, e^{-z} J_0(r), \tag{12}$$

$$\dot{r} = -\phi_r = F(t)\, e^{-z} J_1(r), \tag{13}$$

since

$$J_0'(r) = -J_1(r). \tag{14}$$

Suppose that we have found a solution of equations (12) and (13):

$$z = z(t;\, r_0,\, z_0), \qquad r = r(t;\, r_0,\, z_0), \tag{15}$$

where (r_0, z_0) are the co-ordinates of the particle at time t_0. By eliminating t between these equations, we evidently obtain the equation of the trajectory of the particle. Similarly, to find the equation $z = \zeta(r, t)$ of a surface that moves with the fluid, given $z = \zeta(r, t_0)$—i.e., $z_0 = z_0(r_0)$—we insert $z_0(r_0)$ in equations (15) and eliminate r_0. In this way we can find the equation of the free surface for any given initial condition. Before doing this, let us consider briefly the nature of the flow defined by the velocity potential (11).

The Stokes stream function ψ is defined by the equations

$$\psi_z = -r\phi_r, \qquad \psi_r = r\phi_z. \tag{16}$$

Since

$$J_1'(r) = J_0(r) - \frac{J_1(r)}{r} \tag{17}$$

and $J_0'(r) = -J_1(r)$,

$$\psi(z,\, r,\, t) = F(t)\, r\, e^{-z} J_1(r), \tag{18}$$

and the streamlines $\psi =$ Constant are given by

$$e^z = C r J_1(r). \tag{19}$$

Since the pattern of streamlines does not change with time, the streamlines coincide with the trajectories of fluid particles. We can also obtain this result by noticing that equation (19) is the integral of the equation

$$\frac{dz}{dr} = \frac{J_0(r)}{J_1(r)}, \tag{20}$$

which follows from the equations of motion, (12) and (13).

According to equation (19), one can generate all the stream surfaces by displacing any one of them parallel to the z-axis. The section of a stream surface by a plane through the z-axis resembles an inverted U whose legs asymptotically approach the z-axis and

the wall and whose apex lies directly above the first zero of $J_0(r)$. The flow has an upward component on the axis side and a downward component on the wall side (see Fig. 1).

To find the equation of the free boundary, we integrate the equations of motion (12) and (13). Set

$$Z = e^z , \tag{21}$$

$$v = r^2 , \tag{22}$$

$$T(t) = \int_t^t F(t)\, dt + 1 , \tag{23}$$

$$K(v) = \frac{2J_1(r)}{r} . \tag{24}$$

In terms of the new variables, equations (12) and (13) become

$$\dot{Z} = J_0(v^{1/2}) , \tag{25}$$

$$Z = \frac{vK(v)}{\dot{v}} , \tag{26}$$

where the dot now denotes differentiation with respect to T. Eliminating Z between these equations and using the identity (17), one obtains, after a simple calculation,

$$\frac{v}{v_0} = \frac{(T-1)\,K(v_0)}{Z_0+1} , \tag{27}$$

$$\frac{Z}{Z_0} = \frac{K(v)}{K(v_0)}\,\frac{(T-1)\,K(v_0)}{Z_0+1} . \tag{28}$$

These are the parametric equations of the free surface.

Since the velocity potential (11) is not exact, it cannot satisfy Bernoulli's equation (10) over the entire free surface. Now we are interested primarily in the flow near the vertex, for when that is known, we can find the flow at the sides—at least in an approximate way—by another method (see Sec. II, 3). We shall therefore choose the function $F(t)$ in such a way that Bernoulli's equation is satisfied in a first-order neighborhood of the vertex.

We shall assume that initially the free surface is perfectly flat, so that

$$z_0(r_0) = 0 , \qquad Z_0(v_0) = 1 . \tag{29}$$

To obtain the equation of the free surface, we insert this value of Z_0 in equations (27) and (28) and eliminate v_0. Neglecting terms nonlinear in v (since we are concerned only with a first-order neighborhood of the vertex), we obtain:

$$v = v_0 T , \tag{30}$$

$$e^\zeta = T\left[1 - \frac{v}{8}(1 - T^{-2})\right] . \tag{31}$$

We now substitute the velocity potential (11) in Bernoulli's equation (10), replacing z by ζ, as given by equation (31), and $F(t)$ by $T'(t)$. Equating the coefficient of v in the resulting equation to zero, we obtain a second-order, nonlinear differential equation for the function $T(t)$:

$$T(T^2+1)T'' - T'^2 - T^2(T^2-1) = 0 . \tag{32}$$

Let us verify that the solution of equation (32) has the proper asymptotic behavior. When $t \gg t_0$, $T \gg 1$, and equation (32) becomes, approximately,

$$T'' - T = 0 . \tag{33}$$

Hence

$$F(t) = T'(t) = e^{t+c} \qquad (t \gg t_0) , \tag{34}$$

and

$$\phi = e^{-(z-t-c)} J_0(r) \qquad (t \gg t_0) . \tag{35}$$

From equations (31) and (24) we find

$$\left.\frac{d\zeta}{dt}\right|_{r=0} = \frac{d \log T}{dt} = 1 \qquad (t \gg t_0) . \tag{36}$$

Thus the velocity potential (35) describes a steady state of flow in which the vertex advances with unit velocity. In c.g.s. units the vertex speed is

$$V = \left(\frac{gR}{\beta_1}\right)^{1/2} \approx 0.511 \, (gR)^{1/2} . \tag{37}$$

The experimental values of the numerical coefficient in this formula (Davies and Taylor 1949) lie between this value and that derived by Davies and Taylor (eq. [4]). Although Davies and Taylor used a velocity potential that is equivalent to equation (35), they chose to satisfy Bernoulli's equation at two distinct points ($r = 0$, $r = \frac{1}{2}R$) rather than in a first-order neighborhood of the vertex.

When $t \approx t_0$,

$$T = 1 + \tau(t) \qquad [\tau(t) \ll 1] , \tag{38}$$

and equation (32) becomes, approximately,

$$\tau'' - \tau = 0 . \tag{39}$$

The initial condition (29) requires that

$$\tau(t_0) = 0 . \tag{40}$$

Hence the appropriate solution of equation (39) is

$$\tau(t) = a e^{t_0} \sinh(t - t_0) \qquad (a e^{t_0} \ll 1) , \tag{41}$$

so that

$$F(t) = T'(t) = \tau'(t) = a e^{t_0} \cosh(t - t_0) \tag{42}$$

and

$$\phi = a e^{t_0} \cosh(t - t_0) \, e^{-z} J_0(r) \qquad (t \approx t_0) . \tag{43}$$

The velocity potential (43) is the one given by the linearized theory. We conclude that the solutions of equation (32) have the proper asymptotic form.

To obtain the complete solution of equation (32), we set

$$X(T) = T'^2 . \tag{44}$$

Equation (32) may be written in the form

$$\frac{d}{dT}[X(1 + T^{-2})] = 2(T - T^{-1}) , \tag{45}$$

whence

$$X = T'^2 = F^2 = (1 + T^{-2})^{-1} (T^2 - 2 \log T + \text{const.}) \tag{46}$$

the constant in equation (46) being determined by the asymptotic form of $T(t)$ for $t \approx t_0$. For the sake of simplicity, we choose

$$t_0 = -\infty\,, \qquad a = 2\,. \tag{47}$$

Then equation (41) becomes

$$\tau\,(t) = e^t\,, \tag{48}$$

and the constant in equation (46) $= -1$.

Let $\zeta^*(t)$ denote the co-ordinate of the vertex. The height of the vertex is given by equation (31):

$$\zeta^*\,(t) = \log T\,(t)\,. \tag{49}$$

Combining this equation with equation (46), we obtain, for the vertex speed,

$$V\,(t) = \frac{d\zeta^*}{dt} = \left(\frac{e^{2\zeta^*} - 2\zeta^* - 1}{e^{2\zeta^*} + 1}\right)^{1/2}. \tag{50}$$

The height of the vertex at time t is given implicitly by the formula

$$t\,(\zeta_2^*) - t\,(\zeta_1^*) = \int_{\zeta_1^*}^{\zeta_2^*} \left(\frac{e^{2x}+1}{e^{2x}-1-2x}\right)^{1/2} dx\,, \tag{51}$$

and is plotted in Figure 2.

2. TWO-DIMENSIONAL FLOW BETWEEN PARALLEL WALLS

The extension of the preceding theory to the case of two-dimensional flow between parallel walls presents no new features. We shall therefore quote the results for two-dimensional flow, but we shall omit the working.

We assume that the flow is identical in every plane parallel to the xy-plane. The gravitational field is in the negative y-direction, the walls are at $x = \pm R$, the plane $y = 0$ represents the free surface at time t_0, and the equation of the free surface is $y = \eta(x, t)$. The units of length and time are so chosen that

$$\frac{R}{\pi} \equiv k^{-1} = 1\,, \qquad g = 1\,. \tag{52}$$

The velocity potential is

$$\phi = F\,(t)\; e^{-y} \cos x\,. \tag{53}$$

The streamlines and the trajectories of fluid particles are given by the equation

$$e^y = C \sin x\,. \tag{54}$$

The auxiliary quantity T is defined as before and satisfies the equation

$$T\,(2T^3 + 1)\,T'' + (T^3 - 1)\,T'^2 - T^2\,(T^3 - 1) = 0\,, \tag{55}$$

which has the asymptotic solutions

$$T = e^{3^{-1/2}t + c} \qquad (t \gg t_0) \tag{56}$$

and

$$T = 1 + a\,e^{t_0} \sinh\,(t - t_0) \qquad (t \approx t_0)\,. \tag{57}$$

The corresponding velocity potentials are

$$\phi = e^{-(y - 3^{-1/2}t - c)} \cos x \qquad (t \gg t_0)\,, \tag{58}$$

$$\phi = a\, e^{t_0} \cosh (t - t_0)\; e^{-y} \cos x \qquad (t \approx t_0)\,. \tag{59}$$

The vertex speed in the steady state is

$$V = 3^{-1/2} \left(\frac{gR}{\pi}\right)^{1/2} \approx 0.326\, (gR)^{1/2}. \tag{60}$$

The vertex speed for arbitrary t is

$$V(t) = \left[\frac{e^{3\eta^*} - 3\eta^* - 1}{3\,(e^{3\eta^*} + \frac{1}{2})}\right]^{1/2}, \tag{61}$$

and the vertex height is given implicitly by the formula

$$t(\eta_2^*) - t(\eta_1^*) = \int_{\eta_1^*}^{\eta_2^*} \left[\frac{3\,(e^{3x} + \frac{1}{2})}{e^{3x} - 1 - 3x}\right]^{1/2} dx \tag{62}$$

and is plotted in Figure 2.

3. VALIDITY OF THE APPROXIMATION; NATURE OF THE FLOW NEAR THE WALLS

We shall explicitly consider the case of tubular flow; but the following discussion, with some obvious modifications, also applies to two-dimensional flow. In the quasi-steady state, the flow at depths greater than about $1.5R$ below the vertex is nearly parallel to the wall of the tube. Using this fact, together with Bernoulli's equation and the equation of continuity, Davies and Taylor (1950) wrote down the equations

$$\pi R^2 V = \pi\,(R^2 - r^2)\; q = \pi\,(R^2 - r^2)\,[2g\,(\zeta^* - z)]^{1/2}, \tag{63}$$

where V is the vertex speed. These equations, rather than the theory of Section II, 1, should be used to calculate the shape of the interface in the region where the fluid runs parallel to the wall.

According to the second of equations (63), $q \propto (-z)^{1/2}$ for large negative values of z. The approximate theory of Section II, 1, gives $q \propto \exp(-z)$. Unfortunately, it does not seem possible to develop a simple unified approximation that will yield both the correct vertex speed and the correct asymptotic flow for large negative values of z. The following discussion will bring out the nature of the difficulty.

The velocity potential (11) describes the simplest kind of axially symmetric flow that satisfies the fixed-boundary conditions of the present problem *and is free of singularities in the entire tube.* The most general flow of this kind is given by the velocity potential,

$$\phi = \sum_{k=1}^{\infty} F_k(t)\; e^{-\beta_k z/\beta_1} J_0 \frac{\beta_k r}{\beta_1}, \tag{64}$$

where the β_k's are the zeros of the Bessel function $J_1(r)$. We see at once that this velocity potential cannot have the proper asymptotic form for large negative values of z and $t \gg t_0$. Consequently, the exact velocity potential cannot be free of singularities in the entire tube: it must contain terms that represent sources in the region not actually occupied by the fluid.

Symmetry requires the sources to lie on the z-axis. Let $z^*(t)$ denote the co-ordinate of the highest source (or the limit point of a continuous distribution of sources). Then expansion (64) holds only for $z \geq z^*$.

We can form a rough idea of how z^* varies with time by examining the limiting cases $t \gg t_0$ and $t \approx t_0$. In the quasi-steady state the quantity $(\zeta^* - z^*)$ is constant in time. Inspection of the flows that have been calculated for various distributions of sources (Milne-Thomson 1950) suggests that $\zeta^* - z^* \approx R$. At the other limit, $t \to t_0$, the ve-

locity potential (11) becomes exact. Hence $\zeta^* - z^* \to +\infty$ as $t \to t_0$. These two limiting cases suggest the approximate rule

$$\zeta^* - z^* \approx -\zeta_{rr}^{-1}(0, t). \tag{65}$$

That is, the highest singularity coincides approximately with the center of curvature of the vertex.

The theory of Section II, 1, probably describes the flow above the plane $z = z^*$ with good accuracy. To describe the rest of the flow, one can use equations (63), together with the requirement that the volume of fluid below the plane $z = 0$ equals the volume not occupied by fluid above the plane $z = 0$.

III. INSTABILITY OF AN INFINITE PLANE INTERFACE

1. PERIODIC FLOWS

In Section II we considered flows confined by tubes and by parallel plane walls. We shall now extend the results to unconfined, but spatially periodic, flows. In the case of two-dimensional flow between parallel walls the extension is trivial: we may evidently regard the walls as mathematical planes of symmetry. To extend the results for tubular flow, consider an infinite array of right cylinders whose walls intersect any plane $z =$ Constant in a network of regular hexagons. We may reasonably assume that the flow in a hexagonal cylinder of mean radius R resembles the flow in a circular cylinder of radius R, except in the neighborhood of the walls. We may therefore use the expression derived in Section II, 1, for the vertex speed. Near the walls, however, the fluid will tend to flow into the corners, forming long spikes rather than a uniform curtain. If the flow is the same in every cylinder, it will not be affected by the walls, which we may therefore regard as mathematical planes of symmetry.

The fluid displaced by a rising bubble runs down into six spikes, each of which serves three bubbles; hence there are two spikes for every bubble. Assuming that the spikes have circular cross-sections of radius $a(z)$, we can determine $a(z)$ approximately from Bernoulli's equation and the equation of continuity. Considerations of continuity approximately fix the rate of growth of the spikes (see the final paragraph of Sec. II, 3).

2. APERIODIC FLOWS

The periodic flows arise from initial conditions that are very unlikely to be realized in nature. However, the theoretical description of more general flows presents great difficulty. In the present section we shall try to get some insight into the nature of aperiodic flows by qualitative arguments based on our knowledge of special flows.

Consider an arbitrary two-dimensional disturbance. In the initial phase of growth $\eta(x, t)$ is a superposition of independent Fourier amplitudes,

$$A_k(t) = A_k \exp\left[(gk)^{1/2}t\right], \tag{66}$$

where

$$A_k = \frac{1}{2\pi}\int_{-\infty}^{\infty} \eta(x, 0)\, e^{-ikx} dx. \tag{67}$$

According to equation (66), the Fourier amplitudes corresponding to large values of k (i.e., small wave lengths) grow faster than those corresponding to small values of k (i.e., large wave lengths). On the other hand, the phase of exponential growth lasts longer for the latter than for the former. Now the Fourier amplitudes begin to interfere badly with one another when the mean amplitude of the disturbance becomes comparable with the mean wave length. From the preceding remarks it is clear that at this stage the predominant wave numbers will come from a relatively narrow subrange of the range of wave numbers for which the coefficients A_k are appreciable. Fourier amplitudes cor-

responding to the largest wave numbers will have been outstripped; those corresponding to the smallest wave numbers will not have had time to develop. Thus the initial competition between Fourier amplitudes tends to establish a nearly periodic pattern of flow.

As the mean amplitude of the disturbance becomes comparable with the mean wave length, the competition between noninterfering Fourier amplitudes goes over into a competition between individual bubbles. To see what effects are introduced by small departures from periodicity at this stage, let us consider a simple example. Figure 3 shows three well-developed bubbles, the middle one being slightly narrower than its companions. In general, the pattern of flow will resemble that for periodic flow. However, the flow pattern associated with the middle bubble will be slightly compressed at the top, while the flow patterns associated with the bubbles on either side will be correspondingly dilated. This is indicated in Figure 3 by the bending of the streamlines SS and $S'S'$. That the channel defined by these streamlines must, in fact, narrow from bottom to top follows from the requirement that the flow be continuous on SS and $S'S'$ and the fact that the vertex speed of the two large bubbles exceeds that of the small

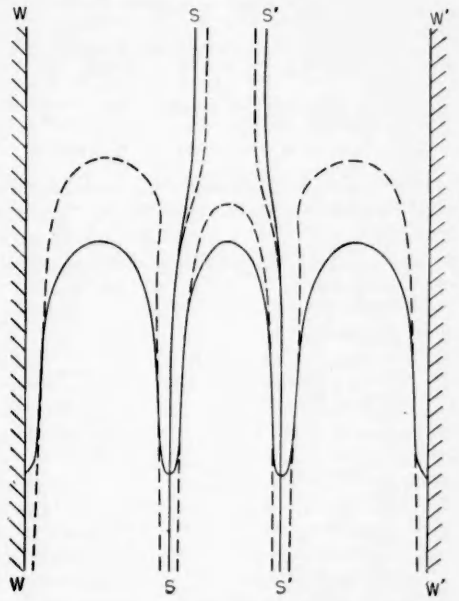

FIG. 3.—Illustrating the competition between well-developed bubbles in two-dimensional flow. The middle bubble is crowded out by the larger bubbles on either side. SS and $S'S'$ are streamlines.

bubble. The large bubbles will therefore expand, thereby acquiring a higher vertex speed, while the small bubble will shrink and slow down. This development, which is indicated in Figure 3 by the broken lines, shows up clearly in some experiments by D. J. Lewis (1950). Ultimately, the two large bubbles will fill the entire channel, the middle bubble having been washed downstream. Since perfectly periodic flow can never be attained in practice, the number of bubbles per unit length will continually diminish. The foregoing remarks apply, with some obvious modifications, to the more general case of three-dimensional flow.

Finally, we shall consider briefly the question whether an arbitrary disturbance tends

to develop into a two-dimensional system of cylindrical troughs and crests or a three-dimensional system of bubbles and spikes. From equations (37) and (60) we see that the final vertex speed of a bubble in a tube of diameter $2R$ is higher, by a factor $(3\pi/\beta_1)^{1/2}$, than the final vertex speed of a cylindrical wave in a channel of width $2R$. This suggests that a well-developed two-dimensional disturbance would tend to break up into a system of bubbles and spikes.

I am indebted to Capt. Ralph Pennington for pointing out to me that equation (32) has a first integral, and to Capt. Pennington and Mr. Robert Goerss for performing the quadratures on which Figure 2 is based. Professor John A. Wheeler directed my attention to the problems discussed herein and made several valuable suggestions for improving the readability of the paper. The qualitative description of aperiodic flow contained in Section III, 2, was largely worked out in the course of a conversation with Professor Wheeler.

REFERENCES

Chandrasekhar, S. 1955*a*, *Proc. Cambridge Phil. Soc.*, **51**, 162.
———. 1955*b*, *Quart. J. Mechanics*, **8**, 1.
Cole, R. H. 1948, *Underwater Explosions* (Princeton: Princeton University Press), p. 247.
Davies, R. M., and Taylor, G. I. 1950, *Proc. R. Soc. London, A*, **200**, 375.
Frieman, E. 1954, *Ap. J.*, **120**, 18.
Harrison, W. J. 1908, *Proc. London Math. Soc.* (2), **6**, 396; **7**, 107.
Hide, R. 1955, *Proc. Cambridge Phil. Soc.*, **51**, 179.
Lamb, H. 1932, *Hydrodynamics* (New York: Dover Publications), chap. ix.
Lewis, D. J. 1950, *Proc. R. Soc. London, A*, **202**, 81.
Milne-Thomson, L. M. 1950, *Theoretical Hydrodynamics* (New York: Macmillan Co.).
Pennington, R. 1952, unpublished Princeton University report.
Spitzer, L., Jr. 1954, *Ap. J.*, **120**, 1.
Taylor, G. I. 1950, *Proc. R. Soc. London, A*, **201**, 192.
Wheeler, J. A., Carter, D., Frieman, E., and Pennington, R. 1952, unpublished.

OBSERVABLE TESTS ON THE NATURE OF THE COSMOLOGICAL RED SHIFT

S. N. MILFORD
Department of Physics, St. John's University, Brooklyn, New York
Received August 4, 1954; revised March 7, 1955

ABSTRACT

This paper develops tests on the red shift in the spectra of distant galaxies, in order to distinguish between the Doppler velocity interpretation of the red shift and some other cause. Section I discusses the previous tests proposed by McCrea and by Hubble and Tolman. Section II sets up new theoretical tests in a nonstatic relativistic cosmological model; section *a* describes the cosmological model used; *b* finds the equation for the time rate of variation of brightness of a star in the model universe employed; and *c* discusses the observed frequency of distant events in the same model. In Section III the tests are cast into their observable form. The most promising test expresses the rate of decline of the light-curve of a distant supernova in terms of the red shift in its spectrum and is given in equation (26). This supernova test is probably free from the evolutionary objections to the galaxy counts test. In Section III, c, the test on the frequency of novae and supernovae is discussed. Finally, there is a brief discussion of the practicality of the tests, and it is concluded that the supernova light-curve test could be carried out with existing equipment.

I. INTRODUCTION

At present there are many cosmological theories which fit the broad features of the observed universe (Bondi 1952; McCrea 1953) but very few detailed observational tests which can be used to discriminate between these theories. One of the most important observational facts is the red shift in the spectra of all but the nearest galaxies, which, when interpreted as a Doppler velocity shift, indicates large velocities of recession. Red shifts corresponding to a velocity of 20 per cent of the velocity of light have already been measured (Humason 1954), and, at the photographic limit of the 200-inch, extrapolation gives velocities of the order of 40 per cent of the velocity of light. The velocity interpretation of the red shift not only has led to nonstatic cosmological theories which allow for large-scale expansion of the universe but also leads to appreciable corrections to the apparent magnitudes for distant galaxies (much more than 1 mag. for $\delta\lambda/\lambda = 0.5$). There have been some doubts raised about the reality of such enormous velocities; and alternative explanations of the red shift—such as (1) photons lose energy with the passage of time, or (2) the physical "constants" of nature change with time—have been put forward. These are discussed by Omer (1949). None of the alternative explanations so far advanced seems likely to supplant the Doppler interpretation.

In view, however, of the importance of the red shift, further tests on its nature are desirable. The present paper derives relations between the red shift and several observable quantities in a relativistic expanding universe, the most promising test referring to the gradient of the light-curve of a supernova. If the red shift comes to be accepted as a definite velocity effect on other grounds, then the present tests could be used as checks on the validity of the laws used in deriving the tests, e.g., the relativity formula for time dilatation and possibly also to help find the values of such cosmological parameters as the curvature of space.

Several possible tests on the red shift have been proposed in the past. McCrea (1935) pointed out that any periodic phenomenon in a galaxy must show the same Doppler effect as does the radiation, if the red shift is due to velocity, and mentioned the particular case of the period of Cepheids. Although McCrea did not actually propose this as a test on the red shift, it could in principle be so used if it were possible to identify the

period of a Cepheid either uniquely or statistically from the shape of its light-curve (see, e.g., Payne-Gaposchkin 1951). McCrea also found the relation

$$[\log (\text{apparent brightness})]_{\text{av}} - [\log (\text{apparent area})]_{\text{av}} = 4 \log D + \text{constant}$$

for galaxies, where the averages are over all galaxies for each value of $D = 1 + \delta\lambda/\lambda$. Unfortunately, such a test requires the constancy of the brightness and size of the galaxies over periods (for the most distant galaxies for which the red shift has been measured so far) of the order of 500 million years. This has always seemed rather unlikely, and the results of Stebbins and Whitford (Whitford 1954) now make it probable that the galaxies evolve considerably during such intervals of time.

Hubble and Tolman (1935) set out to find methods of investigating the nature of the red shift and formulated their two well-known tests. The first of these relates the distribution of luminosity over the surface of images of galaxies to the red shift and the apparent magnitude, i.e., it is essentially the same as the McCrea test discussed previously. It has not yet been applied, because at large distances the image of a galaxy becomes comparable in size with the microphotometer aperture and the grain of the plate.

We should like to point out that this difficulty could perhaps be overcome by taking the angular distance between physical pairs of galaxies as a measure of $\delta\theta$, since this would be much easier to measure accurately than the diameter of a galaxy. Most optical pairs could be eliminated by choosing pairs of galaxies with the same red shift. Again, any evolutionary changes would interfere with the test—in this case, changes in the average separation of galaxy pairs with time. The extension to three or more galaxies is obvious.

Their second test relates the counts of galaxies out to a given limiting magnitude with the red shift. This test has been much discussed, because it was applied and led to rather unlikely conclusions on the size, density, and time scale of the universe (Omer 1949). However, in view of the various extrapolations and approximate magnitude scales used, it is now considered that any application of this test must await further work with the 200-inch. As Hubble and Tolman state, these tests are applicable only in a universe where the average luminosity and surface brightness of galaxies do not change with time.

More recently Zwicky (1951) has suggested using clusters of galaxies to decide between the short and long time scales. These cluster tests could perhaps be used to test the red shift, provided that certain assumptions are made about the evolution of clusters. One could, for example, as suggested earlier, measure the diameter of clusters of galaxies.

Of the four separate tests discussed, only the Cepheid one is free from the assumption that evolutionary changes in the galaxies are small enough to be neglected, and Cepheids are not bright enough to be observed in the regions of large red shifts. The supernova test derived in the present paper is free from assumptions about the evolution of galaxies or the universe and, because of the brightness of supernovae, seems to be within the possibilities of observation. The new tests will be derived in the following sections.

II. THEORETICAL TESTS FOR THE RED SHIFT IN A NONSTATIC RELATIVISTIC MODEL UNIVERSE

a) ASSUMPTIONS AND COSMOLOGICAL MODEL USED

If the red shift is a Doppler effect, then the local physical laws which give rise to the Doppler effect must be valid out to the distances of the galaxies concerned, and it is reasonable to assume that other physical laws which are valid in our local neighborhood are also true out to these distances. In particular, it is assumed that the general theory of relativity holds. If, then, the tests derived on the basis of these assumptions are satisfied, there will be strong evidence that the red shift is due to velocity and that the general theory of relativity can be used over these large distances. In the case that the tests are not satisfied, any or all of the velocity, the relativity theory, or the model used can be questioned.

A nonstatic relativistic homogeneous isotropic model is assumed for the universe. If

later work indicates that the actual universe is not homogeneous isotropic, the present tests can be derived equally well for the model which most closely fits the observed universe. For example, if it were found that the distribution of matter is nonhomogeneous but isotropic with respect to our Galaxy, the tests could be set up in the nonhomogeneous model investigated by Omer (1949).

Assuming, further, that co-moving co-ordinates can be employed, the line element may be written as follows:

$$ds^2 = -e^{g(t)}\left(\frac{dr^2}{1-r^2/R^2} + r^2 d\theta^2 + r^2 \sin^2\theta d\phi^2\right) + c^2 dt^2, \tag{1}$$

where r is a co-ordinate distance related to the usual radial co-ordinate and $g(t)$ is the function which describes the rate of increase of the proper distance between two particles in the universe. This and a number of equations which will be required are conveniently set out in Tolman (1934*a*) and will be quoted, with slight modifications, using c.g.s. units instead of the relativistic units in Tolman. Let the origin of co-ordinates O be in our Galaxy. Consider a star i which is always at rest relative to the matter in its neighborhood which defines the co-moving co-ordinates. Then r_i is always constant. Suppose that certain "events" at the star, such as the passing through maximum light for a variable star, are accompanied by simultaneous emission of light-signals. If two events at the star i occur at times t_i and $t_i + \delta t_i$, and the light from these events arrives at the origin at times t_{io} and $t_{io} + \delta t_{io}$, respectively, then the red shift x_{io} in the spectrum of the star as observed at the origin is given by

$$1 + x_{io} = \frac{\lambda_i + \delta\lambda_{io}}{\lambda_i} = \frac{\delta t_{io}}{\delta t_i} = \exp\tfrac{1}{2}(g_{io} - g_i), \tag{2}$$

where any quantity f associated with the star i at time t_i will be denoted by $f_i = f(t_i)$ when measured by an observer co-moving with the star, and by $f_{io} = f(t_{io})$ when measured at O.

b) THE VARIATION OF LUMINOSITY WITH TIME IN A NONSTATIC UNIVERSE

It is proposed to find the light-curve observed at O for a variable star in a distant galaxy exhibiting a red shift. Let $z_i(\nu_i, t_i)d\nu_i$ be the number of photons emitted by the star per second at time t_i in the frequency interval ν_i to $\nu_i + d\nu_i$, so that the total light-energy emitted per second is

$$L_i(t_i) = \int_0^\infty z_i(\nu_i, t_i)\, h\nu_i d\nu_i. \tag{3}$$

Note that L_i is a function of time via the spectrum-luminosity function z_i. The apparent luminosity measured by an observer at O at time t_{io}, then, is

$$l_{io}(t_{io}) = \frac{\text{Constant} \times L_i(t_i)}{[r_i^2\{1 + x_{io}(t_{io})\}^2 \exp g_{io}(t_{io})]}. \tag{4}$$

Compare the magnitude m_{io} of the star with a constant source of luminosity l, magnitude m (e.g., a laboratory source):

$$m_{io} - m = -\frac{5}{2}\log_{10}\frac{l_{io}}{l} = -\frac{5}{2E}\log_e \frac{L_i}{r_i^2(1 + x_{io})^2 \exp g_{io}} + \text{constant}, \tag{5}$$

where $E = \log_e 10$. Differentiation of equation (5) with respect to the time of emission t_i gives

$$\frac{dm_{io}}{dt_i} = -\frac{5}{2E}\left(\frac{1}{L_i}\frac{dL_i}{dt_i} - \frac{2}{1 + x_{io}}\frac{dx_{io}}{dt_i} - \frac{dg_{io}}{dt_i}\right). \tag{6}$$

Applying equation (6) to each of two stars $i = 1, 2$, and substracting, we obtain

$$\frac{dm_{10}}{dt_1} - \frac{dm_{20}}{dt_2} = -\frac{5}{2E}\left(\frac{1}{L_1}\frac{dL_1}{dt_1} - \frac{1}{L_2}\frac{dL_2}{dt_2} - \frac{2}{1+x_{10}}\frac{dx_{10}}{dt_1} + \frac{2}{1+x_{20}}\frac{dx_{20}}{dt_2} - \frac{dg_{10}}{dt_1} + \frac{dg_{20}}{dt_2}\right). \tag{7}$$

Since the absolute luminosity L_i cannot be measured accurately at O, it is desirable to seek conditions under which the terms $(1/L_1)(dL_1/dt_1) - (1/L_2)(dL_2/dt_2)$ vanish from equation (7). If an observer is permanently located at 10 parsecs from star i, i.e., he co-moves with the star, then he measures its absolute magnitude at any time t_i as

$$M_i(t_i) = -\frac{5}{2E}\log_e L_i(t_i) + \text{constant} \tag{8}$$

and the gradient of its magnitude-time light-curve as

$$\frac{dM_i}{dt_i} = -\frac{5}{2E}\frac{1}{L_i}\frac{dL_i}{dt_i}. \tag{9}$$

Evidently, the L_i terms will vanish from equation (7) if

$$\left(\frac{dM_1}{dt_1}\right)_{t_1} = \left(\frac{dM_2}{dt_2}\right)_{t_2}, \tag{10}$$

where t_i is uniquely determined by the time of observation t_{io}, since the radial null-geodesic for light traveling from star i to the origin O (θ = Constant, ϕ = Constant), on employing the line element (1), gives

$$\int_{r_i}^{0} \frac{dr}{(1 - r^2/R^2)^{1/2}} = -c\int_{t_i}^{t_{io}} e^{-1/2\varphi(t)}\,dt, \tag{11}$$

where the integral on the left side is a constant. Equation (10) then suggests the two following conditions: (*a*) observe only those stars which are known *from other evidence* to have exactly the same light-curves; (*b*) choose the times of observation t_{10} and t_{20} so that the corresponding t_1 and t_2 given by equation (11) were times when the stars 1 and 2 were at exactly the same points on their light-curves, e.g., both at maximum. Suppose, in order to see how restrictive condition *a* is, that star i with emission function $z_i(\nu_i, t_i)$ were replaced by a star with emission function $Az_i(\nu_i, t_i)$, where A is a constant. Then the near-by observer would find a larger absolute magnitude but would find that the gradient of the light-curve was unchanged by equations (3) and (9). It follows that condition (10) can be satisfied by two stars, 1 and 2, which are identical, except that one star emits A times as many photons as the other, i.e., is intrinsically brighter. This is an important point observationally, because the spectrum and light-curve can be determined with much more certainty than can the absolute magnitude.

Assuming that the observations satisfy conditions *a* and *b* and using equation (2) to express the proper time intervals δt_i in terms of the observed time intervals δt_{10}, equation (7) becomes

$$\frac{dm_{10}}{dt_{10}} = \frac{1+x_{20}}{1+x_{10}}\frac{dm_{20}}{dt_{20}} - \frac{5}{2E}\frac{1}{1+x_{10}}\left\{\frac{-2}{1+x_{10}}\frac{dx_{10}}{dt_1} + \frac{2}{1+x_{20}}\frac{dx_{20}}{dt_2} - (1+x_{10})\frac{dg_{10}}{dt_{10}} + (1+x_{20})\frac{dg_{20}}{dt_{20}}\right\}. \tag{12}$$

On the right side of equation (12) the first term arises from the intrinsic variability of the star, modified by the time dilatation, and vanishes for a nonvariable star. All the other terms are due to the nonstatic model used, and their values depend only on the distances of the objects considered and not on their nature. The quantities dx_{io}/dt_i and dg_{io}/dt_{io} are not directly observable. It is possible to express $g(t)$ and dx/dt in terms of observable quantities only by assuming either some particular detailed cosmological model to be valid (arbitrary choice) or by assuming a particular functional form for $g(t)$ or $x(t)$ as a function of t and finding the numerical coefficients of the function by fitting it to the observed universe. The latter approach is employed here, following Tolman's (1930) procedure of expanding $g(t)$ as a power series about the present time $t_{10} = 0$:

$$g(t) = 2\sum_{n=1}^{\infty} k_n t^n . \tag{13}$$

Since $t_{10} - t_{20}$, the time difference between observations of two variable stars, is, at most, of the order of 100 years (speaking in 1955!), whereas $t_{io} - t_i$ is of the order of 10^6–10^9 years, it is sufficiently accurate for the treatment here to take $t_{20} = t_{10} = 0$. The coefficients k_n are found empirically as follows. Suppose that the star (or galaxy) described by equation (8) has a constant magnitude. Then equations (4) and (8) give the co-ordinate distance of the star in terms of its red shift, etc.,

$$r_i = 10^{1+0.2(m_{io}-M_i)} \times (1 + x_{io})^{-1} \exp(-\tfrac{1}{2} g_{io}) , \tag{14}$$

where, by equation (13), $g_{io} = 0$ for $i = 1$ or 2. In order to compare with the red-shift magnitude observations, r_i on the left side must be expressed in terms of the red shift x_{io}. A Maclaurin series expansion is used, and the required derivatives are found by beginning with

$$\frac{dr_i}{dx_{io}} = \frac{dr_i/dt_i}{dx_{io}/dt_i} . \tag{15}$$

Note that dr_i/dt_i here does not refer to the change of r_i with time for a particular star (it will be recalled that r_i = Constant for a particular star) but rather refers to the $r = r(t)$ relation for a ray of light traveling radially inward toward O; from the line element (1) we obtain

$$\frac{dr_i}{dt_i} = -c\left(1 - \frac{r_i^2}{R^2}\right)^{1/2} \exp(-\tfrac{1}{2} g_i) . \tag{16}$$

Equations (2) and (16) substituted in equation (15) and the resulting expression evaluated at $x_{io} = 0$, $r_i = 0$, and $t_{io} = 0$ give the first derivative in the Maclaurin series. The higher derivatives can similarly be found from equations (2), (15), and (16). The results are

$$\left[\frac{dr_i}{dx_{io}}\right]_{x_{io}=0} = \frac{c}{k_1}, \qquad \left[\frac{d^2 r_i}{dx_{io}^2}\right]_{x_{io}=0} = \frac{2ck_2}{k_1^3},$$

$$\left[\frac{d^3 r_i}{dx_{io}^3}\right]_{x_{io}=0} = \frac{c}{k_1^5}\left(\frac{-c^2k_1^2}{R^2} - 2k_1^2k_2 - 6k_1k_3 + 12k_2^2\right), \ldots ,$$

giving

$$r_i = \sum_{n=1}^{\infty} a_n x_{io}^n = \frac{c}{k_1}\left\{x_{io} + \frac{k_2}{k_1^2}x_{io}^2 + \frac{1}{k_1^4}\left(\frac{-c^2k_1^2}{6R^2} - \tfrac{1}{3}k_1^2k_2 - k_1k_3 + 2k_2^2\right)x_{io}^3 + \ldots\right\} , \tag{17}$$

which defines the coefficients a_n introduced for later convenience. Combining equations (14) and (17), we have

$$\sum_{n=1}^{\infty} a_n x_{io}^n = (1+x_{io})^{-1} \times 10^{1+0.2(m_i-M_i)}. \tag{18}$$

To determine the k's, equation (18) is then fitted to the observed results for red shift versus magnitude for objects of known absolute magnitude; k_1 and k_2 follow immediately, but k_3 cannot be separated from the curvature $1/R^2$ without additional information. In practice, even the value of k_1 is presently undergoing revision. Eventually, when the magnitude scales have been revised, it should be possible to get a good value for k_1, some idea of the order of k_2, and limits on the size of the higher coefficients (Tolman 1934*b*).

To return to equation (12), the dx_{io}/dt_i terms are rewritten, using equation (2), in terms of the g's, so that

$$-\frac{2}{1+x_{10}}\frac{dx_{10}}{dt_1}+\frac{2}{1+x_{20}}\frac{dx_{20}}{dt_2}=\frac{dg_1}{dt_1}-\frac{dg_2}{dt_2}+(1+x_{20})\frac{dg_{20}}{dt_{20}}-(1+x_{10})\frac{dg_{10}}{dt_{10}}. \tag{19}$$

The dg_i/dt_i terms are expanded as a Maclaurin series in x, the first derivative being

$$\frac{d}{dx_{io}}\left(\frac{dg_i}{dt_i}\right)=\frac{d^2g_i}{dt_i^2}\frac{dt_i}{dx_{io}}.$$

For this and the higher derivatives the values

$$\left[\frac{dt_i}{dx_{io}}\right]_{x_{io}=0}=-\frac{1}{k_1}, \qquad \left[\frac{d^2t_i}{dx_{io}^2}\right]_{x_{io}=0}=\frac{k_1^2-2k_2}{k_1^3}, \tag{20}$$

$$\left[\frac{d^3t_i}{dx_{io}^3}\right]_{x_{io}=0}=\frac{1}{k_1^5}(-2k_1^4+6k_1^2k_2+6k_1k_3-12k_2^2), \ldots,$$

are required. These give

$$\left[\frac{d}{dx_{io}}\left(\frac{dg_i}{dt_i}\right)\right]_{x_{io}=0}=-\frac{4k_2}{k_1}, \left[\frac{d^2}{dx_{io}^2}\left(\frac{dg_i}{dt_i}\right)\right]_{x_{io}=0}=\frac{1}{k_1^3}(4k_1^2k_2+12k_1k_3-8k_2^2),$$

$$\left[\frac{d^3}{dx_{io}^3}\left(\frac{dg_i}{dt_i}\right)\right]_{x_{io}=0}=\frac{1}{k_1^5}(-8k_1^4k_2-36k_1^3k_3+24k_1^2k_2^2 \tag{21}$$

$$-48k_1^2k_4+96k_1k_2k_3-48k_2^3), \ldots$$

$$\frac{1}{2}\frac{dg_i}{dt_i}=\sum_{n=0}^{\infty} b_n x_{io}^n$$

$$=k_1-\frac{2k_2}{k_1}x_{io}+\frac{1}{k_1^3}(k_1^2k_2+3k_1k_3-2k_2^2)x_{io}^2 \tag{22}$$

$$+\frac{1}{k_1^5}(-\tfrac{2}{3}k_1^4k_2-3k_1^3k_3+2k_1^2k_2^2-4k_1^2k_4+8k_1k_2k_3-4k_2^3)x_{io}^3+\ldots,$$

where the b_n's are introduced for convenience. Although not directly needed here, the expansion for the time when a signal is emitted in terms of the red shift of the star concerned will be quoted for its interest, since it follows immediately from equation (20),

$$t_i = -\frac{1}{k_1} x_{io} + \frac{1}{k_1^3}(\tfrac{1}{2}k_1^2 - k_2)\, x_{io}^2 + \frac{1}{k_1^5}(-\tfrac{1}{3}k_1^4 + k_1^2 k_2 + k_1 k_3 - 2k_2^2)\, x_{io}^3 + \ldots . \quad (23)$$

Equations (13), (19), and (22) plus the foregoing choice of $t_{10} = 0$ transform equation (12) into the desired observable form:

$$\frac{dm_{10}}{dt_{10}} = \frac{1 + x_{20}}{1 + x_{10}} \frac{dm_{20}}{dt_{20}} - \frac{5}{E} \frac{1}{1 + x_{10}} \sum_{n=0}^{\infty} b_n (x_{10}^n - x_{20}^n) , \quad (24)$$

where every quantity is directly observable except the coefficients b_n, which are determined empirically via equations (17), (18), and (22). The difference between special and general relativity enters only in the coefficients $b_2, b_3, \ldots$, which depend on the curvature $1/R^2$ (which is zero for a special relativity model).

It should be noted that this result is valid only for those regions where there is a systematic red shift, i.e., in the actual universe regions not too close to our Galaxy. A useful result is obtained by considering the case of nonvariable stars, letting r_1 be large and r_2 be very small, so that $x_{20} = 0$, $dm_{20}/dt_{20} = dm_2/dt_2 = 0$, since the stars are nonvariable. Then when stars 1 and 2 are compared by the observer at O, equation (24) shows that the apparent magnitude change of star 1 is given by the expansion term $-5\Sigma b_n x_{10}^n/E(1 + x_{10})$, which is explicitly due to the expansion of the universe. An upper limit to the size of the expansion term can then be found from existing observations of nonvariable stars in external galaxies and shows that the expansion term is negligible here in comparison with the first term in equation (24). Finally, the usual transformation has to be made from the theoretical magnitudes used to the observed magnitudes, by allowing for the absorption by the atmosphere and the telescope and the spectral sensitivity of the receiver.

In order to apply equation (24) practically, it is necessary to have a class of very bright objects which can be recognized at great distances and which can be stated with a reasonable degree of probability to have identical intrinsic light-curves. Type I supernovae seem to be the only objects which satisfy all these criteria, although Cepheids lack only the requirement of great brightness; both cases are discussed in Section III.

c) THE OBSERVED FREQUENCY OF EVENTS IN AN EXPANDING UNIVERSE

If it be assumed that the frequency of a particular type of event is the same at all times and all places, then the observed frequency F_{10} of such events in a distant region should be less than that observed in a near-by region by the red-shift ratio of equation (2),

$$F_{10} = \left(\frac{1 + x_{20}}{1 + x_{10}}\right) F_{20} \quad (25)$$

if no events are missed. In principle, this would provide another observable relation which could be used to check the velocity interpretation of the red shift. In practice, the test is more complicated, since the only types of events which are available are the flare-ups of novae, supernovae, and irregular fluctuations in the light-curves of these; and, because of the dispersion in magnitude of both novae and supernovae, great care must be taken to insure that the same events are measured for both near and distant regions.

III. OBSERVABLE FORM OF THE RED-SHIFT TESTS

a) THE LIGHT-CURVE OF A SUPERNOVA AS A FUNCTION OF THE RED SHIFT

There are two main types of supernovae, those of type I being 2 or 3 mag. brighter than those of type II. Here only those of type I are of immediate interest, since they have a partially regular behavior. According to Baade[1] (1945), this type of supernova has a light-curve which first descends from the maximum with "minor variations in the widths and heights of the maxima," and at about 100 days after the maximum a steady decline sets in, with a linear gradient which is substantially the same for all type I supernovae so far observed, being

$$\frac{d\,m_{p20}}{d\,t_{20}} = 0.0137 \pm 0.0012 \qquad \text{magnitudes per day},$$

where m_p is the photographic magnitude. It is possible that some small revision of this figure may be necessary because of the current revision of the magnitude scales.

Although there is as yet no satisfactory theory of the flare-up of a supernova, this does not matter here, because only the fact of the linear decline is used, not its mechanism. It is conceivable that, because of chemical or other differences, the decline could be linear, thus identifying a type I supernova, and yet have a different *rate* of decline. In the absence of any evidence that such is the case, it is assumed here that the linear decline of the light-curve *with the foregoing rate* is an intrinsic property of type I supernovae at all times and in all regions of the universe. On this assumption it is seen that type I supernovae satisfy the requirements stated at the end of Section II, *a*, allowing equation (24) to be applied to the gradient of their light-curves.

Now equation (24) is in terms of bolometric magnitudes measured outside the earth's atmosphere. To convert to the observed photographic magnitudes, the correction term $\log p$ of Hubble and Tolman (1935) can be used. Since only magnitude *differences* occur in the gradient formula, if a supernova had the same intrinsic color throughout its light-curve, then the bolometric magnitude could be replaced by the photographic magnitude with an absolutely negligible error. However, the color of a supernova changes as it fades, and the correction term $2.5\, d/dt_{10} \log (p_2/p_1)$, although still small, may have to be included when accurate observations of distant supernovae are made. The photographic correction must, of course, be made accurately when using equation (18) to find the coefficients k_n. The expansion term can be neglected in the supernova case, as stated earlier, for the following reason. When equation (24) is applied to a nonvariable star, the first term on the right side vanishes, leaving only the change in magnitude due to expansion. There is at present no evidence that the magnitudes of all stars or galaxies at a certain distance, either near our Galaxy or at great distances, are systematically decreasing or increasing; as a reasonable figure, assume that the magnitudes of nonvariable objects have not changed by more than one-tenth of a magnitude during ten years of observation. (The true figure is most probably smaller by many orders of magnitude.) This is about 0.2 per cent of the rate at which the supernova declines; so, for the present, the expansion terms on the right side of equation (24) can be omitted when applied to a supernova.

Summing up, if supernova 2 is very near to O, so that $x_2 = 0$, the expected rate of decline of the light-curve of a distant type I supernova, in terms of photographic magnitudes, is given, to a good approximation, by

$$\frac{d\,m_{p10}}{d\,t_{10}} = \frac{1}{1 + x_{10}} \frac{d\,m_{p20}}{d\,t_{20}}. \tag{26}$$

This result is the same as the special relativity approximate result given by Milford (1953). Three points should be made about equation (26): It was derived without any

[1] I am indebted to Dr. Baade for a letter about type I supernovae.

assumptions about the evolution of galaxies or their populations. The major assumption was that all type I supernovae have the same value for the linear gradient. Lastly, it is pleasing to note that the times t_{10} and t_{20} need only be chosen on the observed linear portion of the light-curve in order to satisfy condition (10).

b) THE PERIOD-LUMINOSITY-CURVE FOR CEPHEIDS

Since the discovery of W Virginis Cepheids there are grave doubts about assuming that the period-luminosity relation for Cepheids in another galaxy is the same as that in our Galaxy. It may well be that, owing to differences of chemical composition or for other reasons, the relation may vary from one galaxy to another by more than the difference between classical and W Virginis Cepheids. This makes the setting-up of a theoretical test on the red shift employing Chepheids very difficult, even apart from the practical difficulty that Cepheids cannot be seen in galaxies far enough away to have an appreciable red shift. For its theoretical interest, however, the result is noted here that the slope of the apparent period-magnitude-curve for Cepheids in a distant galaxy will be given by equation (26) in terms of the proper slope.

c) THE FREQUENCY OF NOVAE AND SUPERNOVAE

Zwicky (1951) proposed using the frequency of occurrence of supernovae in distant galaxies as a measure of the evolution of stellar populations. One could in the same way use the galaxy counts or galaxy diameter tests as measures of the evolution of galaxies.

It is unlikely that the change in frequency of supernovae, for example, due to evolution in stellar populations would be exactly the same as the apparent change, equation (25), due to the expansion of the universe. For this reason it seems worth while to set up the equations for this frequency test on the red shift, even though the practical application seems some distance in the future. It should be noted that any evolutionary change in frequency would distort the observed frequency by an unknown amount.

Since there is considerable dispersion of magnitudes for novae and supernovae, only the brighter ones will be seen at large distances, making it necessary to guard against observational selection. The method of observation would be to control a number of clusters of galaxies, each of known red shift, for frequency per galaxy of new stars down to a chosen absolute brightness. The apparent photographic magnitude corresponding to the absolute magnitude M_p is given by equation (18) and the Hubble and Tolman (1935) correction term, K,

$$m_{p10} = M_{p1} - 5 + 5 \log_{10} \{ a_1 x_{10} + (a_1 + a_2) x_{10}^2 + (a_2 + a_3) x_{10}^3 + \ldots \} + K . \quad (27)$$

This method of counting only stars brighter than a definite absolute magnitude should insure that the same types of stars are counted in near-by and distant galaxies, independently of the luminosity function of the new stars. Note that the velocity interpretation of the red shift enters in the magnitude equation (27) just as much as in the frequency equation (25), against which the counts are tested.

This test can be compared with the galaxy counts test. The observations are more difficult because novae can be seen only in near-by galaxies where the red shift is very small, and supernovae occur only about once per galaxy in 300 years, while galaxies are there all the time! Also, it requires the same assumption that the evolution of galaxies and their populations is either small or known. On the other hand, this test would not be significantly modified by a nonhomogeneous distribution of the galaxies, whereas in such a universe the galaxy counts test could be set up only by employing extra assumptions about the nature of the inhomogeneity.

Another irregular process which could, in principle, be used in the same way as the frequency test would be any irregular fluctuation in brightness (or color or spectrum) of bright stars, for which fluctuations the time dilatation should again be given by equation

(2), assuming that the intrinsic variability averaged over a large number of stars is the same at all times and places. As possible objects, the brightest variables in galaxies, investigated by Hubble and Sandage (1953), suggest themselves. At the moment this fluctuation test is not a practical possibility.

IV. DISCUSSION

An interesting point which emerges from the discussion in Sections II and III is that, for present practical applications, there is no appreciable practical difference between the special and general relativity expressions for these particular tests on the red shift. This is gratifying because it is generally considered that the special theory of relativity has been better verified than the general theory.

It is worth emphasizing again that, although a homogeneous isotropic cosmological model was used, the tests could be derived for a more general model; in fact, if the application of galaxy counts, etc., and these tests indicate that the model disagrees with the observed universe, it would be necessary to try fitting other models to the observations.

Since any evolutionary changes in galaxies also undermine the validity of the red-shift magnitude relation for larger distances, where galaxies are used as standard magnitudes, there are practical difficulties in determining $k_1, k_2, \ldots$; again it is an advantage of the supernova light-curve test that it does not require these coefficients for its practical application. It is possible that the rate of change of the color could be used instead of the total photographic light.

To carry out the light-curve test, only the *difference* of magnitudes need be measured and the time for this change; thus it is not necessary to have an accurate zero point for the scale of magnitudes used. The procedure would be, first, to measure the gradients of a large number of near-by type I supernovae to find the dispersion, if any, in their gradients; second, to discover distant supernovae by means of, for example, the Palomar 48-inch Schmidt; and, third, to follow these supernovae down as far as possible with the 200-inch. Unfortunately, the linear part of the light-curve starts about 3 mag. below the maximum, so that, even if 2 mag. of the linear portion are sufficient to measure the gradient, the supernova must be bright enough for it to be seen at 5 mag. below maximum.

The average absolute magnitude of type I supernovae at maximum was estimated by Baade (1938) to be about -14; but, with the revision of the distance scale, this will probably be changed by some 2 mag. or more. In the present discussion of the faintest supernovae for which the light-curve can be measured, the old magnitude and distance scales will be retained—the revision will not change the following estimates by very much. In order to record 2 mag. of the linear part of the light-curve with the 200-inch, the distance modulus of an average supernova of type I would have to be smaller than 32 mag., corresponding to a red shift of approximately 0.05. Since the brightest supernovae are 2 or 3 mag. brighter than the average, there will be less frequent cases where the light-curve could be measured at a modulus of 34 mag., red shift 0.12. Some few well-observed instances of the latter may be sufficient to test the velocity interpretation of the red shift.

The frequency of discovery of supernovae has been discussed by Zwicky (1942). Type II supernovae occur more frequently than type I, but, being much fainter, their contribution to the observed frequency is greatly diminished by observational selection. Evolutionary changes, as well as those in the total frequency of supernovae, may cause the relative frequency of bright and faint supernovae or that of types I and II to vary, and hence may again invalidate the frequency test.

In summary, the paper has suggested three tests on the red shift, involving the gradient of the light-curve of a supernova, the frequency of occurrence of novae and supernovae, and the period-luminosity relation for Cepheids. The most promising of these is the supernova light-curve one. It requires fewer assumptions than any of the other tests so far proposed and also appears to be a practical possibility. When equation (26) for the

gradient of the light-curve is applied, it should decide whether the red shift is due to velocity or to some other cause.

Note added in proof.—Dr. O. C. Wilson has kindly drawn my attention to his note in *Ap. J.*, **90**, 634, 1939. This prior note of Dr. Wilson also suggested using supernova light-curves as a test on the red shift and stated the time dilatation effect on the light-curve. Unfortunately, I was not aware of this earlier paper; but, since the present paper develops the relativistic and luminosity effects as well as the time effects, there is not much duplication.

I would like to thank Dr. G. C. McVittie for extensive criticism and discussion which helped me to clarify various points in the paper and also for drawing my attention to McCrea's paper (1935).

REFERENCES

Baade, W. 1938, *Ap. J.*, **88**, 285.
———. 1945, *ibid.*, **102**, 309.
Bondi, H. 1952, *Cosmology* (Cambridge: At the University Press).
Hubble, E., and Sandage, A. 1953, *Ap. J.*, **118**, 353.
Hubble, E., and Tolman, R. C. 1935, *Ap. J.*, **82**, 302.
Humason, M. L. 1954, *A.J.*, **59**, 185.
McCrea, W. H. 1935, *Zs. f. Ap.*, **9**, 290.
———. 1953, *Rept. Prog. Phys.*, **16**, 346.
Milford, S. N. 1953, *A.J.*, **58**, 43.
Omer, G. C. 1949, *Ap. J.*, **109**, 164.
Payne-Gaposchkin, Cecilia. 1951, *Astrophysics*, ed. J. A. Hynek (New York: McGraw-Hill Book Co., Inc.), pp. 500–503.
Tolman, R. C. 1930, *Proc. Nat. Acad. Sci.*, **16**, 409.
———. 1934*a*, *Relativity, Thermodynamics, and Cosmology* (Oxford: Oxford Univeristy Press), §§ 178-179, 182.
———. 1934*b*, *ibid.*, §§ 182–185.
Whitford, A. E. 1954, *Ap. J.*, **120**, 599.
Zwicky, F. 1942, *Ap. J.*, **96**, 28.
———. 1951, *Pub. A.S.P.*, **63**, 17.

ON STELLAR STATISTICS

ALLADI RAMAKRISHNAN
Department of Physics, University of Madras, India
Received February 23, 1955

ABSTRACT

The problem of the distribution of stellar intensities when the interstellar matter consists of (1) discrete clouds and (2) a wildly fluctuating density field is formulated in a general manner from a stochastic point of view, and some results are obtained in particular cases.

I. INTRODUCTION

Recently, Chandrasekhar and Münch (1950*a*, *b*; 1951) formulated and solved the following stochastic problem of fluctuations in brightness of the Milky Way. It is given (1) that there is a deterministic contribution of amount $\beta d\tau$ from the element of length $d\tau$ at $t = \tau$ (this is due to stars occurring with a uniform distribution along t) to the intensity of radiation; (2) that clouds occur with a Poisson distribution $e^{-\lambda t}(\lambda t)^n/n!$ in any element of length t, where λ is the probability per unit t that a cloud will occur; and (3) that a cloud has a transparency factor q with a probability density $\psi(q)$. What is the probability $g(u; \epsilon)du$ that an observer at $t = 0$ will measure an intensity between u and $u + du$ when the astrophysical system extends from $t = 0$ to $t = \epsilon$?

Later, Chandrasekhar and Münch (1952) replaced the picture of discrete clouds by that of a wildly fluctuating density field. The mathematical implications of such a field were discussed by the author (Ramakrishnan 1954) in a previous contribution to this *Journal*.

We shall now formulate a more complicated stochastic process than that stated before. It is hoped that this formulation will be of some interest in the light of Chandrasekhar's comments on Ambarzumian's paper (Ambarzumian 1953) regarding this problem.

II. FORMULATION OF THE PROBLEM

Chandrasekhar and Münch (1950, 1951, 1952) assumed that the contribution to the intensity u is deterministic. This contribution comes from stars which are "uniformly" distributed in space, i.e., *they did not take into consideration the "discrete" nature of these sources.*

A further random element can be introduced by assuming that in an element $d\tau$ a star occurs with a probability $\mu d\tau$ and a given star has intensity between η and $\eta + d\eta$, with a probability $\phi(\eta)d\eta$. Thus the mean contribution to the intensity u by the element $d\tau$ is

$$\mu E\{\eta\}\, d\tau\ , \tag{1}$$

where

$$E\{\eta\} = \int_\eta \eta\phi\ (\eta)\ d\eta\ . \tag{2}$$

Here $\mu E\{\eta\}d\tau$ corresponds to $\beta d\tau$ in the previous problem.

We can now ask two questions: (1) What is the distribution of u, the total intensity, i.e., the sum of the intensities of the stars? (2) What is the distribution of the stars in intensity?

[1] In this paper $\int_x$ denotes integration over the entire domain of x, and $E\{y\}$ denotes the expectation value of the stochastic variate y.

The second question raises the well-known problem of the statistical distribution of "particles" in a continuum. A simpler form of this question is: What is the probability $\pi(n, \eta; \epsilon)$ of observing n stars, each with intensity greater than η? Simpler still, what are the moments of n? If we want to deal with π directly, we may have to use the "method of regeneration points," now familiar in stochastic theory, but we shall show that this is not possible in this astrophysical problem. To obtain the moments of n, we can use the method of product densities.

As stated, we are interested in two random variables: (1) the total intensity u and (2) the number of stars n above a certain intensity η, i.e., $n(\eta)$. If $f_1(\eta; \epsilon)$ and $f_2(\eta_1, \eta_2; \epsilon)$ are the product densities of degrees 1 and 2, then, according to the theory of product densities,[2] $f_1(\eta; \epsilon)d\eta$ represents the probability that a star has intensity (as measured by the observer) between η and $\eta + d\eta$, and $f_2(\eta_1, \eta_2; \epsilon)d\eta_1 d\eta_2$ represents the joint probability that a star has an intensity between η_1 and $\eta_1 + d\eta_1$ and another has an intensity between η_2 and $\eta_2 + d\eta_2$. Also we have

$$\sum_n n\pi(n, \eta; \epsilon) = \int_\eta^\infty f_1(\eta'; \epsilon)\, d\eta', \tag{3}$$

and

$$\sum_n n^2\pi(n, \eta; \epsilon) = \int_\eta^\infty f_1(\eta'; \epsilon)\, d\eta' + \int_\eta^\infty \int_\eta^\infty f_2(\eta_1', \eta_2'; \epsilon)\, d\eta_1' d\eta_2'. \tag{4}$$

We can define a random variable $u(\eta)$, which is the sum of the intensities of stars with intensity greater than η:

$$E\{u(\eta)\} = \int_\eta^\infty \eta' f_1(\eta'; \epsilon)\, d\eta', \tag{5}$$

$$E\{u^2(\eta)\} = \int_\eta^\infty \eta'^2 f_1(\eta'; \epsilon)\, d\eta' + \int_\eta^\infty \int_\eta^\infty \eta_1'\eta_2' f_2(\eta_1', \eta_2'; \epsilon)\, d\eta_1' d\eta_2'. \tag{6}$$

Let the probability frequency function of the total intensity, i.e., $u(0)$ or simply u, be $g(u; \epsilon)$. Then

$$E\{u\} = \int_0^\infty u\, g(u; \epsilon)\, du = \int_0^\infty \eta f_1(\eta; \epsilon)\, d\eta. \tag{7}$$

Note that $g(u; \epsilon)$ and $f_1(\eta; \epsilon)$ are functions with entirely different meanings. The difference will be apparent if we consider the second moment of u:

$$E\{u^2\} = \int_0^\infty u^2 g(u; \epsilon)\, du = \int_0^\infty \eta^2 f_1(\eta; \epsilon)\, d\eta + \int_0^\infty \int_0^\infty \eta_1\eta_2 f_2(\eta_1, \eta_2; \epsilon)\, d\eta_1 d\eta_2. \tag{8}$$

III. STELLAR INTENSITIES ASSUMING A DISCRETE CLOUD PICTURE

Let us write the diffusion equations for f_1 and f_2, assuming that the interstellar matter consists of discrete clouds. Before doing so, we must examine the mathematical implications of the absorption function. In their papers Chandrasekhar and Münch were assuming that the probability per unit t that a given cloud will reduce the intensity u to a value lying between uq and $u(q + dq)$ is $\psi(q)dq$. In this problem we have analyzed the total intensity as having been made up of the component intensities of various stars. Let us assume that a star of given intensity, say η, drops to a value between ηq and $\eta(q + dq)$ with probability $\omega(q)dq$ per unit thickness. What is the relation between $\psi(q)$

[2] For the formulation of the theory of product densities and proof of eqs. (4) and (5) see Ramakrishnan (1950, 1953).

and $\omega(q)$? We can think of two possibilities: (1) If $\psi \equiv \omega$, it means that the absorption processes of the individual stars are correlated in a "gearbox" manner, i.e., if one of the stars is reduced in intensity by a factor q (this occurs with a probability $\omega[q]dq$), then all the others *are* reduced in intensity by the same factor. *Thus this absorption process differs completely from that discussed for, say, electrons in cascade processes.* (2) If the absorption processes are independent, ψ and ω are related in a very complicated manner. Obviously, in an astrophysical problem, we must make the assumption of "gearbox" correlation, since the transitions are due to the interceptions and there is no reason why the cloud should "distinguish" between intensities from different stars.

If we assume "gearbox" correlation of absorption, *it is quite clear that the regeneration-point method cannot be applied, since we do not have independent primaries of stochastic processes at the point of regeneration.* Then we employ the product-density technique:

$$\frac{\partial f_1(\eta;\epsilon)}{\partial \epsilon} = -\lambda f_1(\eta;\epsilon)\int_0^1 \psi(q)\,dq + \lambda\int_q f_1\left(\frac{\eta}{q};\epsilon\right)\frac{\psi(q)\,dq}{q} + \mu\phi(\eta) \tag{9}$$

and

$$\frac{\partial f_2(\eta_1,\eta_2;\epsilon)}{\partial \epsilon} = -\lambda f_2(\eta_1,\eta_2;\epsilon)\int_0^1 \psi(q)\,dq + \lambda\int_q f_2\left(\frac{\eta_1}{q},\frac{\eta_2}{q};\epsilon\right)\frac{\psi(q)\,dq}{q^2} + \mu\{f_1(\eta_1;\epsilon)\phi(\eta_2) + f_1(\eta_2;\epsilon)\phi(\eta_1)\}. \tag{10}$$

This is a new type of equation. Contrast it with the well-known stochastic process of cosmic-ray cascades,[3] where the particles with energies η_1 and η_2 behave independently. Apply the Mellin transformations,

$$p_1(s;\epsilon) = \int_\eta f_1(\eta;\epsilon)\,\eta^{s-1}d\eta\,, \quad p_2(s,r;\epsilon) = \int_{\eta_1}\int_{\eta_2} f_2(\eta_1,\eta_2;\epsilon)\,\eta_1^{s-1}\eta_2^{r-1}d\eta_1 d\eta_2\,, \tag{11}$$

and

$$q_s = \int_0^1 \psi(q)\,q^{s-1}dq\,, \qquad \eta_s = \int_0^\infty \phi(\eta)\,\eta^{s-1}d\eta\,.$$

Then

$$\frac{\partial p_1(s;\epsilon)}{\partial \epsilon} = -\lambda(1-q_s)\,p_1(s;\epsilon) + \mu\eta_s\,, \tag{12}$$

$$\frac{\partial p_2(s,r;\epsilon)}{\partial \epsilon} = -\lambda(1-q_{s+r-1})\,p_2(s,r;\epsilon) + \mu\{p_1(s;\epsilon)\,\eta_r + p_1(r;\epsilon)\,\eta_s\}. \tag{13}$$

Hence we have

$$p_1(s;\epsilon) = \frac{1-\exp-[\lambda(1-q_s)\epsilon]}{\lambda(1-q_s)}\,\mu\eta_s\,, \tag{14}$$

$$p_2(s,r;\epsilon) = \exp-[\lambda(1-q_{s+r-1})\epsilon]\int_0^\epsilon \exp[\lambda(1-q_{s+r-1})\tau]\,\{p_1(s;\tau)\,\eta_r + p_1(r;\tau)\,\eta_s\}\mu d\tau\,. \tag{15}$$

Note that $p_2(1,1;\epsilon) = [p_1(1;\epsilon)]^2$, giving a Poisson distribution for the total number of stars.

Inverting $p_1(s;\epsilon)$ and $p_2(s,r;\epsilon)$, we get $f_1(\eta;\epsilon)$ and $f_2(\eta_1,\eta_2;\epsilon)$, whence we obtain the

[3] For a comprehensive summary of this problem see, for example, Ramakrishnan and Mathews (1954).

first and second moments of $\pi(n, \eta; \epsilon)$. If we are interested in the first and second moments of the total intensity, they are given by (see eqs. [7] and [8])

$$E\{u\} = p_1(2; \epsilon), \tag{16}$$

$$E\{u^2\} = p_1(3; \epsilon) + p_2(2, 2; \epsilon). \tag{17}$$

We can also write the diffusion equation for $g(u; \epsilon)$ thus:

$$\frac{\partial g(u; \epsilon)}{\partial \epsilon} = -(\lambda+\mu)\, g(u; \epsilon) + \lambda \int_q g\left(\frac{u}{q}; \epsilon\right) \psi(q)\, \frac{dq}{q} + \mu \int_\eta g(u-\eta; \epsilon)\, \phi(\eta)\, d\eta. \tag{18}[4]$$

The moments of u can be obtained by iteration from equation (18) by multiplying both sides by u^n and integrating over all values of u from 0 to ∞ and writing $u^n = (u - \eta + \eta)^n$ in the expression containing $u - \eta$ on the right-hand side. We give here the first three moments:

$$E\{u\} = \frac{\mu E\{\eta\}}{\lambda(1-q_1)}\{1 - \exp-[\lambda(1-q_1)\epsilon]\}, \tag{19}$$

$$E\{u^2\} = \frac{\mu E\{\eta^2\}}{\lambda(1-q_2)}\{1 - \exp-[\lambda(1-q_2)\epsilon]\} + \frac{2\mu^2}{\lambda^2}[E\{\eta\}]^2 \left\{\frac{1}{(1-q_1)(1-q_2)} + \frac{\exp-[\lambda(1-q_1)\epsilon]}{(1-q_1)(q_2-q_1)} + \frac{\exp-[\lambda(1-q_2)\epsilon]}{(1-q_2)(q_1-q_2)}\right\}, \tag{20}$$

$$E\{u^3\} = \frac{\mu E\{\eta^3\}}{\lambda(1-q_3)}\{1 - \exp-[\lambda(1-q_3)\epsilon]\} + \frac{3\mu^2 E\{\eta^2\}E\{\eta\}}{\lambda^2(1-q_2)} \times \left\{\frac{1-\exp-[\lambda(1-q_3)\epsilon]}{1-q_3} + \frac{\exp-[\lambda(1-q_3)\epsilon] - \exp-[\lambda(1-q_2)\epsilon]}{q_2-q_3}\right\} + \frac{6\mu^2[E\{\eta\}]^3}{\lambda^3} \times \left\{\frac{1-\exp-[\lambda(1-q_3)\epsilon]}{(1-q_1)(1-q_2)(1-q_3)} + \frac{\exp-[\lambda(1-q_2)\epsilon] - \exp-[\lambda(1-q_3)\epsilon]}{(1-q_2)(q_1-q_2)(q_2-q_3)} + \frac{\exp-[\lambda(1-q_1)\epsilon] - \exp-[\lambda(1-q_3)\epsilon]}{(1-q_1)(q_2-q_1)(q_1-q_3)}\right\}. \tag{21}$$

These expressions agree with those obtained from equation (17). In the case when $\psi(q') = \delta(q' - q)$, where δ is the Dirac delta function, the formal Laplace transform solution of $g(u; \epsilon)$ has been obtained by S. K. Srinivasan (see appendix); but, for the calculation of the first few moments, it is easier to adopt the method outlined here.

We shall now consider a special case of the general problem discussed. We shall assume

$$\psi(q') = \delta(q' - q), \qquad \phi(\eta) = \delta(\eta - 1). \tag{22}$$

In such a case we can obtain the actual distribution $\pi(n, \eta; \epsilon)$. We first note that η can take only the discrete values 1, q, q^2, . . . , q^m, ... Thus, instead of speaking of

[4] Compare this with eq. (18) of Chandrasekhar and Münch (1950*a*).

$\pi(n, \eta; \epsilon)$, the probability that there are n stars with the intensity *greater* than η, we shall define $\pi(n, m; \epsilon)$ as the probability that there are n stars with intensity greater than q^m, i.e., equal to or greater than q^{m-1}. Then $\pi(n, m; \epsilon)$ can be computed by simple probability arguments.

The system extends from $t = 0$ (the origin where the observer is) to $t = \epsilon$. The mth cloud (counted from the origin) occurs between τ and $\tau + d\tau$, with probability,

$$e^{-\lambda\tau} \frac{(\lambda\tau)^{m-1}}{(m-1)!} \lambda d\tau, \tag{23}$$

where λ is the probability per unit distance that a cloud will occur. Any star occurring between 0 and τ must have an intensity greater than q^m. Any star occurring beyond τ must have an intensity equal to or less than q^m.

Thus the joint probability that the mth cloud will occur between 0 and ϵ and that there are n stars above the intensity q^m is

$$\int_0^\epsilon e^{-(\lambda+\mu)\tau} \frac{(\mu\tau)^n}{n!} \frac{(\lambda\tau)^{m-1}}{(m-1)!} \lambda d\tau. \tag{24}$$

The mth cloud occurs beyond ϵ with probability

$$1 - \int_0^\epsilon e^{-\lambda\tau} \frac{(\lambda\tau)^{m-1}}{(m-1)!} \lambda d\tau. \tag{25}$$

Thus

$$\pi(n, m; \epsilon) = \int_0^\epsilon e^{-(\lambda+\mu)\tau} \frac{(\mu\tau)^n}{n!} \frac{(\lambda\tau)^{m-1}}{(m-1)!} \lambda d\tau + \left[1 - \int_0^\epsilon e^{-\lambda\tau} \frac{(\lambda\tau)^{m-1}}{(m-1)!} \lambda d\tau\right] e^{-\mu\epsilon} \frac{(\mu\epsilon)^n}{n!} \tag{26}$$

$$= \frac{\lambda^m \mu^n}{(\lambda+\mu)^{m+n}} \frac{\Gamma[m+n, (\lambda+\mu)\epsilon]}{n!\,(m-1)!} + \left[1 - \frac{\lambda^{m-1}}{(m-1)!} \Gamma(m, \lambda\epsilon)\right] \frac{e^{-\mu\epsilon}(\mu\epsilon)^n}{n!},$$

where

$$\Gamma(n, x) = \int_0^x e^{-\tau} \tau^{n-1} d\tau.$$

Without loss of generality, either λ or μ (not both) can be put equal to 1 by suitably choosing a unit of t.

IV. STELLAR INTENSITIES, ASSUMING A FLUCTUATING DENSITY FIELD

We shall now assume that the interstellar matter is continuous but wildly fluctuating in density. We recall the following results obtained by the author, regarding the stochastic model of the fluctuating density field.

1. Since ρ, the density of the interstellar matter, is a stochastic variable, $M(t)$, the optical thickness of matter of extension t is also a stochastic variable. Hence

$$M(t) = k \int_0^t \rho(\tau')\, d\tau',$$

where k is the absorption coefficient. Without loss of generality, k can be chosen to be $1/E\{\rho\}$, and hence

$$M(t) = \int_0^t \rho'(\tau')\, d\tau'$$

if we define $\rho' = \rho/E\{\rho\}$. It was proved by the author that, for a certain model of the density field,

$$E\{e^{-nM(t)}\} = e^{-nE\{M(t)\}}\{1 + n^2\alpha^2\tau_0 t\} + O(\tau_0^2), \tag{27}$$

where

$$E\{M(t)\} = t, \qquad \alpha^2 = \frac{E\{\rho^2\} - [E\{\rho\}]^2}{[E\{\rho\}]^2},$$

and τ_0 is a small constant, such that second and higher powers of τ_0 can be neglected.

2. It was also proved that $M(t_1)$ and $M(t_2)$ are uncorrelated if the intervals t_1 and t_2 have no common point and $t_1, t_2 \gg \tau_0$. An immediate consequence of this result is that if the interval of length t_2 lies entirely within the interval of length t_1, then

$$E\{M(t_1)\,M(t_2)\} = E\{M^2(t_2)\} + E\{M(t_2)\}E\{M(t_1 - t_2)\}, \tag{28}$$

or, more generally, if $\pi(M_1, M_2; t_1, t_2)dM_1\,dM_2$ is the joint probability that $M(t_1)$ lies between M_1 and $M_1 + dM_1$ and $M(t_2)$ lies between M_2 and $M_2 + dM_2$, then

$$\pi(M_1, M_2; t_1, t_2) = \pi(M_2; t_2)\,\pi(M_1 - M_2; t_1 - t_2), \tag{29}$$

if the interval of length t_2 lies inside the interval of length t_1.

We shall use these two results to derive the product densities of stars. We define, as before, $f_1(\eta; \epsilon)$ as the product density of degree 1 of stars, i.e., $f_1(\eta; \epsilon)d\eta$ as the probability that a star has an intensity, as measured by the observer, between η and $\eta + d\eta$, ϵ being the extent of the astrophysical system. If the observed intensity of a star is η and if the star has occurred at a distance τ from the observer, then its intensity at the point of occurrence must have been $\eta e^{M(\tau)}$. Thus

$$f_1(\eta; \epsilon) = \int_0^\epsilon \mu\phi\,[\eta\, e^{M(\tau)}]\,\pi(M, \tau)\, e^{M(\tau)}\,d\tau. \tag{30}$$

Using similar arguments, if $f_n(\eta_1, \eta_2, \ldots, \eta_n; \epsilon)$ is the product density of degree n, we obtain

$$\begin{aligned} f_n(\eta_1, \eta_2, \ldots, \eta_n; \epsilon) = \int_0^\epsilon \int_0^\epsilon \cdots \int_0^\epsilon \int_{M_1} \int_{M_2} \cdots \int_{M_n} \mu^n \phi(e^{M_1}\eta_1)\,\phi(e^{M_2}\eta_2) \cdots \\ \phi(e^{M_n}\eta_n)\,\pi(M_1, M_2, \ldots, M_n; \tau_1, \tau_2, \ldots, \tau_n)\, e^{M_1} e^{M_2} \cdots \\ e^{M_n} d\tau_1 d\tau_2 \cdots d\tau_n dM_1 dM_2 \cdots dM_n. \end{aligned} \tag{31}$$

It is not possible to write an expression for π in the integrand unless we know the relative order of $\tau_1, \tau_2, \ldots, \tau_n$. If we assume, for example, that $\tau_1 < \tau_2 < \ldots < \tau_n$, we can write

$$\begin{aligned} \pi(M_1, M_2, \ldots, M_n; \tau_1, \tau_2, \ldots, \tau_n) = \pi(M_1; \tau_1)\,\pi(M_2 - M_1; \tau_2 - \tau_1) \\ \cdots \pi(M_n - M_{n-1}; \tau_n - \tau_{n-1}). \end{aligned} \tag{32}$$

Since the integrand is to be integrated with respect to each of the variables $\tau_1, \tau_2, \ldots, \tau_n$ over the whole domain 0 to ϵ, the relative order of these variables changes, and this change has to be considered before writing an expression for π according to equation (32).

In view of this difficulty, it is not possible to obtain even a formal general solution of equation (31), though, for any given n, the equation can be solved by using elementary combinatorial analysis in the determination of the relative order. We give here the solution for product densities of degrees 1 and 2.

Defining $p_1(s;\epsilon)$ and $p_2(s, r;\epsilon)$ as the Mellin transforms of f_1 and f_2, as in equation (11), we obtain, after a simple calculation,

$$p_1(s;\epsilon) = \mu\eta_s \frac{1-\exp-[(s-s^2a^2\tau_0)\epsilon]}{s-s^2a^2\tau_0}, \tag{33}$$

$$p_2(s, r;\epsilon) = \frac{\mu^2\eta_s\eta_r}{\{(r+s)-(r+s)^2a^2\tau_0\}}\left\{\frac{1-\exp-[(r-r^2a^2\tau_0)\epsilon]}{r-r^2a^2\tau_0} + \frac{1-\exp-[(s-s^2a^2\tau_0)\epsilon]}{s-s^2a^2\tau_0}\right\}. \tag{34}$$

The moments of the total intensity are given by

$$E\{u\} = p_1(2\epsilon); = \mu E\{\eta\}\frac{1-\exp-[(1-a^2\tau_0)\epsilon]}{1-a^2\tau_0} = \mu E\{\eta\}[1e^{-\epsilon}+a^2\tau_0(1-e^{-\epsilon}-\epsilon e^{-\epsilon})]+O(\tau_0^2), \tag{35}$$

$$E\{u^2\} = p_1(3;\epsilon)+p_2(2, 2;\epsilon) = \mu E\{\eta^2\}\frac{1-\exp-[2(1-2a^2\tau_0)\epsilon]}{2(1-2a^2\tau_0)}+\mu^2[E\{\eta\}]^2\frac{1-\exp-[(1-a^2\tau_0)\epsilon]}{(1-a^2\tau_0)(1-2a^2\tau_0)} \tag{36}$$

$$= \frac{\mu E\{\eta^2\}}{2}[1-e^{-2\epsilon}+2a^2\tau_0(1-e^{-2\epsilon}-2\epsilon e^{-2\epsilon})] + \mu^2[E\{\eta\}]^2[1-e^{-\epsilon}+a^2\tau_0(3-3e^{-\epsilon}-\epsilon e^{-\epsilon})]+O(\tau_0^2).$$

To compare this with the discrete case, in equations (19) and (20), we write $q = e^{-\tau*}$, choose $\tau_* \ll 1$, and set $\mu = 1/\tau_*$. Then the solutions for $E\{u\}$ and $E\{u^2\}$ in the discrete and continuous cases are identical if we recognize that τ_* corresponds to $2a^2\tau_0$.

My thanks are due to Mr. P. M. Mathews for his helpful suggestions in the preparation of this paper and to Mr. S. K. Srinivasan for permitting me to include his solution of $g(u;\epsilon)$ in the form of an appendix.

APPENDIX

S. K. Srinivasan has obtained the formal solution of $g(u;\epsilon)$ in the discrete case when $\psi(q') = \delta(q'-q)$ by first defining $g_n(u;\epsilon)du$ as the joint probability that n clouds have occurred in the range $t=0$ to $t=\epsilon$ and the intensity measured lies between u and $u+du$; g_n satisfies the equation

$$\frac{\partial g_n(u;\epsilon)}{\partial\epsilon} = -(\lambda+\mu)g_n(u;\epsilon)+\mu\int_\eta g_n(u-\eta;\epsilon)\phi(\eta)\,d\eta+\frac{\lambda}{q}g_{n-1}\left(\frac{u}{q};\epsilon\right). \tag{A.1}$$

Defining

$$\rho_n(s;\epsilon) = \int_0^\infty g_n(u;\epsilon)\,e^{-su}du, \tag{A.2}$$

he obtained

$$\frac{\partial\rho_n(s;\epsilon)}{\partial\epsilon} = -(\lambda+\mu)\rho_n(s;\epsilon)+\mu\rho_n(s;\epsilon)\sigma(s)+\lambda\rho_{n-1}(sq;\epsilon), \tag{A.3}$$

where

$$\sigma(s) = \int_0^\infty \phi(\eta)\, e^{-s\eta} d\eta\,. \tag{A.4}$$

By writing equation (A.3) in the iterative form,

$$\rho_n(s;\epsilon) = \int_0^\epsilon \lambda \exp - \{ [\lambda + \mu - \mu\sigma(s)](\epsilon - \tau) \} \rho_{n-1}(sq;\tau)\, d\tau \tag{A.5}$$

with

$$\rho_0(s;\epsilon) = \exp - \{ [\lambda + \mu - \mu\sigma(s)]\epsilon \}, \tag{A.6}$$

he obtained the solution as follows:

$$\rho_n(s;\epsilon) = \frac{\lambda^n}{\mu^n} \sum_{k=0}^{n} \frac{\exp - \{ [\lambda + \mu - \mu\sigma(sq^k)]\epsilon \}}{\prod_{\substack{j=0 \\ j \neq k}}^{j=n} \{ \sigma(sq^j) - \sigma(sq^k) \}}, \tag{A.7}$$

$$\rho(s;\epsilon) = \sum_{n=0}^{\infty} \rho_n(s;\epsilon)\,. \tag{A.8}$$

The moments of u obtained from this equation are in agreement with those obtained by the author.

REFERENCES

Ambarzumian, W. A. 1953, *Math. Rev.*, **14**, 192 (review by Chandrasekhar).
Chandrasekhar, S., and Münch, G. 1950*a*, *Ap. J.*, **112**, 380.
———. 1950*b*, *ibid.*, p. 393.
———. 1951, *ibid.*, **114**, 110.
———. 1952, *ibid.*, **115**, 103.
Ramakrishnan, Alladi. 1950, *Proc. Cambridge Phil. Soc.*, **46**, 595.
———. 1953, *ibid.*, **49**, 483.
———. 1954, *Ap. J.*, **119**, 443.
Ramakrishnan, Alladi, and Mathews, P. M. 1954, *Prog. Theoret. Phys. (Japan)*, **11**, 95.

A TABLE OF THE RADIATIVE OPACITIES OF A NUMBER OF GAS MIXTURES

GEOFFREY KELLER*
Perkins Observatory
AND
ROLAND E. MEYEROTT†
Argonne National Laboratory
Received February 19, 1955

ABSTRACT

Rosseland mean opacities have been computed for gas mixtures at temperatures ranging from 10^5 to 2×10^7 degrees and for a range of densities dependent upon the temperatures. Thirteen mixtures, most of which are rich in hydrogen and helium, have been investigated.

PURPOSE

The purpose of this article is to make available the results of an extensive series of opacity calculations which have been in progress for a number of years. The results of other related investigations and computations will be published at a later date, including a number of auxiliary tables, which should be of assistance in the computation of opacities of mixtures which have not been considered here.

BRIEF DESCRIPTION OF METHOD

The quantities given here are Rosseland mean opacities and have been computed according to the general principles set forth by Strömgren (1932) and developed by Morse (1940). Several tables and other information have been obtained from Mayer (1947).

In this work the opacity due to bound-bound (line) absorption has been omitted. It is felt that in most cases the omission does not cause a serious error. Further investigations of this problem are currently being made, however.

Calculations of the absorption due to bound-free transitions have been based on electron occupation numbers which were corrected for electron screening and pressure ionization according to the method described by Keller and Meyerott (1952*a*, *b*). Approximate Gaunt factors for elements heavier than helium have been estimated from the use of Hartree-type wave functions (Meyerott 1954). For hydrogen and helium the Gaunt factors given by Menzel and Pekeris (1935) and tabulated by Mayer (1947) have been employed.

Free-free absorption has also been included, and here an average Gaunt factor of unity has been used for the heavier elements. For *H* II and *He* III an approximation for the gaunt factor has been obtained from the expressions of Menzel and Pekeris (1935). Aside from the renormalization factor, our expression agrees with that given by Kulsrud (1954) in the approximation to which his expression is valid; but our use of a higher order of approximation introduces new corrections of up to 50 per cent of the zero-order term. We have not employed Kulsrud's renormalization and cannot agree with the argument by which he derives it. Our objection is essentially that the electron does not move in a box of dimensions equal to the interproton distances but *is* free to move throughout the entire volume. At large distances from the proton with which it is in the process of photo-

* This research of this author was supported in part by the Argonne National Laboratory under a consultant subcontract based on work performed under the auspices of the United States Atomic Energy Commission.

† Now at the RAND Corporation, Santa Monica, California.

absorption, the potential varies as $\exp[-ar]/r \approx 0$; and, on the average, it behaves like a plane wave, so that Sommerfeld's normalization is correct. If one wishes to look at the detailed picture, one can say that the electron's normalization is indeed influenced by the potential fields of the protons other than the one with which it is in the process of photoabsorption, but in that case its normalization will be affected in the opposite sense by the proximity to the other electrons.

It is not yet certain that the free-free transition probabilities are not seriously affected by pressure effects, however, even if the renormalization just discussed is not necessary. Dr. Kulsrud has advised the authors that a more precise computation shows that interactions between an electron and several other particles simultaneously may be more important than indicated in his 1954 paper. It was not deemed advisable to delay the opacity computations until the question could be settled completely, and in this work the pressure effects on the wave-function amplitudes have been neglected.

The effects of pressure on the transition probabilities mentioned by Tsao (1954) have been taken into account to the extent that they are important in the range of temperatures and densities which we have investigated. This is to say that the effect of shielding upon ionization potentials has been allowed for, but the effect of the shield upon the free-free transition probability in hydrogen has been neglected.

The free-free Gaunt factors which we have employed for hydrogen agree rather well with those of Zirin (1954) for the range of electron and photon energies which is of practical importance.

Scattering by free electrons is computed by the Klein-Nishina formula as given by Heitler (1944). The dependence of the cross-section upon frequency was taken into account during the process of computation of the Rosseland mean.

Computation of the positions and heights of the various absorption edges was performed by hand. These data were then punched into IBM cards, and computation of the mean opacity (for any selected composition) was made on an IBM card-programmed calculator. Opacities for mixtures other than those given here might be obtained in a similar manner, provided that a sufficient need for them were felt.

COMPARISON WITH OTHER TABLES

The values given here have been compared with those given by Zirin (1954) and Epstein and Motz (1954). In both these investigations the free-free opacity of hydrogen has been taken into account. The present authors have not used exactly the same compositions as those employed by Zirin and by Motz and Epstein. However, interpolation between our groups VII and VIII gives a composition comparable to Zirin's first mixture. We find that, in general, our values lie within 25 per cent on either side of Zirin's, except for his cases with $T = 12.56 \times 10^6$, for which there appears to be some sort of error, as may be seen by comparing his tabular values with the plotted points in his Figure 1. An equally good agreement is obtained by comparison of our groups I and II with Zirin's second mixture.

By extrapolation of our groups VII, IV, and I toward a case with a combined fraction of elements other than hydrogen and helium $(1 - X - Y)$ of 0.002, one can obtain opacities which should be comparable to those of Epstein and Motz. These authors compute the Rosseland mean opacity for absorption alone and then combine it with the mean scattering opacity according to a rule given by Chandrasekhar (1939). Using this rule, we find as good agreement with our results as could be expected in view of the uncertainties of our extrapolation procedure. In all cases the discrepancies appear to be less than 25 per cent and may actually be considerably less.

COMPOSITION OF MIXTURES

Table 1 lists the fractions by weight of the various elements assumed to be present in the gas, where thirteen different mixtures or groups have been considered. The numbers

TABLE 1

COMPOSITION OF MIXTURES

Z	Group I	Group II	Group III	Group IV
1	.99000	.49500	.00000	.97000
2	.00000	.49500	.99000	.00000
6	.00041	.00041	.00041	.00123
7	.00081	.00081	.00081	.00243
8	.00297	.00297	.00297	.00891
10	.00448	.00448	.00448	.01344
13	.00043	.00043	.00043	.00129
19	.00062	.00062	.00062	.00186
26	.00028	.00028	.00028	.00084
A	.99500	.74750	.50000	.98500

Z	Group V	Group VI	Group VII	Group VIII
1	.48500	.00000	.9000	.4500
2	.48500	.97000	.0000	.4500
6	.00123	.00123	.0041	.0041
7	.00243	.00243	.0081	.0081
8	.00891	.00891	.0297	.0297
10	.01344	.01344	.0448	.0448
13	.00129	.00129	.0043	.0043
19	.00186	.00186	.0062	.0062
26	.00084	.00084	.0028	.0028
A	.74250	.50000	.9500	.7250

Z	Group IX	Group X	Group XI	Group XII	Group XIII
1	.0000	.485000	.0000	.000	.00000
2	.9000	.485000	.5000	.000	.50000
6	.0041	.001844	.0205	.041	.47123
7	.0081	.003606	.0405	.081	.00243
8	.0297	.012420	.1485	.297	.00891
10	.0448	.006231	.2240	.448	.01344
13	.0043	.001914	.0215	.043	.00129
19	.0062	.002760	.0310	.062	.00186
26	.0028	.001245	.0140	.028	.00084
A	.5000	.742500	.5000	.500	.50000

TABLE 2

Density (gms/cm^3) = B (α_e)/A

B (α_e) x 10^{-n}

(n is given to the right of each number)

T x 10^{-6}	.116	n	.232	n	.581	n	1.16	n	2.32	n
α_e										
3	x		x		x		x		1.40	0
4.5	x		x		x		x		3.2	-1
5	x		x		x		6.8	-2	x	
6	x		x		8.9	-3	2.5	-2	7.1	-2
6.5	x		x		5.4	-3	x		x	
7	x		8.2	-4	3.3	-3	9.2	-3	2.6	-2
8	1.07	-4	3.0	-4	1.20	-3	3.4	-3	9.6	-3
10	1.45	-5	4.1	-5	1.63	-4	4.6	-4	1.30	-3
12	1.97	-6	5.6	-6	2.2	-5	6.2	-5	1.76	-4

T x 10^{-6}	4.06	n	5.81	n	8.13	n	11.6	n	23.2	n
α_e										
0	x		x		x		2.4	2	6.9	2
1	x		x		x		1.05	2	3.0	2
2	x		1.46	1	2.4	1	4.1	1	1.17	2
3	3.2	0	x		x		1.56	1	4.4	1
4	x		2.1	0	3.4	0	5.8	0	1.67	1
4.5	7.3	-1	x		x		x		x	
5	x		7.6	-1	x		2.1	0	6.1	0
6	1.64	-1	2.8	-1	4.6	-1	7.9	-1	2.2	0
7	6.0	-2	x		x		x		x	
8	2.2	-2	3.8	-2	6.2	-2	1.07	-1	3.0	-1
10	3.0	-3	5.1	-3	x		x		x	
12	4.1	-4	6.9	-4	1.14	-3	1.97	-3	5.6	-3

TABLE 3

Number of Free Electrons n_f per atom

Carbon Z = 6

i_Z

T x 10^{-6} / α_e	.116	.232	.581	1.16	2.32	4.06
3					5.5	5.7
4.5				x	5.7	5.8
5			x	5.1	x	x
6			4.1	5.4	5.9	5.9
6.5		x	4.3	x	x	x
7	x	3.8	4.4	5.7	6.0	6.0
8	3.4	3.9	4.8	5.9	6.0	6.0
10	3.9	4.0	5.3	6.0	6.0	6.0
12	4.0	4.0	5.8	6.0	6.0	6.0

Oxygen Z = 8

i_Z

T x 10^{-6} / α_e	.116	.232	.581	1.16	2.32	4.06	5.81
2					x	x	7.3
3					6.8	7.5	x
4					6.9	7.5	7.6
4.5				x	7.1	7.7	x
5			x	5.9	x	x	7.9
6			5.6	6.2	7.5	7.9	7.9
6.5		x	5.8	x	x	x	x
7	x	4.8	5.8	6.6	7.8	7.9	x
8	3.3	5.3	5.9	7.0	7.9	8.0	8.0
10	4.0	5.8	6.0	7.6	8.0	8.0	8.0
12	4.7	6.0	6.1	7.9	8.0	8.0	8.0

Neon Z = 10

i_Z

T x 10^{-6} / α_e	.232	.581	1.16	2.32	4.06	5.81	8.13
2				x	x	7.8:	7.6
3				7.1:	8.0:	x	x
4			x	7.9	8.9	9.4	9.5
4.5			x	8.3	9.1	x	x
5		x	7.7	x	x	9.7	x
6		7.2	8.0	9.0	9.7	9.9	9.9
6.5	x	7.3	x	x	x	x	x
7	5.0	7.5	8.2	9.4	9.9	x	x
8	5.7	7.7	8.3	9.6	10.0	10.0	10.0
10	6.7	8.0	8.6	9.9	10.0	10.0	x
12	7.2	8.0	9.1	10.0	10.0	10.0	10.0

TABLE 4

OPACITY (cm^2/gm)

a_e / Group	$T = 0.116 \times 10^6$ 8	10	12	7	$T = 0.232 \times 10^6$ 8	10	12
I	280	35	5.7	93	35	5.4	1.19
II	810	96	13.8	560	210	28	4.2
III	830	82	11.1	830	310	42	5.9
IV	320	40	6.7	125	49	7.5	1.49
V	800	99	15.0	670	250	34	5.0
VI	820	84	12.3	970	350	48	6.7
VII	390	52	9.3	191	79	12.6	2.2
VIII	770	105	18.4	820	310	44	6.2
IX	790	92	16.0	1150	430	60	8.2
X	810	101	15.8	660	260	37	5.3
XI	610	131	26	1320	540	75	10.1
XII	340	113	20	700	360	62	9.0
XIII	880	160	25	960	380	52	7.2

$T = 0.581 \times 10^6$

a_e / Group	6	6.5	7	8	10	12
I	35	25	17.0	7.4	1.56	.59
II	54	39	27	12.3	2.3	.59
III	70	49	33	15.4	2.8	.57
IV	70	48	31	12.3	2.3	.74
V	105	75	50	21	3.6	.76
VI	127	91	62	27	4.5	.79
VII	154	101	65	24	4.1	1.08
VIII	220	150	97	37	5.8	1.18
IX	270	184	120	48	7.1	1.23
X	87	61	41	17.3	3.0	.69
XI	670	440	280	101	15.3	2.6
XII	980	640	411	147	23	3.7
XIII	167	116	80	37	7.9	1.47

$T = 1.16 \times 10^6$

a_e / Group	5	6	7	8	10	12
I	16.0	6.7	3.1	1.57	.63	.45
II	21	8.7	3.8	1.76	.57	.36
III	26	10.5	4.4	1.91	.50	.28
IV	32	13.3	5.9	2.8	.84	.49
V	38	15.6	6.7	3.1	.79	.40
VI	44	17.7	7.5	3.3	.72	.31
VII	85	35	15.3	6.9	1.52	.60
VIII	92	38	16.3	7.3	1.48	.52
IX	98	40	17.2	7.5	1.43	.43
X	39	16.2	7.1	3.2	.81	.40
XI	390	162	69	30	5.2	1.07
XII	750	310	132	58	9.8	1.82
XIII	167	74	31	13.9	2.4	.66

TABLE 4 (Con't)

$T = 2.32 \times 10^6$

α_e / Group	3	4.5	6	7	8	10	12
I	22	8.7	2.9	1.55	.91	.51	.41
II	25	10.0	3.2	1.58	.85	.42	.32
III	28	11.0	3.4	1.60	.78	.32	.22
IV	49	18.7	5.8	2.9	1.46	.62	.44
V	54	21	6.2	2.9	1.41	.52	.34
VI	58	23	6.6	3.0	1.35	.42	.24
VII	133	50	15.1	7.0	3.2	.92	.49
VIII	141	53	15.6	7.2	3.1	.82	.40
IX	148	55	16.1	7.3	3.1	.72	.30
X	54	22	7.0	3.3	1.57	.54	.34
XI	600	230	68	31	12.5	2.3	.56
XII	1140	440	132	60	24	4.2	.86
XIII	230	97	34	15.0	6.1	1.13	.34

$T = 4.06 \times 10^6$

α_e / Group	3	4.5	6	7	8	10	12
I	5.6	2.9	1.28	.77	.50	.42	.40
II	5.6	2.9	1.23	.69	.46	.32	.30
III	5.6	2.9	1.17	.61	.37	.23	.20
IV	12.7	6.5	2.5	1.28	.76	.45	.40
V	12.8	6.6	2.5	1.21	.68	.35	.30
VI	12.8	6.6	2.5	1.13	.59	.26	.21
VII	37	18.5	6.5	2.9	1.43	.54	.40
VIII	37	18.7	6.6	2.9	1.35	.46	.31
IX	37	18.8	6.6	2.8	1.27	.37	.22
X	11.8	6.0	2.3	1.15	.65	.35	.30
XI	174	86	29	12.0	4.9	.91	.31
XII	340	170	57	23	9.5	1.86	.41
XIII	30	13.6	4.6	2.1	1.01	.34	.24

$T = 5.81 \times 10^6$

α_e / Group	2	4	5	6	8	10	12
I	4.2	1.62	1.02	.70	.45	.40	.39
II	4.2	1.54	.93	.61	.36	.31	.30
III	4.2	1.45	.83	.51	.26	.21	.199
IV	8.3	3.2	1.81	1.08	.52	.41	.39
V	8.3	3.1	1.71	.98	.42	.32	.30
VI	8.3	3.0	1.60	.87	.33	.22	.20
VII	22	8.4	4.4	2.3	.72	.44	.39
VIII	22	8.4	4.3	2.2	.63	.35	.30
IX	22	8.3	4.2	2.1	.53	.26	.21
X	7.8	3.0	1.68	.96	.42	.32	.30
XI	103	38	19.0	8.9	1.60	.44	.24
XII	200	76	37	17.3	2.9	.64	.27
XIII	10.4	5.5	2.8	1.36	.44	.25	.21

TABLE 4 (Con't)

$T = 8.13 \times 10^6$

α_e / Group	2	4	6	8	12
I	2.3	.96	.54	.42	.39
II	2.2	.85	.44	.32	.29
III	2.1	.73	.33	.23	.20
IV	4.0	1.57	.69	.45	.39
V	3.9	1.45	.58	.35	.29
VI	3.8	1.34	.47	.26	.20
VII	10.0	3.6	1.13	.54	.38
VIII	9.9	3.5	1.02	.44	.29
IX	9.8	3.4	.91	.34	.20
X	4.0	1.47	.59	.36	.29
XI	44	15.0	3.2	.73	.22
XII	87	30	6.1	1.17	.23
XIII	5.3	1.63	.53	.27	.20

$T = 11.6 \times 10^6$

α_e / Group	0	1	2	3	4
I	3.1	1.84	1.29	.91	.67
II	2.9	1.74	1.18	.80	.57
III	2.8	1.63	1.05	.68	.46
IV	3.8	2.5	1.95	1.35	.93
V	3.7	2.4	1.83	1.23	.83
VI	3.6	2.3	1.70	1.12	.72
VII	6.6	4.8	4.2	2.8	1.79
VIII	6.5	4.7	4.0	2.7	1.69
IX	6.4	4.6	3.9	2.6	1.58
X	4.1	2.8	1.99	1.36	.89
XI	22	17.3	16.4	11.0	6.4
XII	41	33	32	21	12.5
XIII	7.6	4.1	2.5	1.46	.90

$T = 11.6 \times 10^6$

α_e / Group	5	6	8	12
I	.53	.46	.40	.39
II	.43	.36	.30	.29
III	.33	.26	.21	.20
IV	.66	.52	.41	.38
V	.56	.42	.32	.29
VI	.45	.32	.22	.20
VII	1.07	.71	.44	.37
VIII	.97	.62	.35	.28
IX	.86	.52	.26	.20
X	.59	.44	.32	.29
XI	3.1	1.50	.45	.20
XII	5.8	2.7	.65	.21
XIII	.54	.36	.23	.20

TABLE 4 (Con't)

$T = 23.2 \times 10^6$

α_e / Group	0	1	2	3	4
I	1.17	.84	.64	.52	.45
II	1.03	.72	.54	.42	.36
III	.89	.59	.42	.32	.26
IV	1.37	1.02	.78	.61	.50
V	1.23	.90	.66	.51	.40
VI	1.08	.76	.54	.40	.30
VII	2.0	1.58	1.19	.89	.65
VIII	1.87	1.44	1.06	.78	.55
IX	1.70	1.29	.93	.66	.45
X	1.30	.95	.72	.55	.43
XI	5.1	4.1	2.9	1.98	1.21
XII	9.2	7.4	5.3	3.5	2.1
XIII	2.2	1.25	.77	.51	.36

$T = 23.2 \times 10^6$

α_e / Group	5	6	8	12
I	.41	.40	.38	.38
II	.32	.30	.29	.29
III	.22	.21	.194	.191
IV	.44	.40	.38	.38
V	.34	.31	.29	.28
VI	.25	.22	.196	.191
VII	.51	.43	.37	.36
VIII	.42	.34	.29	.28
IX	.33	.25	.20	.191
X	.35	.32	.29	.28
XI	.72	.44	.24	.192
XII	1.19	.65	.28	.193
XIII	.28	.23	.20	.191

listed under Z are the atomic numbers of the elements concerned. The quantity $A = (1 + x_1)/2$ gives the number of electrons present in the gas for each unit of atomic weight and is a measure of the importance of opacity due to free electron scattering.

Groups I–IX form a set in which the relative abundances of elements heavier than helium are fixed. The authors are indebted to Drs. Aller, Greenstein, and Schwarzschild for their suggestions in this connection.

Group X was considered in order to test the sensitivity of the results to the assumed abundance of neon. If the opacities of this group are compared with those of group V, it will be seen that the maximum differences are of the order of 20 per cent and occur at a temperature of 0.5×10^6 degrees.

Groups XI and XII were computed in order to permit a study of the effect of depletion of helium upon the opacity. In these cases it has been assumed that the consumed helium has been converted into heavier elements having the same relative proportions as those in groups I–IX.

Group XIII is a mixture obtained on the assumption that all hydrogen has been consumed giving group VI and then that the helium has been converted to carbon to the point where only 50 per cent of the mass remains in the form of helium.

DENSITIES

In the process of calculation of the opacities, various pairs of values of the temperature and free-electron density have been assumed. The two parameters which have been employed to specify the foregoing quantities are T (the temperature itself) and α_e (introduced in Keller and Meyerott 1952*b*). By definition,

$$\rho_{e0} = 8\pi \sqrt{2} h^{-3} \left(\frac{m_e}{\beta}\right)^{3/2} F(-\alpha_e),$$

where ρ_{e0} is the free-electron density at large distances from a nucleus, $\beta = 1/kT$, m_e is the electron mass, and F is the Fermi-Dirac function. When $\alpha_e \geq 2$, one has the approximate relation

$$\alpha_e \approx \log_e \frac{G(T)}{N_e} = \log_e \left\{\frac{2(2\pi m_e kT)^{3/2}}{h^3 \rho_{e0}}\right\},$$

where $N_e \approx \rho_{e0}$ and $\log_e [G(T)/N_e]$ is the density parameter used by a number of authors (Chandrasekhar 1939, p. 269).

In some problems one may wish to know the value of the gas density corresponding to a given pair of values α_e and T. The gas densities depend on the relative abundances and degrees of ionization of the constituent elements. For this reason a common density table cannot be given for all mixtures. For the purpose of computing the density, we may assume that the hydrogen and helium are completely ionized in all the cases considered here. For the mixtures rich in these elements (groups I–X) the fact that the heavier elements are only partially ionized can be neglected, and, to an accuracy of 5 per cent, one can use Table 2, employing the values of A appearing in Table 1.

For the mixtures which are poor in hydrogen and helium, it may be desirable to use a more precise expression,

$$A = \sum_Z \frac{x_Z \bar{\imath}_Z}{A_Z},$$

where the A_Z's are the atomic numbers of the elements in question and the $\bar{\imath}_Z$'s, the average number of free electrons per atom, are given in Table 3 for some of the more important constituents.

OPACITIES

The results appear in Table 4. Enough digits have been carried in the computations to produce results which are correct to 10 per cent (it is hoped!), assuming, of course, that the theoretical basis of the computation is sound. The omission of line absorption may be serious, although at the present time it is thought not to be. There remains some uncertainty in the difficult matter of Gaunt factors, but, aside from the question of renormalization, the agreement between various authors is encouraging.

In general, the opacities appear to behave in a fashion which is in accord with the computations and predictions of earlier authors. There is one effect, however, that may be deserving of special mention. It is well known that the strongest absorption occurs close to the shortest wave-length absorption edges of the more abundant elements. At low temperatures, where the maximum of the Planck distribution is shifted toward longer wave lengths, it is the photoionization of *K* and *L* electrons of *H* and *He* which makes the major contribution to the opacity. In a mixture such as group XII, these elements are not present, and, with decreasing temperature, the opacity tends to depend more and more on the relatively ineffectual absorption of the higher edges of *C*, *N*, *O*, and *Ne* and on free-free effects. Such weakening of the absorption at lower temperatures could be even more marked if nuclear processes were to deplete the elements of the oxygen group. It is interesting to speculate on whether the resulting abnormal temperature dependence of the opacity would contribute to an instability which would make sustained Cepheid pulsation possible.

The authors are very much indebted to Mrs. Mary Fenwick and Mrs. Jean Kelley for the preliminary computations performed at the Perkins Observatory. They are particularly grateful to Mrs. Lucille Renick, who supervised CPC computations, and to the members of the Argonne National Laboratory computing group, who gave us such willing assistance.

REFERENCES

Chandrasekhar, S. 1939, *An Introduction to the Study of Stellar Structure* (Chicago: University of Chicago Press), p. 272.
Epstein, I., and Motz, L. 1954, *Ap. J.*, **120**, 156.
Heitler, W. 1944, *The Quantum Theory of Radiation* (2d ed.; Oxford: Oxford University Press), p. 157.
Keller, G., and Meyerott, R. E. 1952*a*, *Argonne National Laboratory Report*, ANL 4771.
———. 1952*b*, *Argonne National Laboratory Report*, ANL 4856.
Kulsrud, R. M. 1954, *Ap. J.*, **119**, 386.
Mayer, H. 1947, *Los Alamos Scientific Laboratory Report*, LA-647.
Menzel, D. H., and Pekeris, C. L. 1935, *M.N.*, **96**, 77.
Meyerott, R. E. 1954, *Phys. Rev.*, **95**, 72.
Morse, P. M. 1940, *Ap. J.*, **92**, 27.
Strömgren, B. 1932, *Zs. f. Ap.*, **4**, 118.
Tsao, H. T. H. 1954, *Ap. J.*, **119**, 70.
Zirin, H. 1954, *Ap. J.*, **119**, 371.

STELLAR PULSATION AS A LIMIT-CYCLE PHENOMENON

WASLEY S. KROGDAHL
Dearborn Observatory, Northwestern University
Received February 19, 1955

ABSTRACT

It is shown how the equations of motion for a pulsating star may be modified so as to make the system one possessing self-excitation. Limit-cycle solutions have been calculated for several illustrative cases. Indications as to how the corresponding velocity-curves relate to the observed curves for Cepheids are given.

Theoretical investigations of stellar pulsation have dealt primarily with pulsations that are linear in form and appropriate to conservative systems (Rosseland 1949). Latterly, some attention has been given to anharmonic or nonlinear pulsations of conservative systems. To treat a pulsating star as a conservative dynamical system is inappropriate, however; for, as has been remarked by Ledoux (1952), such a star is, in fact, a real (as opposed to ideal) thermodynamic engine. As such it can exhibit features (such as self-excitation) not possible in truly conservative mechanisms.[1] It is the purpose of this investigation to see how the present anharmonic theory may be modified to describe nonconservative self-excited systems.

The pulsation equations in their customary form are derived from the equations of motion of an isotropic fluid medium. In tensor notation these are

$$\frac{\delta v_s}{\delta t} = F_s - \frac{1}{\rho}\frac{\partial p}{\partial x^s}, \tag{1}$$

where $\delta v_s/\delta t$ is the intrinsic derivative of $v_s = g_{sn}dx^n/dt$ (g_{sn} is the covariant fundamental tensor), F_s is a force field (in this case gravitation), ρ is the mass density, and p is the total pressure. For a radially pulsating star possessing radial symmetry we have

$$F_1 = -\frac{GM(r)}{r^2}, \qquad F_2 = 0 = F_3, \tag{2}$$

in spherical co-ordinates. Moreover, if mass is to be conserved, it is necessary that

$$M[r(a, t)] = M(a) \tag{3}$$

or, taking differentials,

$$M(r + dr) - M(r) = 4\pi r^2 \rho dr = 4\pi a^2 \rho_0 da = M(a + da) - M(a), \tag{4}$$

where $a = r_0$ is the mean or equilibrium value of r for some layer of the star and a zero subscript denotes the value of a quantity in the unperturbed state of the star. Combining equations (2) and (3) gives

$$F_1 = -\frac{GM(a)}{r^2}. \tag{5}$$

Using equation (4) in the form

$$\rho dr = \frac{a^2}{r^2}\rho_0 da, \tag{6}$$

[1] "Only non-conservative non-linear systems are physically significant" (Andronow and Chaikin 1949).

we also have

$$\frac{1}{\rho}\frac{\partial p}{\partial r}=\frac{r^2}{a^2}\frac{1}{\rho_0}\frac{\partial p}{\partial a}. \tag{7}$$

With equations (5) and (7), equation (1) may now be written

$$\ddot{r}=-\frac{GM(a)}{r^2}-\frac{r^2}{a^2}\frac{1}{\rho_0}\frac{\partial p}{\partial a}. \tag{8}$$

We make use of the further relation,

$$p=p_0(a)\left(\frac{\rho}{\rho_0}\right)^{\gamma}. \tag{9}$$

The quantity (ρ/ρ_0) may be eliminated with the aid of equation (4), according to which

$$\frac{\rho}{\rho_0}=\left[\frac{r^2}{a^2}\frac{\partial r}{\partial a}\right]^{-1}=\left(\frac{\partial r^3}{\partial a^3}\right)^{-1}. \tag{10}$$

Equation (8) is now

$$\ddot{r}=-\frac{GM(a)}{r^2}-\frac{r^2}{a^2}\frac{1}{\rho_0}\frac{\partial}{\partial a}\left[p_0\left(\frac{\partial r^3}{\partial a^3}\right)^{-\gamma}\right]. \tag{11}$$

Let us introduce the variables

$$y=r^3\,,\qquad r=y^{1/3}\ (\dot{r}=\tfrac{1}{3}y^{-2/3}\dot{y}\,,\ \ddot{r}=\tfrac{1}{3}y^{-2/3}\ddot{y}-\tfrac{2}{9}y^{-5/3}\dot{y}^2)\,, \tag{12}$$

$$x=a^3\,,\qquad a=x^{1/3}\,.$$

Equation (11) takes the form

$$\ddot{y}-\frac{2}{3}\frac{\dot{y}^2}{y}=-GM(x)-\frac{9}{\rho_0}y^{4/3}\frac{\partial}{\partial x}\left[p_0\left(\frac{\partial y}{\partial x}\right)^{-\gamma}\right]. \tag{13}$$

Inasmuch as $y=x$ is a particular solution, we take for y an expression of the form

$$y=x+g(x,t)\,, \tag{14}$$

where $g(x,t)$ is assumed to be small in comparison to x. Upon substituting equation (14) in equation (13) and carrying out the expansions, we have for $g(x,t)$,

$$\begin{aligned}
\frac{\ddot{g}}{x}=&\frac{9}{\rho_0}\Big\{-x^{1/3}\frac{\partial p_0}{\partial x}\Big[\frac{4}{3}\frac{g}{x}-\gamma g'\Big]+\gamma p_0 x^{1/3}g''\Big\}\\
&+\frac{9}{\rho_0}\Big\{-x^{1/3}\frac{\partial p_0}{\partial x}\Big[\frac{g^2}{x^2}-\frac{4\gamma}{3}\frac{g\,g'}{x}+\frac{\gamma(\gamma+1)}{2}g'^2\Big]+\gamma p_0 x^{1/3}\Big[\frac{4}{3}\frac{g}{x}-(\gamma+1)g'\Big]\Big\}\\
&+\frac{2}{3}\frac{\dot{g}^2}{x^2}+\frac{9}{\rho_0}\Big\{x^{1/3}\frac{\partial p_0}{\partial x}\Big[\frac{4}{81}\frac{g^3}{x^3}+\frac{2\gamma}{9}\frac{g^2g'}{x^2}-\frac{2\gamma(\gamma+1)}{3}\frac{g\,g'^2}{x}+\frac{\gamma(\gamma+1)(\gamma+2)}{6}g'^3\Big]\\
&+\gamma p_0 x^{1/3}g''\Big[\frac{2}{9}\frac{g^2}{x^2}-\frac{4}{3}(\gamma+1)\frac{g\,g'}{x}+\frac{(\gamma+1)(\gamma+2)}{2}g'^2\Big]\Big\}-\frac{2}{3}\frac{\dot{g}^2g}{x^3}+\cdots\,.
\end{aligned} \tag{15}$$

We seek to solve this partial differential equation by substituting a solution of the form

$$g(x,t)=x\sum_n\phi_n(x)\,q_n(t)\,, \tag{16}$$

where either the ϕ_n or the q_n forms a complete orthogonal set in the fundamental intervals for which they are defined. Writing

$$-\frac{9}{\rho_0}\,x^{1/3}\frac{dp_0}{dx}=J(x),\quad \frac{9p_0}{\rho_0}\,x^{1/3}=H(x)\,, \tag{17}$$

and taking the ϕ_n to be even functions of $\xi = x/X$ ($X^{1/3}$ = outer radius), orthogonal in the interval (0, 1) with weight function $W(\xi)\equiv 1$,[2] equation (15) becomes

$$\frac{\ddot{g}}{x}=\ddot{q}_1+(1-3\xi^2)\,\ddot{q}_2+\ldots=\{JP_1+HP_2\}+\{JP_3+HP_4\}+P_5 + \{JP_6+HP_7\}+P_8+\ldots\,, \tag{18}$$

where

$$P_1=(\tfrac{4}{3}-\gamma)\,q_1+[(\tfrac{4}{3}-\gamma)+(9\gamma-4)\,\xi^2]\,q_2+\ldots\,,$$

$$P_2=-18\gamma\xi q_2+\ldots\,,$$

$$P_3=\left[\frac{4-15\gamma+9\gamma^2}{18}\right]q_1^2+\left[\frac{4-15\gamma+9\gamma^2}{9}-\frac{4-21\gamma+27\gamma^2}{3}\,\xi^2\right]q_1q_2 + \left[\frac{4-15\gamma+9\gamma^2}{18}-\frac{4-21\gamma+27\gamma^2}{3}\,\xi^2+\frac{4+9\gamma+81\gamma^2}{2}\,\xi^4\right]q_2^2+\ldots\,,$$

$$P_4=[(-6\gamma+18\gamma^2)\,\xi]\,q_1q_2+[(-6\gamma+18\gamma^2)\,\xi-(90\gamma+162\gamma^2)\,\xi^3]\,q_2^2+\ldots$$

$$P_5=\tfrac{2}{3}\dot{q}_1^2+[\tfrac{4}{3}-4\xi^2]\,\dot{q}_1\dot{q}_2+[\tfrac{2}{3}-4\xi^2+6\xi^4]\,\dot{q}_2^2+\ldots\,,$$

$$\begin{aligned}P_6=&\left[\frac{27\gamma^3-27\gamma^2-18\gamma+8}{162}\right]q_1^3+\left[\left(\frac{8-18\gamma-27\gamma^2+27\gamma^3}{54}\right)\right.\\&\left.+\left(\frac{-8+30\gamma+9\gamma^2-81\gamma^3}{18}\right)\xi^2\right]q_1^2q_2+\left[\left(\frac{8-18\gamma-27\gamma^2+27\gamma^3}{54}\right)\right.\\&\left.-\left(\frac{8-30\gamma-9\gamma^2+81\gamma^3}{9}\right)\xi^2+\left(\frac{8+30\gamma-189\gamma^2+243\gamma^3}{6}\right)\xi^4\right]q_1q_2^2\\&+\left[\left(\frac{8-18\gamma-27\gamma^2+27\gamma^3}{162}\right)-\left(\frac{8-30\gamma-9\gamma^2+81\gamma^3}{18}\right)\xi^2\right.\\&\left.+\left(\frac{8+30\gamma+189\gamma^2+243\gamma^3}{6}\right)\xi^4-\left(\frac{8+594\gamma+1215\gamma^2+729\gamma^3}{6}\right)\xi^6\right]q_2^3+\ldots\,,\end{aligned} \tag{19}$$

$$\begin{aligned}P_7=&[(2\gamma-3\gamma^2-9\gamma^3)\,\xi]\,q_1^2q_2+[(4\gamma-6\gamma^2-18\gamma^3)\,\xi\\&+(60\gamma+198\gamma^2+162\gamma^3)\,\xi^3]\,q_1q_2^2+[(2\gamma-3\gamma^2-9\gamma^3)\,\xi\\&+(60\gamma+198\gamma^2+162\gamma^3)\,\xi^3-(846\gamma+1539\gamma^2+729\gamma^3)\,\xi^5]\,q_2^3+\ldots\,,\end{aligned}$$

$$\begin{aligned}P_8=&-\tfrac{2}{3}q_1\dot{q}_1^2+(-\tfrac{4}{3}+4\xi^2)\,q_1\dot{q}_1q_2+(-\tfrac{2}{3}+4\xi^2-6\xi^4)\,q_1\dot{q}_2^2+(-\tfrac{2}{3}+2\xi^2)\,\dot{q}_1^2q_2\\&+(-\tfrac{4}{3}+8\xi^2-12\xi^4)\,\dot{q}_1q_2\dot{q}_2+(-\tfrac{2}{3}+6\xi^2-18\xi^4+18\xi^6)\,q_2\dot{q}_2^2+\ldots\,.\end{aligned}$$

[2] It has been customary to choose the ϕ_n to be the solutions of the linearized pulsation equation. However, there is no particular advantage in so doing when one considers the complete nonlinear problem. In fact, it is usually simpler to choose the ϕ_n according to convenience.

If we now multiply both sides of equation (18) by $\phi_n d\xi$ and integrate from 0 to 1, we may isolate $\ddot{q}_n$ on the left side and, by integration, eliminate ξ as a variable on the right-hand side.

As a first approximation we set $q_n \equiv 0$ for all $n > 1$ and, by using the notations

$$j_m^n = \left(\int_0^1 \phi_m^2 \, d\xi\right)^{-1} \int_0^1 J(\xi)\, \phi_m(\xi)\, \xi^n d\xi\,,$$
$$h_m^n = \left(\int_0^1 \phi_m^2 \, d\xi\right)^{-1} \int_0^1 H(\xi)\, \phi_m(\xi)\, \xi^n d\xi\,, \tag{20}$$

we derive for $q_1 \equiv q$ the differential equation

$$\ddot{q} = (\tfrac{4}{3} - \gamma)\, j_1^0 q + \left(\frac{4 - 15\gamma + 9\gamma^2}{18}\right) j_1^0 q^2 + \tfrac{2}{3}\dot{q}^2 + \left(\frac{8 - 18\gamma - 27\gamma^2 + 27\gamma^3}{162}\right) j_1^0 q^3 - \tfrac{2}{3} q\,\dot{q}^2 + \ldots\,. \tag{21}$$

At this point we must adopt some definite model in order to have numerical values for the j_1^0. For simplicity, we choose the homogeneous model, for which

$$J(\xi) = 3\left(\frac{4\pi G \rho_0}{3}\right). \tag{22}$$

Adopting a new scale of time according to the relation

$$\tau = \left(\frac{4\pi G \rho_0}{3}\right)^{1/2} t\,, \tag{23}$$

equation (21) reduces to

$$\frac{d^2 q}{d\tau^2} = (4 - 3\gamma)\, q + \tfrac{1}{6}(4 - 15\gamma + 9\gamma^2)\, q^2 + \tfrac{2}{3}\left(\frac{dq}{d\tau}\right)^2 (1 - q) + \tfrac{1}{54}(8 - 18\gamma - 27\gamma^2 + 27\gamma^3)\, q^3 + \ldots\,. \tag{24}$$

Giving γ the value $\frac{5}{3}$, we have

$$\frac{d^2 q}{d\tau^2} = -q + \tfrac{2}{3} q^2 + \tfrac{14}{27} q^3 + \ldots + \tfrac{2}{3}(1 - q)\left(\frac{dq}{d\tau}\right)^2 + \ldots\,. \tag{25}$$

Equation (25) or its analogue is the equation which we wish to modify in such a manner as to describe more realistically the nonconservative, self-excited behavior of a pulsating star. To be self-excited, the star must be unstable at least for small amplitudes; such an instability would be assured by the presence of a term of the form $\mu(dq/d\tau)$ ($\mu > 0$) on the right-hand side of equation (25). However, in order that the oscillations shall not increase exponentially without limit, a damping must become effective for larger amplitudes; such a stability would be assured by the presence of an additional term of the form $-\nu q^2(dq/d\tau)$ ($\nu > 0$) on the right-hand side of equation (25).

It is proposed that terms of the forms suggested be added to equation (25). That their addition is not wholly arbitrary may be asserted on the ground that (*a*) actual Cepheids are statically unstable stars and (*b*) any real thermodynamic system is mechanically dissipative. The presence of such terms is desirable on the ground that (*a*) the modified equation possesses at least some solutions which are oscillations independent of the initial conditions, determined by parameters occurring in the equation rather than by physical-

ly irrelevant starting values and (*b*) at no time does the pulsating configuration pass through the equilibrium state, a desideratum emphasized by Milne (1934).

The presence of such terms may be expected if any deviations from the adiabatic relation (9) occur, for we could then write

$$p = p_0 \left(\frac{\rho}{\rho_0}\right)^{\gamma} + u\,(a, t)\,, \tag{9'}$$

where $u(a, t)$ represents the deviation. However, in a configuration which does not retrace itself at any time during a single period, a function such as $u(a, t)$ may also be expressed as a single-valued function $u(r, \dot{r})$ of the pulsational displacement and velocity. The terms $\mu dq/d\tau$ and $-\nu q^2 dq/d\tau$ may be looked upon as the leading terms arising from the substitution of equation (9') for equation (9). Such an interpretation implies that nonadiabatic conditions are directly responsible for the unstable equilibrium of Cepheids. This view has been advanced by Eddington (1941) and more recently by S. A. Jevakin (1953). Though a relation between the added terms and the deviation function $u(r, \dot{r})$ seems clear enough, it does not seem feasible or desirable to establish the explicit connection between them in view of the proximate nature of the remainder of the theory.

In the interest of mathematical convenience we set $\nu = \mu/\lambda^2$ and append the term $\mu(1 - q^2/\lambda^2)(dq/d\tau)$ to equation (25). We propose, therefore, to consider the solutions of the modified pulsation equation

$$\frac{d^2q}{d\tau^2} = -q + \tfrac{2}{3}q^2 + \tfrac{14}{27}q^3 + \ldots + \tfrac{2}{3}(1-q)\left(\frac{dq}{d\tau}\right)^2 + \ldots + \mu\left(1 - \frac{q^2}{\lambda^2}\right)\frac{dq}{d\tau}. \tag{26}$$

From its general similarity to the Van der Pol equation, we can anticipate that it will have limit-cycle solutions whose character will be functions of μ and λ.

Equation (26) has a singular point at $q = 0$, $dq/d\tau = 0$ in the $(q, dq/d\tau)$ plane or phase plane. The character of this singularity can be determined from the nature of the roots of Liapounoff's characteristic equation (Minorsky 1947), which in this case is

$$S^2 - \mu S + 1 = 0 \qquad \text{or} \qquad S = \tfrac{1}{2}\,(\mu \pm \sqrt{\mu^2 - 4})\,.$$

This implies that the singularity is an unstable focal point if $0 < \mu < 2$ and an unstable nodal point if $\mu > 2$; the singularity is a stable one for all negative μ. For any positive value of μ, therefore, the origin of the phase plane is a point of unstable equilibrium—i.e , the equilibrium configuration is unstable.

To emphasize the physical significance of the parameters μ and λ, we note that, since the configuration becomes unstable only for positive μ, this parameter must be related to the energy source of the pulsation, for unless there is a positive source of energy for the maintenance of the motion, it will be damped to arbitrarily small amplitude. On the other hand, as $\lambda \to 0$ with μ positive, the term containing it becomes arbitrarily large numerically and of sign opposite $dq/d\tau$. In short, $\lambda = 0$ leads to no motion, and λ may be seen to be inversely related to the damping constant.

For convenience in calculating, let us make the substitution

$$q = \lambda Q\,.$$

Then equation (26) becomes

$$Q'' = -Q + \tfrac{2}{3}\lambda Q^2 + \tfrac{14}{27}\lambda^2 Q^3 + \mu\,(1 - Q^2)\,Q' + \tfrac{2}{3}\lambda\,(1 - \lambda Q)\,Q'^2 + \ldots\,, \tag{27}$$

where primes indicate differentiation with respect to τ. When $\lambda = 0$, we have the Van der Pol equation; for small values of λ the solutions should differ but little from the limit-cycle solutions of that equation. Within a considerable range of initial values, all solutions for a given μ and λ asymptotically approach one and the same curve and thus

represent a periodic self-excited system. It should be emphasized that this is true for all positive μ, *no matter how small*. Thus the pulsation will be independent of initial values even for values of μ very close to zero (conservative system), though, to be sure, convergence to the limit cycle is then exceedingly slow. This is a major respect in which the theory of nonconservative systems is superior to the theory of conservative systems.

For the sake of illustration, limit-cycle solutions have been calculated for several pairs of values of λ and μ. Figure 1 shows four of these solutions plotted in the $(r, dr/d\tau)$ plane or phase plane. The parameter values for curves *1*, *2*, *3*, and *4* are: (*1*) $\mu = 0.01$, $\lambda = 0.1$; (*2*) $\mu = 0.1$, $\lambda = 0.15$; (*3*) $\mu = 0.5$, $\lambda = 0.1$; and (*4*) $\mu = 1.0$, $\lambda = 0.04$. The curve for a fifth case (*5*) $\mu = 0.1$, $\lambda = 0.1$, differs too little from curve *1* to be readily distinguished from it on the scale of the drawing. The segments represent intervals of τ. In curve *1* the interval is $\Delta\tau = 0.18$; in the other curves, $\Delta\tau = 0.24$.

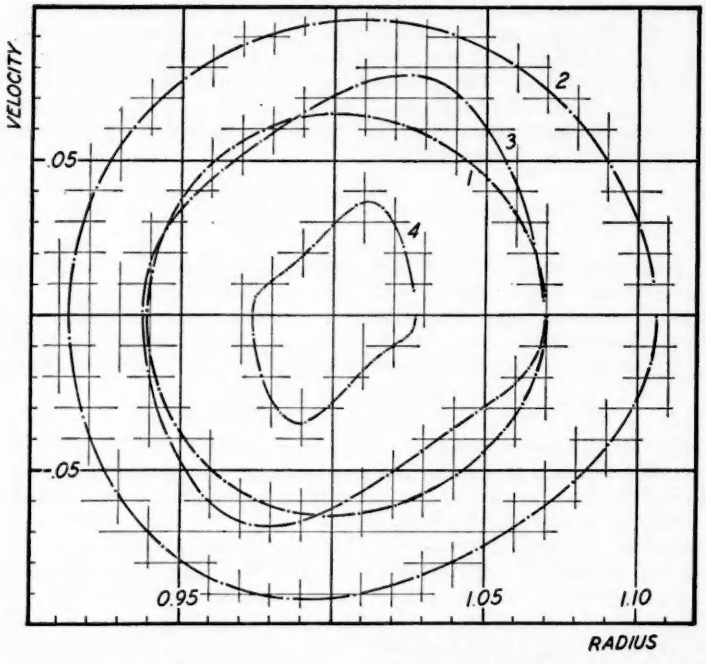

FIG. 1.—Curves *1*, *2*, *3*, and *4* are the phase-plane limit-cycle solutions of eq. (28) for cases (1) $\mu = 0.01$, $\lambda = 0.1$; (2) $\mu = 0.1$, $\lambda = 0.15$; (3) $\mu = 0.5$, $\lambda = 0.1$; and (4) $\mu = 1.0$, $\lambda = 0.04$. Curve segments between dots represent intervals of τ. In curve *1*, $\Delta\tau = 0.18$; in the rest, $\Delta\tau = 0.24$. The velocity is in units of $dr/d\tau$.

A few general conclusions may be readily drawn from these curves. Comparison of curves *1* (or *5*) and *2* shows that both possess near-symmetry in the r-axis but that *2* is slightly asymmetric in the r'-axis. This asymmetry is to be attributed to the greater value of λ in *2*. Any desired amount of such asymmetry could be achieved by a sufficient increase of λ. However, λ must remain small to fulfil the conditions under which the mathematical approximation remains valid. Moreover, values of λ sufficient to introduce much asymmetry correspond to pulsation amplitudes appreciably greater than those of actual Cepheids. It is clear, therefore, that only small values of λ are to be considered.

Comparison of curves *1* (or *5*) and *3* shows that larger values of μ introduce an asymmetry into the origin without appreciable modification of the amplitude of pulsation. This point is emphasized by curve *4*, for which μ is greater and λ less.

Ledoux (1952) has considered the asymmetry of Cepheid phase-plane-curves and used the virial theorem to derive an equation for the phase-plane diagrams in the conservative nonlinear case. For the sake of comparison, Figure 2 shows the phase-curves of cases *4* and *5*, together with the phase-curves calculated from Ledoux's formula. The latter are chosen to have the same maximum radius. It will be seen that the amplitudes are almost the same. Moreover, for small μ, the phase-curve is nearly identical.

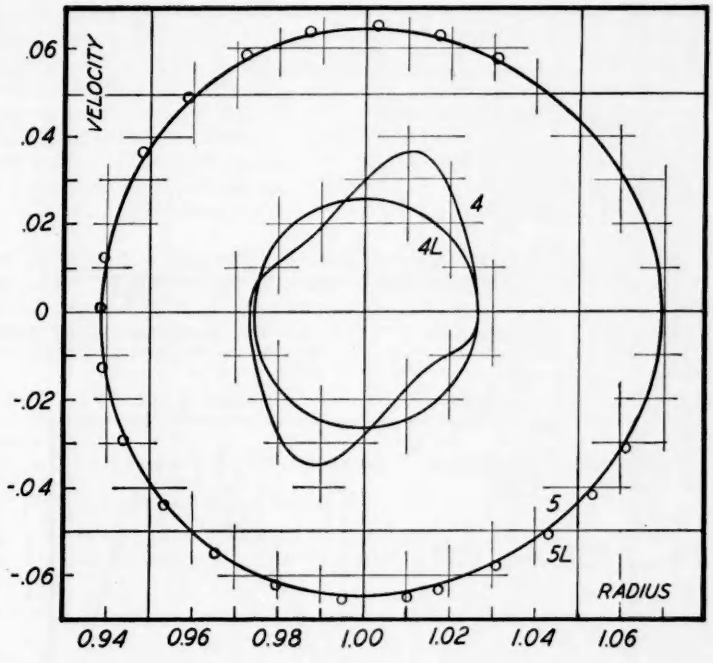

FIG. 2.—The phase-plane limit-cycle curves *4* and *5* represent cases (4) $\mu = 1.0$, $\lambda = 0.04$, and (5) $\mu = 0.1$, $\lambda = 0.1$. Curve *4L* is Ledoux's phase-plane-curve having the same maximum radius as *4*. Curve *5L*, giving Ledoux's curve for the same maximum radius as *5*, is so little different from *5* that the curve has not been drawn. Instead, points on the curve are indicated by the small circles. The velocity is in units of $dr/d\tau$.

For large μ, however, the phase-curve calculated here is considerably more asymmetric, even for small λ, than that given by Ledoux's equation. It would seem, therefore, that, to secure asymmetry, the nonconservatism is as essential to the problem as the nonlinearity.

Figure 3 shows the radial velocity-curves which correspond to cases *5*, *3*, and *4*. In discussing these, several points are to be noted. First, the pulsation here considered is not a running wave. Thus it does not correspond to current opinion that Cepheid pulsations are of the nature of running waves, at least near the star's surface. It must be added, however, that the present theory would give a wave whose phase at any instant is a function of distance from the center if in equation (16) we were to include more than

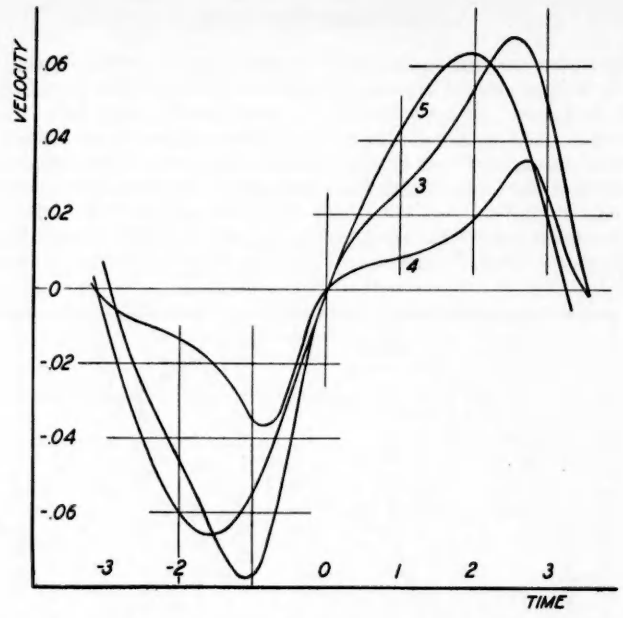

FIG. 3.—Curves *3*, *4*, and *5* represent the limit-cycle velocity-curves for cases (3) $\mu = 0.5$, $\lambda = 0.1$; (4) $\mu = 1.0$, $\lambda = 0.04$; and (5) $\mu = 0.1$, $\lambda = 0.1$. The time is in units of τ, and the velocity in units of $-dr/d\tau$.

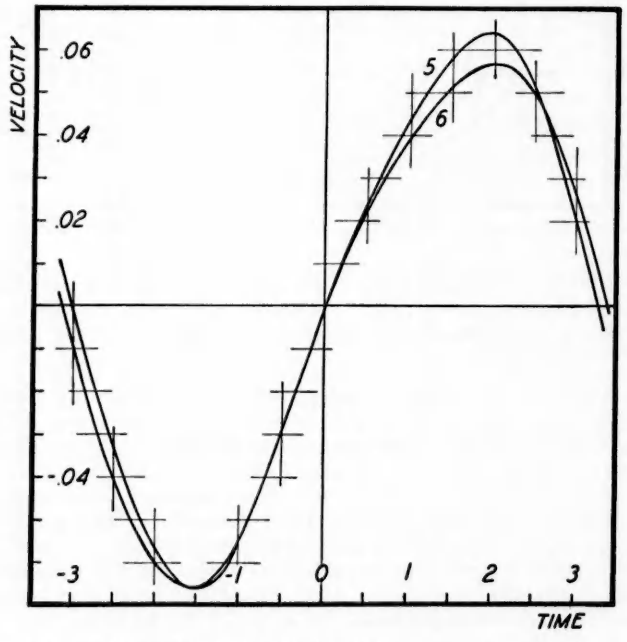

FIG. 4.—Curves *5* and *6* represent the limit-cycle velocity-curves for cases (5) $\mu = 0.1$, $\lambda = 0.1$, $\epsilon = 0$ and (6) $\mu = 0.1$, $\lambda = 0.1$, $\epsilon = -1.0$. The time is in units of τ, and the velocity in units of $-dr/d\tau$.

one term. Only mathematical intractability has prevented the present solution from having the properties of a running wave.

Second, observations indicate that the expansion of a Cepheid is in the manner of a shock wave. The maximum velocity of such a wave, however, corresponds to a kinetic temperature of the order of 10^{5}° K or less. Therefore, the wave need not be a shock wave at depths corresponding to temperatures as great as 10^{5}° K or greater. In short, the shock-wave characteristics may appear only very near the surface of the star. What is more, the contraction velocity may be expected to be that of free fall. It may be preferable, then, to visualize a pulsating star as a core, comprising nearly the whole of the star's radius, surrounded by an envelope in which is induced an expanding shock wave followed by a contraction not of the shock-wave type. If this may be done, comparison of observed and calculated velocity-curves should be limited to the interval of initial expansion. The calculated curves are then to be thought of as the velocity-curves of the core, curves not directly observable.

To test the sensitivity of the solution to the form of the dissipative terms appended to the equations of a conservative system, a slightly modified set of terms was used for an additional calculation. Thus, in place of $\mu(1 - Q^2)Q'$ in equation (27), the term $\mu(1 + \epsilon Q - Q^2)Q'$ was used. (Cases *1–5* represent pulsations with $\epsilon = 0$.) Figure 4 compares the velocity-curves of case *5* ($\lambda = 0.1$, $\epsilon = 0$, $\mu = 0.1$) and case *6* ($\lambda = 0.1$, $\epsilon = -1$, $\mu = 0.1$). The curves do not differ significantly.

It is a pleasure to acknowledge my indebtedness to Drs. S. Chandrasekhar and M. Schwarzschild for helpful discussions and correspondence. I wish also to express gratitude to the Graduate School of Northwestern University for a grant of funds for assistance in computing.

REFERENCES

Andronow, A., and Chaikin, C. 1949, *Theory of Oscillations* (Princeton: Princeton University Press), p. 102.
Eddington, A. S. 1941, *M.N.*, **101**, 182.
Jevakin, S. A. 1953, *Astr. Zhur.*, **30**, 161. Summarized in *Astronomical News Letter*, No. 72 (February 20, 1954), p. 10.
Ledoux, P. 1952, *Bull. Acad. R. Belg.*, 5e ser., **38**, 354.
Milne, E. A. 1934, *M.N.*, **94**, 418.
Minorsky, N. 1947, *Nonlinear Mechanics* (Ann Arbor, Mich.: Edwards Bros.), p. 114.
Rosseland, S. 1949, *The Pulsation Theory of Variable Stars* (Oxford: Oxford University Press), chaps. iii and iv.

WAVE FUNCTIONS, SPIN-ORBIT, AND SPIN-SPIN PARAMETERS FOR THE $1s^2 2s^2 2p^4$ ISOELECTRONIC SEQUENCE

HAROLD ZIRIN
Harvard College Observatory
Received February 11, 1955

ABSTRACT

Variational wave functions are presented for the $1s^2 2s^2 2p^4$ isoelectronic sequence, for the ions *O* I through *Ca* XIII. These wave functions make possible the computation of the spin-orbit and spin-spin parameters for the ions noted. The results agree well with empirical values.

Recently I calculated (Zirin 1955; referred to hereafter as "Paper I") the values of the spin-orbit parameter ζ and the spin-spin parameter η for the $1s^2 2s^2 2p^2$ isoelectronic sequence, using variational wave functions on the scheme of Morse, Young, and Haurwitz (1935). I have applied here the same treatment to the $1s^2 2s^2 2p^4$ sequence from *O* I to *Ca* XIII.

These are the trial functions used:

$$1s: \; u_1(r) = \left(\frac{\mu^3 a^3}{\pi}\right)^{1/2} e^{-\mu a r};$$

$$2s: \; u_2(r) = \left(\frac{\mu^5}{3\pi N}\right)^{1/2} \left[r\, e^{-\mu r} - \left(\frac{3A}{\mu}\right) e^{-\mu b r} \right];$$

$$2p: \; u_3(r) = \left(\frac{\mu^5 c^5}{\pi}\right)^{1/2} r \cos\vartheta \cdot e^{-\mu c r},$$

$$u_4(r) = \left(\frac{\mu^5 c^5}{2\pi}\right)^{1/2} r \sin\vartheta \cdot e^{i\varphi - \mu c r},$$

$$u_5(r) = \left(\frac{\mu^5 c^5}{2\pi}\right)^{1/2} r \sin\vartheta \cdot e^{-i\varphi - \mu c r}.$$

Paper I sets forth the details of the wave-function calculations, except that the total potential energy of each atom is, in this case (using the symbols of Morse, Young, and Haurwitz),

$$V = -2Z(V_1 + V_2 + 2V_3) + 4V_{12} + 8V_{13} + 8V_{23} + V_{11} + V_{22} + 3V_{34} + 3V_{45} - 2X_{12} - 4X_{13} - 4X_{23} - 2X_{34} - X_{45}$$

and the kinetic energy is

$$T = 2T_1 + 2T_2 + 4T_3.$$

The tables of Morse and Yilmaz (1955) give the various components of V and T, which may be combined on an IBM card-programmed electronic calculator to give the total energy $W = -V^2/4T$ for many values of the parameters a, b, and c. A graphical minimization of W leads to the energy of each ion as well as the correct values of μ, a, b, and c. Table 1 lists the energies and wave-function parameters for each ion.

The formulae of Paper **I** give the spin-orbit parameter ζ and the spin-spin parameter η, except that the subsidiary quantity ξ is now equal to $\xi_{\text{nucleus}} + 2\xi_{1s} + 2\xi_{2s} + 3\xi_{2p}$, since the 2p electron moves in this case in the field of three other 2p electrons. Table 2 lists the resultant values of ζ and η, along with Garstang's (1951) empirical values. In contrast to the ζ's for the $1s^2 2s^2 2p^2$ sequence, which ran systematically about 2 or 3 per cent higher than the corresponding empirical parameters, our $1s^2 2s^2 2p^4$ results are about 5 per cent lower. Presumably, the increased number of interacting electrons has reduced our accuracy. The theoretical η's agree quite well with the empirical ones.

The present theoretical values for ζ and η represent an improvement (as was also the case for $1s^2 2s^2 2p^2$) over those obtained by Garstang from the Hartree-type wave functions, as Table 3 clearly shows. Finally, Garstang (1952) uses an extrapolated value of $\zeta = 21{,}690$ cm^{-1} and $\eta = 56$ cm^{-1} for *Ca* XIII ($Z = 20$). Our corresponding values are 20,790 cm^{-1} and 63.4 cm^{-1}. Thus Garstang's values appear quite reasonable, especially since our ζ's are systematically lower than the empirical ones.

TABLE 1

ENERGIES AND WAVE-FUNCTION PARAMETERS FOR THE $1s^2 2s^2 2p^4$ ISOELECTRONIC SEQUENCE

Z	W (Atomic Units)	a	b	c	μ
8	149.124	3.35	2.94	0.965	2.3
9	197.230	3.22	2.85	1.025	2.7
10	252.320	3.15	2.84	1.080	3.07
11	314.370	3.07	2.75	1.083	3.49
12	383.50	2.88	2.5	1.063	4.05
13	459.61	2.77	2.25	1.05	4.58
14	542.74	2.72	2.25	1.063	5.02
15	632.89	2.60	2	1.025	5.65
16	730.30	2.60	2	1.05	6.03
17	834.23	2.57	2	1.05	6.49
18	945.38	2.55	2	1.065	6.92
19	1063.54	2.55	2	1.075	7.33
20	1188.07	2.53	2	1.075	7.78

TABLE 2

THEORETICAL AND EMPIRICAL SPIN-ORBIT PARAMETERS ζ AND SPIN-SPIN PARAMETERS η FOR THE $1s^2 2s^2 2p^4$ ISOELECTRONIC SEQUENCE

Z	Ion	ζ_{theoret}	ζ_{emp}	η_{theoret}	η_{emp}
8	*O* I	124 cm^{-1}	146.6 cm^{-1}	1.18 cm^{-1}	1.33 cm^{-1}
9	*F* II	280	320.4	2.29	2.26
10	*Ne* III	577	607	3.96	4.3
11	*Na* IV	963	1041	5.86	5.8
12	*Mg* V	1562	1673	8.65	7.8
13	*Al* VI	2404	2565	12.05	10.9
14	*Si* VII	3579	3760	16.43	14
15	*P* VIII	4974	5350	21.0	.....
16	*S* IX	7032	7370	27.5	.....
17	*Cl* X	9397	.....	34.3	.....
18	*A* XI	12650	.....	43.4	.....
19	*K* XII	16410	.....	52.9	.....
20	*Ca* XIII	20790	.....	63.4	.....

I should like to thank Miss Marie M. Connors, of the Massachusetts Institute of Technology, Office of Statistical Services, for supervising the CPC calculations. The work reported herein was accomplished under the sponsorship of the Air Force Cambridge Research Center, Geophysics Research Directorate, through Contract AF19 (604)-146.

TABLE 3

COMPARISON OF THEORETICAL PARAMETERS (ALL IN CM^{-1})

Ion	Theoretical (Garstang)		Theoretical (Zirin)		Empirical (Garstang)	
	ζ	η	ζ	η	ζ	η
O I	184.6	1.15	124	1.18	146.6	1.33
Ne III	690	3.7	577	3.96	607	4.3

REFERENCES

Garstang, R. H. 1951, *M.N.*, **111**, 115.
———. 1952, *Ap. J.*, **115**, 569.
Morse, P. M., and Yilmaz, H. Unpublished (to be published in the *Astrophysical Supplements*).
Morse, P. M., Young, L. A., and Haurwitz, E. S. 1935, *Phys. Rev.*, **48**, 948.
Zirin, H. 1955, *Ap. J.*, **121**, 528.

VIBRATIONAL TRANSITION PROBABILITIES OF DIATOMIC MOLECULES; COLLECTED RESULTS. III. N_2, NO, O_2, O_2^+, OH, CO, CO^+*

W. R. JARMAIN, P. A. FRASER,† AND R. W. NICHOLLS
Department of Physics, University of Western Ontario, London, Canada
Received December 30, 1954

ABSTRACT

Arrays of approximate vibrational transition probabilities (i.e., overlap integral squares or "Franck-Condon factors") are presented for bands of the following molecular transitions of astrophysical interest:

N_2: $a\,^1\Pi_g \rightarrow X\,^1\Sigma_g^+$ (Lyman-Birge-Hopfield)
NO: $B\,^2\Pi \rightarrow X\,^2\Pi$ (β system)
O_2: $A\,^3\Sigma_u^+ \rightarrow X\,^3\Sigma_g^-$ (Herzberg)
$B\,^3\Sigma_u^- \rightarrow X\,^3\Sigma_g^-$ (Schumann-Runge)
O_2^+: $b\,^4\Sigma_g^- \rightarrow a\,^4\Pi_u$ (first negative)
OH: $A^2\Sigma^+ \rightarrow X\,^2\Pi$
CO: $a\,^3\Pi \rightarrow X\,^1\Sigma^+$ (Cameron)
$a'\,^3\Sigma^+ \rightarrow a\,^3\Pi$ (Asundi)
CO^+: $A\,^2\Pi \rightarrow X\,^2\Sigma^+$ (comet-tail)

INTRODUCTION

The spontaneous dipole transition probability for the transition giving rise to the emission of the $(v' \rightarrow v'')$ diatomic molecular band is proportional to the cube of the quantum energy and also to the vibrational transition probability $p(v', v'')$ which has been defined as

$$p(v', v'') = |\int \psi_1^{v'} R_e(r)\, \psi_2^{v''} d\boldsymbol{r}|^2$$

where $\psi_1^{v'}$ and $\psi_2^{v''}$ are the vibrational wave functions of the levels v' and v''; r is the internuclear separation; and $R_e(r)$ is the electronic dipole transition integral (Fraser 1954*a*).

The vibrational transition probability is the factor which largely controls the distribution of intensity among the bands of a molecular band system. Data on $p(v', v'')$ is thus essential to the interpretation of measured band intensities in terms of source conditions. In attempts to determine arrays of $p(v', v'')$ by theoretical means, it has been convenient to assume that $R_e(r)$ is a slowly varying function of r and therefore that

$$q(v', v'') = |\int \psi_1^{v'} \psi_2^{v''} d\boldsymbol{r}|^2$$

is an acceptable approximation to $p(v', v'')$. It has been suggested by Bates (1952) that $q(v', v'')$ should be called the "Franck-Condon factor" because the amount of overlap of $\psi_1^{v'}$ and $\psi_2^{v''}$ is one basis for the Franck-Condon principle; $q(v', v'')$ has also been termed the "overlap integral square."

A combination of recent theoretical and experimental studies on certain band systems has shown that the assumption of constancy of $R_e(r)$ is by no means necessarily valid (Fraser 1954*a*; Turner and Nicholls 1954*a*; Nicholls 1954; Wallace and Nicholls 1955).

* The research reported in this paper has been sponsored by the Geophysics Research Directorate, Air Force Cambridge Research Centre, Air Research and Development Command, under Contract AF 19(122)-470.

† Now at Department of Physics, University College, London, England.

It has nevertheless been shown (Fraser 1954*a*) that when R_e is not independent of r, it is often possible to write

$$p(v', v'') = R_e^2(\bar{r}_{v'v''})\, q(v', v''),$$

where $\bar{r}_{v'v''}$ is an average value of internuclear separation encountered in the $v' \rightarrow v''$ transition and is defined by

$$\bar{r}_{v'v''} = \frac{\int \psi^{v'} r \psi^{v''} d\tau}{\int \psi^{v'} \psi^{v''} d\tau}.$$

Indirect methods of evaluation of $\bar{r}_{v'v''}$ which do not involve lengthy computation have been developed, as has a method of determination of R_e as a function of r (Fraser 1954; Jarmain and Nicholls 1955).

THE FRANCK-CONDON FACTORS

The foregoing discussion shows that it remains important to accumulate data on $q(v', v'')$ for molecular band systems. A variety of methods of computation of $q(v', v'')$ are available (Pillow 1951; Bates 1952; Wu 1952; Fraser and Jarmain 1953; Jarmain and Fraser 1953; Jarmain and Nicholls 1954).

In Papers I and II of this series (Jarmain, Fraser, and Nicholls 1953; Fraser, Jarmain, and Nicholls 1954) an approximate method (Fraser and Jarmain 1953) was mentioned which enables the rapid computation of arrays of $q(v', v'')$ for a wide range of band systems. The basis of the method was to render the overlap integrals capable of analytic evaluation by means of an approximation. The approximation was to set the parameters a_1 and a_2 involved in the assumed Morse potentials,

$$U_i(r) = D_i[1 - \exp\{-a_i(r - r_{ei})\}]^2 \qquad (i = 1, 2),$$

of the electronic states 1 and 2 equal to some intermediate value a and to adjust the a-dependent parameters accordingly.

While this method was at once applicable to a wide range of band systems for which the approximation was valid, a series of improvements have now been made which widen the limits of application to almost any system, the potentials of which may be represented by Morse functions. These improvements are (*a*) the "r_e-shift," which improves the accuracy of the approximation (Jarmain and Fraser 1953); (*b*) development of remainder formulae (Jarmain and Fraser 1953), which avoid heavy numerical cancellation; and (*c*) an application of perturbation theory which allows corrections of the $q(v', v'')$ from neighboring entries in the table (Fraser 1954*b*). The amount of calculation involved in the method is now sufficiently reduced so that an array of about thirty values of $q(v', v'')$ for a system may be computed on a desk calculator in about a day.

RESULTS

Arrays of q-values for band systems of N_2, NO, O_2, O_2^+, OH, CO, and CO^+ are shown in Tables 1–9. The perturbation theory correction was applied in Tables 2, 5, 6, and 8. The basic molecular constants used in this calculation are given in Table 10, and Table 11 shows the value of a employed for each system. Classification of these results into the three sections employed in Papers I and II (namely, "Excellent," "Satisfactory," and "Indicative of trends") has been indicated on each table.

DISCUSSION

The q-values have been calculated to three significant figures, and, to preserve uniformity with previous papers of this series, tables have been set up to show three decimal places in most cases. The third decimal place is merely suggestive. However, in

TABLE 1*

N_2: a $^1\Pi_g \rightarrow X\ ^1\Sigma_g^+$ (LYMAN-BIRGE-HOPFIELD)

$q\ (v', v'')$

v'	v''							
	0	1	2	3	4	5	6	7
0	0.05_1	0.16_7	0.25_7	0.24_4	0.16_1	0.07_9	0.02_9	0.00_9
1	$.13_2$	$.19_4$	$.06_5$	$.00_4$	$.10_4$	$.19_0$	$.16_9$	
2	$.18_5$	$.08_2$	$.01_0$	$.11_8$	$.07_2$	0.00_0		
3	$.19_0$	$.00_5$	$.09_1$	$.05_5$	0.00_9			
4	$.15_8$	$.01_6$	$.09_3$	0.00_1				
5	$.11_4$	$.06_4$	0.03_4					
6	$.07_4$	0.09_9						
7	0.04_4							

* Classification: Excellent.

TABLE 2*

NO: B $^2\Pi \rightarrow X\ ^2\Pi$ (β SYSTEM)

$q\ (v', v'')$

v'	v''												
	0	1	2	3	4	5	6	7	8	9	10	11	12
0	0.00_0	0.00_1	0.00_7	0.02_3	0.05_2	0.09_1	0.12_7	0.14_7	0.13_2	0.12_4	0.10_7	0.08_6	0.06_6
1	$.00_1$	$.00_7$	$.02_8$	$.06_2$	$.09_1$	$.08_9$	$.06_2$	$.04_4$	$.05_0$	$.05_0$	$.07_3$	$.08_4$	$.08_4$
2	0.00_3	0.01_7	0.04_8	0.07_1	0.06_5	0.03_7	0.05_4	0.04_9	0.06_0	0.04_2	0.01_6	0.01_8	0.04_9

* Classification: $v' \leq 1$ and $v'' \leq 7$, Excellent. Remainder of table, Indicative of trends. q-values for $\frac{3}{2} \rightarrow \frac{3}{2}$ have been combined with those for $\frac{1}{2} \rightarrow \frac{1}{2}$ in the ratio 2:1.

TABLE 3*

O_2: A $^3\Sigma_u^+ \rightarrow X\ ^3\Sigma_g^-$ (HERZBERG)

$q\ (v', v'')$

v'	v''										
	0		1	2	3	4	5	6	7	8	9
0	0.00_0	$6.5_1\times10^{-7}$	0.00_0	0.00_0	0.00_1	0.00_3	0.01_2	0.03_0	0.06_2	0.10_4	0.14_4
1	$.00_0$	$5.4_8\times10^{-6}$	$.00_0$	$.00_1$	$.00_4$	$.01_5$	$.03_9$	$.07_3$	$.10_0$	0.09_7	
2	$.00_0$	$2.4_4\times10^{-5}$	$.00_0$	$.00_3$	$.01_2$	$.03_3$	$.06_5$	$.08_4$	0.06_6		
3	$.00_0$	$7.6_9\times10^{-5}$	$.00_1$	$.00_6$	$.02_3$	$.05_1$	$.07_2$	0.05_7			
4	$.00_0$	$1.9_3\times10^{-4}$	$.00_2$	$.01_2$	$.03_5$	$.06_1$	0.05_7				
5	$.00_0$	$4.0_4\times10^{-4}$	$.00_4$	$.01_8$	$.04_4$	0.05_8					
6	$.00_1$	$7.5_1\times10^{-4}$	$.00_6$	$.02_5$	0.05_0						
7	$.00_1$	$1.2_5\times10^{-3}$	$.00_9$	0.03_1							
8	$.00_2$	$1.9_2\times10^{-3}$	0.01_3								
9	$.00_3$	$2.7_6\times10^{-3}$									
10	0.00_4	$3.7_1\times10^{-3}$									

* Classification: Excellent. Vibrational assignment according to Herzberg (1952).

TABLE 4*

O_2: B $^3\Sigma_u^- \rightarrow$ X $^3\Sigma_g^-$ (SCHUMANN-RUNGE)
Small q (v', v'')

v'	v''			v'	v''		
	0	1	2		0	1	2
0	$2.3_1\times10^{-9}$	$6.2_5\times10^{-8}$	$8.1_2\times10^{-7}$	8	$6.1_2\times10^{-5}$	$8.1_2\times10^{-4}$	$4.8_0\times10^{-3}$
1	$2.6_9\times10^{-8}$	$6.6_4\times10^{-7}$	$7.8_4\times10^{-6}$	9	$1.0_8\times10^{-4}$	$1.3_2\times10^{-3}$	$7.0_7\times10^{-3}$
2	$1.6_4\times10^{-7}$	$3.6_9\times10^{-6}$	$5.6_1\times10^{-5}$	10	$1.8_0\times10^{-4}$	$2.0_2\times10^{-3}$	$9.7_2\times10^{-3}$
3	$6.9_4\times10^{-7}$	$1.4_3\times10^{-5}$	$1.3_9\times10^{-4}$	11	$2.7_9\times10^{-4}$	$2.8_9\times10^{-3}$	$1.2_5\times10^{-2}$
4	$2.2_8\times10^{-6}$	$4.3_2\times10^{-5}$	$3.8_0\times10^{-4}$	12	$4.1_6\times10^{-4}$	$3.9_4\times10^{-3}$	$1.5_4\times10^{-2}$
5	$6.3_0\times10^{-6}$	$8.4_8\times10^{-5}$	$8.6_4\times10^{-4}$	13	$5.8_8\times10^{-4}$	$5.1_3\times10^{-3}$	$1.8_2\times10^{-2}$
6	$1.5_0\times10^{-5}$	$2.3_7\times10^{-4}$	$1.7_1\times10^{-3}$	14	$7.9_2\times10^{-4}$	$6.4_2\times10^{-3}$	$2.0_4\times10^{-2}$
7	$3.1_8\times10^{-5}$	$4.6_2\times10^{-4}$	$3.0_0\times10^{-3}$	15	$1.0_4\times10^{-3}$	$7.7_4\times10^{-3}$	$2.2_2\times10^{-2}$

* Classification: Indicative of trends.

TABLE 5*

O_2^+: b $^4\Sigma_g^- \rightarrow$ a $^4\Pi_u$ (FIRST NEGATIVE)
$q(v', v'')$

v'	v''							
	0	1	2	3	4	5	6	7
0	0.26_5	0.29_6	0.20_9	0.11_9	0.06_0	0.02_8	0.01_3	0.00_9
1	$.42_9$	$.02_2$	$.04_3$	$.13_0$	$.13_6$	$.10_4$	0.07_4	
2	$.24_3$	$.18_2$	$.14_3$	$.00_6$	$.02_2$	0.01_1		
3	$.05_8$	$.35_1$	$.02_6$	$.16_0$	0.08_7			
4	$.00_5$	$.14_4$	$.34_5$	0.03_1				
5	$.00_0$	$.01_6$	0.26_7					
6	$.00_0$	0.00_3						
7	0.00_0							

* Classification: $v' + v'' \leq 6$, Excellent. $v' + v'' = 7$, Indicative of trends.

TABLE 6*

OH: A $^2\Sigma^+ \rightarrow$ X $^2\Pi$
$q(v', v'')$

v'	v''							
	0	1	2	3	4	5	6	7
0	0.90_7	0.08_9	0.00_3	0.00_0	0.00_0	0.00_0	0.00_0	0.00_0
1	$.08_8$	$.71_6$	$.18_6$	$.01_2$	$.00_0$	$.00_0$	0.00_0	
2	$.00_6$	$.16_9$	$.51_4$	$.28_0$	$.03_2$	0.00_0		
3	$.00_0$	$.02_3$	$.23_7$	$.32_1$	0.32_9			
4	$.00_0$	$.00_2$	$.05_4$	0.25_3				
5	$.00_0$	$.00_0$	0.00_7					
6	$.00_0$	0.00_0						
7	0.00_0							

* Classification: $v' + v'' \leq 6$, Excellent. $v' + v'' = 7$, Indicative of trends.

TABLE 7*

CO: a $^3\Pi \rightarrow X\ ^1\Sigma^+$ (CAMERON)

$q(v', v'')$

v'	v''						
	0	1	2	3	4	5	6
0	0.26_8	0.38_6	0.23_9	0.08_8	0.02_1	0.00_4	0.00_0
1	$.32_0$	$.02_8$	$.10_5$	$.26_8$	$.18_9$	0.05_1	
2	$.21_9$	$.05_4$	$.15_8$	$.00_0$	0.15_2		
3	$.11_3$	$.16_1$	$.00_8$	0.13_5			
4	$.04_9$	$.16_3$	0.03_9				
5	$.01_9$	0.10_9					
6	0.00_7						

* Classification: Excellent.

TABLE 8*

CO: a′ $^3\Sigma^+ \rightarrow$ a $^3\Pi$ (ASUNDI)

$q(v', v'')$

v'	v''			v'	v''		
	0	1	2		0	1	2
0	0.03_7	0.14_3	0.24_3	7	0.05_9	0.10_2	0.00_1
1	$.10_3$	$.19_5$	$.09_7$	8	$.03_6$	$.09_9$	$.00_6$
2	$.16_2$	$.10_9$	$.00_0$	9	$.02_1$	$.08_2$	$.02_3$
3	$.18_1$	$.01_9$	$.05_0$	10	$.01_9$	$.06_4$	$.04_1$
4	$.16_5$	$.00_3$	$.05_9$	11	$.01_2$	$.05_0$	$.05_2$
5	$.12_9$	$.03_9$	$.06_7$	12	0.00_7	0.03_8	0.05_5
6	0.09_1	0.08_1	0.02_4				

* Classification: $v' \leq 9$ and $v'' \leq 1$, Excellent. Remainder of table, Satisfactory.

TABLE 9*

CO^+: A $^2\Pi \rightarrow X\ ^2\Sigma^+$ (COMET-TAIL BANDS)

$q(v', v'')$

v'	v''							
	0	1	2	3	4	5	6	7
0	0.04_2	0.14_9	0.24_6	0.24_9	0.17_4	0.08_9	0.03_5	0.01_1
1	$.11_3$	$.19_1$	$.08_3$	$.00_0$	$.08_4$	$.18_3$	0.18_0	
2	$.16_6$	$.09_9$	$.00_2$	$.10_4$	$.08_9$	0.00_1		
3	$.18_0$	$.01_5$	$.07_1$	$.07_2$	0.00_2			
4	$.15_9$	$.00_4$	$.09_6$	0.00_1				
5	$.12_2$	$.04_1$	0.05_1					
6	$.08_5$	0.07_8						
7	$.05_5$							
8	0.03_4							

* Classification: Excellent.

two cases—for the Herzberg and Schumann-Runge systems of O_2 (Tables 3 and 4)—where q-values are very small, they have been reported to two significant figures. These values, particularly for bands of small v'', may be of use in atmospheric absorption studies. While the numbers in Table 4 are unimproved, the relative magnitudes should nevertheless be useful.

In Table 3, for the Herzberg system, no change was made in the molecular constants from which the q-values were computed, because of the revision of vibrational assignment suggested by Broida and Gaydon (1954), as this small change in vibrational assignment will not make a very large change in the q-values (see, e.g., Dr. Pillow's work

TABLE 10

MOLECULAR CONSTANTS*

Molecule	State	α (A^{-1})	$K=\omega_e/\omega_e x_e$	r_e (A)
N_2	a $^1\Pi_g$	2.3050	132.28	1.213
	X $^1\Sigma_g^+$	2.4505	163.23	1.094
NO	B $^2\Pi_{3/2}$	1.835	136.6	1.385
	B $^2\Pi_{1/2}$	1.835	136.4	1.448
	X $^2\Pi_{3/2}$	2.488	136.3	1.1508
	X $^2\Pi_{1/2}$	2.488	136.3	1.1508
O_2	A $^3\Sigma_u^+$†	2.560	55.98	1.5341
	B $^3\Sigma_u^-$	1.9486	87.52	1.604
	X $^3\Sigma^-$	2.3934	130.90	1.20740
O_2^+	b $^4\Sigma_g^-$	2.848	70.03	1.27953
	a $^4\Pi_u$	2.220	99.68	1.38126
OH	A $^2\Sigma^+$	2.3107	33.504	1.0121
	X $^2\Pi$	2.1582	45.106	0.9706
CO	a' $^3\Sigma^+$	1.97	128.00	1.359
	a $^3\Pi$	2.426	120.2	1.2093
	X $^1\Sigma^+$	2.3400	161.22	1.1282
CO^+	A $^2\Pi$	2.3461	115.43	1.24368
	X $^2\Sigma^+$	2.4835	146.02	1.11506

* Except where otherwise indicated, the source is G. Herzberg, *Molecular Spectra and Molecular Structure*, Vol. 1: *Diatomic Molecules* (2d ed.; New York: D. Van Nostrand Co., 1950).

† Herzberg (1952).

TABLE 11

CHOSEN MEAN α-VALUES *

Molecule	Transition	α (A^{-1})	Molecule	Transition	α (A^{-1})
N_2	a→X	2.3778	O_2^+	b→a	2.534
NO	$B(\frac{3}{2})\rightarrow X(\frac{3}{2})$	2.161	OH	A→X	2.2344
NO	$B(\frac{1}{2})\rightarrow X(\frac{1}{2})$	2.045	CO	a→X	2.383
O_2	A→X	2.477	CO	a'→a	2.38
O_2	B→X	2.0520	CO^+	A→X	2.4148

* The α-dependent parameters are adjusted to correspond to the chosen mean α as in Fraser and Jarmain (1953) and Jarmain and Fraser (1953).

on the same system, 1953*a*, *b*). It should be noted, however, that an observed band which was previously called (v', v'') should now have its intensity compared with $q(v' + 1, v'')$ as a result of this change in assignment.

Because of the splitting of the upper and lower states of the *NO* β system, q-values were calculated separately for each of the electronic transitions involved ($\Omega = \frac{3}{2} \rightarrow \frac{3}{2}$; $\Omega = \frac{1}{2} \rightarrow \frac{1}{2}$) and then combined in the ratio of the statistical weights (2:1) for comparison with the observed individual bands.

REFERENCES

Bates, D. R. 1952, *M.N.*, **112**, 614.
Broida, H. P., and Gaydon, A. G. 1954, *Proc. R. Soc. London, A*, **222**, 181.
Fraser, P. A. 1954*a*, *Canad. J. Phys.*, **32**, 515.
———. 1954*b*, *Proc. Phys. Soc. A*, **67**, 939.
Fraser, P. A., and Jarmain, W. R. 1953, *Proc. Phys. Soc. London, A*, **66**, 1145.
Fraser, P. A., Jarmain, W. R., and Nicholls, R. W. 1954, *Ap. J.*, **119**, 286.
Herzberg, G. 1952, *Canad. J. Phys.*, **30**, 185.
Jarmain, W. R., and Fraser, P. A. 1953, *Proc. Phys. Soc. London, A*, **66**, 1153.
Jarmain, W. R., Fraser, P. A., and Nicholls, R. W. 1953, *Ap. J.*, **118**, 228.
Jarmain, W. R., and Nicholls, R. W. 1954, *Canad. J. Phys.*, **32**, 201.
———. 1955, *Scientific Report No. 20* (Contract AF 19(122)-470, Department of Physics, University of Western Ontario).
Nicholls, R. W. 1954, *Phys. Rev.*, **94**, 1423.
Pillow, M. E. 1951, *Proc. Phys. Soc. London, A*, **64**, 772.
———. 1953*a*, *ibid.*, **66**, 733.
———. 1953*b*, *ibid.*, p. 1064.
Turner, R. G., and Nicholls, R. W. 1954*a*, *Canad. J. Phys.*, **32**, 468.
———. 1954*b*, *ibid.*, p. 475.
Wallace, L. V., and Nicholls, R. W. 1955, *J. Terr. and Atm. Phys.*, Vol. **6** (in press).
Wu, T. Y. 1952, *Proc. Phys. Soc. London, A*, **65**, 965.

THE SPECTRUM OF NGC 7027

L. H. ALLER, I. S. BOWEN, AND R. MINKOWSKI
University of Michigan Observatory
Mount Wilson and Palomar Observatories
Carnegie Institution of Washington, California Institute of Technology
Received January 31, 1955

ABSTRACT

A total of 263 lines was observed in the spectrum of NGC 7027 with the spectrographs of the 100- and 200-inch telescopes. Intensity measurements and identifications were made for most of these lines. This nebula shows an exceedingly wide range of ionization, forty ions ranging from *Mg* I to *Fe* VII being observed. The 4F–nG and 5G–nH series of *He* II were followed to $n = 29$ and $n = 40$, respectively, and the somewhat abnormal progression of observed intensities along these series was given a theoretical interpretation.

I. INTRODUCTION

A comprehensive study of the physical state and chemical composition of gaseous nebulae is dependent upon an accurate knowledge of their spectra. The most detailed studies were those of Bowen and Wyse (1939), who investigated NGC 6572, NGC 7027, and NGC 7662, and of Wyse (1942), who extended the investigation to six additional planetaries and the Orion Nebula. These studies, carried out with the aid of the Lick 36-inch refractor and a spectrograph equipped with Bowen's (1938) image slicer, gave the wave length, identifications, and approximate intensities of nebular lines observed between the Balmer limit and λ 6755. The wave lengths, the identifications, and even the reality of many of the fainter lines required confirmation by the more powerful spectrographic equipment that has been developed in the last fifteen years. The intensities published by Wyse represent eye-estimates made with the aid of scale plates; they should be replaced by photometrically measured intensities whenever possible.

The most rewarding of planetary nebulae for a detailed spectroscopic study is NGC 7027. This object shows the richest line spectrum of all gaseous nebulae. Probably every line observable in any planetary is represented here. There is a huge range in excitation from *N* I to *Fe* VII. Furthermore, the nebula has a higher surface brightness than any other planetary nebula. All observable radiation comes from the nebular lines plus continuum. There is no direct contribution from any central star. The latter must have a temperature well in excess of 150,000° K. A number of observers have published reproductions of the spectrum (see, e.g., Wyse 1942 and Aller 1954).

II. OBSERVATIONAL PROCEDURE

The present investigation comprises two sets of data: (*a*) wave lengths and identifications of the nebular lines based on plates taken with the coudé spectrograph of the Hale 200-inch telescope and (*b*) relative line intensities primarily from a photometric study carried out with the 100-inch reflector and Cassegrain spectrograph.

The detailed spectrophotometric procedures will be described in a separate communication (Minkowski and Aller 1955). They consisted in photographing the spectrum of NGC 7027 beside that of a suitable comparison star thrown out of focus on a ground-quartz diffuser placed in front of the slit. Vega and ε Persei served as comparison stars. A laboratory calibration provided the transmissivity of the diffuser. Step-slit spectra of a lamp, obtained with the photometric calibration accessory of the 100-inch coudé, provided the density-intensity relationship. In addition to the Mount Wilson data, which covered the spectral range λλ 3600–9000, observations of the λλ 3200–5000 range

were obtained at the McDonald Observatory with the Cassegrain spectrograph equipped with quartz prisms.

The essential information relative to the equipment, emulsions, and dispersions employed at Palomar is given in Table 1. Successive columns give the plate number, the camera used, the order of the grating, the wave-length region, the dispersion in A/mm, the emulsion type, and the exposure times. Overlapping order occurred in some spectral regions.

III. OBSERVATIONAL RESULTS

Table 2 contains the essential results of this investigation. The four columns give the wave length, the ion, the electron transition, and the intensity measured at the brightest part of the nebula.

The plates used for the intensity measures had a much lower dispersion than those employed for the wave lengths. Hence many of the lines whose intensities are measured as blends are resolved on the Palomar plates. Accordingly, we have used tracings of the Palomar plates to allocate the relative intensity contributions in blends. Unfortunately, the earlier Palomar plates were secured before the calibration spectrograph was available; hence they contain no calibration. We can interpolate the relative intensities of the lines in a blend with the aid of other lines on the plate whose intensities had been determined photometrically. The continuum is so very strong that even on the calibrated Palomar plates the intensities of the weaker lines can be measured only very roughly. The footnotes to the table contain remarks on certain individual lines. A colon (:) means that the tabulated line intensity is very uncertain.

TABLE 1

OBSERVATIONS OF NGC 7027 OBTAINED AT PALOMAR

Plate	Camera	Grating Order	Wave-Length Range (A)	Dispersion (A/Mm)	Emulsion	Exposure (Min.)
Pc 151	36-in	3–4	3300–5000	6.7–9.0	Baked 103-O	1265
Pe 358	8.4-in	2	5700–6700	56	103*a*-E	435
Pd 1039	18-in	2	5500–8500	27	103*a*-F+IN	1132
Pd 1040	18-in	2	5400–8100	27	103*a*-F+IN	100
Pd 1042	18-in	2–3–4	3300–5400	13.5–18–27	Baked 103*a*-J	1192
Pd 1555	18-in	2	5300–8600	27	103*a*-D+IN	430
Pe 1556	8.4-in	2	4700–5700	56	103*a*-D	330
Pe 1811	8.4-in	3	4400–5000	38	Baked II*a*-O	440
Pe 1814	8.4-in	3	3700–4400	38	Baked II*a*-O	425

The intensities of the far-ultraviolet lines λ 3202 *He* I and λ 3133 are adopted from earlier work by one of us (Aller 1941). Their intensities relative to the nearest lines for which we have photometric data from the present study have been utilized to reduce them to the present system. The intensities of all lines are given on the scale $I(H\beta) = 100$.

A comparison of the present relative intensities with those given by Wyse shows that his eye-estimates were remarkably accurate, considering the crudeness of his calibration. No sizable scale error appears to have existed, but the zero point of his intensity scale in the visual region appears to be shifted with respect to the intensity in the photographic region.

IV. THE PROBLEM OF THE IDENTIFICATIONS

The Palomar plates showed many weak lines that could not be resolved or observed on the Mount Wilson spectra. On the other hand, there were a few lines that were ob-

TABLE 2

SPECTRUM OF NGC 7027

Wave Length	Ion	Transition	Intensity
3132.82	*O* III	$3p\,^3S-3d\,^3P_2$	20:
3203.15	*He* II	3^2D-5^2F	7:
3299.58	*O* III	$3s\,^3P_0-3p\,^3S$	3.5
3312.35	*O* III	$3s\,^3P_1-3p\,^3S$	11.3
3340.78	*O* III	$3s\,^3P_2-3p\,^3S$	16.0
3345.82	[*Ne* V]	$^3P_1-^1D$	24:
3386.03	.....	.....	0.5
3411.84	*O* IV	$3^2P_{3/2}-3^2D_{5/2}$	1.1
3425.84	[*Ne* V]	$^3P_2-^1D$	60:
3428.70	*O* III	$3p\,^3P_1-3d\,^3P_2$	
3444.05	*O* III	$3p\,^3P_2-3d\,^3P_2$	30:
3554.4	*He* I	2^3P-10^3D	0.3
3587.05	*He* I	2^3P-9^3D	0.8
3634.20	*He* I	2^3P-8^3D	0.8
3666.00	*H* I	2^2P-27^2D	.....
3667.68	*H* I	2^2P-26^2D	.....
3669.47	*H* I	2^2P-25^2D	.....
3671.48	*H* I	2^2P-24^2D	0.6
3673.70	*H* I	2^2P-23^2D	0.8
3676.31	*H* I	2^2P-22^2D	0.9
3679.39	*H* I	2^2P-21^2D	0.9
3682.81	*H* I	2^2P-20^2D	1.0
3686.88	*H* I	2^2P-19^2D	1.1
3691.53	*H* I	2^2P-18^2D	1.3
3697.21	*H* I	2^2P-17^2D	1.4
3703.81	*H* I	2^2P-16^2D	1.7
3705.04	*He* I	2^3P-7^3D	0.7
3711.95	*H* I	2^2P-15^2D	1.8
3715.27	*He* II	4^2F-29^2G	0.7
3721.81	*H* I	2^2P-14^2D [*S* III] $^3P_1-^1S$	4.3
3725.99	[*O* II]	$^4S-^2D_{3/2}$	9.4
3728.76	[*O* II]	$^4S-^2D_{5/2}$	4.6
3732.97	*He* II	4^2F-26^2G	0.7
3734.34	*H* I	2^2P-13^2D	2.3
3736.70	*O* IV	$3p\,^4D_{7/2}-3d\,^4F_{9/2}$	0.9
3740.16	*He* II	4^2F-25^2G	0.6
3744.78	.....	.....	.....
3748.77	*He* II	4^2F-24^2G	0.6
3750.19	*H* I	2^2P-12^2D	2.7
3754.69	*O* III	$3s\,^3P_1-3p\,^3D_2$	1.4
3757.24	*O* III	$3s\,^3P_0-3p\,^3D_1$	0.8
3759.87	*O* III	$3s\,^3P_2-3p\,^3D_3$	3.8
3768.86	*He* II	4^2F-22^2G	0.7
3770.66	*H* I	2^2P-11^2D	3.3
3773.95	*O* III	$3s\,^3P_1-3p\,^3D_1$	0.7
3781.74	*He* II	4^2F-21^2G	0.8
3791.29	*O* III	$3s\,^3P_2-3p\,^3D_2$	0.7
3797.91	*H* I	2^2P-10^2D	3.5
3813.50	*He* II	4^2F-19^2G	0.7
3819.66	*He* I	2^3P-6^3D	1.1
3833.75	*He* II	4^2F-18^2G	0.6
3835.41	*H* I	2^2P-9^2D	4.6
3839.57	[*Fe* V]	$^5D_3-^3F_3$	.....
3851.81	[*Fe* V]	$^5D_3-^3F_2$	.....
3856.17	*Si* II	$3p^2\,^2D_{5/2}-4^2P_{3/2}$	0.3
3857.99	*He* II	4^2F-17^2G	0.8
3862.67	*Si* II	$3p^2\,^2D_{3/2}-4^2P_{1/2}$	0.3
3868.73	[*Ne* III]	$^3P_2-^1D$	51.
3888.91	*H* I	2^2P-8^2D *He* I 2^3S-3^3P	8.8

TABLE 2—*Continued*

Wave Length	Ion	Transition	Intensity
3891.28	[*Fe* V]	$^5D_4-{}^3F_4$	0.4
3895.61	[*Fe* V]	$^5D_3-{}^3P_2$	0.4
3920.89	*C* II	$3^2P_{3/2}-4^2S$	
3923.56	*He* II	4^2F-15^2G	0.6
3926.50	*He* I	2^1P-8^1D	0.4
3956.82			0.2
3964.88	*He* I	2^1S-4^1P	24.4
3967.46	[*Ne* III]	$^3P_1-{}^1D$	
3970.07	*H* I	2^2P-7^2D	
3997.36	[*F* IV]	$^3P_1-{}^1D$	0.2
4003.28			
4009.17	*He* I	2^1P-7^1D	0.4
4026.12	*He* I	2^3P-5^3D *He* II 4^2F-13^2G	2.0
4060.26	[*F* IV]	$^3P_2-{}^1D$	0.3
4068.62	[*S* II]	$^4S-{}^2P_{3/2}$	4.5
4070.27	*C* III	$4^3F_4-5^3G_5$ [*Fe* III] $^5D_4-{}^3G_5$	0.4
4072.14	[*Fe* V]	$^5D_2-{}^3P_1$	0.3
4076.33	[*S* II]	$^4S-{}^2P_{1/2}$	2.2
4089.15	*O* II	$3d^4F_{9/2}-4f^4G_{11/2}$	
4097.37	*N* III	$3^2S-3^2P_{3/2}$	2.0
4100.08	*He* II	4^2F-12^2G	16.3
4101.74	*H* I	2^2P-6^2D	
4103.46	*N* III	$3^2S-3^2P_{1/2}$	
4119.16	*O* II	$3p^4P_{5/2}-3d^4D_{7/2}$	
4120.80	*He* I	2^3P-5^3S	0.3
4122.60	[*K* V]	$^4S-{}^2D_{5/2}$	0.2
4128.74			0.3
4143.76	*He* I	2^1P-6^1D	0.5
4146.05			
4156.35	*C* III	$3^3D_2-5^3F_3$	0.4
4163.33	[*K* V]	$^4S-{}^2D_{3/2}$	0.3
4180.92	[*Fe* V]	$^5D_1-{}^3P_0$	0.2
4186.98	*C* III	4^1F-5^1G	0.5
4189.84	*O* II	$3p^2F_{7/2}-3d^2G_{9/2}$	
4199.88	*He* II	4^2F-11^2G	1.5
4227.37			0.5
4267.13	*C* II	3^2D-4^2F	0.9
4325.74	*C* III	$3s\ ^1P-3p^1D$	
4338.62	*He* II	4^2F-10^2G	33
4340.44	*H* I	2^2P-5^2D	
4363.19	[*O* III]	$^1D-{}^1S$	21
4379.07	*N* III	4^2F-5^2G	0.5
4387.97	*He* I	2^1P-5^1D	1.7
4437.59	*He* I	2^1P-5^1S	
4471.50	*He* I	2^3P-4^3D	3.9
4510.79	[*K* IV]	$^1D-{}^1S$	0.7:
4541.60	*He* II	4^2F-9^2G	2.3
4552	*Si* III	$4^3S-4^3P_2$	0.4
4571.24	*Mg* I	$3^1S-3^3P_1$	0.9
4606.51	[*Fe* III]	$^5D_4-{}^3F_3$	0.5
4625.54	[*A* V]	$^1D-{}^1S$	0.5
4631.96			
4634.15	*N* III	$3^2P_{1/2}-3^2D_{3/2}$	2.8
4640.62	*N* III	$3^2P_{3/2}-3^2D_{5/2}$	3.6
4641.93	*N* III	$3^2P_{3/2}-3^2D_{3/2}$	0.6
4647.46	*C* III	$3^3S-3^3P_2$	1.4
4649.08	*O* II	$3s^4P_{5/2}-3p^4D_{7/2}$	0.4
4650.27	*C* III	$3^3S-3^3P_1$	0.6
4657.68			1.6
4658.42	*C* IV	5^2G-6^2H [*Fe* III] $^5D_4-{}^3F_4$	
4685.71	*He* II	3^2D-4^2F	45

TABLE 2—*Continued*

Wave Length	Ion	Transition	Intensity
4701.45	[*Fe* III]	$^5D_3-{}^3F_3$	.....
4711.34	[*A* IV]	$^4S-{}^2D_{5/2}$	2.8
4713.17	*He* I	2^3P-4^3S	0.7
4714.26	[*Ne* IV]	$^2D_{5/2}-{}^2P_{3/2}$	0.8
4715.65	[*Ne* IV]	$^2D_{5/2}-{}^2P_{1/2}$	0.5
4724.16	[*Ne* IV]	$^2D_{3/2}-{}^2P_{3/2}$	1.3
4725.60	[*Ne* IV]	$^2D_{3/2}-{}^2P_{1/2}$	1.3
4733.68	[*Fe* III]	$^5D_2-{}^3F_2$	.....
4740.20	[*A* IV]	$^4S-{}^2D_{3/2}$	11
4754.9	[*Fe* III]	$^5D_3-{}^3F_4$	0.4
4859.32	*He* II	4^2F-8^2G	100
4861.30	*H* I	2^2P-4^2D	
4893.42	*Fe* VII	$^3F_2-{}^3P_1$	0.6
4921.96	*He* I	2^1P-4^1D	3.1
4930.97	[*O* III]	$^3P_0-{}^1D$	<0.5
4944.01	[*Fe* VII]	$^3F_3-{}^3P_2$	.....
4950.48	.....	.....	.....
4958.95	[*O* III]	$^3P_1-{}^1D$	420
4972.12	[*Fe* VI]	$^4F_{5/2}-{}^2G_{7/2}$	.....
5006.88	[*O* III]	$^3P_2-{}^1D$	1170
5015.55	*He* I	2^1S-3^1P	.....
5041.31	*Si* II	$4^2P_{1/2}-4^2D_{3/2}$	1.6
5047.92	*He* I	2^1P-4^1S	1.4
5056.45	*Si* II	$4^2P_{3/2}-4^2D_{5/2}$	1.5
5090	.....	.....	0.5
5112	*O* V	3^1S-3^1P	0.5
5131.18	.....	.....	0.6
5145.78	[*Fe* VI]	$^4F_{7/2}-{}^2G_{7/2}$	0.9
5158.94	[*Fe* VII]	$^3F_3-{}^3P_1$	0.6
5161.67	.....	.....	
5176.42	[*Fe* VI]	$^4F_{9/2}-{}^2G_{9/2}$	0.9
5191.81	[*A* III]	$^1D-{}^1S$	0.9:
5197.95	[*N* I]	$^4S-{}^2D_{3/2}$	1.2:*
5200.41	[*N* I]	$^4S-{}^2D^5/_2$	0.3:*
5216	.....	.....	0.5
5232	.....	.....	0.4
5262.00	.....	.....	.....
5270.28	[*Fe* III]	$^5D_3-{}^3P_2$	0.3:
5277.76	[*Fe* VII]	$^3F_4-{}^3P_2$	0.3:
5309.17	[*Ca* V]	$^3P_2-{}^1D$	1.7
5323.26	[*Cl* IV]	$^1D-{}^1S$	1.0
5335.22	[*Fe* VI]	$^4F_{3/2}-{}^4P_{1/2}$	1.2
5345.98	.....	.....	1.2
5411.54	*He* II	4^2F-7^2G	9
5423.87	[*Fe* VI]	$^4F_{5/2}-{}^4P_{3/2}$	0.4:
5426.57	[*Fe* VI]	$^4F_{7/2}-{}^4P_{5/2}$	0.2:
5470.93	.....	.....	0.4:
5484.79	[*Fe* VI]	$^4F_{5/2}-{}^4P_{1/2}$	0.5:
5517.72	[*Cl* III]	$^4S-{}^2D_{5/2}$	1.0
5537.80	[*Cl* III]	$^4S-{}^2D_{3/2}$	2.7
5577.36	[*O* I]	$^1D-{}^1S$	1.5
5592.17	*O* III	$3s^1P-3p^1P$	1.1
5604	[*K* VI]	$^3P_1-{}^1D$	0.6
5614.65	[*Ca* VII]	$^3P_2-{}^1D$	.....
5630.88	[*Fe* VI]	$^4F_{7/2}-{}^4P_{3/2}$	0.7
5677.01	[*Fe* VI]	$^4F_{9/2}-{}^4P_{5/2}$	1.1
5696.06	*C* III	3^1P-3^1D	.....
5721.13	[*Fe* VII]	$^3F_2-{}^1D$	1.2

* These lines correspond to the 3726/2729 pair of [*O* II]. Their intensity ratio, which does not agree with the theoretical predictions of Ufford and Gilmour (*Ap. J.*, **111**, 580, 1950) and of Garstang (*Ap. J.*, **115**, 506, 1952), is probably affected by collisional effects, as is the 3727 pair of [*O* II].

TABLE 2—*Continued*

Wave Length	Ion	Transition	Intensity
5726.12			
5754.59	[*N* II]	$^1D-^1S$	12
5776.37	[*Mn* VI]	$^3F_3-^3P_1$	
5786.59	*He* II	5^2G-40^2H	
5790.85	*He* II	5^2G-39^2H	
5794.64	*He* II	5^2G-38^2H	
5801.38	*C* IV	$3^2S-3^2P_{3/2}$	2.2
5806.29	*He* II	5^2G-36^2H	
5812.12	*C* IV	$3^2S-3^2P_{1/2}$	1.1
5820.14	*He* II	5^2G-34^2H	
5828.64	*He* II	5^2G-33^2H	
5836.50	*He* II	5^2G-32^2H	0.3:
5847.14	*He* II	5^2G-31^2H	
5858.33	*He* II	5^2G-30^2H	
3862.34			
5864.81	[*Mn* V]	$^4F_{7/2}-^2G_{7/2}$	
5867.82	*He* II	5^2G-29^2H *Si* II $3p4s^4P_{5/2}-3p4p^4P_{5/2}$	
5875.63	*He* I	2^3P-3^3D	24
5882.35	*He* II	5^2G-28^2H	
5885.90			
5890.98	[*Mn* V]	$^4F_{9/2}-^2G_{9/2}$	
5894.01	[*Mn* VI]	$^3F_4-^3P_2$	
5896.87	*He* II	5^2G-27^2H	
5913.52	*He* II	5^2G-26^2H	
5932.22	*He* II	5^2G-25^2H	0.8
5953.00	*He* II	5^2G-24^2H	0.9
5977.05	*He* II	5^2G-23^2H	0.7
6004.81	*He* II	5^2G-22^2H	1.2
6037.16	*He* II	5^2G-21^2H	1.1
6074.30	*He* II	5^2G-20^2H	1.1+
6086.88	[*Ca* V]	$^3P_1-^1D$ [*Fe* VII] $^3F_3-^1D$	2.5:
6101.76	[*K* IV]	$^3P_2-^1D$	2.5:
6118.31	*He* II	5^2G-19^2H	1.1+
6151.43			
6166.22	[*Mn* V]	$^4F_{7/2}-^4P_{5/2}$	0.3
6170.73	*He* II	5^2G-18^2H	1.1
6218.64			
6221.04	[*Mn* V]	$^4F_{5/2}-^4P_{1/2}$	
6228.41	[*K* VI]	$^3P_2-^1D$	
6233.80	*He* II	5^2G-17^2H	0.9
6300.31	[*O* I]	$^3P_2-^1D$	20
6312.10	[*S* III]	$^1D-^1S$	16
6347.54	*Si* II	$4^2S-4^2P_{3/2}$	
6363.82	[*O* I]	$^3P_1-^1D$	10
6371.34	*Si* II	$4^2S-4^2P_{1/2}$	0.3:
6393.62	[*Mn* V]	$^4F_{9/2}-^4P_{5/2}$	
6406.53	*He* II	5^2G-15^2H	0.8
6435.11	[*A* V]	$^3P_1-^1D$	5.2
6462.14			
6518.34	[*Mn* VI]	$^3F_2-^1D$	
6527.31	*He* II	5^2G-14^2H	0.8:
6548.09	[*N* II]	$^3P_1-^1D$	80
6560.24	*He* II	4^2F-6^2G	
6562.90	*H* I	2^2P-3^2D	650
6583.36	[*N* II]	$^3P_2-^1D$	240
6598.76	[*Fe* VII]	$^3F_4-^1D$	
6678.16	*He* I	2^1P-3^1D	10
6716.52	[*S* II]	$^4S-^2D_{5/2}$	5.4
6730.74	[*S* II]	$^4S-^2D_{3/2}$	7.5
6890.80	*He* II	5^2G-12^2H	2.1
7005.67	[*A* V]	$^3P_2-^1D$	14

TABLE 2—*Continued*

Wave Length	Ion	Transition	Intensity
7065.31	*He* I	2^3P-3^3S	20
7135.78	[*A* III]	$^3P_2-{}^1D$	56
7170.62	[*A* IV]	$^2D_{3/2}-{}^2P_{3/2}$	3:
7177.77	*He* II	5^2G-11^2H	2:
7237.26	[*A* IV]	$^2D_{5/2}-{}^2P_{3/2}$	2.6
7262.77	[*A* IV]	$^2D_{3/2}-{}^2P_{1/2}$	3.1
7281.32	*He* I	2^1P-3^1S	2.8
7319.92	[*O* II]	$^2D_{5/2}-{}^2P$	77
7330.19	[*O* II]	$^2D_{3/2}-{}^2P$	
7530.54	[*Cl* IV]	$^3P_1-{}^1D$	1.4
7592.79	*He* II	5^2G-10^2H	1.2†
7726.51	[*S* I]	$D-{}^1S$	.....
7751.04	[*A* III]	$^3P_1-{}^1D$	20
8045.58	[*Cl* IV]	$^3P_2-{}^1D$	5.3
8196.61	.....	.....	2.0
8236.64	*He* II	5^2G-9^2H	5.2
8502.5	*H* I	3^2D-16^2F	0.6
8545.53	*H* I	3^2D-15^2F	0.8
8598.35	*H* I	3^2D-14^2F	2.6
8665.0	*H* I	3^2D-13^2F	2.7
8750.5	*H* I	3^2D-12^2F	3.1
8862.8	*H* I	3^2D-11^2F	3.5
9014.9	*H* I	3^2D-10^2F	5.5
9069	[*S* III]	$^3P_1-{}^1D$	40:

† In atmospheric absorption band.

served by Wyse and that seemed to appear on the Mount Wilson spectra but were not found on the Palomar plates. In view of the higher dispersion and greater effective exposure of the latter, we are inclined to regard the lines not confirmed by the Palomar plates as largely spurious and have omitted most of them. We have listed all the lines that appear definitely on one or more Palomar plates and a few of the more uncertain lines that are readily identified with ions whose lines appear in the spectrum. Weak, elusive features that appear on only one plate and for which we have no identification are likely to be spurious. We have not listed these possible lines, although some of them may turn out to be real.

One fact to be emphasized is that the limiting intensity reached differs from one region of the spectrum to another. For example, in the infrared region of the spectrum the plates are less sensitive, while in the ultraviolet the lowered transparency of the corrector plate in the Schmidt camera of the spectrograph cuts down the transmitted intensity. Furthermore, the blaze of the grating renders it more efficient in some spectral regions than in others. The presence of an underlying continuum also influences the detectability of weak lines. If a faint continuum exists, weak lines may be seen that would otherwise be lost below the threshold of the plate.

In general, the identification of lines can be made with some certainty in the cases in which the wave lengths are accurately known from laboratory or other measurements and in which the relative intensities of the lines in a given multiplet can be predicted from theory. These conditions are satisfied for most of the permitted lines and for a substantial part of the forbidden lines (cf. Bowen 1955). For some of the fainter forbidden lines, however, the wave lengths are still uncertain by an angstrom or more, and no information is available at the present time for predicting relative intensities. In these cases identification may be very uncertain; for instance, the assignment of a few lines to [*Ni* II] and [*Ni* VII] suggested by one of us (Aller 1954*a*) is probably to be ruled out.

V. THE DEGREE OF EXCITATION OF THE NEBULA

Lines of the following ions are represented in NGC 7027: *H*, *He* I, *He* II, *C* II, *C* III, *C* IV, *N* I, *N* II, *N* III, *O* I, *O* II, *O* III, *O* IV, *O* V, *F* IV, *Ne* III, *Ne* IV, *Ne* V, *Mg* I, *Si* II, *Si* III, *S* I, *S* II, *S* III, *Cl* III, *Cl* IV, *A* III, *A* IV, *A* V, *K* IV, *K* V, *K* VI, *Ca* V, *Ca* VII, *Mn* V, *Mn* VI, *Fe* III, *Fe* V, *Fe* VI, and *Fe* VII. This list differs from those of Bowen and Wyse and of Wyse in a few particulars. For example, the $^5D-{}^3F$ multiplet of [*Fe* III] is well represented, as is the $^5D-{}^3P$ multiplet of [*Fe* V]. There is no evidence for [*F* II], although [*F* IV] is definitely present.

Phosphorus does not appear; its lines fall in an unfavorable region of the spectrum. Among the heavier elements, no definite evidence is found for nickel, which is perhaps not surprising in view of the weakness of the forbidden lines of much more abundant iron.

As has been remarked by previous observers, NGC 7027 shows a wide range in excitation from *Mg* I to *Fe* VII. A careful search has failed to reveal any lines of [*Fe* X]. Since the lines of [*Fe* VII] appear in exposures 1/25 as long as the longest exposures (which do not reveal [*Fe* X]) and since all the [*Fe* X] radiation is concentrated in one line, while that of *Fe* VII is spread over several lines, we may conclude that the abundance of *Fe* X is less than 3 per cent of that of *Fe* VII. Hence this nebula, although as high in excitation as any planetary, is not so high as T Coronae Borealis or RS Ophiuchi in their coronal-line stages or even CI Cygni in its highest excitation phase.

One of the most interesting features of the spectrum of NGC 7027 is the behavior of the Pickering (4^2F-n^2G) or Brackett series of ionized helium and of the Pfund (5^2G-n^2G, etc.) series of this ion. The latter series is followed to $n = 40$, whereas the former (whose alternate members nearly coincide with the Balmer lines) cannot be followed quite so far. On the hypothesis of the "primary mechanism" of excitation, i.e., recombination followed by cascade, the emission in ergs per cubic centimeter per second per unit volume is given by (Menzel 1937)

$$E_{nn'} = N_i N_\epsilon \frac{KZ^4}{T_\epsilon^{3/2}} b_n \frac{g}{n'} \frac{2hRZ^2}{n^3} e^{X_n}, \tag{1}$$

where Ni is the number of doubly ionized helium atoms, $N\epsilon$ is the electron density, $Z = 2$ for ionized helium, K is a constant numerically equal to 3.26×10^{-6}, n' is the quantum number of the lower level of the transition ($n' = 4$ for the Pickering and 5 for the Pfund series), n is the quantum number of the upper level, and R is the Rydberg constant. The Kramers-Gaunt factor, g, has been tabulated by Menzel and Baker (1938). The electron temperature T_ϵ is also involved in the exponent

$$X_n = \frac{hRZ^2}{n^2 kT_\epsilon}. \tag{2}$$

The factor b_n measures the deviation of the population of the nth level from that appropriate to thermodynamic equilibrium. If T_ϵ is 20,000° K, Menzel and Baker's "case B" ($Z = 2$) yields the dependence of b_n on n shown in the accompanying table.

n	9	10	15	20	25	30
b_n	0.244	0.271	0.371	0.428	0.464	0.486

We select case B because it applies to an optically thick nebula. If the relative intensities of the Pfund series lines are computed by equation (1) and plotted against n, it is found that the values fall off nearly as $1/n^3$ for the higher members. The observed intensities

(which are subject to large accidental errors) fall off roughly in accord with theoretical expectations for the earlier members of the series, but for $n > 15$ the decline in intensity with n is very slow. Allowance for the effects of space absorption only aggravates the discordance between theory and observation.

The trouble probably lies in the values of the b_n's. As n increases without bounds, b_n approaches 1, and it is possible that this limiting value is reached near $n = 30$ or 40 as a consequence of the redistribution of atoms among the higher levels by collisions. In fact, there is no reason why b_n could not exceed unity before the limiting value is reached. Further speculation is unwarranted until the problem of the collisional redistribution is treated quantitatively. The Pfund lines of ionized helium have been found by Wilson (1954) with about the expected intensities in certain O-type stars.

The Pickering lines are observed to $n = 29$ and have a behavior somewhat similar to that of the Pfund series, since the higher members of this series likewise seem to be abnormally strong, falling off in intensity at a rate much slower than $1/n^3$. The fact that this series cannot be followed quite so far as the Pfund series appears to be a consequence of observational selection. The higher members of the Pickering series (Brackett) lines are lost between the Balmer lines.

VI. CORRECTION OF THE OBSERVED INTENSITIES FOR SPACE ABSORPTION

The correction of a stellar magnitude for the effects of space absorption is found from the color excess, but for gaseous nebulae no normal "color" exists. Hence the space absorption must be evaluated from a critical examination of the line intensities them-

TABLE 3

CORRECTION $\Delta \log I$ TO BE ADDED TO LOGARITHMS OF LINE INTENSITIES TO ALLOW FOR SPACE ABSORPTION

λ 3200..	+0.53	λ 4000..	+0.27	λ 4800..	+0.02	λ 5400..	−0.13	λ 6500..	−0.37
3400..	+ .45	4200..	+ .20	4861..	.00	5600..	− .17	7000..	− .47
3600..	+ .39	4400..	+ .14	5000..	− .04	5800..	− .21	7500..	− .57
3800..	+0.33	4600..	+0.08	5200..	−0.08	6000..	−0.26	8000..	−0.66

selves. For example, we might compare Paschen and Balmer lines that arise from the same upper level or auroral and transauroral lines that fall in widely separated spectral regions. The difficulty in comparing the Balmer and Paschen lines is that the latter have been measured on plates of very low dispersion and considerable difficulty is found in estimating the position of the continuum. The forbidden lines are difficult to use because of uncertainties in the intensities and transition probabilities.

Perhaps the most reliable estimate can be made from the observed Balmer decrement. Observations of a large number of planetaries show that their Balmer decrements follow Menzel and Baker's case B unless they are affected by space absorption (Aller 1951). Hence, by comparing the decrement in NGC 7027 with this theoretical decrement and assuming that the law of space absorption is that given by Whitford (1947), it is possible to evaluate the amount of extinction (cf. Aller 1954*b*). In order to bring the observed and theoretical decrements into harmony, a differential correction for space absorption amounting to 2.75 mag. between λ 4220 and λ 10,300 A is required. This correction depends on the lower members of the Balmer series and is not affected by the deviation from case B which may be expected to occur for high members of the *H* series, similar to the deviations found in the *He* II series. The surface brightness of the nebula, as observed in the radiation of the green nebular lines, is cut down by about a factor of 10. Table 3 gives the correction to be applied to the observed line intensities as a function of wave length in order to allow for the effects of selective extinction. These corrections should

be applied to the observed line intensities when they are used, for example, for theoretical discussions.

VII. COMPARISON WITH OTHER SPECTROPHOTOMETRIC DATA: FURTHER OBSERVATIONS NEEDED

A comparison of the present observations with those of Aller (1941) shows that the latter appear to be affected by a scale error in the sense that the weaker lines are systematically too weak. Evidently the continuum was drawn too high. The photoelectric observations of Liller and Aller (1954) and of Code and Whitford (1954) indicate that the intensity ratio of the green nebular lines to $H\beta$ was measured too small. Code and Whitford have kindly sent us their photoelectric line intensities for the stronger lines (down to about 11 on our scale) in NGC 7027. Except for N_1 and λ 3727, the agreement is excellent, the average deviation between the measured intensities being less than 10 per cent. In particular, there is no indication of any scale error in the photographic results. The great strength of the green nebular lines makes them difficult subjects for photographic photometry, whereas the photoelectric observation of the λ 3727 intensity can be explained by blending with near-by lines.

No checks are available for the weaker lines, and none appear to be forthcoming in the near future. The intensities of the very weakest lines are subject to large accidental errors, but we feel that the intensities are free from serious scale errors.

With the telescopic and spectrographic equipment at present available, it is not likely that many new lines can be added in the region from λ 3600 to λ 8200. On the other hand, the identifications and intensities can be greatly improved in the region from λ 3600 to the limit of transmission of the earth's atmosphere. It is our intention to make observations in this region as soon as appropriate spectrographic equipment is available.

REFERENCES

Aller, L. H. 1941, *Ap. J.*, **93**, 236.
———. 1951, *ibid.*, **113**, 125.
———. 1954*a*, *Nuclear Transformations, Stellar Interiors, and Nebulae* (New York: Ronald Press Co.), chap. 4, Fig. 7.
———. 1954*b*, *Ap. J.*, **120**, 401. The following misprints should be corrected. The second term in the denominator of eq. (11) should read $(A_{32} + A_{31})\varpi_3/C$, while in eq. (12) Ω_{13} should be replaced by Ω_{23} and A_{23} by A_{21}.
Bowen, I. S. 1939, *Ap. J.*, **88**, 113.
———. 1955, *Ap. J.*, **121**, 306.
Bowen, I. S., and Wyse, A. B. 1939, *Lick Obs. Bull.*, **19**, 1.
Code, A., and Whitford, A. E. 1954, private communication.
Liller, W., and Aller, L. H. 1954, *Ap. J.*, **120**, 48.
MacRae, D., and Stock, J. 1954, *Nature*, **173**, 589.
Menzel, D. H. 1937, *Ap. J.*, **85**, 330.
Menzel, D. H., and Baker, J. G. 1938, *Ap. J.*, **88**, 52.
Minkowski, R., and Aller, L. H. 1955, *Ap. J.* (in press).
Whitford, A. E. 1948, *Ap. J.*, **107**, 102.
Wilson, R. 1953, *M.N.*, **113**, 557.
Wyse, A. B. 1942, *Ap. J.*, **95**, 356.

STUDIES OF RV TAURI STARS. I. U MONOCEROTIS*

HELMUT A. ABT†
Lick Observatory, University of California
Received December 20, 1954

ABSTRACT

High-dispersion spectrograms of the low-velocity RV Tauri star U Monocerotis have been obtained regularly for $6\frac{1}{2}$ months, or for more than four light-minima. The results from these plates are compared with a few photoelectric observations and an A.A.V.S.O. light-curve. The spectrograms show that the radial-velocity-curve has a discontinuity at each light-maximum. Displacements of the atmosphere, computed from the radial-velocity-curve, are as large as 55×10^6 km; they are large during cycles of deep light-minima and small during cycles of shallow minima. Curves of growth have been constructed from line intensities on 17 spectrograms, including some with double absorption lines. Large apparent abundance changes during times of single lines are attributed to a variable continuous opacity within the regions of line formation. Ionization temperatures computed with numerical values of the variable continuous opacity are probably in agreement with other determinations of the temperature. Within their probable errors, the rates of change of ionization temperature and of electron pressure with displacement are independent of cycle or direction of motion.

I. INTRODUCTION

This, the first of a series of papers on RV Tauri stars, is concerned with U Monocerotis; other papers will deal with R Scuti and AC Herculis. All three of these stars are members of the low-velocity group of RV Tauri stars (Joy 1952), but it will be seen that in the behavior of their atmospheres these stars more closely resemble W Virginis than the classical Cepheids. The principal observations of U Monocerotis discussed are high-dispersion spectrograms taken at the Lick Observatory at an average interval of 10 days for $6\frac{1}{2}$ months. In addition, a few photoelectric observations in two colors and a visual light-curve from the A.A.V.S.O. are given.

In this paper we attempt to locate the regions of formation of the absorption lines and to obtain some information about the nature of these regions from a study of line intensities. The analysis generally follows standard methods for normal stars. If it should eventually be shown that this star is so abnormal in certain respects that these methods should not have been applied, the corresponding results must be disregarded.

II. PHOTOMETRIC OBSERVATIONS

The A.A.V.S.O. visual light-curve of U Monocerotis for the winter of 1952–1953 (when the spectra were being obtained) was provided by Mrs. M. W. Mayall from observations made principally by Messrs. Yamada, of Japan, and Elias, of Greece. The curve (Fig. 1) shows, successively, a deep light-minimum, a shallow one, two moderate ones, and part of a deep one.

A few photoelectric observations were obtained by O. J. Eggen and by the author, as shown in Table 1. Eggen's observations were obtained with a 1P21 photomultiplier and the Lick 12-inch refractor; his magnitudes and colors have been converted to the ***P***, ***V*** system (Eggen 1951*b*). The author's measures were obtained with an E.M.I. photomultiplier and the 12-inch refractor. A conversion to the ***P***, ***V*** system was made from observations of the Harvard C-12 region on two nights. On most of the nights a comparison was made simply with the neighboring stars HD 59692 ($V = 7.53$, $P - V = -0.03$)

* *Contributions from the Lick Observatory*, Ser. II, No. 57.

† Now at the Yerkes and McDonald Observatories.

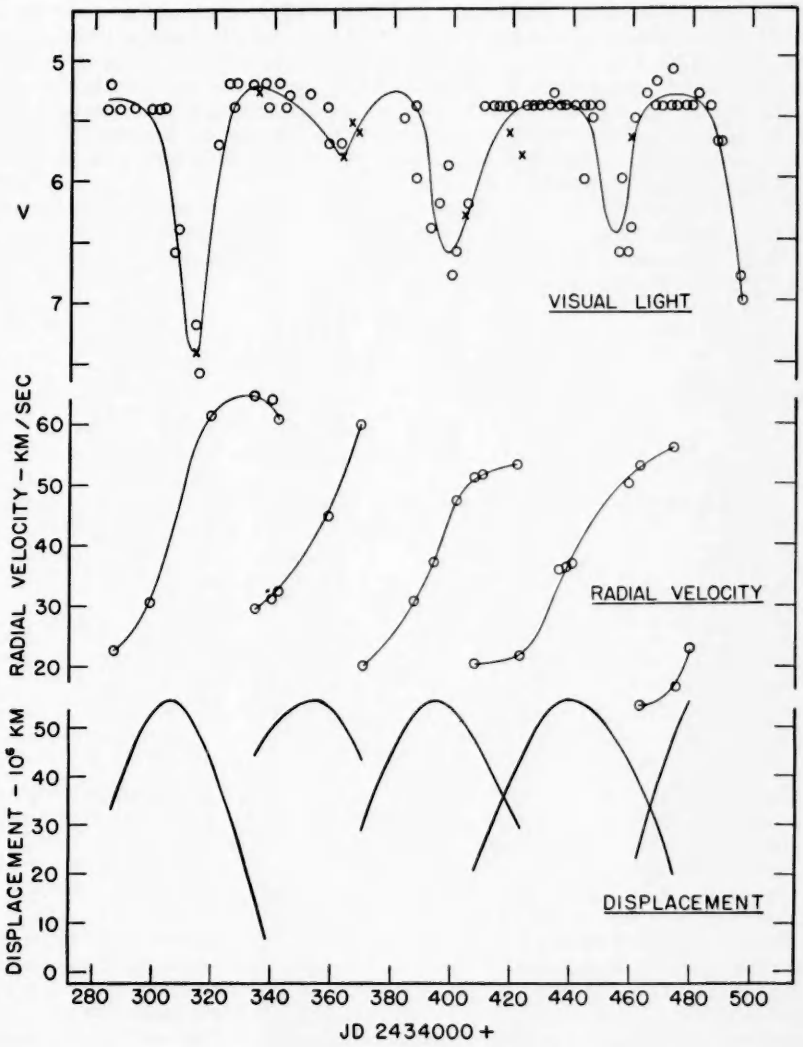

FIG. 1.—*Top:* photoelectric (*crosses*) and A.A.V.S.O. (*circles*) visual magnitudes. The latter were adjusted to the former by a scale correction. *Center:* radial-velocity measures. *Bottom:* displacements, $r - r_n$, from unknown zero points, r_n, for each cycle, n, computed from the radial-velocity-curve without assuming a limb-darkening correction factor. For purposes of this illustration we have set all the maximum displacements equal.

and HD 59730 ($V = 6.44$, $P - V = +1.56$). The photoelectric observations are given in the first three columns of Table 1.

A comparison of the photoelectric visual light-observations with those by the A.A.V.S.O. shows the latter to be systematically fainter near light-maxima but in agreement at $V = 7.4$. This difference is probably due to the assumed magnitudes of the brighter comparison stars used by the A.A.V.S.O. A correlation between the two scales was found, and the A.A.V.S.O. values were adjusted accordingly. All observations are plotted in Figure 1. In the case of a large discrepancy between the few photoelectric observations (e.g., JD 2434419 and 2434424) and the many visual estimates, the proper weighting of the two determinations is unknown.

The colors show very little correlation with light; the star is often as blue during a light-minimum as during a maximum, or even bluer. It will be seen later that the colors and their small variation with phase are probably consistent with the spectroscopic data, except for the last color observation.

TABLE 1

PHOTOELECTRIC OBSERVATIONS AND TEMPERATURES

JD 2434000+	V	$P-V$	Observer	T_e (° K)		T_{ion} (° K)	
				$E_{P-V}=0$	$E_{P-V}=0.13$	Short	Long
313.89	7.41	1.05	Abt	4270	4460	4500	
336.00	5.25	0.91	Abt	4500	4710	4850	.....
364.78	5.81	0.80	Abt	4710	4990	.....	4750
367.94	5.55	0.77	Abt	4750	5040	5040	.....
369.90	5.63	0.732	Eggen	4800	5140	4990	.....
404.85	6.33	0.96	Abt	4420	4620	4460	
419.79	5.63	0.95	Abt	4420	4670	.....	4800
424.83	5.83	0.937	Eggen	4460	4670	5200	4990
460.80	5.68	1.535	Eggen	3730	3850	4580	

III. RADIAL VELOCITIES

Most of the spectrograms were obtained with the Mills spectrograph (dispersion 11 A/mm at λ 4500) attached to the 36-inch refractor; the remainder were obtained at the 36-inch with another spectrograph, giving a dispersion of 22 A/mm at λ 4500. The measured radial velocities were corrected for telescope flexure in the case of the Mills spectrograms. Table 2 gives the plate numbers, spectrograph, heliocentric times of observation, and radial velocities of the metallic absorption lines during five cycles.

The radial-velocity variation is a discontinuous one, as in the case of W Virginis (Sanford 1952). Just before each light-maximum a weak set of lines appears, displaced shortward with respect to the stronger lines. These lines quickly strengthen, move longward, and then fade during the next light-maximum (see Fig. 1). These successive sets of lines are numbered 1 through 5 in Table 2, and this numbering will be used to refer to these five cycles as well as to the corresponding five light-minima. The times of the beginning and end of each segment of the velocity-curve are sometimes uncertain because of the infrequency of the observations. The average separation of the double lines is 35 km/sec, or about 0.5 A, so at times the components of some of the strongest lines are unresolved (see Fig. 2).

The radial-velocity-curves are different for each cycle, but they have a periodicity that corresponds to the time between successive light-minima, a fact indicating that this interval is the fundamental period rather than twice this quantity. For the remainder

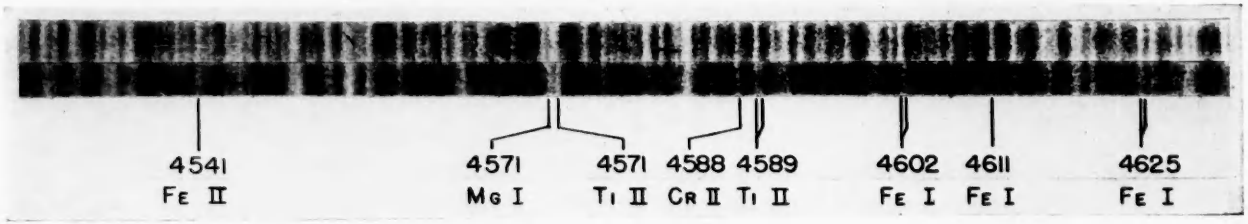

FIG. 2.—Two spectra of U Monocerotis. *Above:* with single lines (JD 2434479); *below:* with many lines doubled (JD 2434422). The shortward components of the lower spectrum have been aligned with the corresponding lines in the upper spectrum. Note that the longward component of 4602.94 *Fe* I (lower E.P. = 1.48 ev) is stronger than the shortward component, while for 4611.28 *Fe* I (lower E.P. = 3.64 ev) and for 4625.05 *Fe* I (lower E.P. = 3.23 ev) the reverse is true. This observation indicates a much higher excitation temperature for the shortward lines than for the longward.

of this paper we shall refer to the time between successive minima (about 46 days) as the period of the variable.

We wish to integrate the radial-velocity-curve to find radial displacements of the regions where the lines are formed. To perform this integration, we must know the velocity of the center of mass of the star. We cannot arbitrarily assume that the mean of the observed velocities over any time interval represents the γ-velocity, because the atmosphere may be continually expanding, as well as pulsating, or it may show an apparent systematic contraction, like solar prominences. However, we may compare the mean observed velocity with the γ-velocity if we assume that this star resembles RV Tauri stars in globular clusters. Since the peculiar motions of stars in globular clusters are probably of the order of only 5 km/sec (Wilson and Coffeen 1954), the integrated-light velocities of the clusters should closely represent the γ-velocities of individual stars in the clusters. In Table 3 we compare mean velocities of the W Virginis stars and RV Tauri stars in

TABLE 2

SPECTROSCOPIC OBSERVATIONS AND RADIAL VELOCITIES

PLATE LS	SPECTRO-GRAPH	HELIO. JD 2434000+	RADIAL VELOCITIES (KM/SEC)				
			1	2	3	4	5
35742	III/16″	286.021	+22.6	.....	.....	.....	.....
802	Mills	299.012	+30.3	.....	.....	.....	.....
949	Mills	319.988	+61.3	.....	.....	.....	.....
36010	Mills	334.028	+64.5	+29.6	.....	.....	.....
052	Mills	339.984	+63.9	+31.3	.....	.....	.....
081	Mills	342.013	+60.5	+32.6	.....	.....	.....
129	Mills	358.945	.....	+44.6	.....	.....	.....
185	III/16″	369.868	.....	+59.8	+19.4	.....	.....
217	Mills	387.869	.....	.....	+30.2	.....	.....
235	III/16″	393.843	.....	.....	+36.9	.....	.....
247	III/16″	400.821	.....	.....	+46.9	.....	.....
273	III/16″	407.898	.....	.....	+51.2	+20.1	.....
289	Mills	410.791	.....	.....	+51.8	.....	.....
333	Mills	422.811	.....	.....	+53.4	+21.8	.....
419	Mills	435.696	.....	.....	.....	+35.9	.....
425	III/16″	438.797	.....	.....	.....	+36.3	.....
427	Mills	439.691	.....	.....	.....	+36.4	.....
480	Mills	459.691	.....	.....	.....	+50.4	.....
488	Mills	462.694	.....	.....	.....	+53.3	+13.1
533	Mills	474.695	.....	.....	.....	+56.2	+16.3
540	Mills	479.693	.....	.....	.....	.....	+23.1

clusters (Joy 1949) with the integrated-light cluster velocities (Mayall 1946). The weights W_I and W_M are those assigned by Mayall and Joy, respectively, to their velocity measures. The weight of a difference between two velocities is given by the product of the weights divided by the sum; this quantity is given in the last column of the table. Only those stars in Joy's list were used for which there were enough observations to define velocity-curves. The weighted difference of $+2 \pm 6$ km/sec between the mean velocities of the variables and the integrated-light cluster velocities shows that there is probably no significant difference between these velocities. This result was first pointed out by Joy (1949). It shows that there is no predominantly outward or inward motion of the atmospheric material in RV Tauri and W Virginis stars. We shall therefore assume that the mean observed velocity of U Monocerotis is the γ-velocity. It should be noted that a continuous velocity-curve, such as would be obtained for this star with a spectro-

graph of lower dispersion, would give the same mean velocity as that of the observed discontinuous curve.

Sanford (1933) found a variation in the mean velocity of U Monocerotis with a range of 40 km/sec and a period of about 2300 days. Our observations indicate a small decrease in mean velocity from +40.9 km/sec for cycle 2 to +37.7 km/sec for cycle 4. A comparison with Sanford's mean velocities suggests a corrected period of 2640 or possibly 1980 days. We shall adopt a mean velocity that varies linearly from +42.6 km/sec on JD 2434280 to +36.6 km/sec on JD 2434480.

The mean photographic absolute magnitude of U Monocerotis is probably of the order of −2.5 (Rosino 1951), and its mean spectral type is about G5 *Ib*. These values indicate a mean photospheric radius of about 65×10^6 km. We shall see later that the displacement of the reversing layer may at times be as much as 55×10^6 km or more. Normally, one would introduce a limb-darkening correction factor of about 24/17 (Getting 1934) to the radial velocities, because, when the photosphere and reversing layer are close together, the radial expansion over most of the stellar disk is not directed along the

TABLE 3

VELOCITIES OF VARIABLES IN GLOBULAR CLUSTERS

Type	NGC (M)	Integrated Vel. (Km/Sec) (Mayall)	Wt. W_I	Variable No.	Mean Vel. (Km/Sec) (Joy)	Wt. W_M	Diff. (Mean − Integ.)	Weight
W Vir	5272 (3)	−150	24	154	−153	14.0	− 3	8.84
	6218 (12)	− 32*	4	1	− 42	5.6	−10	2.33
	6254 (10)	+ 73	6	2	+ 67	7.0	− 6	3.23
RV Tau	5904 (5)	+ 45	13	42	+ 54	8.0	+ 9	4.95
	5904 (5)	+ 45	13	84	+ 50	8.0	+ 5	4.95
	6779 (56)	−154	5	6	−132	7.7	+22	3.03
	7089 (2)	− 3	17	11	− 4	10.8	− 1	6.60
Weighted mean							+ 2±6	

* This is a revised unpublished velocity determined by Dr. N. U. Mayall, to whom the author is grateful for this information.

line of sight. In view of the possible large separation of the photosphere and reversing layer, this factor will not be used in this case. Our displacements may therefore be conservative.

The displacements, $r - r_n$, from an arbitrary radius, r_n, can now be calculated for each cycle, n. The discontinuity of the velocity-curve indicates that we observe different material during successive cycles, and therefore the radial velocities give no information on the relative locations of successive segments of the displacement-curve, i.e., on the relative values of the r_n's. In illustrating the displacements in Figure 1, we have arbitrarily given each cycle the same maximum displacement. This procedure probably does not represent the actual situation.

In Table 4 are tabulated the ranges in visual light and displacement and the initial outward velocity (γ-velocity *minus* initial observed velocity) for each of five cycles. All three quantities are directly correlated, a fact indicating (1) that deep light-minima are associated with large expansions, while shallow ones occur during small expansions, and (2) that regions of line formation starting with large outward velocities move to large displacements. The minima in visual light occur about 10 days after maximum expansions of the atmosphere. The first correlation, which was first pointed out for several RV Tauri stars by Sanford (1931) and by McLaughlin (1938, 1941), is such that each

27×10^6-km range in displacement corresponds to a decrease in visual light by 1 mag. This result is only very approximate, since the duration of the segments of the velocity-curve and hence the ranges in displacement depend in part on the frequency of the observations. Since we did not observe the beginning of cycle 1, the initial outward velocity may have been larger than 19.9 km/sec. Our small amount of data indicates that the displacement ranges depend more on the duration of a set of lines than on the velocity ranges (or initial outward velocities) of the lines.

IV. SPECTROPHOTOMETRY

In the following discussion our line intensities have been compared with those computed for a normal stellar atmosphere. Since an atmosphere with two regions of line formation is not normal, the results must be regarded with caution. The only justification for our approach is that, at the outset, we have very little knowledge as to what kind of model actually represents the star. We hope that these preliminary results will be of

TABLE 4

LIGHT, DISPLACEMENT, AND VELOCITY RANGES

Cycle No.	Visual-Light Range (Mag.)	Displacement Range	Initial Outward Velocity (Km/Sec)	Cycle No.	Visual-Light Range (Mag.)	Displacement Range	Initial Outward Velocity (Km/Sec)
1	2.1	56×10^6km	19.9+	4	1.1	36×10^6km	18.9
2	0.4	12	11.5	5	1.7+	.....	23.9
3	1.2	27	20.5				

aid in deciding between models and that the basic data may then be used to test the models. We see no a priori reason for doubting the results obtained during times of single lines, but when the lines are double, continuous opacities associated with the two-line spectra may affect the observed line intensities. The size of the corrections for this effect cannot be determined with the information available, i.e., the total opacities and relative locations of the two regions of line formation are not known. It is significant that reasonable values of the physical parameters have been derived at these times without applying any corrections. Within the completeness of our measures in this star, as well as in W Virginis, we have found no evidence for dilution of radiation (except in the zero-volt *Fe* I lines), stratification, or departures from local thermodynamic equilibrium (except for large differences between ionization and excitation temperatures, a result which is also often obtained in nonvariable stars). All the *Fe* absorption-line intensities (except for the zero-volt lines) are those to be expected, within our accuracy of measurement, from a specification of the abundances, excitation temperature, ionization temperature, continuous opacity, turbulent velocity, and damping constant for each set of lines present. We shall not discuss the *TiO* bands present at deep light-minima or the *H* emission lines observed during increasing light.

Equivalent widths for lines of *Fe* I and *Fe* II were measured on the fifteen Mills and on two of the III/16″ plates. The method of reduction is essentially that described for W Virginis (Abt 1954). To compare measures on the III/16″ plates with those on the Mills plates, we made a comparison of two plates of α Persei taken with these two spectrographs. It was found that on the lower-dispersion spectrograms the lines were measured 15 per cent shallower and wider than on the higher-dispersion plates, so that equivalent widths are 12 ± 12(p.e.) per cent larger. Corrections of this amount were applied to the III/16″ measures. A comparison of the Mills equivalent widths for α Persei with

those determined by Greenstein (1948) showed the former to be 17 ± 12(p.e.) per cent smaller. Table 5 gives the equivalent widths, W, expressed as $-\log W/\lambda$. For plates with double lines, separate columns are used for the shortward and longward components. For the III/16″ plates the corrected values are given. The f-values used are those given in the paper on W Virginis; these were taken from laboratory, solar, and stellar sources.

The empirical curves of growth were compared with theoretical ones (Wrubel 1949) for a Milne-Eddington model atmosphere. Some justification will be given later for the use of this model rather than a Schuster-Schwarzschild model. The results are tabulated in Table 6, whose first two columns give the plate number and the component measured. Column 3 gives the number of lines measured. These numbers are small because of the very limited spectral range available; there were just barely enough lines to construct curves of growth. However, this spectral range ($H\gamma$ to λ 4650) is one in which the lines are almost entirely free of blends. The double lines are generally not completely separated, but the observed changes in line strengths are so large that useful results can nevertheless be obtained. The damping parameter, a, cannot be determined when all the lines are weak: assumed values for these times are followed by a colon in column 4 of Table 6.

The variation in Doppler velocity, V, is given in column 5 and is shown in Figure 3. This velocity increases during each expansion and during the subsequent contraction from an initial value of about 3 to about 7 km/sec. The accuracy of measurement is about ±1 km/sec on each plate. The velocities are too large to be due to thermal motion; they may be due either to some form of turbulent motion or to a dispersion in the pulsation velocity.

The excitation temperatures, T_{ex}, are also shown in Figure 3. Their behavior from cycle to cycle is irregular, perhaps due in part to the low precision of ±500° of their determination. At times of double lines the shortward component always seems to have the higher excitation temperature. At times of large displacement the zero-volt *Fe* I lines do not fit the curve of growth chosen for the 1.5 to 3.5 ev lines, and consequently for these times the zero-volt lines were not used in the determination of T_{ex}. The reason for this discrepancy will be considered in the discussion of R Scuti, for which we have better material in this regard.

In the absence of absolute f-values for *Fe* II, we converted the line strengths of *Fe* I and *Fe* II to abundances relative to those in α Persei. From the degree of ionization of *Fe* I in α Persei (Greenstein 1948) we then derived the degree of ionization in U Monocerotis. Columns 7 and 8 in Table 6 give the logarithms of the relative apparent abundances, N/κ, in U Monocerotis compared to α Persei for *Fe* I and *Fe* II, respectively. Column 9 gives the degree of ionization of *Fe* I. These numbers are plotted in Figure 4, where the abundances marked with a vertical line (and by a colon in Table 6) are uncertain; they were derived from incomplete curves of growth that depend on assumed values of a, V, and T_{ex}. Those marked with an arrow in Figure 4 and an inequality in Table 6 are maximum values obtained from an absence of that component.

V. DISCUSSION

A striking feature of Figure 4 is that, although the apparent abundances are observed to vary by a factor of more than 1000, the corresponding degrees of ionization are nearly constant; at only one time does the degree of ionization differ from the mean by more than a factor of 2. The degree of ionization is a function of the ionization temperature (T_{ion}), electron pressure (P_e), and—for a detached shell—the dilution factor. The *Fe* I lines show no dilution effects (except in the zero-volt lines) in the sense of intensity differences for lines originating from metastable and stable levels. Therefore, it appears that P_e (which varies over a range of 10^3) and T_{ion} vary in such a manner that the ionization of *Fe* I is constant.

At this point we shall consider the possible reasons for time variations in the apparent

TABLE 5

VALUES OF $-\log W/\lambda$

λ	Element	Multiplet No.	Plate No. and Component										
			35742	35802	35949	36010		36052		36081		36129	36185	
						Short	Long	Short	Long	Short	Long		Short	Long
4389.24	Fe I	2										4.03		
4404.75	Fe I	41	3.77			3.98	4.10	3.84		3.90	4.13	3.77	3.90	
16.82	Fe II	27				4.42		4.22		4.32		4.19		
27.31	Fe I	2	3.85		3.79			3.76		4.03	4.08	3.88		
32.57	Fe I	797												
47.72	Fe I	68	4.27	4.17	4.14	4.26		4.18				4.19	4.57	5.16
72.92	Fe II	37	4.18	3.98	4.36	4.36		4.20		4.21		4.23	4.52	
76.02	Fe I	350	4.31	4.14	4.25			4.16		4.16		4.20	4.40	5.04
84.23	Fe I	828	4.20		4.25	4.25		4.19		4.39		4.31	4.47	
85.68	Fe I	830				4.55								
89.18	Fe II	37						4.18		4.15		4.22		
89.74	Fe I	2	4.03	3.79	3.91							3.98	4.30	
91.40	Fe II	37	4.30	4.16	4.37	4.27	4.69	4.23		4.20		4.28	4.38	
94.57	Fe I	68	4.11	3.94	4.16					4.16	4.20	4.01		
4504.84	Fe I	555	4.89	4.42				4.98		4.88				
08.28	Fe II	38	4.17	4.19	4.23	4.24	4.48	4.25	4.74	4.20	4.62	4.21	4.23	
15.34	Fe II	37	4.13	4.12	4.23	4.24	4.47	4.21		4.18	4.76	4.15	4.29	4.77
20.23	Fe II	37	4.09	4.05	4.26	4.24	4.66	4.24		4.21		4.08		
22.63	Fe II	38	4.02	3.80	4.13	4.05	4.27	4.02	4.36	4.02	4.45	4.03	4.20	
28.62	Fe I	68	4.08	3.86	4.14							3.99	4.24	4.31
41.52	Fe II	38	4.31	4.09	4.30	4.30	4.72	4.26	4.84	4.25		4.20	4.50	4.77
76.33	Fe II	38	4.37	4.20		4.39	4.69	4.30	4.70	4.37		4.25	4.60	4.88
82.83	Fe II	37	4.37			4.39		4.32		4.29				
83.83	Fe II	38	4.07	4.04	4.05	3.97	4.30	3.99	4.75	4.08		3.97		
87.13	Fe I	795	4.99	4.38				4.93		5.22		5.09		
4602.00	Fe I	39	4.61	4.20	4.41			4.56		4.71		4.56		
02.94	Fe I	39	4.30	4.09	4.26	4.27	4.46	4.22		4.29		4.15	4.93	
11.28	Fe I	826	4.54	4.19	4.50	4.68	5.04	4.44		4.51		4.38		
20.51	Fe II	38	4.46	4.27	4.71	4.43		4.42		4.42		4.42	4.55	5.16
25.05	Fe I	554	4.54	4.28	4.48	4.44		4.47		4.41		4.50	4.83	
32.92	Fe I	39	4.49	4.17				4.68		4.32		4.39		
43.47	Fe I	820		4.23						4.69		4.66		
47.44	Fe I	409	4.41	4.14		4.40				4.29		4.42		

TABLE 5—*Continued*

λ	Element	Multiplet No.	Plate No. and Component												
			36217	36289		36333		36419	36427	36480	36488		36533		36540
				Short	Long	Short	Long				Short	Long	Short	Long	
4389.24	*Fe* I	2	3.94	.....	3.93	.....	3.93	4.18	4.09	4.02	.....	4.20	.....	.....	.....
4404.75	*Fe* I	41	3.72	.....	3.77	.....	3.88	3.84	3.80	3.81	.....	3.91	3.91	4.11	3.69
16.82	*Fe* II	27	.....	.....	.....	.....	.....	.....	4.22	.....	.....	.....	4.16	.....	4.17
27.31	*Fe* I	2	3.83	.....	3.84	.....	3.91	3.94	3.88	3.90	.....	3.93	4.06	4.25	4.02
32.57	*Fe* I	797	4.54	.....	4.90	.....	3.91	.....	.....	.....	.....	.....	.....	.....	.....
47.72	*Fe* I	68	4.22	.....	4.22	4.44	4.36	.....	.....	4.17	.....	4.30	4.22	.....	4.16
72.92	*Fe* II	37	4.10	.....	4.27	4.30	.....	4.27	4.24	4.23	.....	4.34	4.08	.....	4.10
76.02	*Fe* I	350	4.23	.....	4.18	4.41	4.49	4.33	4.32	4.20	.....	4.36	4.15	.....	4.15
84.23	*Fe* I	828	4.09	.....	.....	4.41	.....	4.43	4.28	.....	.....	4.63	.....	.....	4.05
85.68	*Fe* I	830	.....	.....	.....	.....	.....	.....	.....	.....	.....	.....	.....	.....	.....
89.18	*Fe* II	37	.....	.....	.....	.....	.....	.....	.....	.....	.....	.....	.....	.....	.....
89.74	*Fe* I	2	3.87	.....	3.89	.....	4.00	4.03	4.00	3.98	.....	4.06	.....	.....	.....
91.40	*Fe* II	37	4.24	.....	.....	4.24	4.96	4.27	4.24	4.23	.....	.....	4.07	.....	4.15
94.57	*Fe* I	68	4.02	.....	4.04	4.13	4.29	4.12	4.04	4.05	.....	4.15	4.22	.....	3.94
4504.84	*Fe* I	555	4.50	.....	5.47	5.03	.....	.....	.....	.....	.....	5.00	.....	.....	4.58
08.28	*Fe* II	38	4.15	4.76	4.20	4.15	4.36	4.18	4.15	4.20	4.76	4.16	4.31	.....	4.21
15.34	*Fe* II	37	4.18	4.73	4.16	4.23	4.39	4.20	4.16	4.20	4.63	4.26	4.22	.....	4.08
20.23	*Fe* II	37	4.12	4.65	4.19	4.22	4.64	4.16	4.16	4.17	.....	4.16	4.21	.....	4.04
22.63	*Fe* II	38	3.91	4.61	3.95	4.05	4.21	4.00	3.93	3.98	4.43	4.13	.....	.....	3.88
28.62	*Fe* I	68	4.04	.....	3.95	.....	.....	4.00	4.04	4.03	.....	4.04	.....	.....	3.99
41.52	*Fe* II	38	4.18	.....	4.21	4.15	.....	4.32	4.22	4.30	.....	4.36	.....	.....	4.18
76.33	*Fe* II	38	4.30	.....	4.23	4.37	4.59	4.33	4.33	4.34	.....	.....	4.39	.....	4.23
82.83	*Fe* II	37	4.16	.....	.....	.....	.....	4.33	4.27	.....	4.66	4.34	4.17	.....	4.18
83.83	*Fe* II	38	4.00	.....	3.96	3.95	.....	3.99	4.04	4.01	4.50	4.08	3.98	.....	3.90
87.13	*Fe* I	795	4.58	.....	5.00	.....	.....	.....	4.99	.....	.....	5.26	.....	.....	4.69
4602.00	*Fe* I	39	4.34	.....	4.45	.....	.....	4.74	4.61	4.49	.....	4.66	4.36	.....	4.28
02.94	*Fe* I	39	4.23	.....	4.17	4.51	4.34	.....	4.22	4.16	.....	4.31	4.23	.....	4.13
11.28	*Fe* I	826	4.23	.....	.....	4.56	.....	4.52	4.42	4.42	.....	4.63	4.38	.....	4.23
20.51	*Fe* II	38	4.34	.....	4.37	4.45	.....	4.52	4.36	4.45	.....	.....	4.35	.....	4.32
25.05	*Fe* I	554	4.32	.....	4.45	4.48	4.83	4.56	4.47	4.46	.....	.....	4.35	.....	4.28
32.92	*Fe* I	39	4.20	.....	4.27	4.64	4.56	4.46	4.40	4.30	.....	4.59	4.35	.....	4.12
43.47	*Fe* I	820	4.33	.....	4.70	4.76	.....	4.75	4.50	4.84	.....	5.15	4.58	.....	4.31
47.44	*Fe* I	409	4.24	.....	4.20	4.42	4.53	4.40	4.24	4.43	.....	.....	4.24	.....	4.12

TABLE 6

SPECTROPHOTOMETRIC RESULTS

Plate LS (1)	Component (2)	n (3)	log a (4)	V (Km/Sec) (5)	T_{ex} (6)	log $[(N'/\kappa)_v/(N'/\kappa)_a]$ (7)	log $[(N''/\kappa)_v/(N''/\kappa)_a]$ (8)	log (N''/N') (9)	log $\bar{\kappa}$ (10)	T_{ion} (11)	log P_e (12)	log P (13)	log ρ (14)	log g_e (15)
35742	.....	27	−1.8	3.2	3650	+1.65	+1.45	+2.76	−3.34	4540	−2.29	+1.54	− 9.73	−1.50
35802	.....	25	−3.0	4.0	3850	+2.98	+2.18	+2.16	−4.07	3910	−3.29	+0.90	−10.31	−2.87
35949	Long	20	−3.0	6.8	3500	+1.25	+0.62	+2.33	−2.51	4800	−1.38	+2.47	− 8.83	+0.26
	Short	0	.....	.....	.....	.....	<−2.64	.....	.....	.....	.....	.....	.....	.....
36010	Long	11	−2.6:	6.2	3630	+0.20	−0.18	+2.58	−1.71	5540	−0.39	+2.63	− 8.73	+1.22
	Short	20	−2.2	3.8	6000	+0.50	−0.02	+2.44	−2.64	4750	−1.52	+2.33	− 8.96	−0.01
36052	Long	5	.....	.....	.....	.....	−0.63:	.....	.....	.....	.....	.....	.....	.....
	Short	25	−2.2	5.5	4420	+0.93	+0.36	+2.39	−2.25	4850	−1.04	+2.91	− 8.39	+0.96
36081	Long	6	.....	.....	.....	.....	−0.68:	.....	.....	.....	.....	.....	.....	.....
	Short	27	−2.2	5.6	4200	+0.99	+0.53	+2.50	−2.42	4940	−1.23	+2.44	− 8.87	+0.32
36129	Long	27	−2.2	7.2	3650	+1.27	+0.80	+2.49	−2.69	4800	−1.55	+2.20	− 9.10	−0.19
	Short	0	.....	.....	.....	.....	<−2.64	.....	.....	.....	.....	.....	.....	.....
36185	Long	7	.....	.....	.....	.....	−0.36:	.....	.....	.....	.....	.....	.....	.....
	Short	17	−2.2:	4.3	3730	+0.89	+0.64	+2.71	−2.53	4990	−1.35	+2.12	− 9.20	−0.11
36217	.....	27	−2.6	3.6	4340	+2.14	+1.58	+2.40	−3.47	4310	−2.52	+1.56	− 9.69	−1.61
36289	Long	27	−2.2	5.8	3480	+1.71	+1.42	+2.67	−3.31	4500	−2.28	+1.63	− 9.64	−1.38
	Short	4	.....	.....	.....	.....	−1.87:	.....	.....	.....	.....	.....	.....	.....
36333	Long	17	−2.2:	10.0	3050	+1.02	+0.43	+2.37	−2.32	4940	−1.14	+2.59	− 8.72	+0.57
	Short	21	−2.2	3.0	5480	+0.31	+0.58	+3.23	−2.47	5250	−1.44	+1.29	−10.05	−0.88
36419	.....	25	−1.8	5.0	3790	+1.17	+0.93	+2.72	−2.82	4850	−1.69	+1.85	− 9.45	−0.67
36427	.....	28	−1.8	5.2	3850	+1.21	+0.93	+2.68	−2.82	4800	−1.70	+1.95	− 9.35	−0.57
36480	.....	25	−2.2	5.8	3500	+1.58	+1.15	+2.53	−3.04	4580	−1.97	+1.95	− 9.33	−0.79
36488	Long	25	−2.2	5.5	3360	+1.48	+1.27	+2.75	−3.16	4670	−2.09	+1.59	− 9.70	−1.27
	Short	5	.....	.....	.....	.....	−0.88:	.....	.....	.....	.....	.....	.....	.....
36533	Long	2	.....	.....	.....	.....	−2.09:	.....	.....	.....	.....	.....	.....	.....
	Short	22	−2.6	4.6	4000	+1.53	+1.36	+2.79	−3.25	4620	−2.18	+1.54	− 9.74	−1.41
36540	.....	28	−2.6	4.6	4380	+1.83	+1.47	+2.60	−3.36	4460	−2.35	+1.60	− 9.67	−1.46

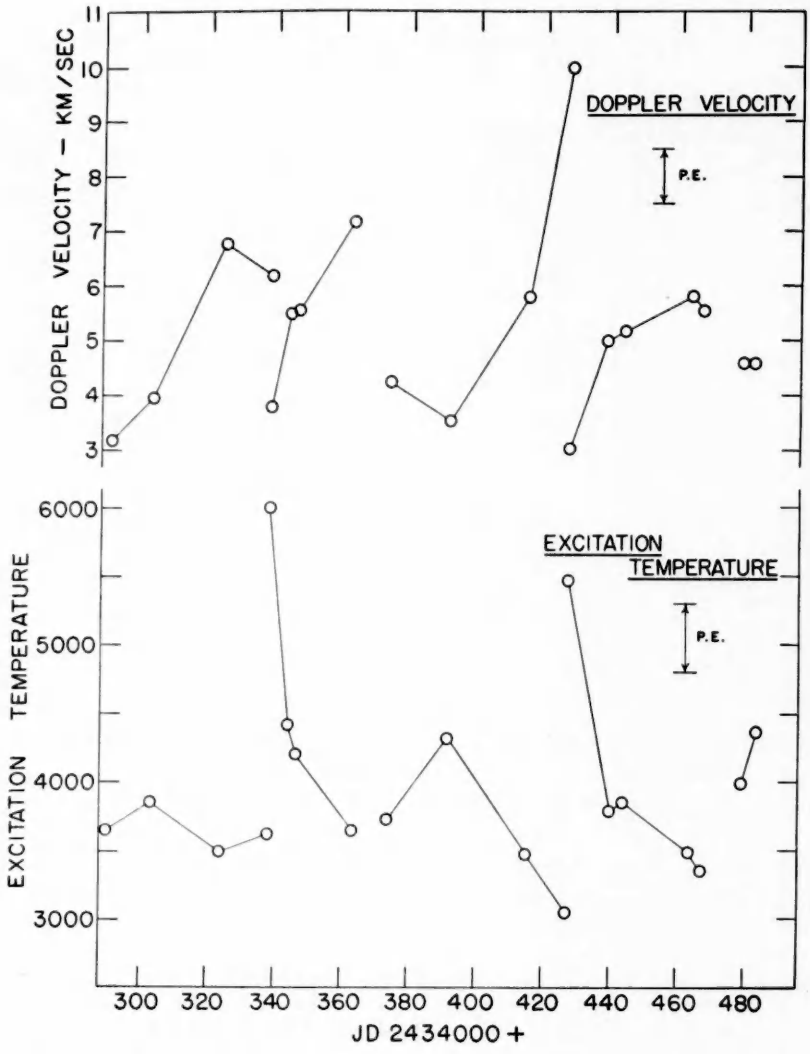

FIG. 3.—*Top:* Doppler velocities; *bottom:* excitation temperatures. The two vertical lines indicate the estimated probable errors in these quantities.

abundances, particularly during times when the lines are single. It will be shown below that at least 99 per cent of the *Fe* atoms are in the form of *Fe* II. Therefore, the *Fe* II abundance-curve gives the variation in *Fe* abundance under conditions of local thermodynamic equilibrium. We see in Figure 4 that, as an extreme case, during cycle 1 the apparent abundance decreased by a factor of 36 between the second and third observations. This change is very apparent in the line strengths on the two spectrograms, both of which had single lines. We now consider four causes for apparent abundance changes.

1. *Variation in surface density.*—If the observations had been reduced with curves of growth for a Schuster-Schwarzschild model, we would have derived values of $\mathfrak{N}H$, the number of *Fe* atoms per square centimeter above the photosphere. These values would have been proportional to the values of N/κ of the Milne-Eddington model. In the case of a transparent expanding shell, $\mathfrak{N}H$ would change because the surface density varies inversely as the square of the radius of the shell. However, for the two spectra mentioned earlier, the abundance per square centimeter decreased as the mean radius of the region of line formation decreased 8.5×10^6 km, i.e., the change in surface density would produce the opposite effect from that observed.

2. *Excess of far-ultraviolet radiation.*—The abundance of *Fe* in U Monocerotis as derived from lines of *Fe* I and *Fe* II could vary through ionization to *Fe* III from an excess of radiation in the vicinity of λ 767, which corresponds to the ionization potential of *Fe* II. The general weakening of all the absorption lines between the times mentioned is not consistent with such selective effects, which depend on a comparison of the ionization potential of each element with the wave-length profile of the proposed ultraviolet excess.

3. *Nonspherically symmetric models.*—Various models (e.g., large filaments, nonspherically symmetric shells, rings, satellites, and spots) can be proposed in which the amount of material projected in front of the disk varies with time. If these are to produce abundance changes by a factor of 36 or more, they are likely to cause significant changes or scatter in the variations in velocity, light, and other quantities. We should not postulate complicated or nonspherically symmetric models unless they are suggested by more than one parameter.

4. *Variable continuous opacity.*—The variation in apparent abundance, N/κ, may be due to a variation in the continuous opacity, κ, in the region where the lines are formed. It will be seen that numerical values of κ then lead to ionization temperatures that are probably in agreement with effective temperatures derived from colors and from spectral types. If the continuous opacity is sufficiently large at most, or all, times to obscure part of the region of line formation, this region as a whole must be opaque in the continuum, i.e., the photosphere is located within this region. In view of our dissatisfaction with the first three causes, we shall provisionally accept this explanation and investigate its consequences. One of these is that a Milne-Eddington model gives a more useful representation of the atmosphere than does a Schuster-Schwarzschild model. We therefore no longer accept those estimates, based on a Schuster-Schwarzschild model, of the thickness of the regions of line formation in W Virginis (Abt 1954).

The curves of growth for *Fe* II yield the quantity

$$\log \frac{[N(Fe\ \text{II})/\kappa]_U}{[N(Fe\ \text{II})/\kappa]_a}.$$

From the degree of ionization in Figure 4, $N(Fe\ \text{I}) < 10^{-2}\ N(Fe\ \text{II})$. With sufficient accuracy, the Saha equation gives

$$\log \frac{N(Fe\ \text{III})}{N(Fe\ \text{II})} - \log \frac{N(Fe\ \text{II})}{N(Fe\ \text{I})} = -\frac{5040}{T_{\text{ion}}}\left[I(Fe\ \text{II}) - I(Fe\ \text{I})\right] = -\frac{41{,}800}{T_{\text{ion}}}, \quad (1)$$

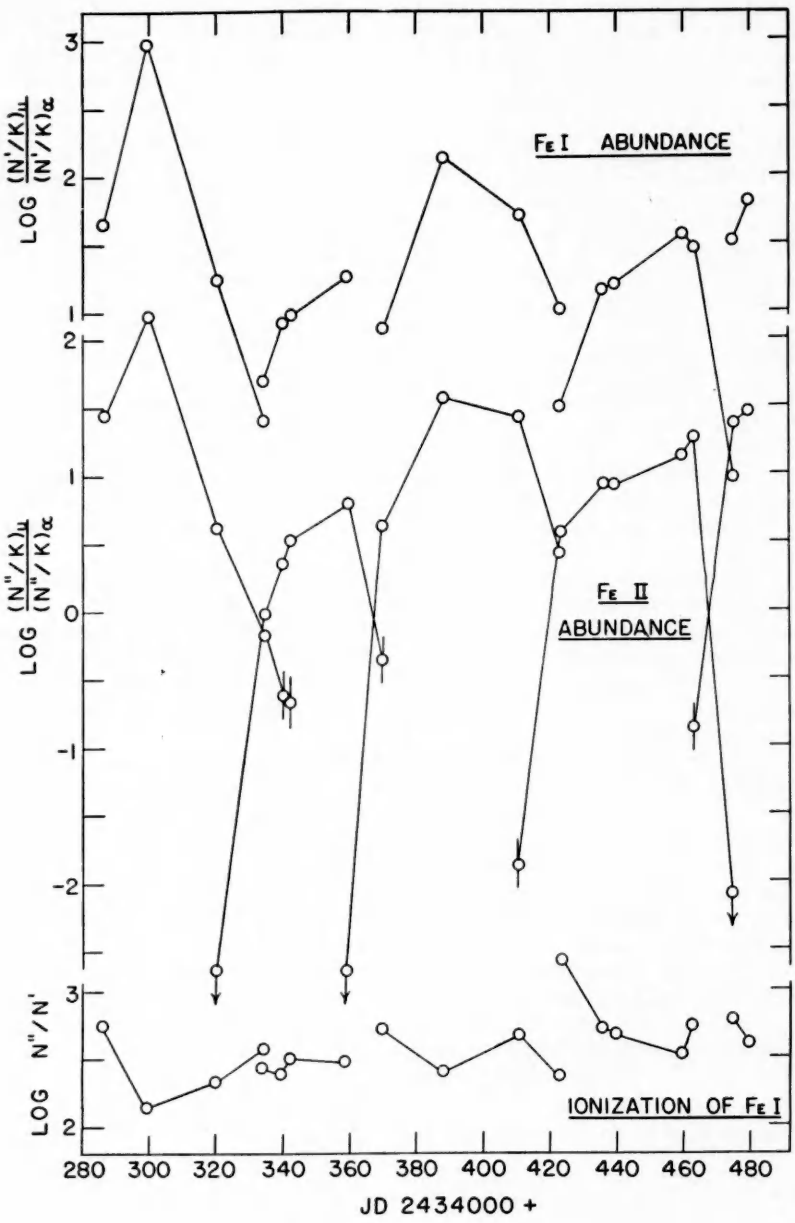

FIG. 4.—*Top and center:* apparent abundances of *Fe* I and *Fe* II, respectively, relative to those in α Persei; *bottom:* the degree of ionization of *Fe* I in U Monocerotis.

where I is the ionization potential. For temperatures of 5500° or less, $N(Fe\ \text{III}) < 10^{-4}\ N(Fe\ \text{II})$. Therefore, with 1 per cent accuracy, $N(Fe) = N(Fe\ \text{II})$. If we assume the same fraction of *Fe* per gram of material in U Monocerotis as in α Persei, we obtain

$$\frac{N(Fe)_U}{N(Fe)_\alpha} = \frac{N(Fe\ \text{II})_U}{N(Fe\ \text{II})_\alpha} = 1. \tag{2}$$

Therefore,

$$\frac{[N(Fe\ \text{II})/\kappa]_U}{[N(Fe\ \text{II})/\kappa]_\alpha} = \frac{\kappa_\alpha}{\kappa_U}. \tag{3}$$

The relation between κ and the mean opacity, $\bar{\kappa}$, is given by Chandrasekhar and Münch (1946). Knowing $\bar{\kappa}$ for α Persei (Greenstein 1948), we derive the values of $\bar{\kappa}$ for U Monocerotis that are given in column 10 of Table 6.

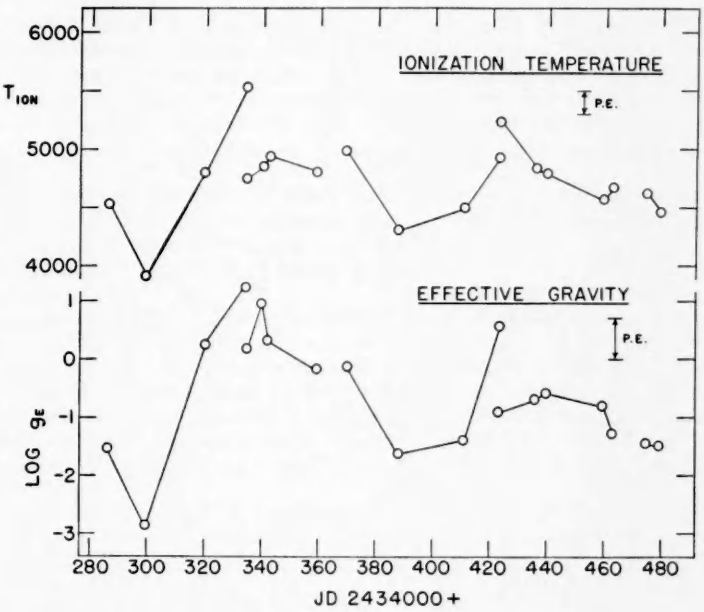

FIG. 5.—*Top:* ionization temperatures; *bottom:* effective gravity determined spectroscopically. The two vertical lines represent the estimated probable errors in these quantities.

The continuous opacity is a function of T_{ion} and P_e (Chandrasekhar and Münch 1946). Similarly, the degree of ionization is a function of these two quantities. For each time of observation, we solved simultaneously for T_{ion} and P_e (in dynes per square centimeter), with the results given in columns 11 and 12 of Table 6. The variation in T_{ion} is shown in Figure 5. The size of the probable errors in the determination of $\bar{\kappa}$, T_{ion}, and P_e cannot be estimated accurately, but a rough check is obtained by comparing results on four pairs of plates for which the time interval between plates is only 3–5 days. The mean differences are ± 0.10 in log $\bar{\kappa}$, $\pm 100°$ in T_{ion}, and ± 0.12 in log P_e. We shall assume probable errors (p.e.) per observation of twice these amounts.

We can now compare the ionization temperatures in the regions where the lines are

formed with the effective temperatures derived from the colors in Table 1. From Eggen's work (1951*a*, *b*) we have the relation between $P - V$ and spectral type for unreddened I*b* supergiants. Keenan and Morgan (1951) give the relation between spectral type and effective temperature, T_e, for population I stars. Table 1 gives the effective temperatures for no interstellar reddening (color excess $E_{P-V} = 0$) and the interpolated values of T_{ion} for one or more components. The ionization temperatures are systematically higher by 260°. However, if we assume that the star has a color excess of 0.13 mag., this systematic difference disappears, and the temperatures agree (except for the last one), with a probable error of ±120°. Stebbins and Huffer (1934) predict a color excess on the C_1 scale of 0.07 mag. for the galactic longitude (194°) and distance (about 500 parsecs) of this star. Since our color system more nearly resembles the (*B*, *V*) system of Johnson and Morgan (1951), the predicted color excess is of the order of 0.14 mag. (Morgan, Harris, and Johnson 1953), if we may extrapolate from their correlations for B-type stars. Therefore, our assumed color excess is of reasonable size. Rosino (1951) estimated the spectral-type range of U Monocerotis to be F8e I*b* to K0p I*b*, for which we would expect (Keenan and Morgan 1951) a range in effective temperature of 5300°–3820°. Our ionization temperatures range from 5540° to 3910°. We conclude that the ionization temperatures computed on the basis of a variable continuous opacity are probably in agreement with the observed spectral types and with the effective temperatures derived from the colors. It should be noted that if $\bar{\kappa}$ were constant, computed values of T_{ion} and of P_e would be nearly constant at all times, since the degree of ionization of *Fe* I shows very little variation.

There are often very large differences (as much as 1900°) between the excitation and ionization temperatures (see Fig. 2). In the spectra the intensity ratios of low- to high-excitation lines give a later spectral type than comparisons of lines from two stages of ionization. For this reason the spectra often are not similar to any standards for spectral classification.

We are now ready to discuss the variation of T_{ion} and P_e with displacement, $r - r_n$, during the course of each cycle. Within the probable errors in T_{ion} and P_e, these quantities decrease during each expansion and increase during the subsequent contraction. However, the values of T_{ion} and P_e at the times of double lines may be only rough approximations, because in the case of the Milne-Eddington model the observed line intensities must be corrected for the composite nature of the spectrum. The variations in T_{ion} and log P_e with time are rather similar in shape, a consequence of the relative constancy of the degree of ionization of *Fe* I.

During each cycle the shapes of the variation in T_{ion} (Fig. 5) and in log P_e are very similar to the corresponding segments of the displacement-curves (Fig. 1). For the two cycles (1 and 3) for which our data extend over large ranges in displacement, the correlations are given roughly by

$$\frac{\Delta T_{\text{ion}}}{\Delta (r - r_n)} = -3.0 \times 10^{-10}\ \text{cm}^{-1}, \tag{4}$$

$$\frac{\Delta \log P_e}{\Delta (r - r_n)} = -5.7 \times 10^{-13}\ \text{cm}^{-1}. \tag{5}$$

We find that with a scatter (computed as a probable error) of ±150° in T_{ion} and ±0.24 in log P_e, equations (4) and (5) hold for all five cycles. This scatter is about the same as the estimated probable errors in the determination of T_{ion} (±200°) and log P_e (±0.24). Therefore, as a rough approximation, the rates of change of temperature and of electron pressure with displacement are the same for all cycles and are numerically the same during expansion as during contraction.

If our values of T_{ion} and P_e have a meaning in the sense that they represent mean conditions in a region that is relatively homogeneous, we may derive the total pressures and densities in the region. The metals are singly ionized, but hydrogen is only slightly ionized. With 1 per cent accuracy, we may write

$$\frac{P_e}{P} = x_H + \frac{1}{A}, \tag{6}$$

where P is the total gas pressure, x_H is the degree of ionization of H, and A is the hydrogen-to-metal ratio. Assuming $A = 10^{4.2}$, we obtain the total pressures, and from the perfect gas law we derive densities, ρ. These quantities are given in columns 13 and 14 of Table 6. The equation of hydrostatic equilibrium is

$$\frac{dP}{d\tau} = \frac{g}{\bar{\kappa}(\tau)}. \tag{7}$$

We shall assume a pressure gradient of this form to obtain a spectroscopically determined effective acceleration, g_e. With sufficient accuracy, it may be shown (Greenstein 1948) that

$$g_e = \frac{P(\tau_0)\ \bar{\kappa}(\tau_0)}{2\tau_0}, \tag{8}$$

where P and $\bar{\kappa}$ are evaluated at the mean optical depth of line formation, τ_0, which we assume to be 0.25. Resulting values of $\log g_e$ are given in column 15 of Table 6 and are plotted in Figure 5. It is probably significant that the g_e's are small at maximum expansions (compare with displacements in Fig. 1) and large at contractions. In fact, the variation in g_e could be used to relate the segments of the displacement-curve if we could believe that the g_e's are directly related to the gravitational g's, whose mean value is of the order of $10^{1.4}$. The range of 10^4 in g_e is much larger than the expected range in g.

We shall not discuss at length the question of what kind of model best fits the observations. As in the case of W Virginis, the observations suggest, at first glance, spherical layers that expand and contract in a time interval greater than that of the ejection of these layers, with successive ones meeting one another. The observed Doppler velocity dispersion is too small if the layers are to fill in the regions between them. However, the problem of the interpenetration of layers is a formidable one. It may perhaps be avoided if the layers are assumed to be nonhomogeneous and to consist of many condensations. This assumption would then lead to the question of how such a layer can be optically thick. It may be that more detailed calculations on the behavior of shock waves in stellar atmospheres will lead to an acceptable model.

One final matter requires discussion, although the relevant data are meager. The colors show very little variation, except for the final measure. For example, the first two observations in Table 1 were taken during a deep light-minimum and the succeeding maximum, but the color difference is only 0.14 mag. Since the light and displacement variations are nearly 180° out of phase (light-minima near maximum expansions), the light-changes must be due predominantly to changes in surface brightness. The color variation is insufficient to account for the light-variation. If the region of line formation is opaque, the photosphere lies in that region, and the light-variation should depend on the area and temperature of the region. Additional photoelectric data are needed, although these would be most meaningful if obtained simultaneously with spectra.

I am grateful to Dr. O. J. Eggen for his photoelectric observations, to the A.A.V.S.O. for the visual observations, and to Drs. J. L. Greenstein, G. H. Herbig, and W. P. Bidelman for reading the manuscript and making helpful suggestions

REFERENCES

Abt, H. A. 1954, *Ap. J.*, suppl., **1**, 63 (No. 3).
Chandrasekhar, S., and Münch, G. 1946, *Ap. J.*, **104**, 446.
Eggen, O. J. 1951*a*, *Ap. J.*, **113**, 367; *Lick Obs. Contr.*, Ser. II, No. 32.
———. 1951*b*, *Ap. J.*, **114**, 141; *Lick Obs. Contr.*, Ser. II, No. 37.
Getting, I. A. 1934, *M.N.*, **95**, 139.
Greenstein, J. L. 1948, *Ap. J.*, **107**, 151; *McDonald Contr.*, No. 145.
Johnson, H. L., and Morgan, W. W. 1951, *Ap. J.*, **114**, 522; *McDonald Contr.*, No. 205.
Joy, A. H. 1949, *Ap. J.*, **110**, 105.
———. 1952, *ibid.*, **115**, 25.
Keenan, P. C., and Morgan, W. W. 1951, *Astrophysics*, ed. J. A. Hynek (New York: McGraw-Hill Book Co.), chap. 1.
McLaughlin, D. B. 1938, *Pub. Univ. Michigan Obs.*, **7**, 57.
———. 1941, *Ap. J.*, **94**, 94.
Mayall, N. U. 1946, *Ap. J.*, **104**, 290; *Lick Obs. Contr.*, Ser II, No. 15.
Morgan, W. W., Harris, D. L., and Johnson, H. L. 1953, *Ap. J.*, **118**, 92; *McDonald Contr.*, No. 224.
Rosino, L. 1951, *Ap. J.*, **113**, 60.
Sanford, R. F. 1931, *Ap. J.*, **73**, 364; *Mt. W. Contr.*, No. 424.
———. 1933, *Ap. J.*, **77**, 120; *Mt. W. Contr.*, No. 465.
———. 1952, *Ap. J.*, **116**, 331.
Stebbins, J., and Huffer, C. M. 1934, *Pub. Washburn Obs.*, Vol. **15**, Part 5.
Wilson, O. C., and Coffeen, M. F. 1954, *Ap. J.*, **119**, 197.
Wrubel, M. H. 1949, *Ap. J.*, **109**, 66.

PASCHEN AND BALMER SERIES IN SPECTRA OF CHI OPHIUCHI AND P CYGNI*

E. MARGARET BURBIDGE AND G. R. BURBIDGE
Cambridge, England
Received February 3, 1955

ABSTRACT

The intensities of the Paschen and Balmer emission lines of hydrogen in χ Oph and P Cyg are given, together with the absorption components in P Cyg. The latter star has a Balmer decrement similar to that of a gaseous nebula, while χ Oph shows differences, similar to those found in other pole-on stars, which may be due to self-absorption. Comparison is made between the populations of the various levels of hydrogen determined from the Paschen and Balmer lines having common upper levels; the results suggest (*a*) a black-body temperature of 15,000° for the emergent continuous radiation of P Cyg and (*b*) support for the self-absorption hypothesis for χ Oph. Estimates of the extents of the emitting regions are given.

I. INTRODUCTION AND OBSERVATIONS

The near-infrared and photographic regions of the spectrum of χ Ophiuchi (B3 Ve) have recently been described by one of us (Burbidge 1952). The separations of the Balmer and Paschen emission components converted to velocities are constant and have the value 110 km/sec over the range λλ 8750–3750. They are consistent with a mean radius for the emitting region of twice the stellar radius of this pole-on star.

The spectrum of P Cygni (B1ep) in the photographic, ultraviolet, and visual regions has been studied by Struve (1935), Struve and Roach (1939), Swings and Struve (1940), Beals (1951), and others. Hiltner (1947) has shown plates of the infrared spectra of both χ Oph and P Cyg. Merrill and Wilson (1934) made some measures of central intensities of Balmer and Paschen lines in P Cyg. They pointed out that intensity measures of lines having the same upper level should enable a simplified treatment of the processes of excitation to be made; this early investigation suggested that the temperature of the star lay between 12,000° and 24,000°.

There appear to be no previous equivalent-width measures in the infrared region of either of these stars (or, so far as the authors are aware, in any similar stars). Therefore, we have thought it worth while to present the results of equivalent-width measures in the infrared and photographic regions, in order to consider the Balmer and Paschen lines together.

In April and May, 1953, one spectrogram each of the region λ 8800–*Hα* of P Cyg and χ Oph was obtained with the 82-inch telescope at the McDonald Observatory, using the coudé grating spectrograph (dispersion 35 A/mm), and Eastman Kodak I-N plates. Two spectrograms each of the photographic region (λλ 4950–3600) were also obtained (dispersion $8\frac{1}{2}$ A/mm). Calibrations in both spectral regions were obtained with the grating calibration spectrograph, which has been briefly described previously (Burbidge and Burbidge 1954); this instrument was used in the first order for the infrared work, with a Wratten "light-red" filter. Microphotometer tracings and reductions were carried out in the usual way.

The equivalent widths of the Balmer emission lines of both stars and the absorption lines of P Cyg have been measured in units of equivalent angstroms of the adjacent continuum, and the means from the pairs of plates are given in Table 1. In χ Oph, where the emission lines from *Hβ* to *H*15 are superposed on broad underlying absorption lines,

* *Contributions from the McDonald Observatory, University of Texas*, No. 255.

their equivalent widths were obtained by drawing in the central parts of the absorption lines as described previously (Burbidge and Burbidge 1953*a;* this paper will hereinafter be described as "Paper I"). Also in χ Oph, where the wings of the broad absorption lines overlap after about $H9$, a small correction was applied to take account of the depression of the continuum (cf. Burbidge and Burbidge 1953*b*, hereinafter referred to as "Paper II"). The results in Table 1 are referred to this corrected continuum. The equivalent widths of the emission components of $H\gamma$–$H23$ in P Cyg have previously been measured

TABLE 1

THE BALMER LINES

Line	Equivalent Widths (Angstroms)			Decrement		
	χ Oph Em.	P Cyg Em.	P Cyg Abs.	χ Oph	P Cyg	Calculated (Nebular)
$H\alpha$	33.9	46.0	.....	2.29	1.58	2.52
$H\beta$	5.79	11.5	.....	1.00	1.00	1.00
$H\gamma$	1.58	4.38	0.77	0.38	0.51	0.51
$H\delta$	1.03	2.08	.73	0.29	0.28	0.31
$H\epsilon$	0.63	1.22	.....	0.19	0.18	0.20
$H\zeta$	0.53	.....	.....	0.17	.....	0.14
$H9$	0.44	0.52	.58	0.15	0.082	0.10
$H10$	0.44	0.44	.46	0.15	0.072	0.076
$H11$	0.41	0.39	.44	0.14	0.064	.....
$H12$	0.36	0.29	.48	0.13	0.046	.....
$H13$	0.41	0.19	.32	0.15	0.032	.....
$H14$	0.44	0.17	.28	0.16	0.030	.....
$H15$	0.44	0.18	.23	0.16	0.030	0.024
$H16$	0.37	.....	.....	0.14	.....	.....
$H17$	0.41	0.08	.18	0.15	0.014	.....
$H18$	0.36	0.11	.14	0.13	0.019	.....
$H19$	0.26	0.06	.14	0.10	0.011	.....
$H20$	0.21	0.08	.12	0.08	0.014	0.011
$H21$	0.19	0.06	.08	0.07	0.011	.....
$H22$	.....	0.05	.08	.....	0.008	.....
$H23$	.....	0.02	.07	.....	0.003	.....
$H24$	.....	0.02	0.05	.....	0.003	.....
$H25$	.....	.....	.....	.....	.....	0.006

by Struve and Roach, and of $H\alpha$–$H\zeta$ by Beals. Comparison shows reasonable agreement, with the exception of $H\alpha$. Owing to its enormous strength, the center of this line falls right at the top of the calibration-curve, and the uncertainty here probably explains the discrepancy. The equivalent widths of the Paschen lines from P 12 to the last visible line are given in Table 2.

II. THE BALMER DECREMENT

The emission-line equivalent widths in Table 1 have been converted to relative intensities by assuming that the stellar continuum can be represented by black-body radiation. The values are referred to $H\beta$ as unity and are also given in Table 1. From its spectral type, the assumed temperature of χ Oph is 18,000° (Keenan and Morgan 1951), and there is no evidence for intrinsic reddening. For P Cyg there has long been uncertainty in the intrinsic color. The Balmer decrement was therefore computed for $T =$ 10,000°, 15,000°, and 22,500° (the latter corresponding to a B1 star with no intrinsic reddening). The value of the decrement is, with the exception of $H\alpha$, rather insensitive to

temperature variation in this range, but, for reasons given in Section III, $T = 15{,}000°$ has been chosen.

The theoretical Balmer decrement for a planetary nebula (Baker and Menzel 1938) has also been given for comparison. The value chosen corresponds to a nebula which is opaque to Lyman-line radiation but transparent to all other line frequencies, and it has been interpolated for an electron temperature of 12,600° (although the decrement is rather insensitive to variation in T_e).

It is at once apparent that the decrement for P Cyg agrees well with the nebular decrement. On the other hand, χ Oph resembles 11 Cam and the other stars studied in Paper II, in that the intensities of the higher Balmer lines are much stronger than the computed nebular values. As before, we interpret these results as suggesting that while in P Cyg self-absorption effects in the lower Balmer lines are negligible, in χ Oph they are of importance. The Paschen decrement referred to P 12 as unity (E_n/E_{12}) is also given in Table 2.

TABLE 2

THE PASCHEN LINES

Line	Equivalent Widths (Angstroms)			E_n/E_{12}	
	χ Oph Em.	P Cyg Em.	P Cyg Abs.	χ Oph	P Cyg
P 12	3.13	0.96	0.34	1.00	1.00
P 13	2.73	.71	.18	0.90	0.77
P 14	3.09	.49	.16	1.05	0.54
P 15	3.72	.47	.26	1.29	0.54
P 16	3.41	.45	.21	1.20	0.52
P 17	2.50	0.33	0.22	0.90	0.38
P 18	2.12	.....	.....	0.77	.....
P 19	2.67	.....	.....	0.98	.....
P 20	1.81	.....	.....	0.67	.....
P 21	1.30	.....	.....	0.48	.....
P 22	1.33	.....	.....	0.50	.....
P 23	1.11	.....	.....	0.42	.....
P 24	0.98	.....	.....	0.37	.....
P 25	0.87	.....	.....	0.30	.....

III. RELATIVE INTENSITIES OF THE PASCHEN AND BALMER EMISSION LINES

We have (cf. Paper I, eq. [11])

$$N_n = 8\pi^2 c \frac{R_*^2}{V} \frac{w}{\lambda^4 A_{nm} (e^{h\nu/kT} - 1)}, \tag{1}$$

where N_n is the population of level n, R_* is the radius of the star, w is the equivalent width of the emission line with n as upper level, and V is the total volume of the emitting region. This equation applies to both Balmer and Paschen lines, with $n = 2$ and 3, respectively, so that two independent determinations of N_n for each value of n are possible. The ratios N_n (Balmer)/N_n (Paschen) are given in Table 3. In equation (1) it is assumed that the stellar continuum is represented by a black-body-curve between λ 3700 and λ 8750. That this is approximately correct is shown by the flux diagram for a hot model atmosphere (Underhill 1950).

P Cyg.—Since there is a nebular Balmer decrement, implying that there is probably no self-absorption, we should find that N_n (Balmer) $\equiv$ N_n (Paschen) for this star. This

is approximately true for the mean of the five lines in Table 3, if $T = 15{,}000°$, and we conclude, therefore, that this is the representative black-body temperature over this wave-length range. Hence there is a small amount of intrinsic reddening. Miss Roman (1951), in a study of the colors of early-type stars in Cygnus, showed that if P Cyg were at the same distance as a concentration of these stars, then its color could be explained wholly by interstellar reddening, and it would have an absolute visual magnitude of -8.3. If the intrinsic color were given by a temperature of 15,000°, corresponding to a B6 star, then the difference in the C_1 color between this and the expected value for a B1 star would be 0.05 (Stebbins, Huffer, and Whitford 1940). This appears to lie within the scatter in color excesses of the group of emission-line stars given by Miss Roman.

χ Oph.—If $T = 18{,}000°$, the mean ratio N_n (Balmer)/N_n (Paschen) = 0.53. To make this ratio unity, it would be necessary to assume that T was of the order of 100,000°, and this is clearly not correct. However, since the Balmer decrement suggests that self-absorption is present, the results in this case can be interpreted by supposing that the cut-

TABLE 3

RELATIVE POPULATIONS DERIVED FROM THE PASCHEN AND BALMER SERIES

n	N_n (BALMER)/N_n (PASCHEN)		n	N_n (BALMER)/N_n (PASCHEN)	
	χ Oph (18,000°)	P Cyg (15,000°)		χ Oph (18,000°)	P Cyg (15,000°)
12	0.49	1.04	17	0.65	0.83
13	.62	0.93	18	.66	.....
14	.59	1.23	19	.38	.....
15	.48	1.27	20	.46	.....
16	0.43	.....	21	0.56	.....

down factor (Paper II, eq. [14]) for the Balmer lines is more pronounced than that for the Paschen lines. From Paper II we have

$$\text{Cut-down factor} = \frac{\bar{D}}{D'}\frac{f}{\tau},$$

where τ is the optical depth at the frequency of the line center, and the other quantities are defined therein. From the definitions of D and D' it is easily shown that D/D' (Balmer) = D/D' (Paschen), for lines having the same upper level. Since the shapes of the lines are determined by the atmospheric velocities, it is reasonable to suppose that the Balmer and Paschen line profiles are similar, so that, averaging over the line widths, $\bar{D}/\bar{D}'$ (Balmer) $\simeq \bar{D}/D'$ (Paschen). Also for $\tau \geq 5$, f is nearly constant (Paper II, Table 3). Now for any line, $\tau \propto \lambda N_n$ times oscillator strength f_{mn}, so that

$$\frac{N_n\,(\text{Balmer})}{N_n\,(\text{Paschen})} = \frac{N_3 f_{3n}\lambda_{3n}}{N_2 f_{2n}\lambda_{2n}}.$$

Using this equation, we have found that the mean value of N_2/N_3 is 7.4. This is the calculated ratio for an atmosphere in thermodynamic equilibrium at 8000°. However, when $\tau < 5$, which may well be the case for the higher values of n, this approximation breaks down, since f/τ then has a complicated dependence on τ.

Qualitatively, we may conclude that the comparison of the Balmer and Paschen line

intensities supports the suggestion that appreciable self-absorption occurs in the outer atmosphere of χ Oph, at any rate in the Balmer lines.

IV. THE DILUTION FACTORS AND THE STRUCTURE OF THE ATMOSPHERES

P Cyg.—Struve and Roach suggested that the dilution factor W could be derived from a comparison of the absorption and emission lines, if it were supposed that they were produced in the same region. By this method for the Balmer lines they found $W > 1$, which is a priori impossible. They suggested that one of the reasons for this result was that the Balmer absorption lines were too strong, owing to metastability of the 2s level, and that the use of the Paschen lines might give a valid result. We have applied this method to the Paschen lines and have found $W \simeq 0.5$. However, this is ten times the dilution factor found by Struve and Roach from the *He* I absorption lines.

In this model the motions of the atmosphere are not considered. On the other hand, Rottenberg (1952) has given an idealized treatment of the redistribution of light by scattering in an expanding shell; the profiles of emission and adjacent absorption components, having equal intensities, are then produced entirely by the motions of the shell. The emission component arising in this way may be added to an intrinsic emission line produced by recombination in a region lying inside the scattering shell. Thus, to apply Rottenberg's results to our measures, the equivalent width of the absorption component should be subtracted from that of the emission component to obtain correct values for the recombination emission lines. However, from Table 1 we see that, from *H*9 onward, the absorption component is the stronger. This can be explained in Rottenberg's picture only by supposing that occultation effects are present. Since the observed effect varies along the series, this would imply that there is stratification in the line production. However, consideration of the transfer of radiation through a shell shows that absorption, as well as scattering, is likely to take place. Also, the separation into an emitting and an outer scattering shell is an oversimplification, in the opposite sense to that of Struve and Roach, and a model lying between the two is indicated.

In view of the complexities of the problem and also the inherent observational errors, it does not seem possible to use the measures to determine quantitatively to what extent each picture applies. We shall conclude by obtaining a rough estimate of the extent of the outer atmosphere by using the total strengths of the *uncorrected* Balmer emission lines, in a similar manner to that used for a static shell in Paper I. Using equation (1) and $T = 15{,}000°$, we find, by summing over the available levels, that

$$\frac{V}{R_*^2}\sum_{n=3}^{24} N_n = 3.1 \times 10^{17}.$$

Since $N_1 \simeq 100\,\Sigma N_n$, $VN_H \simeq 3 \times 10^{19}\,R_*^2$, where N_H is the density of neutral hydrogen. The luminosity of P Cyg is about a hundred times that of a main-sequence star of similar type, so that $R_* \simeq 50\,R_\odot$. In order to determine N_H, the electron density is needed. Previously the value obtained from the Inglis-Teller formula has been used. However, there are considerable uncertainties in this method. In P Cyg the internal motions in the emitting region are more important than the interionic Stark effect in determining the line widths. In view of the uncertainties involved, we shall put $n_e = 10^{11}$/cc, whereas the Inglis-Teller formula gives $n_e = 8 \times 10^{12}$/cc. Assuming a spherical model of the outer atmosphere (Paper I, Fig. 13, *a*), we have $V = (4\pi/3)(a^3 - 1)R_*^3$, where aR_* is the radius of the outer atmosphere. We then find that $a = 1.5$. a is rather sensitive to changes in the assumed value of the electron pressure, and if, for example, n_e were as low as 10^{10}/cc, then a would be 6.5. A value lying between these two is consistent with $W = 0.05$, which was obtained by Struve and Roach from the *He* I absorption lines.

χ *Oph.*—The extent of the outer atmosphere has been determined, again using the Balmer emission lines. Since χ Oph is a pole-on star, we have taken $V = 2\pi(a^2 - 1)R_*^3$, where aR_* is the outer radius of the disk-shaped atmosphere in its equatorial plane (Paper I, Fig. 13, *b*). The measures give

$$\frac{V}{R_*^2}\sum_{n=3}^{21} N_n = 1.1 \times 10^{18},$$

for $T = 18{,}000°$; here $R_* = 4.8\ R_\odot$, and again $N_1 \simeq 100\Sigma N_n$. The Inglis-Teller formula gives $n_e = 2 \times 10^{13}$/cc. Motions are indicated in this atmosphere, since the rotational separation of the double emission lines is 110 km/sec. By analogy with their photospheres, we might expect the electron density in the outer atmosphere to be an order of magnitude greater in χ Oph than in the supergiant P Cyg. If we put $n_e = 10^{12}$/cc and 10^{11}/cc, then $a = 1.3$ and 8.4, respectively. These values may be underestimated, because the effect of self-absorption has been neglected.[1]

The material on which this paper is based was obtained while the authors were working at the Yerkes and McDonald Observatories.

REFERENCES

Baker, J. G., and Menzel, D. H. 1938, *Ap. J.*, **88**, 52.
Beals, C. S. 1951, *Pub. Dom. Ap. Obs. Victoria*, **9**, 1.
Burbidge, E. M. 1952, *Ap. J.*, **115**, 418.
Burbidge, G. R., and Burbidge, E. M. 1953*a*, *Ap. J.*, **117**, 407.
———. 1953*b*, *ibid.*, **118**, 252.
———. 1954, *ibid.*, **120**, 76.
Hiltner, W. A. 1947, *Ap. J.*, **105**, 212.
Keenan, P. C., and Morgan, W. W. 1951, *Astrophysics*, ed. J. A. Hynek (New York: McGraw-Hill Book Co.), p. 23.
Merrill, P. W., and Wilson, O. C. 1934, *Ap. J.*, **80**, 19.
Roman, N. G. 1951, *Ap. J.*, **114**, 492.
Rottenberg, J. A. 1952, *M.N.*, **112**, 125.
Stebbins, J., Huffer, C. M., and Whitford, A. E. 1940, *Ap. J.*, **91**, 20.
Struve, O. 1935, *Ap. J.*, **81**, 66.
Struve, O., and Roach, F. E. 1939, *Ap. J.*, **90**, 727.
Swings, P., and Struve, O. 1940, *Ap. J.*, **91**, 571.
Underhill, A. B. 1950, *Pub. Obs. Copenhagen*, No. 151.

[1] In Paper I the extent of the emitting region of the pole-on star 11 Cam (similar to χ Oph) was wrongly estimated, owing to the omission of a numerical factor and an underestimate for the proportion of hydrogen in the ground state. If we also allow for the uncertainty in the electron density and use the same values as for χ Oph, then $a = 1.2$ and 6.8 for $n_e = 10^{12}$ and 10^{11}, respectively. These values may be compared with the original estimate of $a \simeq 20$ ($n_e = 1.5 \times 10^{13}$, taken from the Inglis Teller-formula).

THE BETA CANIS MAJORIS STARS GAMMA PEGASI, DELTA CETI, AND XI_1 CANIS MAJORIS*

D. H. McNAMARA
Berkeley Astronomical Department, University of California
Received December 20, 1954; revised January 10, 1955

ABSTRACT

The velocity-curves of the three stars γ Pegasi, δ Ceti, and XI_1 Canis Majoris have been determined from Mills spectrograms. The amplitudes of these curves appear to be constant. The profiles of the spectral lines undergo no changes during the velocity cycle. In these respects the stars differ from the other known members of the β Canis Majoris class. A correlation between the periods and the velocity amplitudes is indicated.

I. INTRODUCTION

Our knowledge of the β Canis Majoris or β Cephei group of variable stars has improved in recent years. A summary of our knowledge up until 1952 has been written by Struve (1952). The observational data indicate that the velocity and light vary in the same period, with maximum light occurring when the velocity-curve crosses the γ-axis from positive to negative values. The seven stars investigated up until 1952 were found to have velocity-curves that varied in amplitude. In three of the stars the variation in velocity amplitude has been found to be periodic. With the exception of the star β Cephei, the spectral lines of these stars were found to undergo a change in profile during the short-period cycle. The line broadening is especially pronounced in the stars that have a large velocity range. In this paper the results obtained for three additional members of this group of variable stars are discussed. In certain respects they have been found to differ from the other members of the group. Preliminary results were published previously in a short abstract (McNamara 1953*b*).

II. OBSERVATIONS

The observations described in this investigation were obtained at the Lick Observatory with the Mills spectrograph attached to the 36-inch refractor. This instrument gives a dispersion of 12 A/mm at λ 4500. Since the three stars under investigation were bright, relatively short exposure times were required (10–20 min.). The star lines used for the determination of the radial velocities are given in Table 1. Tables 2, 3, and 4 list

TABLE 1

LIST OF STAR LINES

Wave Length	Element	Wave Length	Element
4471.48.....	*He* I	4574.78.....	*Si* III
4481.23.....	*Mg* II	4590.97.....	*O* II
4552.65.....	*Si* III	4596.18.....	*O* II
4567.87.....	*Si* III		

the individual radial velocities. The lines in the spectra of these stars are very sharp, and hence accurate velocities can be obtained. The probable error of a single velocity in Tables 2, 3, and 4 is of the order of 1 km/sec.

* The observational material presented in this paper was obtained at the Lick Observatory.

III. DISCUSSION

1. γ PEGASI

The spectrum of γ Pegasi has been investigated in great detail. Miss Underhill (1948) has compiled the most recent list of the atomic lines that appear in the spectrum. It is listed as a standard star of spectral type B2 IV in the revised "Atlas of Stellar Spectra" (Johnson and Morgan 1953). Spectrophotometric investigations of γ Pegasi have been made by Aller (1949), Miczaika (1948), and Neven and De Jager (1954) for the purpose of determining atomic abundances.

The variable radial velocity of γ Pegasi was announced by Burns (1911); but, since the amplitude indicated by his observations was so small, it was regarded either with suspicion or without interest because no one investigated further the velocity variation. A series of spectrograms of this star obtained in 1952 showed conclusively that the velocity is variable in the remarkably short period of 3^h38^m (McNamara 1953*a*). The short-period velocity variation and spectral type indicate that γ Pegasi is a member of the β Canis Majoris class of variable stars. The old series of radial velocities obtained in 1952 and a new series obtained in 1953 are listed in Table 2. These velocity observations can be represented by the formula

$$\text{Max. vel.} = \text{JD } 2434266.854 + 0.15175E\,.$$

TABLE 2

RADIAL VELOCITIES OF γ PEG

JD 2434+	Phase (Fraction of P)	Velocity (Km/Sec)	JD 2434+	Phase (Fraction of P)	Velocity (Km/Sec)
238.942	0.066	+6.5	280.865	0.329	+0.6
.956	.158	+5.8	.873	.382	+0.1
.972	.264	+2.0	.888	.481	−0.7
253.853	.233	+1.1	.901	.567	−0.1
.885	.534	−0.1	.913	.646	+0.6
.925	.797	+3.3	.928	.745	+3.0
.960	.033	+6.6	.943	.843	+5.2
.994	.257	+3.5	.957	.936	+6.2
266.821	.784	+4.2	.970	.020	+6.2
.831	.850	+3.4	.981	.092	+6.0
.845	.942	+4.7	638.686	.297	+0.6
.860	.040	+5.8	.700	.389	−0.6
.878	.158	+5.7	.717	.501	−2.4
.889	.231	+4.0	.731	.593	−1.0
.901	.310	+1.2	.749	.712	+1.0
.915	.402	+1.6	.769	.843	+3.6
.928	.488	+0.4	.786	.956	+4.2
.941	.573	−1.3	.806	.086	+3.5
.957	.679	+0.7	.824	.204	+1.3
.967	.745	+3.5	659.750	.099	+3.8
.976	.804	+6.3	.765	.198	+3.3
.987	.876	+5.1	.782	.310	+1.9
.999	.956	+7.5	.799	.422	−2.7
267.006	.000	+6.8	.816	.534	−1.7
280.776	.745	+2.8	.835	.659	+0.1
.786	.811	+6.1	.853	.778	+1.9
.799	.896	+5.6	.874	.916	+5.6
.810	.969	+7.2	.888	.013	+6.2
.822	.046	+5.4	.901	0.099	+5.7
.836	0.138	+2.7			

This is the shortest known period for any star belonging to the β Canis Majoris group of variable stars. The individual velocities of γ Pegasi are plotted against phase in Figure 1. The amplitude of the velocity variation is small; $2K = 7.0$ km/sec. Since the scatter in Figure 1 can be accounted for in terms of errors of measurements, we conclude that the amplitude of the velocity-curve of γ Pegasi is constant. This result is of interest, in view of the amplitude variations observed in the seven stars discussed by Struve (1952). The lines in the spectrum of γ Pegasi are sharp throughout the entire cycle of the velocity variation. Thus in this respect it also differs from the majority of the other stars of its class. Although there is no detectable change in the velocity amplitude, there is a suggestion of a variable γ-velocity. It is true that the displacement of the 1953 observations with respect to the 1952 observations is small, but it is probably real, in view of the displacement of the 1931 velocities (McNamara 1953*a*) from the more recent ones. The light-variability of γ Pegasi has been investigated by Williams (1954*a*), who finds a small light-range of only 0.015 mag. As in the other stars of this group, light-maximum occurs when the velocity crosses the γ-axis from positive to negative values.

2. δ CETI

Like γ Pegasi, δ Ceti is listed as a standard star of spectral type B2 IV in the revised "Atlas of Stellar Spectra" (Johnson and Morgan 1953). The spectrum of δ Ceti has been studied by Aller (1949) and Neven and De Jager (1954) for the purpose of determining the abundances of the elements.

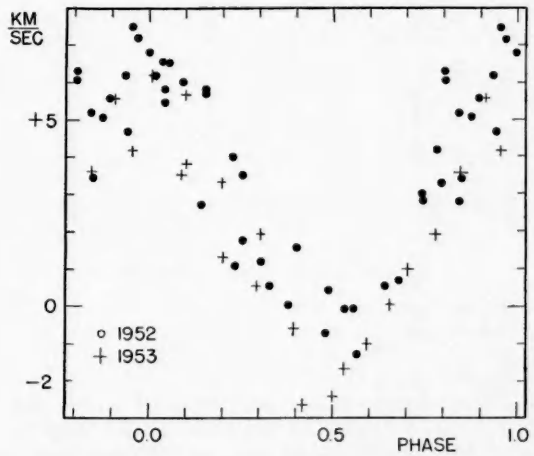

FIG. 1.—Radial velocities of γ Pegasi

The variable velocity of δ Ceti was announced by Frost and Adams (1903). An investigation of the star's velocity was later undertaken by Henroteau (1925), who concluded that the star's velocity was erratic. He later revised this opinion and concluded that δ Ceti was a β Canis Majoris star with a period of 3^h52^m, with a variable velocity amplitude and rapidly varying γ-velocity. The present observations confirm his period but contradict the latter two conclusions. An investigation of the velocity-curve of δ Ceti was also made by Crump (1934), who found a period of 0.1556 day. Crump's period was derived from series of observations obtained on single nights. No attempt was made by

him to represent all the observations with one period, which probably accounts for the discrepancy between his and Henroteau's values of the period.

After Henroteau had announced that δ Ceti is a β Canis Majoris star, Guthnick (1925) and Baker (1926) undertook photometric observations of δ Ceti. They failed to detect any light-variation.

In view of the conflicting spectroscopic periods and negative photometric results, Struve and Swings (1941) considered δ Ceti as only a doubtful member of the β Canis Majoris class.

Photometric observations of δ Ceti were obtained by Walker (1953) at about the same

TABLE 3

RADIAL VELOCITIES OF δ CETI

JD 2434+	Phase (Fraction of P)	Velocity (Km/Sec)	JD 2434+	Phase (Fraction of P)	Velocity (Km/Sec)
288.889	0.881	+12.3	308.935	0.285	+ 6.1
.911	.019	+12.8	350.607	.900	+12.7
.932	.149	+10.9	.632	.056	+13.8
.956	.298	+ 6.2	.653	.186	+11.9
.976	.422	+ 2.3	.676	.329	+ 5.9
.997	.552	+ 2.2	.699	.472	+ 0.8
289.015	.664	+ 3.8	.721	.608	+ 1.5
296.779	.844	+11.4	.742	.738	+ 6.8
.797	.956	+14.3	.769	.906	+12.5
.817	.087	+12.4	630.817	.856	+11.7
.837	.211	+ 8.6	.836	.974	+13.7
.857	.335	+ 2.1	.858	.112	+14.3
.874	.441	+ 1.6	.880	.248	+ 8.6
.892	.552	+ 1.3	.903	.391	+ 3.8
.910	.664	+ 5.7	.924	.521	+ 2.7
.929	.782	+ 8.1	.946	.658	+ 2.0
.950	.912	+13.3	.967	.788	+ 9.6
.973	.050	+14.6	.987	.906	+14.3
308.762	.211	+ 9.5	638.844	.670	+ 3.7
.781	.329	+ 4.4	.862	.782	+ 9.6
.805	.478	+ 1.5	.887	.937	+11.5
.826	.608	+ 2.0	.905	.050	+14.3
.847	.739	+ 7.4	.926	.180	+11.1
.865	.850	+11.2	.947	.310	+ 6.7
.887	.987	+14.3	.966	.428	+ 2.0
.907	.112	+13.2	.985	0.546	+ 1.9
.922	0.205	+ 9.5			

time that the first spectroscopic observations reported in this paper were made. He found that the light is variable, with an amplitude of 0.025 mag. The small amplitude probably accounts for the failure of Guthnick and Baker to detect any light-variation. Walker's photometric observations were consistent with the spectroscopic period derived by Henroteau.

This present investigation of δ Ceti was undertaken for the purpose of ascertaining whether the star is actually a member of the β Canis Majoris class, as Henroteau had originally suggested. This fact was established by the observations obtained on October 3, 1952. The star was subsequently observed on five additional nights in 1952 and 1953, in order to study possible variations in the amplitude of the velocity-curve. The individual velocities are tabulated in Table 3. The phases listed in the second column of Table 3 were computed with the aid of the formula

$$\text{Max. vel.} = \text{JD } 2434288.908 + 0.1611366E\,.$$

This period represents satisfactorily the velocity maximum obtained by Henroteau and Crump, provided that errors in the Julian dates in Crump's paper are corrected. The individual velocities of the present investigation are plotted against phase in Figure 2. As in the case of γ Pegasi, the amplitude of the velocity-curve seems to be constant. The total amplitude, $2K = 12.6$ km/sec, is in excellent agreement with the $2K$ value of 12 km/sec found by Crump. If allowance is made for the precision of Henroteau's observations, his $2K$ values also agree favorably with the $2K$ value of the present investigation. The mean velocity of δ Ceti is +8.2 km/sec. The spectral lines undergo no detectable change in the width during the cycle. In this respect it is also similar to γ Pegasi.

Through a fortunate circumstance, Walker (1953) obtained photometric observations of δ Ceti on the same night (October 3, 1952) on which I obtained radial-velocity ob-

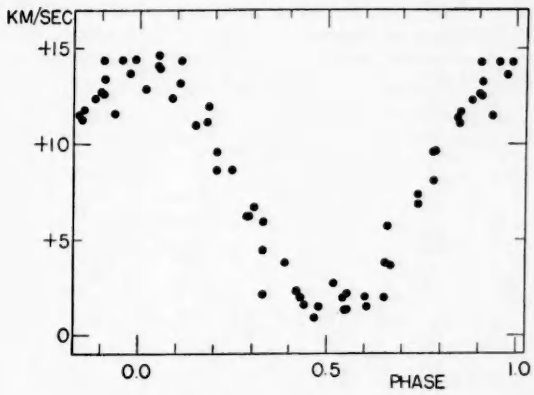

FIG. 2.—Radial velocities of δ Ceti

servations. The combination of the two sets of observations indicates that maximum light occurs when the velocity crosses the γ-axis from positive to negative values.

3. ξ_1 CANIS MAJORIS

The variable velocity of ξ_1 Canis Majoris was discovered by Frost (1907). Henroteau (1921) subsequently observed the star and confirmed the variability but was unable to find a period. ξ_1 Canis Majoris was observed photometrically by Walker (1952), who reported that the star showed no light-variation greater than 0.01 mag. on the two nights that he observed it. A series of spectrograms obtained in 1952 revealed the short-period nature of the velocity variation (McNamara 1953*b*). Further observations were obtained in order to establish the period and to investigate possible changes in the amplitude of the velocity-curve.

The radial-velocity observations of ξ_1 Canis Majoris are listed in Table 4. The phases of maximum velocity can be represented with the formula

$$\text{Max. vel.} = \text{JD } 2434337.026 + 0.209574E\,.$$

The individual velocities plotted against their phases, derived from this formula, are shown in Figure 3. The velocity-curve is symmetrical, and the amplitude is constant with $2K = 36.0$ km/sec. In these respects it is similar to γ Pegasi and δ Ceti.

Additional photometric observations of ξ_1 Canis Majoris were obtained by Williams (1954*b*) in 1953 and 1954. A mean amplitude of 0.04 mag. is indicated by his results. The

light-curve is slightly asymmetric, and light-maximum falls after the velocity has crossed the γ-axis from positive to negative values. Williams' results indicate that the light-amplitude is variable, which probably accounts for Walker's failure to detect any light-variation in 1951. Further photometric observations of this star are highly desirable.

The variable light-range is especially interesting in view of the constant velocity amplitude indicate by the spectroscopic observations. There exists at least a rough correlation between the light-amplitudes and the velocity amplitudes of the β Canis Majoris stars. One would expect, therefore, a change in the velocity amplitude with a change in the light-amplitude, yet there is not the slightest suggestion in my observations extend-

TABLE 4

RADIAL VELOCITIES OF ξ_1 CMA

JD 2434+	Phase (Fraction of P)	Velocity (Km/Sec)	JD 2434+	Phase (Fraction of P)	Velocity (Km/Sec)
326.969.....	0.730	+18.0	381.903.....	0.134	+31.0
.992.....	.840	+29.0	.924.....	.234	+22.6
337.014.....	.945	+38.2	.940.....	.310	+16.6
.033.....	.033	+38.7	399.656.....	.844	+30.4
343.854.....	.582	+ 5.6	.679.....	.954	+39.4
.873.....	.673	+11.7	.705.....	.076	+34.4
.895.....	.778	+22.6	.733.....	.210	+26.3
.913.....	.864	+32.1	.757.....	.324	+15.5
.935.....	.969	+36.4	.777.....	.420	+ 6.4
.951.....	.043	+39.7	.799.....	.525	+ 4.0
.968.....	.124	+32.9	.823.....	.639	+12.0
.987.....	.215	+23.9	.847.....	.754	+21.6
344.005.....	.301	+17.2	679.881.....	.964	+38.7
.020.....	.372	+ 7.9	.898.....	.043	+38.0
381.715.....	.239	+18.0	.917.....	.134	+31.6
.728.....	.301	+16.6	.935.....	.219	+22.3
.753.....	.420	+ 5.7	.953.....	.305	+15.5
.774.....	.520	+ 4.4	.976.....	.415	+ 7.8
.808.....	.682	+11.0	.994.....	.501	+ 4.5
.839.....	.830	+26.6	680.014.....	.596	+ 6.4
.865.....	.954	+37.7	.036.....	.701	+13.9
.885.....	0.048	+38.9	.057.....	0.802	+22.0

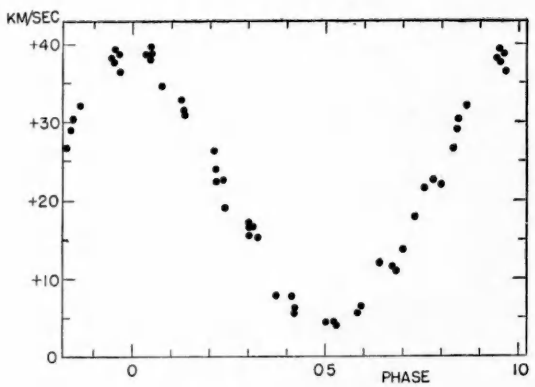

FIG. 3.—Radial velocities of ξ_1 Canis Majoris

ing over a year of a change in the velocity amplitude of ξ_1 Canis Majoris. The possibility exists, of course, that I have not observed the star when the light-amplitude was small. It should be emphasized that no information on the light-curve is available for the nights that the spectrograms were obtained. However, unless future observations prove otherwise, we must regard the velocity amplitude of ξ_1 Canis Majoris as constant.

The spectrum of ξ_1 Canis Majoris is definitely earlier than those of γ Pegasi and δ Ceti. In spectral type it resembles β Canis Majoris and σ Scorpii, although the spectral lines are sharper in the spectrum of ξ_1 Canis Majoris than in the spectra of σ Scorpii and β Canis Majoris, even when the latter two are in the sharp-line stage. As in the case of γ Pegasi and δ Ceti, the lines in the spectrum of ξ_1 Canis Majoris show no detectable change in width during the velocity cycle.

As was pointed out earlier, the seven other known members of the β Canis Majoris group of variable stars have all shown variations in the amplitudes of their velocity-curves; the fact that the three stars investigated here do not show variations suggests that they are unique members of this group of variable stars.

The line broadening that is present in the spectra of the stars with variable velocity amplitudes has recently been satisfactorily explained by Struve (1954) as resulting from the merger of at least two sets of absorption lines in the spectrum that vary in velocity

TABLE 5

SUMMARY OF OBSERVATIONAL DATA

Star	P (Days)	Sp	$(B-V)_i$	$2K$ (Km/Sec)	Light Amp. (Δ Mag.)
γ Peg.....	0.15175	B2 IV	−0.24	7.0	0.015
δ Ceti.....	.1611366	B2 IV	− .245	12.6	.025
ξ_1 CMa.....	0.209574	B1 IV	−0.28	36.0	0.01−0.040

and intensity. Thus the velocity-curve is actually discontinuous at the critical phases when the two sets of absorption lines are present. The line doubling has actually been observed only in the stars 12 Lacertae, BW Vulpeculae, and σ Scorpii, but we can infer that the same phenomenon is taking place in the spectra of the other stars that display this periodic line broadening. On the other hand, γ Pegasi, δ Ceti, and ξ_1 Canis Majoris exhibit neither periodic line broadening nor variable velocity amplitudes. We conclude, therefore, that only one set of absorption lines is observed in the spectra of these three stars. Among the Cepheid variable stars, the line doubling seems to be restricted to the type II variables. Among the β Canis Majoris (type I) stars, however, there are stars which exhibit a single set of sharp absorption lines throughout the entire velocity cycle, as well as stars that show the periodic line doubling.

A summary of the basic observational data pertaining to the three stars discussed here is given in Table 5. The intrinsic colors $(B - V)_i$ on the Johnson-Morgan system ($B - V$ corrected for color excess) have been taken from a recent investigation by McNamara and Williams (1955). The sources of the other information are given in the text.

The velocity amplitudes listed in the fifth column of Table 5 are plotted against their periods in Figure 4. A linear correlation between the periods and the amplitudes is indicated. The line shown in Figure 4 was computed by least squares and is given by the equation

$$2K \text{ km/sec} = -67.75 + 495.5P \text{ days}.$$

The velocity amplitudes of γ Pegasi and δ Ceti fall off this line by only -0.4 and $+0.5$ km/sec, respectively. Although the fit is so good that it can hardly be considered fortuitous, we should consider this relationship a tentative one, in view of the small number of stars. Additional β Canis Majoris stars of this type (constant amplitudes) will have to be found and investigated thoroughly before we can prove or disprove this correlation.

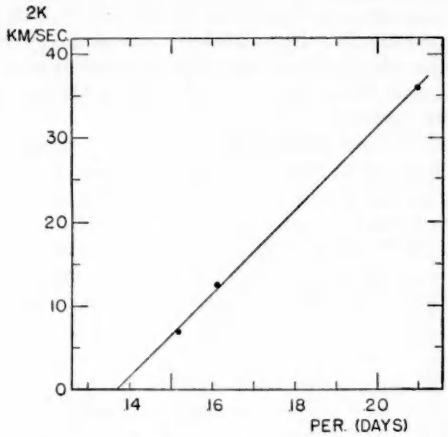

FIG. 4.—The correlation between the periods and the velocity amplitudes

It is of interest to note, however, that an extrapolation of the line would give a zero velocity amplitude for a star with a period of 3^h17^m. Since the spectral type is correlated with the period, this may explain why we have not found any stars belonging to this group that have spectral types later than B2.

REFERENCES

Aller, L. H. 1949, *Ap. J.*, **109**, 244.
Burns, K. 1911, *Lick Obs. Bull.*, **6**, 141.
Crump, C. C. 1934, *Ap. J.*, **79**, 351.
Frost, E. B. 1907, *Ap. J.*, **25**, 64.
Frost, E. B., and Adams, W. S. 1903, *Ap. J.*, **17**, 150.
Henroteau, F. 1925, *Pub. Dom. Ap. Obs. Victoria*, **9**, 23.
Johnson, H. L., and Morgan, W. W. 1953, *Ap. J.*, **117**, 313.
McNamara, D. H. 1953*a*, *Pub. A.S.P.*, **65**, 144.
———. 1953*b*, *ibid.*, p. 193.
McNamara, D. H., and Williams, A. D. 1955, *AP. J.*, **121**, 51.
Miczaika, G. R. 1948, *Milt. d. Badischen Landessternwarte Heidelberg*, No. 60, p. 241.
Neven, L., and Jager, C. de. 1954, *B.A.N.*, **12**, 103.
Struve, O. 1952, *Ann. d'ap.*, **15**, 157.
———. 1954, *Pub. A.S.P.*, **661**, 329, 1954.
Struve, O., and Swings, P. 1941, *Ap. J.*, **94**, 99.
Underhill, A. B. 1948, *Ap. J.*, **107**, 337.
Walker, M. F. 1952, *A.J.*, **57**, 229.
———. 1953, *Pub. A.S.P.*, **65**, 49.
Williams, A. D. 1954*a*, *Pub. A.S.P.*, **66**, 25.
———. 1954*b*, *ibid.*, p. 200.

A MICROPHOTOMETRIC STUDY OF THE SPECTRUM OF SIGMA SCORPII*

SU-SHU HUANG AND OTTO STRUVE
Berkeley Astronomical Department, University of California
Received January 10, 1955

ABSTRACT

Thirteen high-dispersion spectrograms of the β Canis Majoris star, σ Sco (4.5 A/mm), in the same cycle of the radial-velocity variation, have been investigated microphotometrically. The profile of each line changes considerably during the period of oscillation, but its equivalent width remains practically constant. On the descending branch of the radial velocity each line splits into two components in a similar way as in HD 199140, another β Canis Majoris star. We can unambiguously follow on the tracings the growth and decay of the components. On the ascending branch of the radial velocity-curve the lines are comparatively narrow. Because the equivalent width does not vary with phase, the splitting of line profiles must be due to macroscopic motion. In other words, the two streams must be moving in different parts on the star's disk instead of one above the other. At the end of the paper is an appendix which deals with the effect of the exposure time upon the line profile.

I. INTRODUCTION

An interesting feature of some of the β Canis Majoris or β Cephei stars is the change in line widths accompanying variation in radial velocity. In general, the absorption lines show, on the descending branch of the radial velocity-curve, the kind of broadening characteristic of macroscopic motion, such as stellar rotation, mass convection, etc. But at certain phases on the ascending branch of the radial velocity the spectral line becomes much narrower than at any other phase. O. Struve's recent high-dispersion investigation (1954) of HD 199140 = BW Vulpeculae shows, however, that each absorption line in the broad-line stage actually consists of two components. On his spectrograms the growth and fading of these component lines can be clearly seen in two short intervals of less than half an hour, after which the absorption line remains single for the rest of the cycle. On the low-dispersion plates the component lines coalesce into a single line because of the instrumental broadening, and consequently they resemble rotational profiles. The present investigation of σ Sco confirms, in general, this result. We believe, therefore, that in all the β Canis Majoris stars that show changes in line profile during the cycle, the broad-line stage is simply the time when the absorption line splits, for some unknown reason, into several components. Moreover, it is quite possible that the phenomenon of line splitting at a certain stage of the radial-velocity variation should be a fundamental feature of all β Canis Majoris stars, although the splitting of lines in some of these stars might be too small to have been detected.

The present paper treats mainly the analysis of the observational material of a particular star of this type and consequently makes no attempt to explain systematically the phenomena observed in all the β Canis Majoris stars in terms of a single physical picture. However, some plausible suggestions which might help in interpreting the empirical results have been interwoven in the discussion.

II. PRESENTATION OF THE MEASURED RESULTS

The radial velocity-curve of σ Sco has been previously studied by Levee (1952) based on a series of plates taken at the Lick Observatory. He also measured the widths of some absorption lines directly on the plates and noticed their variation during the cycle. Re-

* The spectrograms used in this investigation were obtained by Mr. O. Struve as guest investigator at the Mount Wilson Observatory.

cently, a series of high-dispersion plates of the same star was taken at the Mount Wilson Observatory, enabling us to make a more accurate study of the radial velocity-curve and a microphotometric study of the variation in line profiles. The radial-velocity part is presented in the previous paper (Struve, McNamara, and Zebergs 1955), and the microphotometric part is given here.

Out of fifteen spectrograms, taken on May 16 (5^h59^m–11^h18^m U.T.), 1954, which cover a complete cycle of the radial-velocity variation, thirteen were traced by a microphotometer and reduced to an intensity scale by a semiautomatic instrument. The location upon the velocity-curve of some of these spectrograms, identified by their numbers, is shown in Figure 3, *a*. The identification of the absorption lines was guided by several tables of wave lengths (Struve 1931, 1939; Struve and Dunham 1933; Moore 1945; Underhill 1948). We have selected forty lines which are believed to be free from serious blends and have measured various quantities which will be described presently.

The spectrum of σ Sco, unlike that of ordinary stars, shows such peculiar line profiles that we must first define some measurable quantities before we can describe it. We classify the line profiles into four main categories: (1) S = symmetric, (2) A = asymmetric, (3) D = double, and (4) T = triple. To the D category belong not only all the lines which show two minima of light-intensity but also those which have a hump on either one of the two branches of the line. The hump is not a minimum but is characterized mathematically by two successive points in inflection. The fourth category is only occasionally observed in some uncertain cases and consequently is not important in the present consideration.

For lines of all categories we have measured three quantities, viz.: (1) the maximum depth or depths, (2) the half-width, and (3) the equivalent width. For the S lines, all these three quantities are well defined and need no explanation. For the A lines, the half-width is given as the sum of two parts: the half-half-width (denoted by "hhw." hereafter) on the violet side and the hhw. on the red side. In Table 1 the violet hhw. always precedes the red hhw. The two hhw.'s give us a general idea of the degree of asymmetry but do not give complete information as to the nature of the asymmetry. Thus we sometimes find asymmetrical lines with equal hhw.'s on both the violet and the red side. In the case of a double line, two maximum depths have been measured; the violet one is always given first. It is difficult to define a half-width of a double line. We have measured an hhw. on the violet side with respect to the maximum depth of the violet component and an hhw. on the red side with respect to the red component. Then the separation between the two maximum depths (or the maximum depth and the hump) is measured and added to the two hhw.'s to form a sort of effective half-width. Hence under the column "Half-Width" in Table 1 we find, for the double lines, three entries running as $a + \Delta + b$ in the following order: a = the hhw. on the violet side, Δ = separation between the two maximum depths, and b = the hhw. on the red side. Such a generalized definition of the half-width can be easily extended to lines of more than two components. Thus for a line of three components the half-width is defined by the aggregate of four quantities, $a + \Delta_{12} + \Delta_{23} + b$, where Δ_{12} and Δ_{23} are the separations between two adjacent maximum depths. The half-width thus defined suggests a certain over-all magnitude of the physical quantity which is responsible for the splitting of the absorption line.

Some of the final results of the measurements are given in Table 1 as an illustration. Each listed plate is designated by its coudé number, such as 9206*a*, etc. We are well aware of the uncertainty involved in these measurements. But the spectrum of σ Sco is so peculiar that in some phases the profiles of lines differ greatly among themselves, even on the same spectrogram.

It is difficult to estimate the effect of microphotometric errors. In an ordinary star the symmetry of the spectral lines helps us in smoothing the microphotometric tracing. But in a peculiar spectrum each line imposes upon the investigator a difficult problem during the process of smoothing.

Two notations have been introduced into Table 1 after the symbol of line classification. A colon (:) means that the classification and consequently all the numerical values following it are subject to uncertainty, either due to the blending of neighboring lines or as a result of the blurring of photographic grains. The second notation, an asterisk (*), indicates the doubtful existence of a longward component which is either very broad or is quite far away from the main line (>1 A).

To save space, we have listed only a small part of our results in Table 1 as an illustration. The limited tabulation should be sufficient to show how a complicated spectrum can be described by as few parameters as are given in the table.

III. DIFFERENTIAL STUDY OF THE EQUIVALENT WIDTH

We first investigated, from the material described in Section II, the equivalent widths of the individual lines as a function of phase, and we found no systematic variation. However, the random errors are large. Hence we conclude tentatively that, within the accuracy of our measurements, lines of different excitation and ionization levels remain nearly constant in strength during the entire period.

We next take the average of the equivalent widths measured on different spectrograms of each single spectral line. Not all the forty lines could be measured for every one of the thirteen individual spectra. Because of the uncertainty in the microphotometric tracings, of the broadening at certain phases, etc., many lines had to be discarded in one spectrum or another. Hence the average values, which are listed at the beginning of Table 1, may not have the same statistical weight.

We then plot the equivalent widths from each spectrogram against the mean equivalent widths in Figure 1, *a–c*.

Following Unsöld (1938), we have, for the equivalent width, A_λ,

$$\frac{1}{2R_c}\frac{A_\lambda}{\Delta\lambda_D} = Y(Z, a) = \int_0^\infty \frac{aZH(v, a)\,dv}{1 + aZH(v, a)}, \tag{1}$$

where

$$Z = \frac{Nf}{R_c\Delta\omega_D}. \tag{2}$$

The notations used here have been explained in a previous paper (Huang and Struve 1952).

From equation (1) it follows that, for small aZ, we have

$$A_\lambda \rightarrow \frac{a\,Nf\lambda^2}{2\,c\,\sqrt{\pi}}, \tag{3}$$

i.e., the measured width is independent of the microturbulent velocity. Here we should call attention to the fact that, according to equation (3), the equivalent width of the weak lines increases as λ^2 instead of λ for a given value of Nf. If aZ is large, we have

$$A_\lambda \rightarrow 2R_c\Delta\lambda_D\left[\ln\left(\frac{a}{R_c}\frac{Nf}{\Delta\omega_D}\right)\right]^{1/2} \tag{4}$$

for the case $a = 0$ and

$$A_\lambda \rightarrow \lambda\frac{\pi^{1/4}}{2}\left(\frac{a\,a}{c}R_c Nf\Delta\lambda_D\right)^{1/2} \tag{5}$$

for the case $a \neq 0$.

Let us now consider two atmospheres, denoted hereafter by "I" and "II," respective-

TABLE 1

ILLUSTRATION OF THE MEASURED RESULTS

No.	Wave Length and Identification	Av. Equiv. Width log ($10^5\lambda/\lambda$)	Plate 9206*a*				Plate 9206*d*				Plate 9207*d*			
			Type	Depth	Half-Width (A)	Equiv. Width (A)	Type	Depth	Half-Width (A)	Equiv. Width (A)	Type	Depth	Half-Width (A)	Equiv. Width (A)
1	4661.635 *O* II	1.526	D:	0.116 .056	0.86+1.98 +0.28	0.189	D	0.140 .042	0.58+1.29 +0.52	0.166	S	0.155	0.74	0.110
2	4650.841 *O* II	1.584	S:	.187	1.42	.242	S:	.192	1.21	.225	S:	.172	0.95	.138
3	4649.139 *O* II	1.644	S:	.187	1.37	.242	S:	.188	1.12	.195	S	.208	0.85	.159
4	4647.40 *C* II	1.354	A	.123	0.48+0.65	.120	S	.088	0.96	.081	S	.085	0.69	.082
5	4641.811 *O* II	1.601	S:	.190	1.20	.222	S:	.175	1.08	.194	S:	.159	1.03	.163
6	4638.854 *O* II	1.450	S:	.106	1.29	.131	S	.136	1.16	.150	S:	.128	0.84	.108
7	4630.537 *N* II	1.308	S	.093	1.22	.102	S*	.082	1.20	.099	.....	.....	.....	.....
8	4596.174 *O* II	1.471	S*	.120	1.28	.147	D	.114 .078	0.43+1.07 +0.43	.145	S:*	.143	0.78	.112
9	4590.971 *O* II	1.501	A	.137	0.63+0.68	.196	D	.172 .071	0.34+0.90 +0.69	.169	S	.172	0.77	.155
10	4574.777 *Si* III	1.521	D	.127 .037	0.60+1.36 +0.34	.145	D	.130 .024	0.50+1.31 +0.29	.128	S:*	.164	0.73	.125
11	4567.872 *Si* III	1.688	D	.170 .042	0.59+2.06 +0.39	.230	D	.179 .059	0.42+1.29 +0.69	.218	S:*	.181	0.84	.157
12	4552.654 *Si* III	1.777	D	.218 .088	0.65+1.19 +0.50	.328	D	.212 .104	0.36+1.20 +0.28	.260	D:	.263 .077	0.41+0.99 +0.65	.299
13	4481 *Mg* II	1.446	D:	.076 .031	0.65+1.46 +0.26	.101	D	.107 .044	0.53+1.70 +0.41	.150	S	.141	0.81	.121
14	4416.975 *O* II	1.542	D	.144 .037	0.69+1.12 +0.43	.192	A	.157	0.41+0.62	.155	.....	.....	.....	.....
15	4414.909 *O* II	1.575	D	.154 .073	0.58+0.90 +0.33	.192	A	.125	0.42+0.80	.149	S	.207	0.86	.178
16	4395.95 *O* II	1.204	D:	.062 .037	0.55+1.65 +0.43	.091	S	.079	0.78	.062	.....	.....	.....	.....
17	4369.28 *O* II	0.934	.....	.....	.....	.....	S	.061	1.02	.060	.....	.....	.....	.....
18	4366.896 *O* II	1.410	S*	.098	1.23	.121	D	.108 .063	0.47+1.22 +0.38	.152	S:*	.145	0.65	.096
19	**4349.426 *O* II**	**1.708**	S:*	.216	**1.22**	.250	S:	.227	1.14	.251	S:*	.216	0.69	0.166
20	**4325.77 *O* II**	**1.173**	S:	0.067	0.82	0.054	S	0.044	1.12	0.043	.....	.....	.....	.....

TABLE 1—*Continued*

No.	Wave Length and Identification	Av. Equiv. Width log ($10^6 d\lambda/\lambda$)	Plate 9206*a*				Plate 9206*d*				Plate 9207*d*			
			Type	Depth	Half-Width (A)	Equiv. Width (A)	Type	Depth	Half-Width (A)	Equiv. Width (A)	Type	Depth	Half-Width (A)	Equiv. Width (A)
21	4319.631 *O* II	1.483	S:*	0.125	1.12	0.140	D	0.135 .034	0.60+1.22 +0.43	0.169	S:*	0.172	0.60	0.125
22	4317.139 *O* II	1.439	S	.119	0.93	.099	D	.112 .055	0.52+0.96 +0.33	.143	S:*	.157	.77	.117
23	4267 *C* II	1.589	D	.087 .036	0.52+1.59 +0.43	.138								
24	4189.788 *O* II	1.334	D	.094 .039	0.54+1.66 +0.34	.122	S:	.056	0.96	.055				
25	4185.456 *O* II	1.279	D	.060 .055	0.52+1.07 +0.60	.109	S:	.047	0.96	.042				
26	4153.302 *O* II	1.423	D:	.068 .038	0.68+1.12 +0.43	.116	A	.098	0.44+0.76	.114	S	.141	.86	.121
27	4146.09 *O* II	1.236	D:	.076 .033	0.47+1.17 +0.34	.071					S:	.087	.85	.075
28	4119.221 *O* II	1.436	S:	.102	1.07	.093	S:	.119	0.77	.091	S:	.195	.68	.121
29	4116.104 *Si* IV	1.310	D	.094 .024	0.58+1.13 +0.26	.107	S	.078	0.64	.049	S	.099	.59	.065
30	4092.940 *O* II	1.114	S:	.071	0.63	.047	S	.081	0.77	.062				
31	4078.862 *O* II	1.083	S	.064	0.86	.054	S	.065	0.67	.044				
32	4075.868 *O* II	1.565	D	.147 .063	0.65+0.78 +0.53	.189	S	.125	0.76	.089	S:	.177	.95	.133
33	4072.164 *O* II	1.551	D	.141 .039	0.52+1.10 +0.34	.162	A	.141	0.38+0.46	.127	S:	0.162	0.84	0.131
34	3994.996 *N* II	1.408	D	.126 .036	0.54+1.18 +0.41	.148	S:*	.090	0.86	.082				
35	3955.851 *N* II	1.164					S	.049	0.93	.046				
36	3954.372 *O* II	1.431					S	.077	1.02	.073				
37	3945.048 *O* II	1.350					S	0.076	0.77	0.065				
38	3924.44 *Si* III	1.230	D	.059 .025	0.41+0.94 +0.33	.056								
39	3920.677 *C* II	1.367	A	.074	0.37+0.64	.070								
40	3911.960 *O* II	1.491	D	.114 0.068	0.41+0.83 +0.40	0.145								

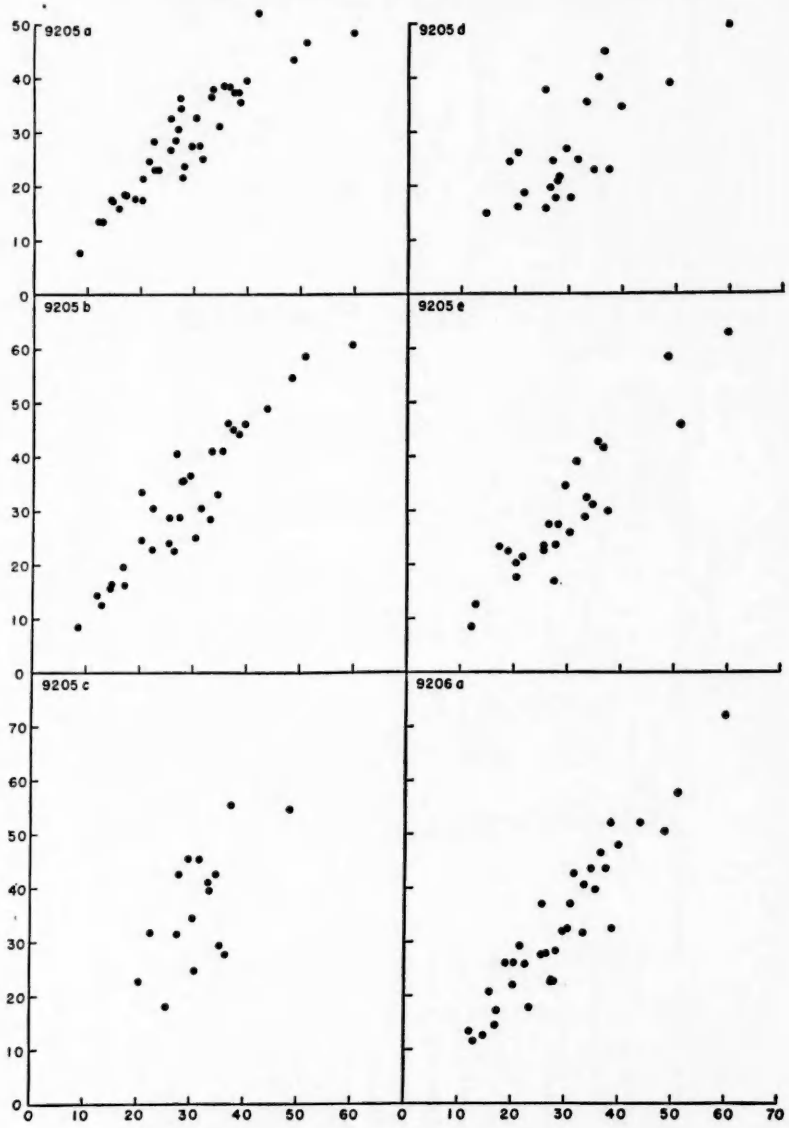

FIG. 1*a*.—The equivalent widths of absorption lines of each spectrogram are plotted against the mean values of the same lines. The value given in the diagram is the magnitude of the quantity $10^6 A\lambda/\lambda$.

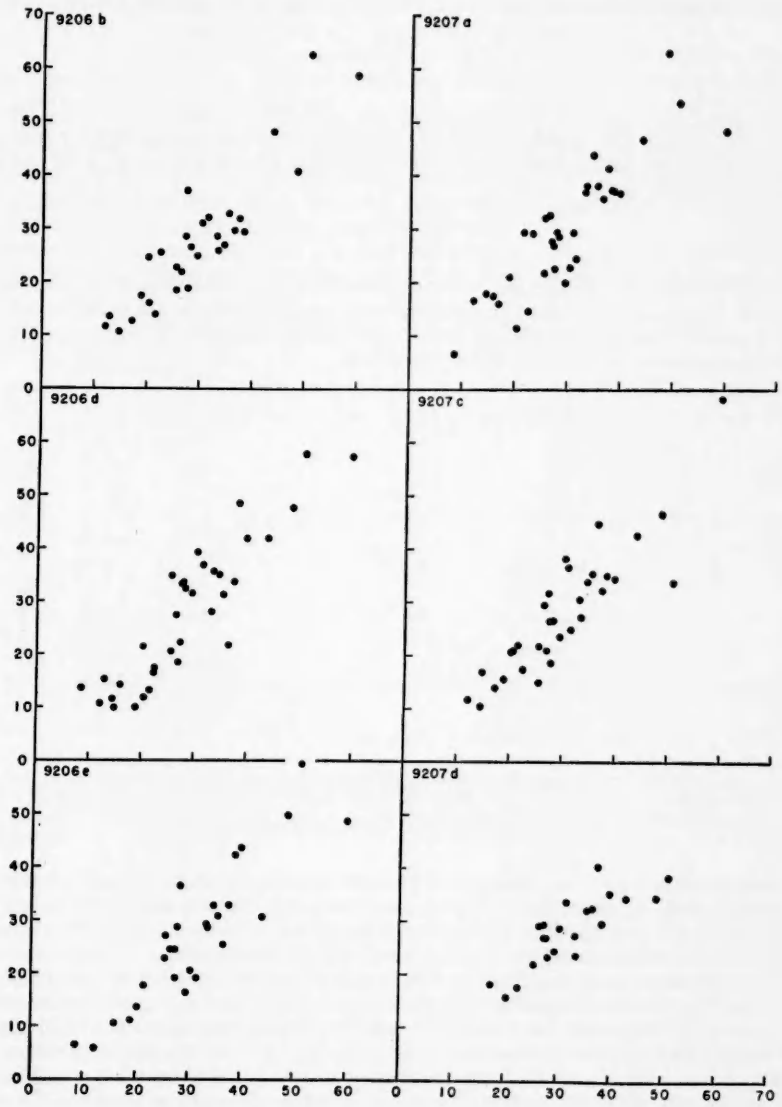

FIG. 1*b*.—The equivalent widths of absorption lines

ly. The two atmospheres are supposed to be built exactly on the same model, except that in case *a* the microturbulent velocities, ξ_s, differ in them by a constant factor n, i.e.,

$$\frac{(\xi_s)_{\text{II}}}{(\xi_s)_{\text{I}}} = \frac{(\Delta\lambda_D)_{\text{II}}}{(\Delta\lambda_D)_{\text{I}}} = n\,,$$

and in case *b* the chemical abundances of the absorbing atoms (in the sense of the Schuster-Schwarzschild model), or the ratio of the selective to the continuous opacities (in the sense of the Milne-Eddington model), differ by a constant factor, n, in the two atmospheres; thus

$$\frac{(Nf)_{\text{II}}}{(Nf)_{\text{I}}} = n\,.$$

We shall study the form of the curve if the equivalent widths of spectral lines in atmosphere II are plotted against those of the same spectral lines in atmosphere I. Without any actual computation, we can predict the general behavior by equations (3)–(5). Let us consider the two cases, *a* and *b*, separately.

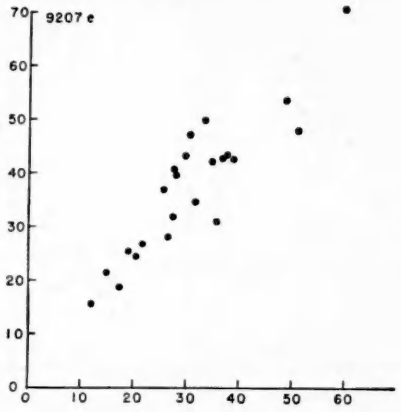

FIG. 1*c*.—The equivalent widths of absorption lines

For case *a* it follows from equation (3) that the A_λ's of very weak lines are independent of the turbulent velocity. Hence the $(A_\lambda)_{\text{II}}$ versus $(A_\lambda)_{\text{I}}$-curve starts at the origin and rises along a 45° straight line. If the damping is extremely small, $(A_\lambda)_{\text{II}}/(A_\lambda)_{\text{I}}$ would approach n according to equation (4), because the square-root factor in equation (4) is an extremely slowly varying function and can therefore be regarded as independent of the turbulent velocity. Hence the tangent of the $(A_\lambda)_{\text{II}}$ versus $(A_\lambda)_{\text{I}}$-curve at the saturation point has a slope equal to n, and it also passes through the origin. The third tangent that we can draw is when absorption lines in both atmospheres have reached the damping branch of the curve of growth. From equation (5) we find that the slope is $n^{1/2}$. The tangent also passes, of course, through the origin. When we know three tangents of a curve at its transition points, the general character of the curve can be easily visualized. Actually, the $(A_\lambda)_{\text{II}}$ versus $(A_\lambda)_{\text{I}}$-curve can be easily written down parametrically. We have illustrated such curves in Figure 2, *a*, for different values of n and a constant value $(= 10^{-2})$ of a.

Case *b* can be similarly studied. Three tangents, all passing through the origin, can be derived from the three limiting equations (3)–(5). The curve starts from the origin

with a slope n, reaches slope unity at the saturation branch, and approaches a straight line of slope $n^{1/2}$ at the damping branch of the curve of growth. Illustrations are given in Figure 2, *b*, for different values of n but with a constant $a = 10^{-2}$.

For most lines the observed points should be located between 0 and 2 in the diagrams; hence the details near the origin in the observed plot will be more important than can be inferred from the present figures.

When both $\Delta\lambda_D$ and Nf are different from one atmosphere to another, the $(A_\lambda)_{II}$ versus $(A_\lambda)_I$-curves will, of course, be more complicated, but they should still all pass through the origin. If an observed curve does not pass through the origin, some systematic error may exist in the measurements. An error in placing the continuum systematically too low or too high, being most likely, will show up here.

Let us now return to Figure 1, *a–c*. The points are scattered around the 45° line passing through the origin, the deviations being quite large. Hence, within the accuracy of

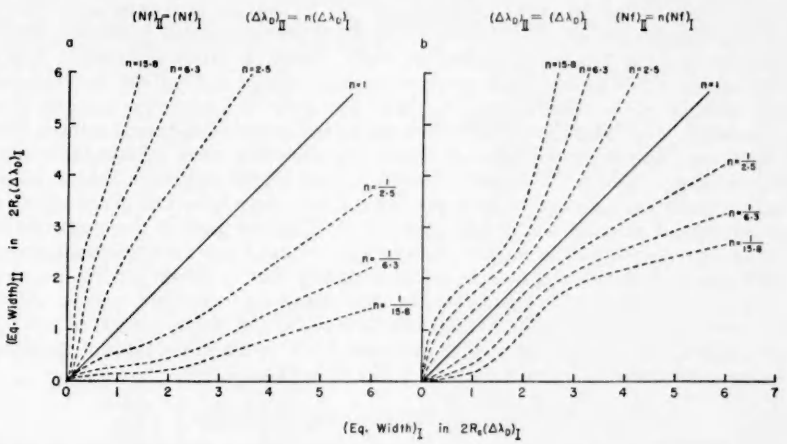

FIG. 2.—Hypothetical behavior of the relationship between the equivalent widths of the same lines that would have been observed in two idealized stellar atmospheres, with (*a*) equal chemical abundances but different microturbulent velocities and (*b*) equal microturbulent velocities but different chemical abundances.

our measurements, we conclude that there is no appreciable change in microturbulent velocities during the cycle of radial-velocity variations. Consequently, the change in line profiles during the cycle must be completely due to the broadening by mass motion. Here the broadening function, which corresponds to the variation in velocities in different parts of the star's disk, is not only very complicated but also changes with time. Wave motions or nonradial oscillations (Ledoux 1951) and prominences (Struve 1951) could all yield the required functions. Unless the spectral lines we have measured all lie on the linear branch of the curve of growth, the present result cannot be easily reconciled with any theory that requires two or more layers, one above the other, which produce different components of a spectral line. For if at a certain stage the star's atmosphere were to consist of two or more layers which produce the same line with a relative shift in frequency due to their velocities, the equivalent width of any line on the transition, on the saturation, or on the damping branches of the curve of growth would increase considerably, and this is contradicted by the empirical results. Besides, there are other difficulties encountered in such theories. According to the radial velocity-curve of HD 199140 obtained recently by Struve, a rising stream in the atmosphere starts to appear

when the falling stream is still observable. If the rising stream were below the falling stream, the two streams would collide. With a mean free path in the atmosphere much smaller than the thickness of the reversing layer, the collision process would convert the energy of mass motions of the two streams into (1) thermal energy and (2) turbulent energy. As a result, we should observe (1) a change in excitation and ionization and (2) an increase in turbulent velocity of small eddies. Neither of these two phenomena has been observed.

If we suppose, on the contrary, that the rising stream were above the falling stream, whence comes the material of the rising stream? If it comes from some gases which were invisible before the multiline stage, we should then expect to see a sequence of phenomena which gradually bring the gases into the visible stage. If the invisibility is due to temperature, we should have a sequence of excitations and ionizations before the gas reaches the same stage of excitation as in the falling stream and another sequence of excitations and ionizations afterward. This again is not observed. If, however, we assume the γ-velocity of the star to be greater than 50 km/sec with respect to the sun, i.e., greater than 60 km/sec with respect to the local centroid, some of the previous objections (but not the one about equivalent width) could be removed, because then the different layers would all be rising and consequently would not collide. But to have a residual velocity whose radial component is greater than 60 km/sec for an early B star is not probable, whether or not the star belongs to the Scorpio-Centaurus stream. Moreover, what will these expanding streams finally become? Why have the remnants of such streams not been observed? It appears, therefore, that all the observational results compel us to abandon the idea of putting one layer above the other. The other alternative is that streams of different radial velocities exist in different parts of the stellar surface. The latter hypothesis fits the present observations without any further assumptions.

The hypothesis of colliding layers was advanced by Struve (1947) for the interpretation of the hydrogen lines in RR Lyrae. In this cluster-type variable, narrow emission lines of hydrogen appear for short intervals of time on the rising branch of the light-curve. It will be necessary to reconsider the case of RR Lyrae in the light of the present discussion. There are no emission lines in σ Sco or in HD 199140.

IV. VARIATION IN THE LINE PROFILE

Levee (1952) found that the change of the line widths has a period identical with that of the radial velocity, and McNamara and Levee (1951) noticed the double structure of some strong absorption lines (i.e., *He* I 4388 and 4471). According to them, the double-line stage occurs when the principal component would be expected to reach its maximum or minimum radial velocity.

Let us now give a general description of the variation of the profiles. The radial velocity-curve of the particular cycle which we have studied is reproduced in Figure 3, *a*. In Figure 3, *b*, some representative profiles are given. They are derived mainly from the two lines *O* II 4590.971 and 4596.174, which belong to the same multiplet. In each of the first four spectra (i.e., 9205*a*–9205*d*) nearly all lines are well represented by the figures. If the form of a particular line deviates from the general one, the deviation can be easily explained by blending effects. Thus, before the radial velocity reaches its maximum (9205*a*), all lines are symmetrical. The asymmetry starts at 9205*b*, which was taken at a time near the velocity maximum. It suggests a weak line on the short-wave-length side of the main component. On the descending branch of the radial velocity-curve, double lines are observed for all lines of medium intensity. The weak lines, being washed out by the broadening, are unobservable. The strong lines remain single but look like rotational profiles. In 9205*c*, the two components of the medium lines are equally strong, but in 9205*d* the component on the long-wave-length side is weaker than that on the short side. In 9205*e*, which corresponds to the stillstand part of the velocity-curve, the component on the long side weakens further, but here the appearance of various lines is quite differ-

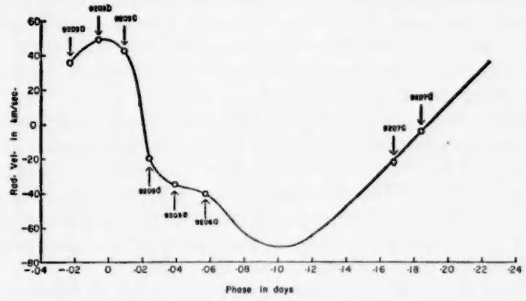

FIG. 3*a*.—The radial velocity-curve. The spectrograms investigated are taken at phases indicated by the arrows, together with their coudé numbers.

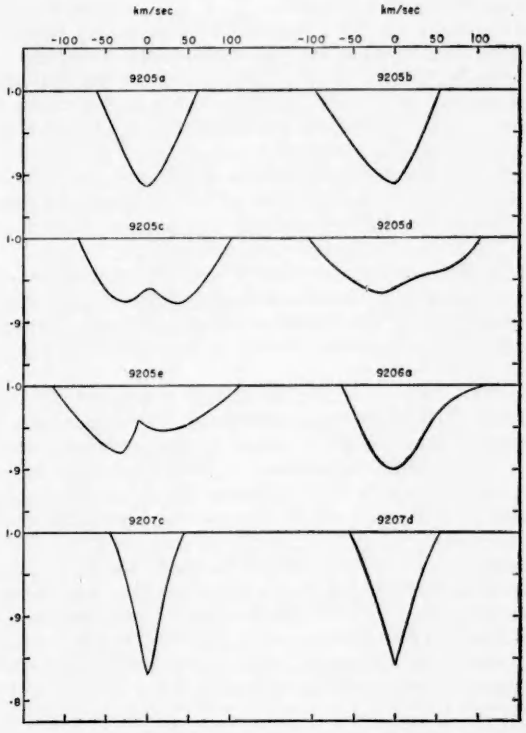

FIG. 3*b*.—The representative line profiles in spectra taken at different phases

ent. Some lines show only slight asymmetry, or they may even be symmetrical while others still have a double structure with a weak component at the long side. In general, the five spectra just described give unambiguously a picture of the growth of the component at the short side and the decay of the original line. The short component makes its first appearance in 9205*b*, increases in strength continuously through stages 9205*c–e*, until it finally becomes the dominant feature in 9206*a*.

It seems advisable to show here the effect on the appearance of profiles of two blending lines. In Figure 4 we have plotted the profiles of two blended lines with different relative separations and with different relative strengths. The relative strength is given in the figure by the ratio in each of the three diagrams. For example, the top diagram has a ratio 1:1, i.e., two lines of equal intensity. The separation is shown by the distance of each short vertical line (under the profiles) from the center of the stronger component. Thus the first profile shows two lines of zero separation, etc.

From these curves we can derive some useful results. Let $\delta\lambda$ be the hhw. of each of the two unblended lines and Δ the separation of the two. The appearance of the blended lines on the microphotometric tracing can be summarized in Table 2. In listing these results, we have considered a slight amount of instrumental broadening as well as the uncertainty arising from photographic grains.

We can now understand why in strong lines we observed rotation-like profiles in 9205*c* and asymmetric lines in 9205*d* instead of the double structure as revealed by the lines of medium intensity. On low-dispersion plates where the instrumental broadening is large, two components of even a medium line cannot be separated, and the spectrum of σ Sco, at any phase on the descending branch of the velocity-curve, would consistently give the observer the impression of rotation.

On the spectrograms taken during the middle of the cycle (i.e., 9206*a*–9207*a*) the lines are either single (symmetric or asymmetric) or with a weak component. But various lines on the same plate do not show a consistent picture, and many of these irregularities might be attributed to microphotometric uncertainty.

In 9207*c* and *d* we come to the sharp-line stage. The representative profiles of these two spectra given in Figure 3, *b*, have been drawn according to the two *O* II lines mentioned previously. In this stage the profiles of different lines in all spectra again become consistent, with only a few exceptions. Nearly all lines are fairly sharp and single. This is especially true in 9207*d*.

There appears to be, at first sight, an inconsistency between our results and those of McNamara and Levee (1951). These authors have stated that "the double-line stage [of the lines *He* I 4388 and *He* I 4471], which in some respects resembles that of 12 Lacertae, occurs when the sharp component . . . would be expected to reach its maximum or minimum radial velocity. At maximum the stronger component is displaced longward of the weaker, and at minimum, shortward." The doubling of the lines is best shown on their spectrogram of June 7, 1951, taken at 6^h11^m U.T. An inspection of Levee's (1952) velocity-curves on page 407 of Volume **115** of this *Journal* shows, however, that this spectrogram—the fourth on June 7, 1951—was taken on the steepest portion of the descending branch of the velocity-curve, preceding the stillstand. It is precisely at this phase that the two components of HD 199140 have similar intensities and are best seen. McNamara and Levee also state that the duplicities were seen only when the total range in radial velocity was exceptionally large. It was 126 km/sec on June 7, 1951.

On May 16, 1954, the total range in velocity was almost the same—123 km/sec. Nevertheless, we do not see the splitting of the *He* I lines on the high-dispersion Mount Wilson plates, but only that of the much weaker lines of *O* II, *Si* III, etc. In order to see the splitting of *He* I lines on our spectrograms, the separation must be much greater than that which we found in the present cycle—50 km/sec. Despite this discrepancy, it seems to us that there is no reason at the present time to conclude that there has been a change

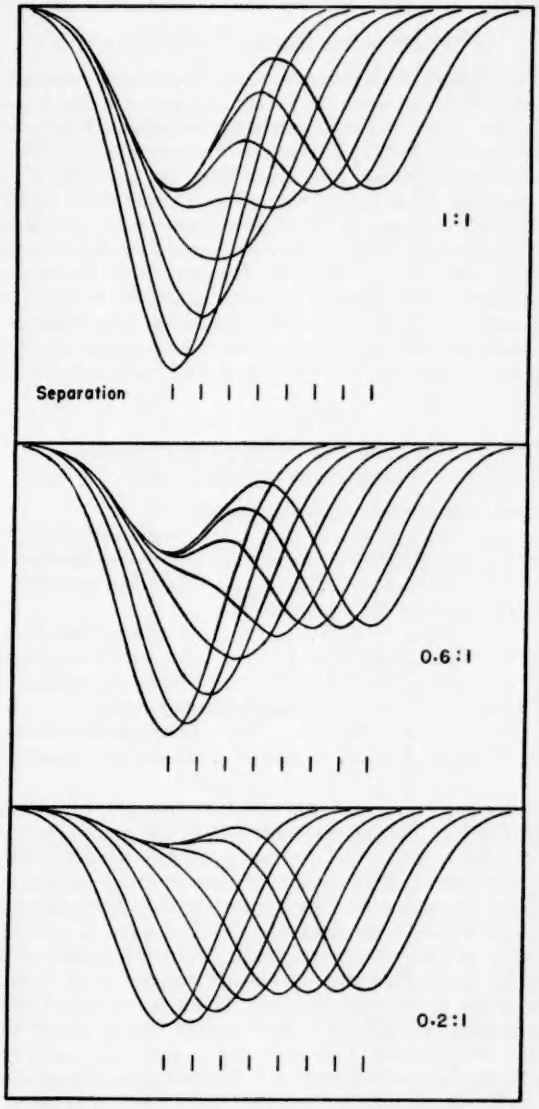

FIG. 4.—Appearance of two blending lines on the microphotometric tracing. The ratio of strengths of one line to the other is given in each of the three diagrams.

in the spectrum of σ Sco or that the phenomenon of line doubling is different in different cycles, except that it becomes less pronounced when the range $2K$ is small.

V. STUDY OF THE MAXIMUM DEPTH OF A LINE

In an ordinary star the half-width measures the broadening on a definite, though nonlinear, scale (Huang 1953). But when the broadening function due to macroscopic motion is peculiar, as in σ Sco, there no longer exists any well-defined half-width. In Section II we defined an effective half-width which can give a general idea of the magnitude of the velocity involved in mass motion but which does not serve as a scale in measuring broadening. For example, let us consider a fictitious atmosphere with a localized prominence moving uniformly outward with a high velocity, with the greater part of the atmosphere remaining quiescent. Such a star would produce a double structure in the spectral lines. The weak component is separated far away from the strong component. According to our previous definition, the effective half-width is very large. This value of the effective half-width would be somewhat misleading. This example bears out clearly a well-known conception involved in the process of broadening by mass motion, i.e., the velocity scale alone does not completely measure the broadening. On the other hand, the

TABLE 2

APPEARANCE OF TWO BLENDING LINES ON MICROPHOTOMETRIC TRACING

I. Two lines of comparable strengths:	
$0 \lesssim \Delta \lesssim \delta\lambda$	A symmetrical line
$\delta\lambda \lesssim \Delta \lesssim 2\delta\lambda$	A rotation-like line
$2\delta\lambda \lesssim \Delta$	Two lines separated
II. Two lines of different strengths:	
$0 \lesssim \Delta \lesssim \delta\lambda$	A symmetrical line
$\delta\lambda \lesssim \Delta\ 2\delta\lambda$	An asymmetrical line
$2\delta\lambda \lesssim \Delta$	Two lines separated
III. A strong line with a very weak companion:	
$0 \lesssim \Delta \lesssim 3\delta\lambda$	A symmetrical line
$3\delta\lambda \lesssim \Delta$	Weak line detectable

maximum depth of a spectral line in our fictitious example will not be greatly changed by the presence of the localized prominence. But as the prominence covers a larger and larger area, the maximum depth will decrease gradually. Hence in such cases the maximum depth of a line offers a better scale for measuring the broadening. Moreover, the maximum depth can be measured more accurately than the half-width. Consequently, we have compared in Figure 5 the maximum depth of a line in the spectrum 9205*a* with that of the same line in every other spectrum. The depth measured in 9205*a* is plotted as the abscissa in all twelve diagrams. The coudé number of the spectrum plotted as the ordinate is given at the top of each diagram. The mean slope of the observed points in each diagram will therefore give us a quantitative idea of the relative extent of the broadening in the two spectra. The slope drawn free hand and represented by the straight lines in Figure 5 is further plotted in Figure 6 against the phase. A slope smaller (or larger) than unity means that the broadening is larger (or smaller) than the one that characterizes Plate 9205*a*. Hence Figure 6 gives a continuous time sequence of broadenings.

Following a previous paper (Huang and Struve 1955), we have studied the relation between the central depth and the equivalent width. Only two spectrograms, i.e., 9205*a* and 9207*d*, have been investigated in this way because they are the only ones with symmetrical lines. In Figure 7 the central depth is plotted against the equivalent width for

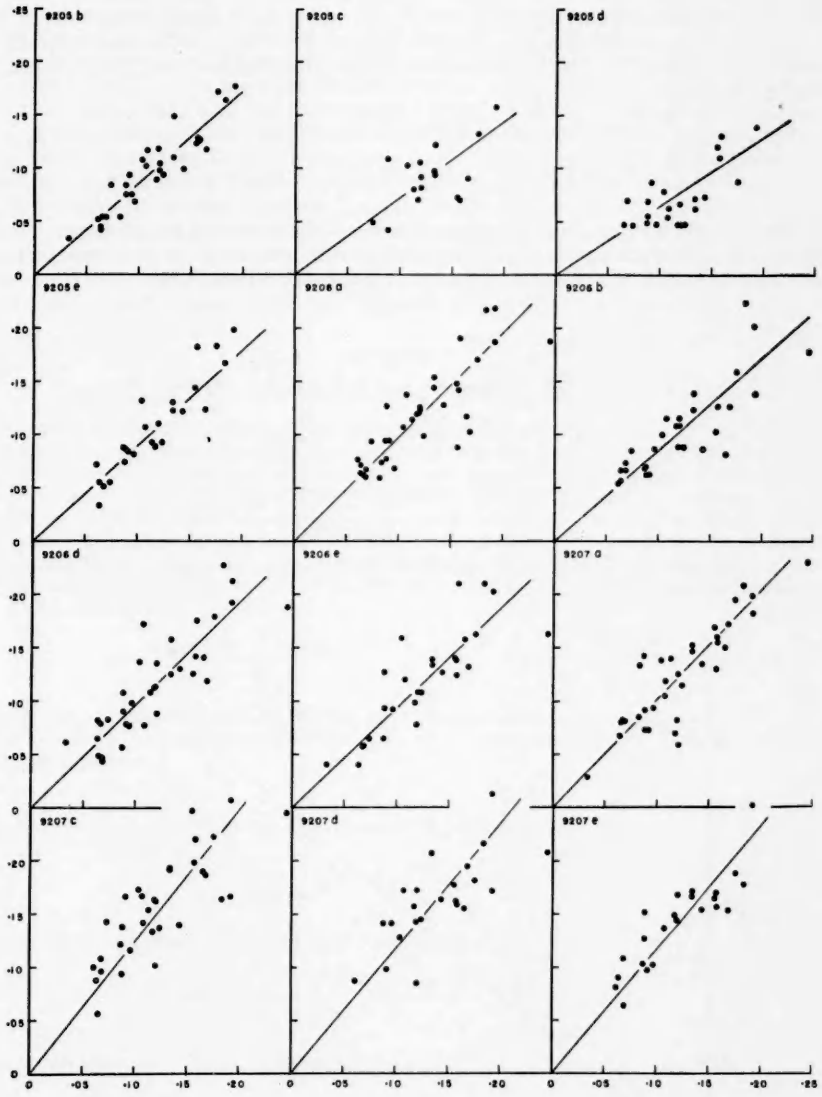

FIG. 5.—The maximum depth of each line in various spectrograms is plotted against that of the same line in Pl. 9205*a*. The mean slope in each plot is determined visually.

both spectrograms. We note that the observed points of each spectrum lie nearly on straight lines passing through the origin. According to the previous paper, this shows that, even in the sharp-line stage (i.e., 9207*d*), the spectrum indicates mass motion. If the motion can be represented by a random velocity ξ_l of large eddies and a random velocity ξ_s of small eddies, we derive from the slope of the observed relation in Figure 7 the following values:

$$\text{For } 9205c: \quad (\xi_l^2 + \xi_s^2)^{1/2} = 40 \text{ km/sec},$$

$$\text{For } 9207d: \quad (\xi_l^2 + \xi_s^2)^{1/2} = 30 \text{ km/sec}.$$

We believe that the velocities of the large eddies contribute mostly to the values. They may, of course, also be due to rotation; the corresponding value of the rotational velocity can be determined only when ξ_s is known (Huang and Struve 1955).

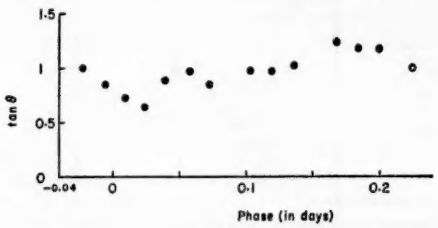

FIG. 6.—The mean slope of each diagram in Fig. 5 is plotted against the phase. It shows the change of broadening during the cycle.

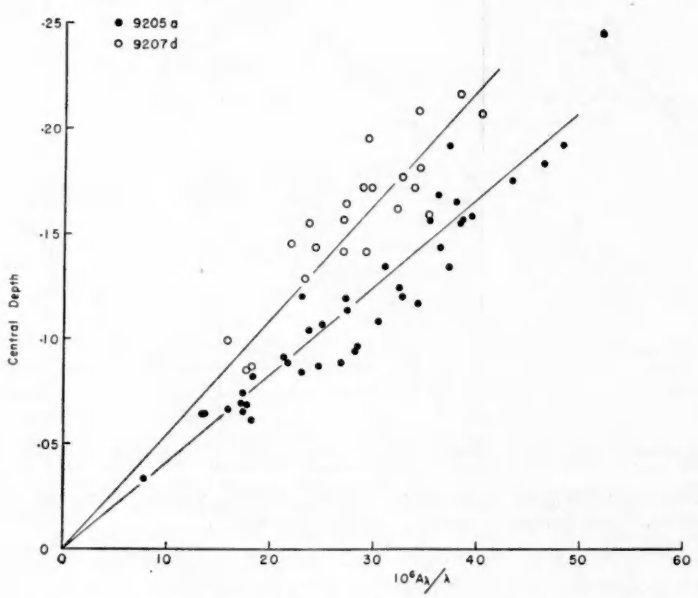

FIG. 7.—The central depth plotted against the equivalent width for two spectrograms

We would like to emphasize the significance of the moderately large widths in the sharp-line stage, because in HD 199140, in which we find a similar phenomenon in the change in the line profile with phase, the line widths in the sharp-line stage are also quite appreciable (McNamara, Struve, and Bertiau 1955). It will be of interest to investigate the correlation between the widths in the sharp-line stage and the phenomenon of line splitting, because the mass motion observed in the sharp-line stage may simply be the rotation of the star. If the lines of stars which show splitting were invariably broad, even at their sharpest stage, the change in profiles might be explained by some kind of mass motion developed by the interaction of rotation and pulsation. The explanation, based on the difference in natural frequency of pulsation due to stellar rotation, at different latitudes on the star's surface (Ledoux 1945), could be given in a manner similar to that proposed by Ledoux (1951). At present this suggestion cannot be regarded too seriously, especially in view of the fact that line splitting has been found not only in the variable stars of early B type which usually rotate (Struve 1950) but also in other kinds of intrinsic variable stars (Struve 1947; Sanford 1949, 1952; Abt 1954).

APPENDIX

EFFECT OF THE EXPOSURE TIME UPON THE LINE PROFILE

Let the original profile be $R(\lambda)$, which would be observed, had the star been moving uniformly. For convenience, the wave length λ is measured from the center of the line that would be formed if the star should stop its relative motion with respect to the sun. Let us now consider the actual star, which is in a state of acceleration. In each infinitesimal time interval, dt, the star can be regarded as moving uniformly with a radial velocity, ξ. Hence, if we take the spectrogram in the interval, dt, there will be no change in line profile, the latter being simply shifted by an amount $\Delta\lambda$ given by $\Delta\lambda = \lambda\xi/c$. In other words, the observed profile should be $R(\lambda - \Delta\lambda)$. If the radiation energy received by the photographic plate in dt is $(dI/dt)dt$, the observed profile, $R'(\lambda)$, will be given by

$$R'(\lambda) = \int_{t_1}^{t_2} R(\lambda - \Delta\lambda) \frac{dI(t)}{dt}\, dt \Big/ \int_{t_1}^{t_2} \frac{dI}{dt}\, dt, \tag{6}$$

where t_1 and t_2 denote, respectively, the beginning and the end of the exposure.

For simplicity, we shall assume that the radiation energy received by the plate per unit time is constant; hence

$$dI \propto dt. \tag{7}$$

Moreover, dt is connected with $d\xi$, and consequently with $d(\Delta\lambda)$ by

$$dt = \frac{dt}{d\xi}\, d\xi = \frac{dt}{d(\Delta\lambda)}\, d(\Delta\lambda). \tag{8}$$

We derive from equations (6)–(8) the required equation:

$$R'(\lambda) = \frac{1}{t_2 - t_1} \int_{(\Delta\lambda)_1}^{(\Delta\lambda)_2} R(\lambda - \Delta\lambda) \frac{dt}{d(\Delta\lambda)}\, d(\Delta\lambda), \tag{9}$$

where $dt/d(\Delta\lambda)$ is given by the radial velocity-curve.

If

$$\Delta\lambda = \alpha t + \beta, \tag{10}$$

i.e., the star is moving with uniform acceleration, we have

$$R'(\lambda) = \frac{1}{(\Delta\lambda)_2 - (\Delta\lambda)_1} \int_{(\Delta\lambda)_1}^{(\Delta\lambda)_2} R(\lambda - \Delta\lambda)\, d(\Delta\lambda). \tag{11}$$

In general, we can always approximate a small section of any radial velocity-curve by a section of a harmonic curve. Thus let

$$\Delta\lambda = (\Delta\lambda)_0 \sin \omega t = \frac{\lambda \xi_0}{c} \sin \omega t . \tag{12}$$

We obtain, from equation (9),

$$R'(\lambda) = \frac{1}{t_2 - t_1} \int_{(\Delta\lambda)_1}^{(\Delta\lambda)_2} \frac{R(\lambda - \Delta\lambda)\, d(\Delta\lambda)}{[(\Delta\lambda)_0^2 - (\Delta\lambda)^2]^{1/2}} . \tag{13}$$

If we denote by v the wave length in units of the Doppler width, $\Delta\lambda_D$, given by

$$\Delta\lambda_D = \frac{\lambda}{\gamma c} , \tag{14}$$

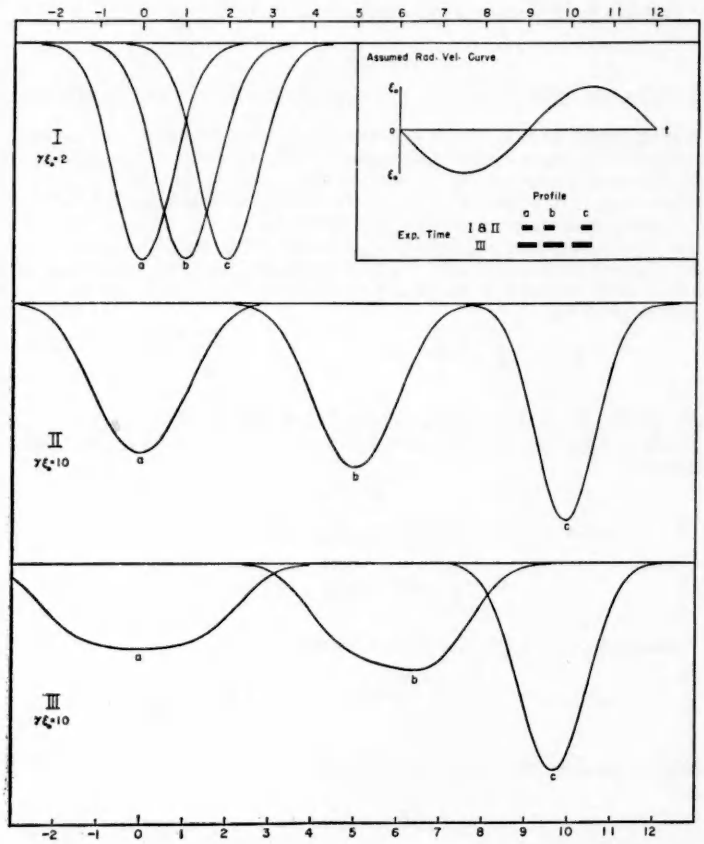

FIG. 8.—Effect of exposure time combined with variable radial velocities upon the profiles of spectral lines. The figure gives not only the shape but also the exact position of the spectral line. Different profiles would be obtained on plates taken with the same length of exposure time but at different phases.

where $1/\gamma$ represents the random velocity associated with the original line profile, $R(\lambda)$, equation (13) can be written as

$$R'(v) = \frac{1}{t_2 - t_1} \int_{v_1}^{v_2} \frac{R(v - v')\, dv'}{\omega\gamma\xi_0 [1 - (v'/\gamma\xi_0)^2]^{1/2}}, \tag{15}$$

where

$$v_i = \gamma\xi_0 \sin \omega t_i \qquad (i = 1, 2). \tag{16}$$

The actual profile observed depends on several parameters: (1) $\gamma\xi_0$, i.e., the ratio of the amplitude of the velocity-curve to the random velocity associated with the original profile; (2) $t_2 - t_1$, i.e., the exposure time; and (3) the position of the exposure time upon the radial velocity-curve. We have illustrated these effects in Figure 8. In the upper right corner we have the idealized radial velocity-curve. Immediately underneath the curve, the black bars denote two sets of exposure times at different phases. Each exposure in the second set (denoted by *III*) is twice as long as each exposure in the first set (denoted by *I* and *II*). For the first set of exposures we have computed two series of line profiles: $\gamma\xi_0 = 2$ (*I*), and $\gamma\xi_0 = 10$ (*II*). For the second set we have only one series, i.e., $\gamma\xi_0 = 10$ (*III*). The computed profiles, given by Figure 8 in three rows, are denoted by *a*, *b*, and *c* corresponding to the three different positions of the exposure time on the velocity-curve. The figures show not only the profiles but also the shift of the line due to the radial velocity. The unit of wave length in Figure 8 is $\Delta\lambda_D$, given by equation (14).

We can derive from these diagrams the following results. First, in ordinary cases where the velocity-curve is not too steep and the exposure time not too long, the change in line profile is not detectable by the eye, as shown in the first row (*I*). The line is simply displaced by an amount depending on the exact position of the velocity-curve at the time of exposure. If the amplitude of the velocity becomes larger and larger, the line profiles at different phases are broadened by different amounts. In the second row (*II*) the three profiles have obviously different half-widths. If the exposure time is increased, we can even detect, without measurement, some asymmetry.

From the drawing we can also see that the exposure time distorts the radial velocity. Approximate correction for this distortion has been worked out by Schlesinger (1916), Petrie (1955), M. Rudkjøbing (unpublished), and others.

REFERENCES

Abt, H. A. 1954, *Ap. J. Supplement*, **1**, 65 (No. 3).
Huang, S.-S. 1953, *Ap. J.*, **118**, 285.
Huang, S.-S., and Struve, O. 1952, *Ap. J.*, **116**, 410.
———. 1955, *ibid.*, **121**, 84.
Ledoux, P. 1945, *Ap. J.*, **102**, 143.
———. 1951, *ibid.*, **114**, 373.
Levee, R. D. 1952, *Ap. J.*, **115**, 402.
McNamara, D. H., and Levee, R. D., 1951, *Pub. A.S.P.*, **63**, 248.
McNamara, D. H., Struve, O., and Bertiau, F. C., S.J. 1955, *Ap. J.*, **121**, 326.
Moore, C. E. 1945, *Contr. Princeton U. Obs.*, No. 20.
Petrie, R. M. 1955, *Pub. Dom. Ap. Obs. Victoria*, Vol. **10**, No. 2.
Sanford, R. F. 1949, *Ap. J.*, **109**, 208.
———. 1952, *ibid.*, **116**, 331.
Schlesinger, F. 1916, *Ap. J.*, **43**, 167.
Struve, O. 1931, *Ap. J.*, **74**, 225.
———. 1939, *ibid.*, **90**, 699.
———. 1947, *Pub. A.S.P.*, **59**, 192.
———. 1950, *Stellar Evolution* (Princeton: Princeton University Press).
———. 1951, *Pub. A.S.P.*, **63**, 138.
———. 1954, *ibid.*, **66**, 329.
Struve, O., and Dunham, T., Jr. 1933, *Ap. J.*, **77**, 321.
Struve, O., McNamara, D. H., and Zebergs, V., 1955, *Ap. J.*, **122**, 122.
Underhill, A. B. 1948, *Ap. J.*, **107**, 337; **108**, 476.
Unsöld, A. 1938, *Physik der Sternatmosphären* (Berlin: J. Springer).

THE RADIAL VELOCITY OF SIGMA SCORPII*

O. STRUVE, D. H. MCNAMARA, AND V. ZEBERGS
Berkeley Astronomical Department, University of California
Received January 10, 1955

ABSTRACT

The fundamental period of σ Scorpii is now $P_2 = 0^d246844$, indicating that there is a slow increase by about 2.3 seconds per century. The individual velocity-curves show a beat period of 8.0 days, corresponding to an interfering period of $P_1 = 0^d255$ or $P_1 = 0^d239$. It is not possible, at the present time, to distinguish between these two values. The fundamental period, P_2, corresponds to $2K_2 = 110$ km/sec. This period is associated with the variation in the profiles of the absorption lines. The interfering period, P_1, corresponds to $2K_1 = 15$ km/sec. The velocities obtained from the hydrogen lines lag behind those obtained from the lines of *O* II, *He* I, *Si* III, *C* II, etc., on the descending branch of the velocity-curve. The γ velocities of the individual curves vary in a period of 34 days. This is interpreted as binary motion with the elements $\gamma = +2.5$ km/sec, $K = 34.0$ km/sec, $e = 0.36$, $\omega = 308°$, $T =$ phase 32.2 days.

The velocity-curve of σ Scorpii was last investigated by R. D. Levee (1952) on the basis of 225 three-prism spectrograms obtained in 1950 and 1951 at the Lick Observatory. The period of the pulsation was found to be 0.246835 day, which is 0.0000014 day longer than the period previously derived by F. Henroteau. The mean velocity obtained from individual cycles varies with a period of about 33 days, and this suggests that σ Scorpii is a spectroscopic binary, like 16 Lacertae, another member of the β Canis Majoris group of pulsating stars. The amplitude of the velocity-curve is variable, between about $2K = 120$ km/sec and $2K = 80$ km/sec, but Levee did not succeed in finding a beat period. The purpose of the present investigation was to study the variation in $2K$ and in the mean velocity. Incidentally, we have also discussed the differences in velocity as determined from the lines of hydrogen and those of other elements. Finally, our material has been used in the succeeding paper (by Huang and Struve) for a study of the periodic variation of the line profiles.

TABLE 1

LIST OF STAR LINES

Wave Length (A)	Element	Plate	Wave Length (A)	Element	Plate	Wave Length (A)	Element	Plate
3964.73	*He* I	C	4120.81	*He* I	C, γ	4416.98	*O* II	C
3973.26	*O* II	C	4143.76	*He* I	C, γ	4471.48	*He* I	C, γ, L
4009.35	*He* I	γ	4267.14	*C* II	γ	4481.23	*Mg* II	C, γ, L
4026.19	*He* I	C, γ	4340.47	*H*γ	C, γ	4552.65	*Si* III	C, L
4069.77	*O* II	γ	4345.56	*O* II	C	4567.87	*Si* III	C, L
4072.16	*O* II	C	4347.42	*O* II	C	4574.78	*Si* III	C, L
4075.87	*O* II	C	4349.43	*O* II	C	4590.97	*O* II	C, L
4101.74	*H*δ	C, γ	4387.93	*He* I	C, γ	4596.17	*O* II	C, L
4119.22	*O* II	C	4414.91	*O* II	C			

Table 1 lists the wave lengths and identifications of the star lines used for the determination of the radial velocities. The letters in the third column have the following meanings: "C" stands for the coudé spectrograph of the 100-inch telescope at Mount Wilson;

* The spectrograms used in this investigation were obtained by Mr. Struve and Mr. McNamara as guest investigators at the Mount Wilson Observatory and by Mr. McNamara at the Lick Observatory.

"γ" stands for the Cassegrain spectrograph of the Mount Wilson 60-inch telescope; and "L" stands for the Mills three-prism spectrograph attached to the 36-inch refractor at the Lick Observatory.

Table 2 gives the radial velocities of 325 spectrograms obtained between April 29 and June 20, 1954 U.T. The Lick spectrograms (designated "L") have a dispersion of 10 A/mm at λ 4500; the Mount Wilson 60-inch plates ("γ") have a dispersion of 29.4 A/mm at λ 4100. The Mount Wilson coudé spectrograms ("C") were obtained with two different cameras: those of May 18 have a dispersion of 10 A/mm, while all others have a dispersion of 4.5 A/mm.

The individual velocities are plotted in Figure 1, *a* and *b*. The open circles represent extensions of velocity-curves obtained by adding or subtracting the period. The phases in Table 2 were computed with the period of 0.247 day from the zero point arbitrarily placed at the maximum radial velocity of each cycle.

The present period $P = 0.246844$ day is appreciably longer than the period derived by Henroteau. There appears to have been a slow increase in the period, amounting to about 2.3 seconds per century.

Table 3 shows the observed epochs of the observed maxima and minima of the individual velocity-curves and the epochs computed with Levee's original epochs and with (*a*) one of his periods, 0.246840 day, and (*b*) our new period of 0.246844 day. The corresponding values of O−C show good agreement for the minima. The maxima indicate a small systematic positive residual, which may be due to a small error in Levee's original epoch of JD 2433804.741. The table also lists the values of γ and $2K$ for the individual dates.

The new values of γ have been plotted as solid dots in Figure 2. The open circles represent Levee's observations. No attempt was made to determine accurately the period of variation of γ. Instead, we have adjusted the two series of values to give the best possible agreement. The resulting velocity-curve leads to the orbital elements of the spectroscopic binary (Table 4) in which the pulsating B2 star is the only visible component.

An attempt to improve the period of the spectroscopic binary by combining Levee's observations with our own leads to the two values, 34.23 days and 33.13 days, depending upon whether 30 or 31 cycles have elapsed between Levee's observed maximum value of γ at JD 2433836.4 and ours at JD 2434863.3. The longer period is probably the correct one, since it agrees with Henroteau's original estimate.

The values of $2K$ listed in Table 3 suggest a beat period of 8.0 days. Table 3 gives them with the phases as computed by the expression:

$$T = \text{JD } 2434878.2 + 8.0E\,.$$

The scatter is large, but the periodicity is undoubtedly real. There are thus two interfering periods: $P_2 = 0.246844$ day, $P_1 = 0.255$ day, or $P_1 = 0.239$ day. We cannot distinguish between these two values of P_1. In the system of 16 Lacertae such a distinction was made from the character of the curve representing the periodic shifts of phase of observed maximum radial velocity plotted against the beat period. In β CMa the distinction was possible because P_1 represented the period of the changes in line profile. In σ Scorpii the phase shifts as recorded in columns "O−C" of Table 3 show too much scatter. The line profiles of σ Scorpii give only the fundamental period, P_2.

The period P_2 is associated with $2K_2 = 100$ km/sec, while P_1 is associated with $2K_1 = 15$ km/sec. The fundamental period, P_2, is the one that characterizes the variation in the line widths. Thus far, only one star, β CMa itself, has its period of line-width variation identical with the period corresponding to the smaller value of the velocity range.

The individual velocity-curves on May 12, 16, 18, 19, June 15, 17, and 20 clearly show a standstill on the descending branches. These standstills are similar to those discovered by R. M. Petrie in HD 199140 = BW Vulpeculae. There can be no doubt that this is a characteristic feature of all β CMa stars possessing large enough amplitudes.

TABLE 2

RADIAL VELOCITIES

JD 2434+	Plate	Radial Velocity (Km/Sec)	Phase (Fraction of Day)	$v_H - v_{all}$ (Km/Sec)	JD 2434+	Plate	Radial Velocity (Km/Sec)	Phase (Fraction of Day)	$v_H - v_{all}$ (Km/Sec)
861.788...	L	+ 14.1	0.056	.....	875.857...	γ	− 20.3	0.050	+21.3
.804...		+ 7.7	.072	.....	.864...		− 26.6	.057	−11.5
.826...		− 14.0	.094	.....	.871...		− 29.2	.064	+ 7.0
.844...		− 22.2	.112	.....	.879...		− 40.2	.072	+ 2.4
.861...		− 13.7	.129	.....	.888...		− 38.2	.081	+ 3.0
.882...		+ 6.8	.150	.....	.896...		− 47.0	.089	+ 3.9
.899...		+ 21.2	.167	.....	.910...		− 51.3	.103	− 3.4
.917...		+ 41.4	.185	.....	.918...		− 47.6	.111	+ 8.4
.940...		+ 65.0	.208	.....	.927...		− 51.1	.120	+ 2.0
.961...		+ 92.6	.229	.....	.936...		− 37.8	.129	+ 3.3
.978...		+100.7	.246	.....	.945...		− 33.6	.138	− 0.6
874.756...	γ	− 3.0	.189	−10.6	.953...		− 33.3	.146	− 1.4
.768...		+ 6.9	.201	+14.4	.961...		− 32.0	.154	−10.8
.775...		+ 15.7	.208	− 2.3	.971...		− 16.4	.164	+ 2.4
.781...		+ 16.7	.214	+ 2.3	.981...		− 3.7	.174	+ 2.5
.789...		+ 22.4	.222	− 7.9	.990...		− 2.5	.183	− 4.8
.797...		+ 31.5	.230	+ 5.1	876.739...	γ	+ 5.5	.196	− 6.6
.805...		+ 33.0	.238	− 5.3	.749...		+ 3.7	.206	+ 0.7
.813...		+ 34.7	.246	+ 7.5	.757...		+ 17.0	.214	−14.4
.822...		+ 33.3	.008	+10.8	.766...		+ 26.0	.223	− 2.0
.833...		+ 21.0	.019	− 5.4	.778...		+ 40.6	.235	− 5.4
.841...		+ 13.0	.027	+10.6	.786...		+ 39.8	.243	+ 1.8
.849...		− 1.7	.035	−25.7	.796...		+ 40.4	.006	+ 5.5
.855...		− 7.0	.041	+ 4.6	.806...		+ 36.2	.016	+13.3
.862...		− 9.9	.048	+ 9.8	.815...		+ 20.0	.025	+ 1.5
.869...		− 8.1	.055	− 5.8	.825...		− 1.6	.035	− 6.9
.876...		− 14.3	.062	− 2.8	.835...		− 10.9	.045	0.0
.884...		− 24.3	.070	+ 2.0	.845...		− 22.7	.055	− 4.5
.897...		− 35.6	.083	− 6.7	.856...		− 24.1	.066	− 1.3
.909...		− 42.3	.095	+ 1.6	.865...		− 33.0	.075	−11.0
.918...		− 45.2	.104	− 5.8	.874...		− 46.9	.084	+ 9.8
.925...		− 49.8	.111	− 4.4	.882...		− 42.8	.092	+ 6.7
.934...		− 48.4	.120	−11.6	.897...		− 51.4	.107	− 1.4
.941...		− 48.4	.127	− 1.8	.911...		− 52.0	.121	+ 6.0
.950...		− 39.0	.136	+ 6.5	.920...		− 46.2	.130	+ 6.6
.961...		− 27.9	.147	+ 8.8	.929...		− 38.0	.139	− 5.7
.968...		− 20.6	.154	+18.2	.938...		− 38.3	.148	+11.3
.979...		− 22.6	.165	− 4.6	.946...		− 30.9	.156	+ 4.9
.987...		− 15.2	.173	− 0.5	.956...		− 24.3	.166	− 1.2
.997...		− 10.4	.183	− 7.6	.965...		− 13.0	.175	+ 7.9
875.740...	γ	− 3.5	.180	+10.9	.974...		− 12.2	.184	− 0.5
.747...		+ 4.1	.187	− 3.4	.987...		+ 4.6	.197	+12.9
.758...		+ 10.3	.198	+ 5.5	877.747...	C	+ 23.3	.211	+ 3.4
.769...		+ 22.6	.209	+ 9.2	.759...		+ 37.3	.223	+ 2.4
.778...		+ 24.2	.218	− 8.6	.768...		+ 39.8	.232	+ 0.7
.786...		+ 28.1	.226	− 2.6	.779...		+ 49.6	.243	− 1.3
.793...		+ 30.9	.233	+ 4.7	.788...		+ 39.5	.005	+ 9.0
.801...		+ 43.0	.241	+ 1.2	.799...		+ 5.0	.016	+20.0
.812...		+ 41.1	.005	+ 8.9	.811...		− 23.4	.028	+ 8.8
.821...		+ 24.1	.014	+ 9.5	.822...		− 29.9	.039	+10.3
.828...		+ 8.6	.021	+ 5.7	878.749...	C	+ 35.9	.224	+ 1.2
.839...		− 3.2	.032	−10.7	.766...		+ 48.9	.241	+ 1.7
.849...		− 15.1	0.042	− 3.2	.781...		+ 42.3	0.009	+ 2.6

TABLE 2—*Continued*

JD 2434+	Plate	Radial Velocity (Km/Sec)	Phase (Fraction of Day)	$v_H - v_{all}$ (Km/Sec)	JD 2434+	Plate	Radial Velocity (Km/Sec)	Phase (Fraction of Day)	$v_H - v_{all}$ (Km/Sec)
878.796...	C	− 20.0	0.024	+18.4	880.870...	C	− 64.5	0.124	+ 4.6
.811...		− 34.8	.039	+ 7.5	.874...		− 60.4	.128	+ 1.2
.829...		− 40.3	.057	+ 7.6	.877...		− 60.2	.131	+11.3
.844...		− 55.2	.072	+15.6	.891...		− 42.5	.145	+ 1.6
.860...		− 68.1	.088	+26.9	.895...		− 38.0	.149	+ 6.3
.875...		− 71.3	.103	+ 2.5	.900...		− 33.4	.154	− 0.6
.891...		− 65.4	.119	+22.1	.907...		− 28.7	.161	+11.2
.908...		− 50.1	.136	+10.1	.911...		− 25.0	.165	− 0.9
.924...		− 35.6	.152	+15.0	.916...		− 20.5	.170	+ 3.5
.940...		− 22.3	.168	− 4.3	881.724...	γ	+ 31.9	.246	+ 9.5
.956...		− 4.6	.184	+ 4.8	.732...		+ 28.6	.007	+ 1.6
.971...		+ 10.1	.199	+15.0	.738...		+ 26.2	.013	+ 0.2
879.731...	γ	+ 31.3	.228	+ 1.6	.745...		+ 18.1	.020	+15.6
.745...		+ 46.2	.242	− 8.0	.752...		+ 1.1	.027	− 7.9
.757...		+ 39.1	.007	− 6.1	.758...		− 8.6	.033	− 4.1
.770...		+ 15.2	.020	+16.1	.764...		− 16.1	.039	+ 4.3
.781...		− 2.5	.031	+ 6.5	.772...		− 16.4	.047	+ 5.7
.792...		− 12.3	.042	− 3.4	.784...		− 22.5	.059	+ 3.9
.815...		− 31.1	.065	+ 8.7	.791...		− 35.6	.066	+ 4.7
.823...		− 37.6	.073	+13.6	.798...		− 37.9	.073	− 2.2
.832...		− 45.3	.082	+18.0	.804...		− 48.7	.079	+11.6
.841...		− 54.6	.091	− 2.5	.811...		− 49.5	.086	− 8.1
.849...		− 62.8	.099	+ 1.9	.820...		− 54.2	.095	+ 8.2
.858...		− 62.1	.108	+10.5	.832...		− 63.6	.107	+ 7.6
.870...		− 61.4	.120	+ 0.3	.843...		− 59.9	.118	+ 4.7
.879...		− 56.8	.129	+ 2.0	.856...		− 57.5	.131	+ 6.0
.893...		− 46.3	.143	+ 1.1	.868...		− 48.1	.143	− 7.6
.906...		− 34.0	.156	− 1.6	.881...		− 40.8	.156	− 0.6
.919...		− 22.7	.169	−19.9	.893...		− 30.4	.168	+ 4.8
.932...		− 9.1	.182	+ 1.0	.906...		− 15.3	.181	− 2.4
.945...		+ 3.2	.195	+ 1.5	.921...		− 2.7	.196	− 1.3
.957...		+ 9.3	.207	+ 0.1	.932...		+ 8.8	.207	+ 3.6
.966...		+ 25.8	.216	+ 4.4	.940...		+ 12.2	.215	+13.2
.973...		+ 24.1	.223	+ 1.3	.947...		+ 17.3	.222	− 2.2
.980...		+ 24.8	.230	+ 3.4	.954...		+ 33.3	.229	+18.3
880.741...	C	+ 32.9	.242	+ 4.6	.959...		+ 27.2	.234	+ 2.0
.749...		+ 23.7	.003	+ 6.9	.966...		+ 31.8	.241	− 0.8
.758...		+ 5.0	.012	+13.1	.974...		+ 31.6	.002	+13.2
.766...		− 18.7	.020	+19.8	882.737...	C	+ 4.8	.025	+ 9.8
.775...		− 27.2	.029	+ 9.6	.752...		− 20.7	.040	+12.8
.783...		− 29.5	.037	+ 8.6	.766...		− 28.5	.054	+11.8
.791...		− 35.0	.045	+ 5.0	.778...		− 42.3	.066	+20.1
.800...		− 37.6	.054	+11.3	.790...		− 57.3	.078	+ 4.9
.806...		− 38.9	.060	+ 5.8	.804...		− 67.4	.092	+14.9
.818...		− 59.5	.072	+11.4	.814...		− 69.6	.102	+ 9.5
.825...		− 65.8	.079	+16.9	.825...		− 71.6	.113	+ 9.6
.831...		− 69.0	.085	+ 5.3	.838...		− 68.4	.126	+ 8.2
.834...		− 71.5	.088	+17.2	.849...		− 61.2	.137	+ 4.2
.840...		− 71.6	.094	+18.7	.860...		− 54.1	.148	+ 1.3
.845...		− 72.0	.099	+17.3	.872...		− 44.0	.160	+ 6.2
.851...		− 72.0	.105	+13.6	.883...		− 34.5	.171	− 1.4
.854...		− 69.4	.108	+14.4	.895...		− 23.3	.183	+ 4.8
.859...		− 69.4	.113	+21.6	.904...		− 15.8	.192	+ 1.1
.861...		− 68.4	.115	+19.2	.914...		− 5.8	.202	+ 3.5
.866...		− 69.4	0.120	+ 4.2	.925...		+ 3.9	0.213	+ 3.4

TABLE 2—*Continued*

JD 2434+	Plate	Radial Velocity (Km/Sec)	Phase (Fraction of Day)	$v_H - v_{all}$ (Km/Sec)	JD 2434+	Plate	Radial Velocity (Km/Sec)	Phase (Fraction of Day)	$v_H - v_{all}$ (Km/Sec)
882.937...	C	+ 16.2	0.225	+ 6.6	910.811...	C	+ 8.2	0.202	− 2.9
.950...		+ 25.0	.238	+ 5.8	.830...		+ 27.6	.221	+ 3.0
883.736...	C	− 18.4	.037	+20.0	.850...		+ 48.4	.241	− 0.3
.749...		− 28.1	.050	+ 5.7	.867...		+ 37.3	.011	+21.6
.761...		− 36.8	.062	+10.0	.891...		− 25.3	.035	+11.7
.773...		− 52.9	.074	+11.6	.910...		− 25.8	.054	+31.0
.786...		− 66.6	.087	+14.3	911.727...	C	− 59.7	.136	+ 1.5
.802...		− 71.6	.103	+11.5	.746...		− 46.6	.155	+14.1
.815...		− 72.4	.116	+ 7.0	.763...		− 27.0	.172	+ 5.4
.827...		− 67.9	.128	+ 4.3	.781...		− 9.0	.190	+ 2.7
.838...		− 60.9	.139	+ 5.4	.798...		+ 10.1	.207	+ 5.1
.854...		− 50.8	.155	+ 1.1	.819...		+ 34.2	.228	+ 0.3
.865...		− 38.8	.166	− 0.9	.837...		+ 49.3	.246	+ 3.0
.877...		− 26.9	.178	+ 3.2	.854...		+ 32.5	.016	+ 8.0
.888...		− 17.4	.189	+ 2.6	.873...		− 13.5	.035	+21.5
.899...		− 5.3	.200	+ 0.5	.890...		− 31.8	.052	+15.1
.913...		+ 8.8	.214	+ 1.5	.910...		− 35.5	.072	+20.0
.925...		+ 23.9	.226	+ 1.6	913.653...	γ	− 49.6	.089	− 0.3
.940...		+ 39.0	.241	− 3.0	.660...		− 52.9	.096	+10.3
.952...		+ 43.7	.006	+ 1.6	.669...		− 57.1	.105	+11.5
.966...		+ 35.5	.020	+ 6.0	.677...		− 57.9	.113	+ 8.4
908.665...	γ	+ 7.4	.033	− 0.7	.688...		− 50.0	.124	− 3.3
.674...		− 5.3	.042	+ 0.4	.701...		− 48.5	.137	+ 0.5
.683...		− 6.2	.051	− 9.6	.710...		− 38.9	.146	+ 8.9
.690...		− 9.9	.058	+ 1.6	.719...		− 37.9	.155	+ 5.1
.697...		− 23.1	.065	+ 7.8	.726...		− 25.5	.162	− 1.8
.703...		− 30.5	.071	+ 5.6	.736...		− 18.0	.172	+ 1.1
.722...		− 47.3	.090	+ 7.6	.745...		− 10.7	.181	− 1.8
.731...		− 49.1	.099	+ 1.9	.754...		− 7.4	.190	+ 4.2
.742...		− 46.9	.110	− 2.2	.765...		+ 3.7	.201	+ 2.8
.753...		− 40.9	.121	− 0.9	.773...		+ 13.8	.209	− 1.6
.763...		− 39.3	.131	+ 1.8	.781...		+ 19.5	.217	+ 3.5
.772...		− 37.3	.140	+ 4.8	.786...		+ 17.8	.222	+ 2.3
.782...		− 26.6	.150	− 1.9	.791...		+ 24.4	.227	− 6.8
.792...		− 20.6	.160	+ 3.1	.796...		+ 33.0	.232	− 1.2
.801...		− 11.6	.169	− 2.1	.800...		+ 26.8	.236	+ 4.0
.811...		− 6.9	.179	+ 2.5	.804...		+ 32.4	.240	+ 1.2
.822...		+ 8.3	.190	+ 2.0	.811...		+ 37.5	.000	+ 8.0
.832...		+ 16.4	.200	− 3.0	.819...		+ 30.7	.008	+ 4.4
.840...		+ 15.8	.208	+ 0.6	.824...		+ 31.3	.013	− 2.0
.847...		+ 29.6	.215	− 2.0	.828...		+ 28.5	.017	+ 2.4
.856...		+ 33.6	.224	+ 6.5	.833...		+ 18.1	.021	+ 3.8
.865...		+ 40.1	.233	− 1.5	.837...		+ 13.9	.026	+ 6.4
.873...		+ 49.7	.241	− 2.9	.841...		+ 2.7	.030	+ 2.0
.881...		+ 49.6	.002	+ 0.7	.845...		− 8.2	.034	− 1.3
.892...		+ 46.0	.013	− 0.3	.851...		− 13.9	.040	+23.6
.901...		+ 31.0	.022	+ 7.8	.856...		− 13.6	.045	− 6.1
.908...		+ 27.4	.029	− 2.3	.861...		− 16.0	.050	− 4.5
910.657...	C	− 30.1	.048	+ 8.2	.867...		− 14.7	.056	− 2.6
.681...		− 44.3	.072	+26.1	.872...		− 7.2	.061	+ 9.2
.703...		− 63.8	.094	+20.1	.876...		− 22.0	.065	+13.5
.723...		− 64.5	.114	+12.2	.881...		− 27.6	.070	+ 6.7
.746...		− 53.1	.137	+24.8	.887...		− 36.1	.076	− 7.0
.766...		− 37.9	.157	+ 1.4	.894...		− 48.3	0.083	− 7.2
.791...		− 15.9	0.182	+ 2.8					

TABLE 3*a*

MINIMUM VELOCITIES, γ

Date (1954)	Observed Epoch (JD 2434+)	E	Comp. Epoch* $P=0^d.246840$ (JD 2434+)	O−C	Comp. Epoch† $P=0^d.246844$ (JD 2434+)	O−C	γ (Km/Sec)	Phase‡ (Days)
Apr. 29	861.844	4282	861.825	+19	861.842	+2	+39	33
May 12	874.925	4335	874.907	+18	874.925	0	− 7	12
13	875.910	4339	875.895	+15	875.912	−2	− 4	13
14	876.898	4343	876.882	+16	876.899	−1	− 5	14
15	.....	.....	.....	.....	.....	.....	− 9	15
16	878.872	4351	878.857	+15	878.874	−2	−10	16
17	879.859	4355	879.845	+14	879.862	−3	− 8	17
18	880.846	4359	880.831	+15	880.849	−3	−19	18
19	881.836	4363	881.819	+17	881.836	0	−24	19
20	882.823	4367	882.806	+17	882.824	−1	−13	20
21	883.808	4371	883.794	+14	883.811	−3	−13	21
June 15	908.734	4472	908.724	+10	908.742	−8	+ 1	12
17	910.714	4480	910.699	+15	910.717	−3	− 7	14
18	.....	.....	.....	.....	.....	.....	− 7	15
20	913.676	4492	913.661	+15	913.679	−3	−10	17

* T = JD 2433804.856 + $0^d.246840E$.

† T = JD 2433804.856 + $0^d.246844E$.

‡ Phase computed with a period of 34 days, zero phase = JD 2434863.

TABLE 3*b*

MAXIMUM VELOCITIES, $2K$

Date (1954)	Observed Epoch (JD 2434+)	E	Comp. Epoch* $P=0^d.246840$ (JD 2434+)	O−C	Comp. Epoch† $P=0^d.246844$ (JD 2434+)	O−C	$2K$ (Km/Sec)	Phase‡ (Days)
Apr. 29	.....	.....	.....	.....	.....	.....	124	7.5
May 12	874.814	4335	874.792	+22	874.810	+ 4	86	4.6
13	875.807	4339	875.780	+27	875.797	+10	97	5.6
14	876.790	4343	876.767	+23	876.784	+ 6	98	6.6
15	877.783	4347	877.754	+29	877.772	+11	122	7.6
16	878.770	4351	878.742	+28	878.759	+11	123	0.6
17	879.750	4355	879.729	+21	879.747	+ 3	112	1.6
18	880.746	4359	880.716	+30	880.734	+12	107	2.5
19	881.725	4363	881.704	+21	881.721	+ 4	94	3.5
	881.970	4364	881.951	+19	881.968	+ 2	98	3.8
20	.....	.....	.....	.....	.....	.....	99	4.5
21	883.948	4372	883.925	+23	883.943	+ 5	118	5.7
June 15	908.879	4473	908.856	+23	908.874	+ 5	100	6.7
17	910.856	4481	908.831	+25	910.849	+ 7	116	0.7
18	911.838	4485	911.818	+20	911.836	+ 2	114	1.6
20	913.811	4493	913.793	+18	913.811	0	96	3.6

* T = JD 2433804.741 + $0^d.246840E$.

† T = JD 2433804.741 + $0^d.246844E$.

‡ Phase computed with a period of 8.0 days, T_0 = JD 2434878.2.

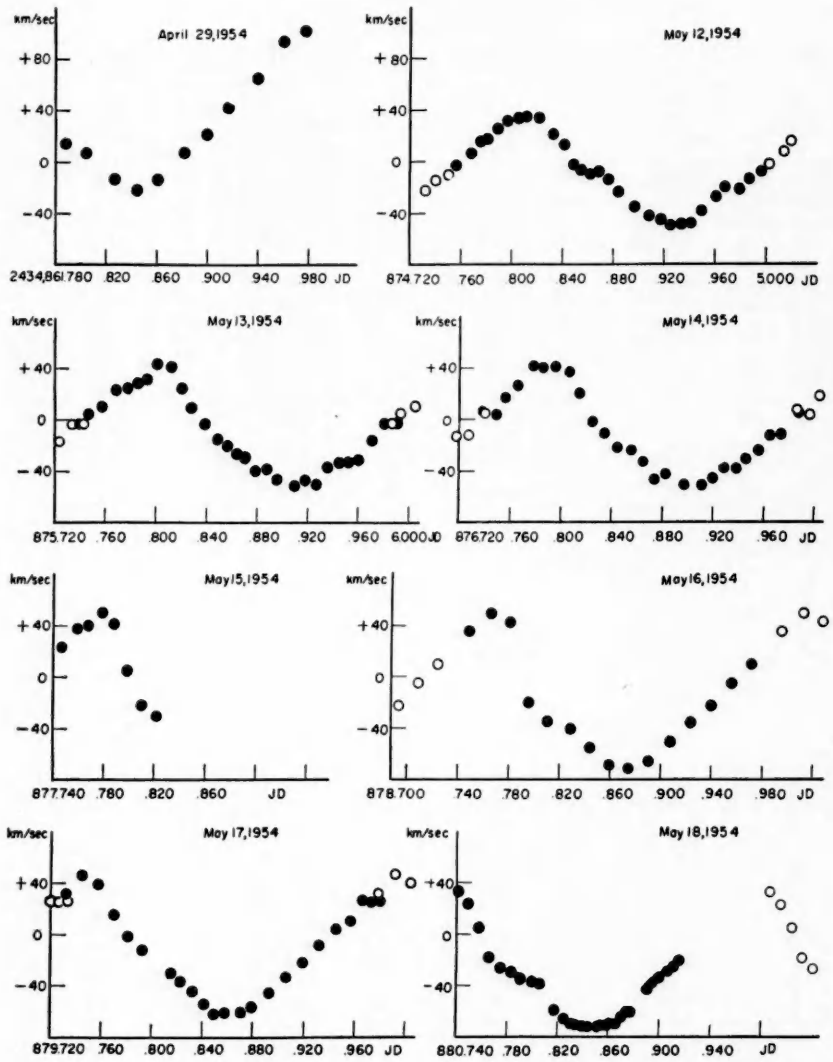

FIG. 1*a*.—Individual velocity-curves of σ Scorpii

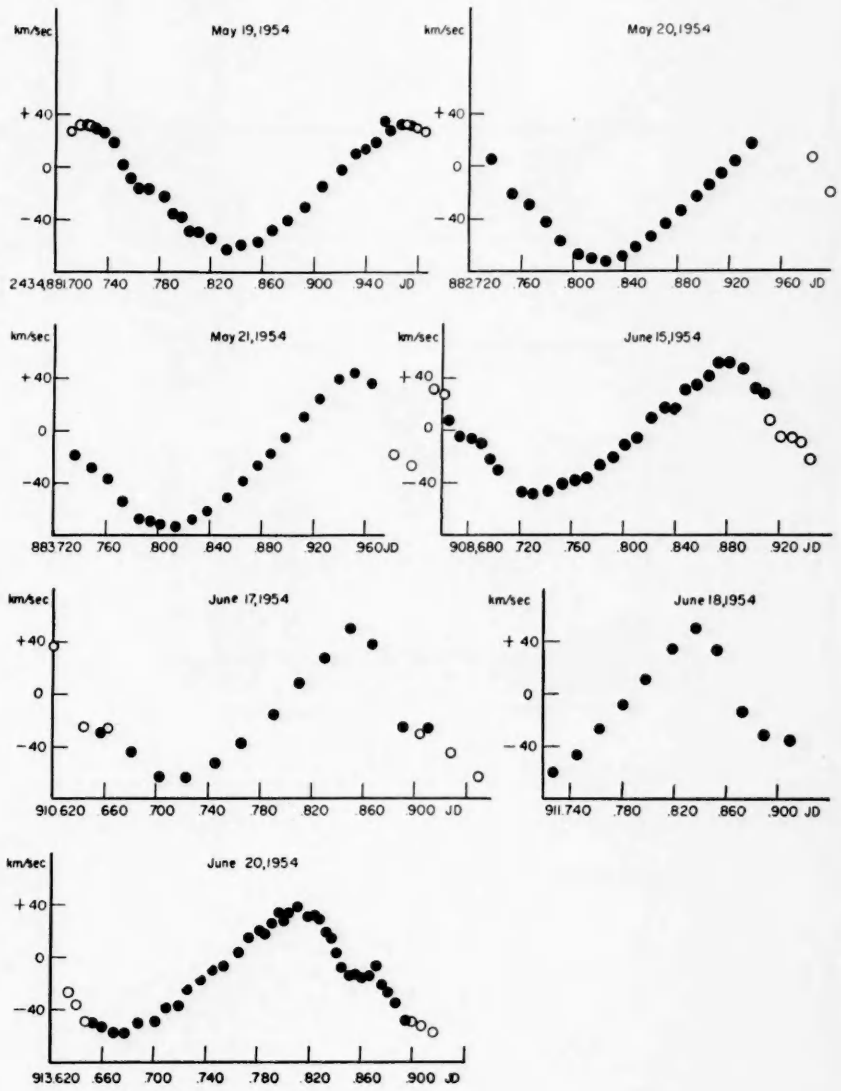
km/sec
May 19, 1954
+40
0
−40
2434.881.700 740 780 820 860 900 940 JD
km/sec
May 20, 1954
+40
0
−40
882.720 760 800 840 880 920 960 JD
km/sec
May 21, 1954
+40
0
−40
883.720 760 800 840 880 920 960JD
km/sec
June 15, 1954
+40
0
−40
908,680 720 760 800 840 880 920 JD
km/sec
June 17, 1954
+40
0
−40
910.620 660 700 740 780 820 860 900 JD
km/sec
June 18, 1954
+40
0
−40
911.740 780 820 860 900 JD
km/sec
June 20, 1954
+40
0
−40
913.620 660 700 740 780 820 860 900 JD

FIG. 1*b*

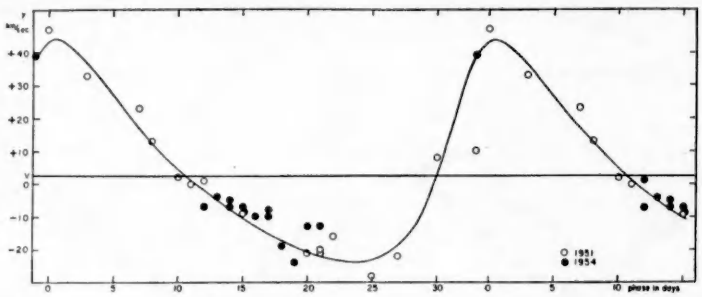

FIG. 2.—Variation of γ-velocity of σ Scorpii

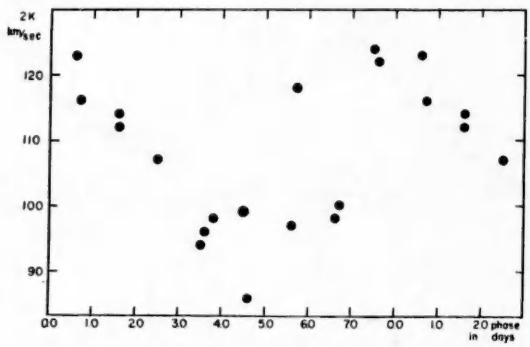

FIG. 3.—Plot of $2K$ with a beat period of 8.0 days

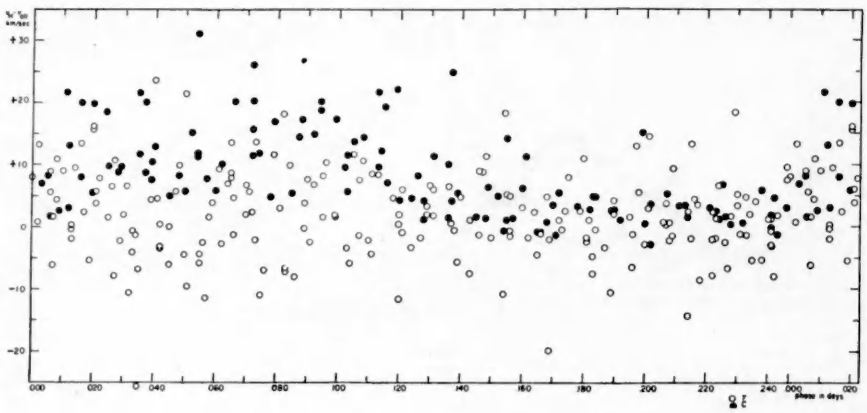

FIG. 4.—Plot of differences in velocity: H − all lines

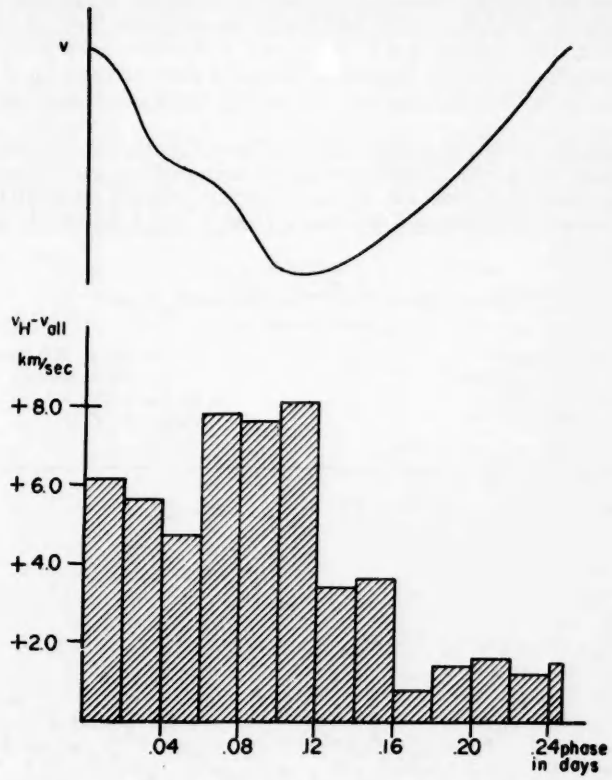

FIG. 5.—Smoothed plot of differences in velocity: H − all lines

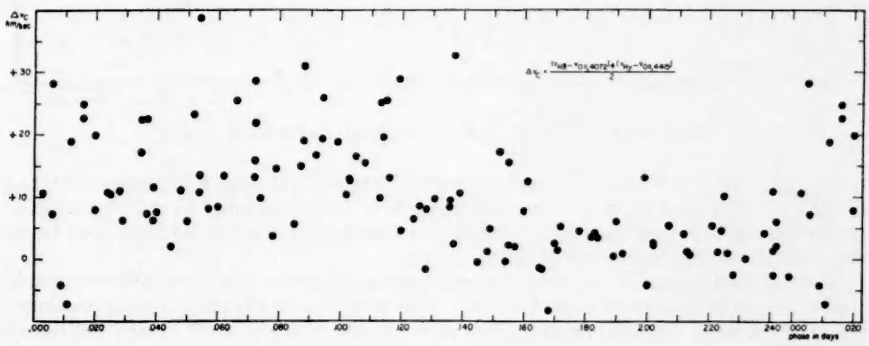

FIG. 6.—Plot of differences H − O II lines from coudé spectrograms

A. Van Hoof has recently discovered a remarkable departure between the velocity-curves of β CMa and 16 Lacertae, obtained, on the one side, from the hydrogen lines and, on the other side, from the lines of *O* II, *N* II, and *C* II. We have recently found that this effect is also conspicuous in BW Vulpeculae. It can be described as a lag of the order of about $0.04P$ in the radial velocities of the *H* lines with respect to those measured in other lines.

In order to study this effect, we have listed in Table 2 for each spectrogram the velocity differences (H − all lines). These values have been plotted against the phase in the short period in Figure 4. The scatter is large, especially between phases 0.000 and 0.150 day, where the lines are broad and indistinct. There is also a systematic difference be-

TABLE 4

ORBITAL ELEMENTS OF SPECTROSCOPIC BINARY
SIGMA SCORPII

P = 34.0 days	T = phase 32.2 days
γ = +2.5 km/sec	K = 34.0 km/sec
e = 0.36	$a \sin i = 1.48 \times 10^7$ km
ω = 308°	$f(\mathfrak{M})$ = 0.112 ⊙

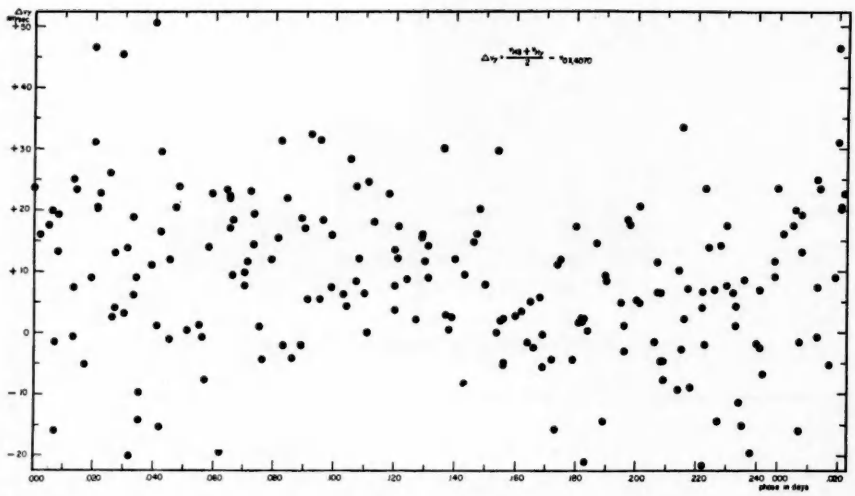

FIG. 7.—Plot of differences H − *O* II lines from Cassegrain plates

tween the coudé ("C") and the Cassegrain ("γ") plates, in the range of phases 0.000 and 0.120 day. This may be due to the distribution of lines measured in the two series of spectrograms, or it may be due to systematic differences in making settings upon broad and sometimes unsymmetrical absorption lines.

If we disregard, for the moment, this systematic difference, we can combine the individual values in groups of width 0.02 day. This was done in Figure 5. The approximate shape of the mean velocity-curve itself is shown at the top. The result clearly indicates a general lag of the hydrogen lines on the descending branch of the velocity-curve—in agreement with Van Hoof's discovery. There is no *clear-cut* indication of two maxima, as in BW Vulpeculae, which correspond, respectively, to the two steep sections of the descending branch of the velocity-curve—the one preceding the standstill, the other fol-

lowing it. But perhaps we may be permitted by analogy to point to the slight minimum in Figure 5 at phase 0.05 day, which closely agrees with the phase of the standstill in σ Scorpii.

In order to ascertain whether the selection of lines in the original measurements had anything to do with this effect, we have plotted in Figures 6 and 7 the values indicated in the diagrams. Since the lines $H\delta$, $H\gamma$, O II 4072, and O II 4415 were measured on all spectrograms plotted in Figure 6, this diagram should be free of any unsuspected influence due to the selection of lines included in the means of Table 2. The result is not essentially different from that of Figure 5. The scatter in Figure 7 is very large, due, no doubt, to the small dispersion of the γ plates. Nevertheless, the general trend is the same as in Figures 5 and 6.

REFERENCES

Levee, R. D., 1952, *Ap. J.*, **115**, 402.

THE VELOCITY-CURVE OF 12 DD LACERTAE*

OTTO STRUVE AND VELTA ZEBERGS
Berkeley Astronomical Department, University of California
Received February 28, 1955

ABSTRACT

Spectrographic observations in November, 1954, confirm the existence of De Jager's beat period of 8.9 days. The principal period $P_1 = 0.19308883$ day, and the secondary period, according to our observations, is 0.197358 day. The corresponding amplitudes are $2K_1 = 37.5$ km/sec. and $2K_2 = 17.5$ km/sec. The hydrogen-line velocities lag behind the average velocity-curve, on the descending branch of the curve, by about 20 minutes. The duplicities of the absorption lines found in 1950 conform to the picture of a discontinuous velocity-curve, as had already been established in the case of BW Vulpeculae and σ Scorpii.

The radial velocity of 12 DD Lacertae was investigated in 1950 from 259 spectrograms obtained at the Mount Wilson, Lick, and McDonald Observatories (Struve 1951). The results of our measurements were later discussed by C. de Jager (1953), who found that this β Canis Majoris type star exhibits a beat period of 8.9079 days. De Jager also found that this beat period is present in the light-curve of DD Lacertae.

The high-dispersion spectrograms of 1950 also led to the discovery of double absorption lines near the maximum and minimum of the principal velocity-curve, whose period is, according to E. A. Fath, 0.19308902 day and, according to De Jager, 0.19308883 day. These duplicities were very striking when the total range in radial velocity, $2K$, was large. They were not seen when $2K$ was small.

The purpose of the present investigation was (*a*) to confirm the existence of De Jager's beat period and (*b*) to investigate whether the duplicities of the spectral lines found in 1950 are compatible with the character of the line duplicities discovered recently in BW Vulpeculae = HD 199140 (Struve 1954) and in σ Scorpii (Huang and Struve 1955).

The new material used in the present work consists of 53 spectrograms obtained with the coudé spectrograph of the 100-inch telescope of the Mount Wilson Observatory, on November 17, 18, and 19, 1954. Those taken on the first two nights were obtained with a 73-inch camera and have a linear dispersion of 4.5 A/mm. Those on November 19 were obtained with a 30-inch camera and have a linear dispersion of 10 A/mm.

Table 1 lists the wave lengths of the star lines, and Table 2 gives the radial velocities. The phases were computed with the formula

$$\text{Phase in days} = T - (\text{JD } 2433508.740 + 0^d19308902E)\,. \qquad (1)$$

The radial velocities are plotted against the time in Figure 1. There is a clear indication of a standstill on the descending branches of all three curves, which resembles the standstill found by R. M. Petrie in BW Vulpeculae and confirmed by us (McNamara, Struve, and Bertiau 1955). Similar standstills are also present in σ Scorpii (Huang and Struve 1955). They seem to be present in many, if not all, the velocity-curves of the β Canis Majoris stars.

Table 3 shows the epochs of maximum and minimum radial velocity read off our curves and the values of O − C computed with three values of the principal period. The period of 0.193175 day was found by Struve to satisfy best the observations of 1950 alone. It does not fit the recent observations and is undoubtedly influenced by the beat

* The spectrograms used in this work were obtained by O. Struve as guest investigator at the Mount Wilson Observatory.

phenomenon. We can disregard it in the future. The period of 0.19308883 day found be De Jager fits our observations satisfactorily.

In order to test De Jager's beat period of 12 Lacertae, we have plotted against the time the observed values of $2K$ from Table 2 of our earlier paper (Struve 1951), but with the omission of the very uncertain value of September 1, 1950. These results are shown as solid dots in Figure 2. Four new values of $2K$ were read off the velocity-curves of Figure 1 and are shown as open circles in Figure 2. All values of $2K$ were plotted with a beat period of 8.9252 days—slightly longer than the one used by De Jager. The resulting

TABLE 1

LIST OF STAR LINES

Wave Length	Element	Wave Length	Element	Wave Length	Element
3964.73	*He* I	4143.76	*He* I	4471.48	*He* I
3973.26	*O* II	4340.47	*Hγ*	4481.23	*Mg* II
4026.19	*He* I	4345.56	*O* II	4552.65	*Si* III
4072.16	*O* II	4347.42	*O* II	4567.87	*Si* III
4075.87	*O* II	4349.43	*O* II	4574.78	*Si* III
4101.74	*Hδ*	4387.93	*He* I	4590.97	*O* II
4119.22	*O* II	4414.91	*O* II	4596.17	*O* II
4120.81	*He* I	4416.98	*O* II		

TABLE 2

RADIAL VELOCITIES

JD 2435+	Radial Velocity (Km/Sec)	Phase (Fraction of Day)	$v_H - v_{all}$ (Km/Sec)	JD 2435+	Radial Velocity (Km/Sec)	Phase (Fraction of Day)	$v_H - v_{all}$ (Km/Sec)
063.610	−27.0	0.117	+ 2.5	064.827	+ 1.1	0.176	+ 1.7
.642	− 6.4	.149	− 0.3	.842	+ 6.8	.191	+13.2
.658	+ 0.3	.165	− 5.5	065.598	− 8.6	.175	− 2.1
.672	+ 5.8	.179	+ 1.2	.608	− 4.0	.185	− 3.4
.687	+ 1.7	.001	+ 1.5	.617	− 4.2	.001	+ 3.8
.703	− 1.3	.017	+ 0.8	.626	− 5.0	.010	+ 1.8
.721	+ 0.9	.035	+ 9.8	.635	− 9.7	.019	+ 2.2
.740	−13.7	.054	+ 0.8	.644	− 9.9	.028	+ 4.4
.756	−27.6	.070	+ 1.8	.653	−12.6	.037	+ 6.0
.771	−33.5	.085	+ 0.9	.662	−12.4	.046	+ 3.2
.786	−30.7	.100	+ 5.9	.672	−13.7	.056	− 2.4
.806	−22.2	.120	− 0.2	.681	−18.0	.065	0.0
.824	−13.1	.138	+ 3.1	.691	−25.0	.075	− 2.9
064.630	+ 3.2	.172	− 3.5	.701	−28.2	.085	− 2.5
.640	+ 5.0	.182	− 9.0	.711	−26.6	.095	0.0
.651	+11.6	.000	− 6.7	.721	−26.5	.105	− 4.7
.661	+12.3	.010	+ 9.3	.730	−24.2	.114	− 2.3
.672	− 2.8	.021	+11.4	.740	−24.0	.124	− 1.1
.688	− 8.4	.037	+ 7.1	.749	−21.3	.133	+ 0.8
.702	−23.7	.051	− 2.5	.760	−18.8	.144	+ 1.4
.717	−32.0	.066	+12.7	.771	−17.3	.155	+ 0.9
.732	−32.8	.081	+ 0.5	.781	−12.0	.165	+ 5.0
.750	−28.9	.099	+ 2.3	.792	− 8.2	.176	− 1.4
.765	−22.1	.114	− 1.7	.803	− 4.8	.187	− 1.4
.779	−14.2	.128	− 1.1	.814	− 2.0	.005	− 2.1
.794	−10.2	.143	+ 4.8	.827	− 4.8	0.013	− 0.7
.812	− 0.5	0.161	− 3.9				

value of the interfering period would then be $P_2 = 0.197358$ day. The scatter of the points in Figure 2 is so large that we are inclined to believe that the velocity-curves contain irregularities other than those which result from the superposition of two harmonic oscillations. A similar conclusion was reached by De Jager with regard to both the variation in brightness and the variation in radial velocity. We agree with him that "it is probably difficult to ascribe them [the remaining residuals] to one single [third] component."

The last column of Table 2 contains the differences in radial velocity as determined

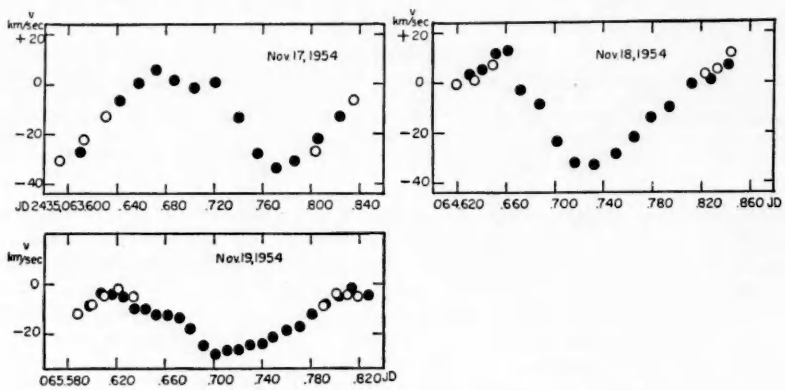

FIG. 1.—Radial velocity-curves of 12 Lacertae

TABLE 3

MAXIMA

(T_0 = JD 2433508.740)

Date (1954)	Observed Epoch (JD 2435+)	Computed Epoch (P = 0d19308902) (JD 2435+)	O−C	Computed Epoch (P = 0d193175) (JD 2435+)	O−C	Computed Epoch (P = 0d19308883) (JD 2435+)	O−C
Nov. 17.....	063.674	063.686	−12	063.606	+68	063.684	−10
18.....	064.657	064.651	+ 6	064.572	+85	064.650	+ 7
19.....	065.616	065.616	0	065.537	+79	065.615	+ 1
	065.814	065.809	+ 5	065.730	+84	065.808	+ 6

MINIMA

(T_0 = JD 2433508.828)

Date (1954)	Observed Epoch (JD 2435+)	Computed Epoch (P = 0d19308902) (JD 2435+)	O−C	Computed Epoch (P = 0d193175) (JD 2435+)	O−C	Computed Epoch (P = 0d19308883) (JD 2435+)	O−C
Nov. 17.....	063.774	063.774	0	063.694	+80	063.772	+ 2
18.....	064.727	064.739	−12	064.660	+67	064.738	−11
19.....	065.704	065.704	0	065.625	+79	065.703	+ 1

from the hydrogen lines alone and from all lines, including those of hydrogen. These values have been plotted in Figure 3 against the principal period, 0.19308902 day, using formula (1). Phase zero corresponds approximately to the epoch of maximum radial velocity. Although the scatter is large, there is a conspicuous excess of positive values between phases 0.01 and 0.05 day, that is, on the descending branch of the velocity-curve. This is a new manifestation of the time lag in the hydrogen velocity-curve as compared to the velocity-curve defined by the lines of other elements. Such an effect was first discovered by A. van Hoof in β Canis Majoris (Van Hoof and Struve 1953) and was later found by him in 16 Lacertae (Van Hoof, De Ridder, and Struve 1954). It has since been found in BW Vulpeculae (McNamara *et al.* 1955) and in σ Scorpii (Struve, McNa-

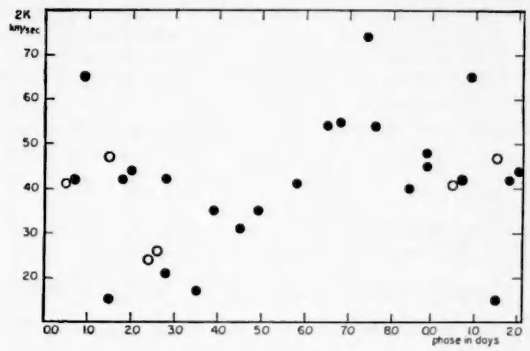

FIG. 2.—Plot of $2K$ against the beat period of 8.9252 days

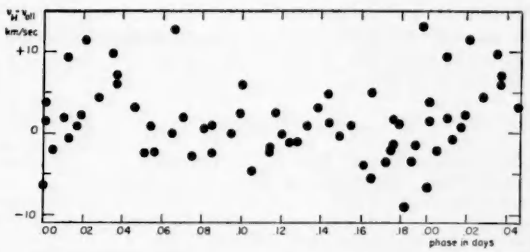

FIG. 3.—Plot of residuals in radial velocity (hydrogen *minus* means of all lines) against the principal period, $P_1 = 0.19308902$ day.

mara, and Zebergs, 1955). In the case of BW Vulpeculae the time lag on the descending branch corresponds to about 7 minutes. In the case of 12 Lacertae this lag corresponds to about 20 minutes, or $0.08P$. There appears to be no time lag on the ascending branch of the velocity-curve.

The new Mount Wilson spectrograms, despite their higher dispersion, fail to show the duplicities of the absorption lines as clearly as did those taken on September 22, 1950. This is due partly to underexposure on November 17 and 18, 1954, when the range in velocity $2K$ was large, and partly to insufficient range $2K$ on November 19, 1954. Nevertheless, the plates of November 17 and 18 do confirm, in a general way, the conclusions derived in our earlier paper.

A re-examination of the spectrograms of September 22, 1950, when the range $2K$ was large, suggests a reinterpretation of the radial velocities, as is demonstrated in Figure 4. There is now no doubt that the character of the velocity-curve resembles that previously found in BW Vulpeculae and σ Scorpii. Since the phenomenon of discontinuous branches of the velocity-curve has now been found in three stars of the β Canis Majoris class, we may conclude that it is a characteristic feature of these stars. It is, however, also certain that those members of the group which, like 12 Lacertae, have large variations in $2K$—partly as a result of the beat phenomenon and partly as a result of irregular fluctuations—show the duplicities only when $2K$ is large.

As to the physical explanation of the double lines, we can only say at this time that in 12 Lacertae, and probably also in BW Vulpeculae, the short intermediate branch of the velocity-curve (Fig. 4) has a marked upward trend. It is therefore *out* of phase when

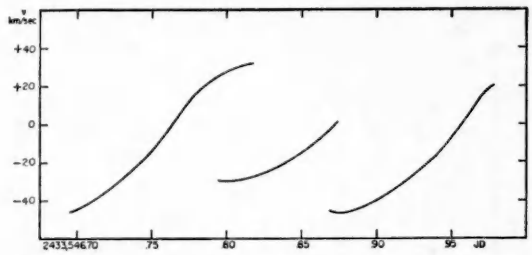

FIG. 4.—Reinterpretation of the velocity-curve of 12 Lacertae obtained on September 22, 1950

compared to the long branches. This would seem to rule out the hypothesis that the two branches represent the two interfering harmonic oscillations: when $2K$ is large, the two oscillations are *in* phase. Hence the slope of the short intermediate branch should be opposite in trend to that actually observed.

In conclusion, we estimate from Figure 2 the amplitudes of the two interfering oscillations as follows: $2K_1 = 37.5$ km/sec, $2K_2 = 17.5$ km/sec.

REFERENCES

Hoof, A. van, Ridder, M. de, and Struve, O. 1954, *Ap. J.*, **120**, 179.
Hoof, A. van, and Struve, O. 1953, *Pub. A.S.P.*, **65**, 158.
Huang, S., and Struve, O. 1955, **122**, 103.
Jager, C. de. 1953, *B.A.N.*, **12**, 81.
McNamara, D. H., Struve, O., and Bertiau, F. C. 1955, **121**, 326.
Struve, O. 1951, *Ap. J.*, **113**, 589.
———. 1954, *Pub. A.S.P.*, **66**, 329.
Struve, O., McNamara, D. H., and Zebergs, V. 1955, **122**, 122.

THE RADIO POSITION OF THE GALACTIC NUCLEUS

J. D. KRAUS AND H. C. KO
Radio Observatory, Ohio State University
Received January 25, 1955

ABSTRACT

Recent radio positions of the galactic nucleus obtained by five different groups of observers are averaged to give a most probable position of the nucleus of $l = 327.^{\circ}79$ and $b = -1.^{\circ}39$. A map showing the individual and average positions is included.

A determination of the position of the nucleus at the center of our Galaxy is a matter of considerable interest. Although obscured by dust from direct optical observation, the nucleus stands out as a sharp peak of high intensity when observed with a narrow-beam antenna at radio wave lengths.

TABLE 1

RADIO DETERMINATIONS OF THE POSITION OF THE GALACTIC NUCLEUS

No.	Observer	Wave Length (Cm)	1950.0		l	b
			α	δ		
1.....	Haddock, Mayer, and Sloanaker (HMS) (1954*a*)	9.4	$17^{h}42^{m}30^{s} \pm 12^{s}$	$-29°01' \pm 5'$	$327.^{\circ}62$	$-1.^{\circ}46$
2.....	Haddock (H) (1954)	3	17 42 30 ±12	−28 55 ± 5	327.70	−1.40
3.....	Hagen and McClain (HM)(1954)	21	17 43	−28 45	327.90	−1.41
4.....	Kraus and Ko (KK) (1954)	120	17 42 48 ±15	−28 50 ±30	327.81	−1.42
5.....	McGee and Bolton (MB) (1954)	75	(17 41 24)	(−28 32)	$327.9 \pm 0.^{\circ}2$	$-1.0 \pm 0.^{\circ}2$
6.....	van de Hulst, Muller, and Oort (VMO) (1954)	21	(17 43 36)	(−28 43)	328.0	−1.5
7.....	Most probable position (MPP)	Composite	17 42 40	−28 50	327.79	−1.39

During the past year a number of relatively accurate radio determinations have been made of the position of the galactic nucleus. These radio observations have been made by Haddock, Hagen, and others at the Naval Research Laboratory (Washington), McGee and Bolton at Sydney, van de Hulst, Muller, and Oort at Leiden, and Kraus and Ko at Ohio State. The positions are summarized in Table 1. Equatorial co-ordinates are 1950.0. Galactic co-ordinates are based on Ohlsson's (Lund) table. Since Ohlsson's table has 1900.0 equatorial co-ordinates, a conversion from 1950.0 to 1900.0 is required in using the tables. Error values are listed only if given by the authors. Where authors give the position only in galactic co-ordinates, the corresponding equatorial co-ordinates are shown in parentheses.

The accuracy of a radio-position determination is a function of both the antenna beam width and the source intensity at the wave length of observation. Thus a wide beam at

longer wave lengths where the intensity is large may yield as precise a position location as a narrow beam at shorter wave lengths where the intensity is small. The galactic nucleus has a spectrum in which the intensity decreases with decreasing wave length. At 120 cm the nucleus (with background deducted) is over 2000 times the minimum detectable intensity as observed with the 1° (in R.A.) by 8° (in Dec.) beam of the Ohio State University radio telescope (Kraus and Ko 1955). This large intensity at 120 cm tends to compensate for the use of a narrower beam at shorter wave lengths where the intensity is smaller.

Using the six positions listed in Table 1, the most probable position for the galactic nucleus was determined as follows. First, an average of all six positions listed in the table was taken. Then since positions 5 and 6 differed considerably from this average, a second

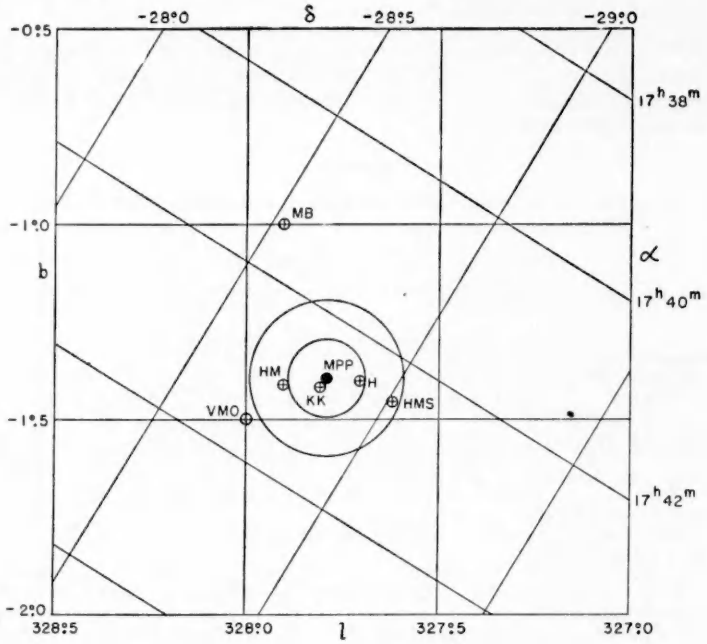

FIG. 1.—Map showing the most probable position (MPP) for the galactic nucleus as based on the six radio observations listed in Table 1. The co-ordinates are galactic (l, b) and equatorial 1950.0 (α, δ).

average was taken of positions 1, 2, 3, and 4 of the table. The first and second averages were then averaged to give what is considered to be the most probable position (MPP) of the galactic nucleus. This position, in galactic co-ordinates, is

$$327°.79 \pm 0°.10 \text{ (longitude)},$$

$$-1°.39 \pm 0°.10 \text{ (latitude)}.$$

This position is shown by the solid dot in Figure 1. Circles of 0°.1 and 0°.2 radius are drawn around the most probable position. Shown also in Figure 1 are the six observed positions listed in Table 1, the observers being indicated by the initial letters of their last names.

It is interesting to note that the longitude for the center of the Galaxy given by Oort (1952), as deduced indirectly from optical data, is 327°. Oort's data included two radio positions, but they are compensating and do not alter the average obtained only by optical means.

As observed with the Ohio State University radio telescope at 120 cm, the beam broadening by the nucleus is equivalent to that from a uniform source at least 1°.5 wide in right ascension. At 21 cm, Hagen and McClain (1954) estimate the diameter to be 0°.5.

The authors are indebted to Dr. Geoffrey Keller, director of Perkins Observatory, for helpful discussions and to Fred T. Haddock, of the Naval Research Laboratory, for communicating his 3-cm position in advance of publication.

Radio astronomy at the Ohio State University is supported by grants from the Development Fund, the Lovejoy Memorial Fund, and the fund for basic research of the Ohio State University and by a grant from the National Science Foundation.

REFERENCES

Haddock, F. T. 1954, private communication, December 3, 1954.
Haddock, F. T., Mayer, C. H., and Sloanaker, R. M. 1954*a*, *Ap. J.*, **119**, 456.
———. 1954*b*, *Nature*, **174**, 176.
Hagen, J. P., and McClain, E. F. 1954, *Ap. J.*, **120**, 368.
van de Hulst, H. C., Muller, C. A., and Oort, J. H., 1954, *B.A.N.*, **12**, 117.
Kraus, J. D., and Ko, H. C. 1954, *Sky and Telescope*, **14**, 22.
———. 1955, *Nature*, **175**, 159.
McGee, R. X., and Bolton, J. G. 1954, *Nature*, **173**, 985.
Oort, J. H., 1952, *Ap. J.*, **116**, 233.

SOME EVIDENCE FOR A REGIONAL VARIATION IN THE LAW OF INTERSTELLAR REDDENING

H. L. JOHNSON AND W. W. MORGAN
Lowell Observatory and Yerkes Observatory
Received March 19, 1955

ABSTRACT

Observations of the colors of early O stars on the (U, B, V) system indicate that the reddening law may be appreciably different in a region in Cygnus ($40° < l < 50°$) from that found for northern galactic longitudes $>70°$. The deviation is in the sense that relatively more ultraviolet light is absorbed in the Cygnus region. A possible explanation in terms of the distance of the absorbing material from the O star is suggested.

TERMINOLOGY

(U, B, V) system: The photometric system described by Johnson and Morgan (1953).

Reddening path: The path in a two-color index diagram occupied by stars of similar intrinsic color, but having differing amounts of interstellar reddening. For a further description of such diagrams, see Morgan, Harris, and Johnson (1953). A reference to earlier work is also given there.

Q index: The quantity defined by

$$Q = (U - B) - \frac{E_{(U-B)}}{E_{(B-V)}}(B - V)$$

(see Johnson and Morgan 1953). The index Q is a measure of the color of an O or B star, corrected for the effect of interstellar reddening. The ratio $E_{(U-B)}/E_{(B-V)}$ was denoted earlier by E_u/E_y; the change has been made for reasons of clarity.

I. INTRODUCTION

To make full use of the gain in accuracy of color determinations with photoelectric photometers, it is necessary to determine accurately the characteristics of the intrinsic radiation of the stars and to correct with precision for the effects of interstellar absorption. The pioneering work in this field has been carried out by Stebbins and Whitford and is given in Parts I and III of "Six-Color Photometry."

The "color-difference" method of W. Becker (1948) furnished a way to evaluate the amount of interstellar absorption and to determine the distances of galactic clusters. A somewhat similar method has been devised by investigators at the Yerkes and McDonald Observatories (Johnson and Morgan 1953; Morgan, Harris, and Johnson 1953) which makes special use of accurate photoelectric colors for the determination of interstellar reddening. For this purpose two calibrating operations are necessary: (1) the derivation of intrinsic colors for the O and B stars—both in $(B - V)$ and $(U - B)$—and (2) the accurate evaluation of the slope, $E_{(U-B)}/E_{(B-V)}$, of the reddening path.

The determination of $(B - V)$ intrinsic colors for the O9–A0 main-sequence stars offers no great difficulty; a sufficient number of sensibly unreddened stars are available for types B2–A0, and clusters can be used to derive intrinsic colors for stars as early as O7–O9. The situation is less satisfactory, however, with regard to operation 2. Two different values have been published for the fundamental ratio $E_{(U-B)}/E_{(B-V)}$ (Johnson and Morgan 1953; Morgan, Harris, and Johnson 1953). The earlier determination gave 0.72; the later, from a selection of stars subjected to a greater range of interstellar reddening, gave 0.886.

The accuracy of the observations is such that the two values are incompatible; the earlier determination rested principally on stars in the winter Milky Way; the later derives most of its weight from several heavily reddened stars of types B0.5 Ia–B1.5 Ia in Cygnus. The aim of the present paper is to attempt to reconcile these differences.

II. THE OBSERVATIONAL DATA

A group of stars having spectral types O5–O7 on the MK system were observed photoelectrically by Johnson with the 20-inch reflector of the Lowell Observatory. To these were added earlier measures by Johnson and by Harris at the McDonald Observatory. The stars are listed in Table 1, *a*, *b*, in order of values of $(B - V)$. The stars in Table 1, *b*, are those located in Cygnus, in the range $40° > l > 50°$.

TABLE 1

PHOTOMETRIC DATA ON O STARS

NAME	MK	V	$B-V$	$U-B$	n	Q
			a			
66811	O5f	2.25	−0.26	−1.11	4	−0.92
47839	O7	4.65	− .25	−1.06	3	− .88
48099	O6	6.36	− .05	−0.94	3	− .91
24912	O7	4.03	+ .01	−0.92	4	− .93
34656	O7	6.79	+ .02	−0.90	4	− .91
54662	O6	6.21	+ .03	−0.88	2	− .90
42088	O6	7.54	+ .05	−0.89	4	− .93
5005	O6	7.76	+ .09	−0.83	4	− .89
46150	O6	6.72	+ .13	−0.82	4	− .91
14434	O6	8.50	+ .16	−0.79	2	− .91
36879	O6	7.58	+ .18	−0.79	4	− .92
12993	O5	9.01	+ .19	−0.81	3	− .94
206267	O6	5.62	+ .21	−0.74	2	− .89
46223	O5	7.25	+ .22	−0.76	4	− .91
210839	O6f	5.04	+ .26	−0.73	4	− .92
242908	O5	9.05	+ .27	−0.72	3	− .91
242926	O6	9.35	+ .32	−0.66	3	− .89
215835	O6	8.58	+ .32	−0.66	3	− .89
46573	O7	7.92	+ .35	−0.66	4	− .91
14442	O5.5	9.24	+ .41	−0.64	2	− .94
14947	O6f	8.04	+ .44	−0.60	3	− .92
16691	O5f	8.70	+ .48	−0.59	3	− .94
+60°497	O7	8.79	+ .57	−0.50	3	− .91
217086	O7	7.64	+ .62	−0.44	3	− .89
15570	O5f	8.12	+0.69	−0.42	3	−0.92
			b			
193514	O7f	7.42	+0.45	−0.51	3	−0.83
193682	O5	8.41	+0.51	− .48	3	− .85
228841	O6.5	8.95	+0.55	− .41	3	− .81
VI Cyg 8A*	O6f	8.98	+1.29	+ .14	4	− .79
VI Cyg 11*	O6f	10.04	+1.43	+ .25	3	− .78
VI Cyg 7*	O6f	10.50	+1.44	+ .30	3	− .74
VI Cyg 9*	O5f	10.80	+1.93	+0.65	4	−0.74

* The association discussed by Johnson and Morgan (1954) has been named VI Cygni. The star VI Cyg 5 has been omitted because it is an eclipsing binary.

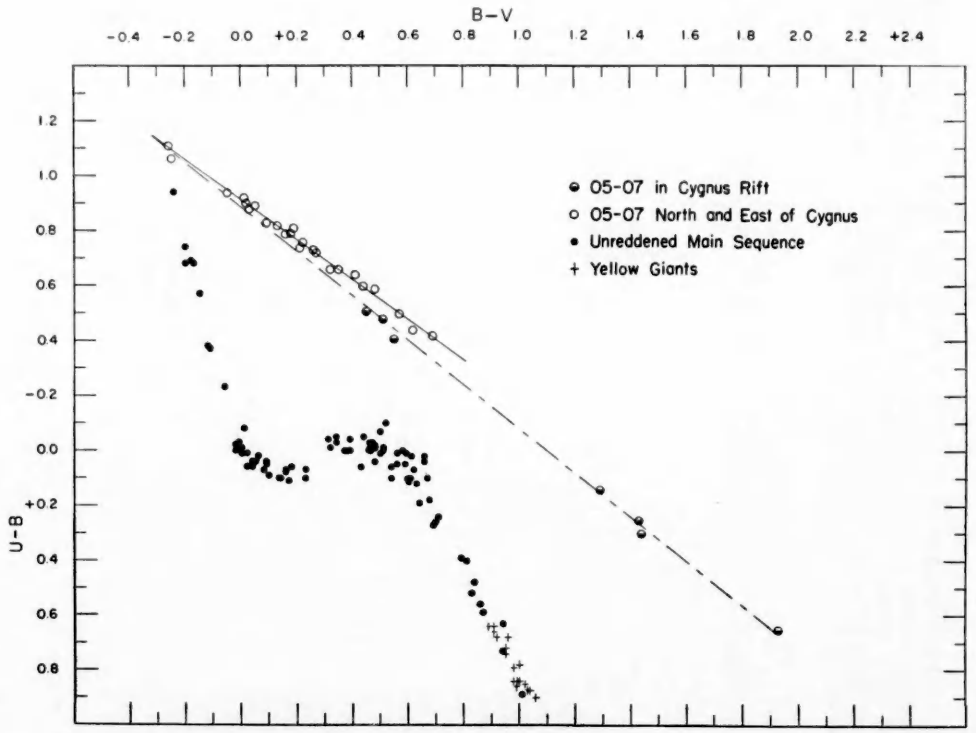

FIG. 1.—Two-color diagram for early O stars. The normal unreddened main sequence is shown from B1 to K3. The two reddening lines have slopes of 0.72 and 0.81, respectively, and pass through the zero point: $(B-V) = -0.32$; $(U-B) = -1.15$.

The columns give the name of the stars, the spectral type, the magnitude V, the values of $(B - V)$ and $(U - B)$, the number of observations, and the quantity Q, defined by

$$Q = (U - B) - 0.72\,(B - V)\,.$$

The intrinsic colors for stars in the spectral interval O5–O7 are similar; the total range in intrinsic $(B - V)$ is probably not more than 0.02 mag. and in $(U - B)$ of the order of 0.03 mag. We are thus justified in considering the stars in Table 1 as of approximately the same intrinsic color.

An inspection of the values of Q in Table 1, *a*, gives strong confirmation to the value of 0.72 for $E_{(U-B)}/E_{(B-V)}$; the mean value of Q from Table 1, *a*, is 0.91, with a range in values of ± 0.03 for the 25 entries.

The result is different in Table 1, *b;* here the values of Q change progressively with the amount of the color excess. The data are plotted in Figure 1, and the divergence in slope of the two relations is clear.

The interpretation of Figure 1 can be made as follows: for stars in the region of the Great Rift of the Milky Way in Cygnus, the interstellar absorption is greater in the ultraviolet relative to that at longer wave lengths. The number of stars observed in the Cygnus region is small, and the overlap in $(B - V)$ is not as great as might be desired; however, the tentative conclusion is indicated that the reddening law is sensibly different for the stars observed in the Cygnus region than for those observed in the Milky Way from Cepheus to Monoceros. The Cygnus region may thus be the second example of abnormal interstellar absorption; the region of the Orion Nebula was found to be peculiar in this respect some years ago (Baade and Minkowski 1937; Stebbins and Whitford 1945; Sharpless 1952).

The slope of the reddening path for O stars in Cygnus does not agree well with the value 0.886; it seems to lie near 0.81. An accurate evaluation of the slope of the reddening path in Cygnus will have to await the completion of a more extended observing program.

There is a possible general explanation of the present observations: the stars listed in Table 1, *a*, are, in general, located in space near the principal absorbing clouds which redden their light; on the other hand, the heavily obscured stars in Cygnus are situated at a considerably greater distance than the dense absorbing material of the Great Rift. It is therefore possible to explain the variations in the reddening law in terms of a modification of dust clouds by their proximity to an O star; the slope of 0.72 would then correspond to dust clouds whose characteristics have been modified because of their nearness to an O star. In the case of distant, heavily reddened O stars, the majority of the reddening material would be located far from the star itself; the slope of around 0.81 would then be the correct one.

More observations will be needed to settle this question. If the foregoing explanation is the correct one, no exceedingly heavily reddened stars should be observed corresponding to the slope 0.72; and for the range of reddening less than $E_{B-V} \sim 1.00$, stars should be found intermediate in position between the two slopes 0.72 and 0.81, which would then be considered to be limiting values.

We are indebted to Dr. D. L. Harris for several informative discussions.

REFERENCES

Baade, W., and Minkowski, R. 1937, *Ap. J.*, **86**, 123.
Becker, W. 1948, *Ap. J.*, **107**, 278.
Johnson, H. L., and Morgan, W. W. 1953, *Ap. J.*, **117**, 313.
———. 1954, *ibid.*, **119**, 344.
Morgan, W. W., Harris, D. L., and Johnson, H. L. 1953, *Ap. J.*, **118**, 92.
Sharpless, S. L. 1952, *Ap. J.*, **116**, 251.
Stebbins, Joel, and Whitford, A. E. 1945, *Ap. J.*, **102**, 318.

COLOR-MAGNITUDE ARRAY FOR STARS IN THE GLOBULAR CLUSTER M13*

ARCHIBALD BROWN†
Yerkes and McDonald Observatories
Received January 18, 1955; revised March 8, 1955

ABSTRACT

The paper gives photovisual and photographic magnitudes for a number of stars in the globular cluster M13, as measured from direct photographs taken at the McDonald Observatory. The photographs were calibrated by means of a sequence of stars in the field whose magnitudes had been determined with a photoelectric photometer. As far as possible, all stars down to apparent magnitude 15.0 (photovisual) were included. The proper motion of these stars was also measured and used to check their identification as members of the cluster. The color-magnitude diagram shows the usual features: a red giant sequence with a sharper boundary on the red side than on the blue, a gap between the blue and yellow stars at zero absolute magnitude, and a few blue stars well away from the main giant sequence.

The present paper is similar to an earlier one (Brown 1951; this paper will be referred to hereafter as "Paper I"), which gave a color-magnitude array for the stars in the globular cluster M15. The observations on M13 (1950, $\alpha = 16^h40^m$, $\delta = +36°33'$) were made in 1949 with the same equipment. As the methods of measuring and reducing the observations were almost identical with those for M15, most of the details can be omitted. To summarize the procedure, photographic and photovisual magnitudes were measured from photographs taken at the Cassegrain focus of the 82-inch reflector of the McDonald Observatory. Several stars in the field were observed photoelectrically to provide a calibration sequence. In drawing up the color-magnitude diagram, a number of stars were eliminated because they showed a recognizable proper motion relative to the cluster. The plates for the proper motions were taken with the 40-inch reflector at the Yerkes Observatory. From the internal evidence, it appears that the proper motions are better determined than for M15, but the magnitudes are less accurate.

I. PHOTOMETRIC OBSERVATIONS

The photoelectric observations were made in October, 1949, with the same equipment as for M15, and the same method of reduction was used (Paper I, pp. 345–348). Table 1 lists the stars observed photoelectrically. The numbers preceded by "L" refer to stars in Ludendorff's (1905) catalogue of M13; the numbers preceded by "N" refer to a supplementary list (Table 12). To determine the zero point of the magnitude scales, N 31 was compared with No. 16 of the North Polar Sequence ($m_{pv} = 11.22$).

Table 2 lists the plates used in the photographic photometry. As with M15, a yellow filter was used with the 103*a*-C plates, and the measurements were made with the Schilt-type photometer at the Yerkes Observatory. The last plate in the list was too heavily exposed to be of much use, but it served as a check on the photographic magnitudes of the faintest stars under consideration. It was not necessary to apply a correction for the background density, as was done for M15, probably because of the restricted use made of the heavy-exposure plate.

The magnitudes obtained from different plates were compared, to see how consistent the results were. (The original intention was to obtain magnitudes with an error of 0.05.) It turned out that the mean-square error was approximately 0.04 mag. for a determination made by taking the mean of the results for three plates.

* *Contributions from the McDonald Observatory, University of Texas*, No. 256.

† Now at the University of Melbourne, Australia.

A comparison of the magnitudes with those obtained by Shapley (1915) showed systematic differences between the two magnitude scales. Table 3 gives the measured magnitudes for a number of stars in the cluster, over the range covered by the present investigation. The fourth and seventh columns give the difference in the two results, Δm, in the sense Brown − Shapley. Figure 1 shows a plot of these differences in magnitude, with Δm as ordinate and Shapley's scale as abscissa. The run of the differences in the photographic magnitudes is fairly regular, except for a group of stars below the general level near $m_{pg} = 13.7$. I have examined my readings for these stars and compared their

TABLE 1

STARS OBSERVED WITH PHOTOELECTRIC PHOTOMETER

Star	Magnitude		Star	Magnitude	
	m_{pv}	m_{pg}		m_{pv}	m_{pg}
N 2	10.63	11.97	L 15	12.90	13.21
N 29	10.76	12.02	N 10	13.35	14.29
N 31	11.30	12.11	L 1043	13.58	14.24
N 13	11.78	12.99	L 22	14.98	15.68
N 17	11.82	12.32	L 1053	15.08	15.10
N 4	12.34	13.28	L 1079	15.37	15.33
L 1087	12.84	13.35			

TABLE 2

LIST OF PLATES USED IN PHOTOGRAPHIC PHOTOMETRY*

McDonald Serial No. CC	Date and Time at Mid-exposure (U.T.) September, 1949	Exposure (Min.)	Emulsion (Kodak)	McDonald Serial No. CC	Date and Time at Mid-exposure (U.T.) September, 1949	Exposure (Min.)	Emulsion (Kodak)
155	17, 3^h31^m	3	103*a*-C	194	25, 2^h33^m	2	103*a*-C
156	17, 3 36	10	103*a*-C	152	17, 2 54	1	103*a*-O
170	19, 2 42	2	103*a*-C	163	18, 2 49	$1\frac{1}{2}$	103*a*-O
171	19, 2 46	2	103*a*-C	175	19, 3 20	1	103*a*-O
193	25, 2 23	6	103*a*-C	196	25, 2 51	4	103*a*-O

* In the corresponding table of Paper I (Table 3), the date should be September, 1949 (instead of 1950), and the serial number of the seventh plate in the list should be CC 182 (instead of 192).

colors and positions in the cluster with those of adjacent stars in Figure 1, but I have not found an explanation for the unusual magnitude difference. So they probably correspond to a real dip in the run of Δm's.

For the photovisual magnitudes, there is a sudden increase in Δm near 13.0, which may be because the magnitude for star N 10 in the calibration sequence is too great. The difference appears to increase slightly to $m_{pv} = 14.65$ and then to fall off at fainter magnitudes. There is probably a small color effect, in the sense that the effective wave length of the present results is longer than that of Shapley's (1915) scale. However, Figure 1 shows that the difference in the scales is a more important effect.

Perhaps it is worth repeating that the calibration of the photoelectric colors was based on stars for which the international color lay between $c' = 0.03$ and $c' = 1.63$ (Paper I,

TABLE 3

COMPARISON OF MAGNITUDES WITH SHAPLEY'S (1915) VALUES

Star No. L	Magnitudes					
	Photographic			Photovisual		
	Shapley	Brown	Δm*	Shapley	Brown	Δm*
222	12.54	(12.5)†	.....	13.06	13.43	+37
1019	12.98	13.13	+15	12.63	12.72	+ 9
15	13.06	13.21	+15	12.80	12.90	+10
1087	13.14	13.35	+21	12.74	12.84	+10
835	13.23	13.63	+40	12.17	12.20	+ 3
973	13.35	13.62	+27	12.08	12.01	− 7
954	13.45	13.64	+19	12.14	12.05	− 9
70	13.45	13.78	+33	12.04	12.12	+ 8
414	13.46	13.67	+21	12.08	12.21	+13
194	13.58	13.83	+25	12.16	12.20	+ 4
199	13.66	13.57	− 9	12.24	12.22	− 2
316	13.68	13.82	+14	12.52	12.56	+ 4
96	13.70	13.69	− 1	12.54	12.43	−11
169	13.71	14.01	+30	12.74	12.80	+ 6
240	13.71	13.71	0	12.37	12.31	− 6
72	13.74	13.58	−16	12.42	12.31	−11
267	13.74	13.64	−10	13.93	14.17	+24
1073	13.75	13.93	+18	12.82	12.83	+ 1
326	13.76	13.81	+ 5	13.88	14.14	+26
687	13.76	13.90	+14	12.96	12.89	− 7
244	13.80	13.85	+ 5	12.64	12.63	− 1
353	13.84	13.93	+ 9	12.87	12.80	− 7
158	13.86	13.89	+ 3	12.70	12.69	− 1
777	13.87	14.00	+13	12.86	12.87	+ 1
919	13.88	14.11	+23	12.92	13.01	+ 9
993	13.90	14.03	+13	13.92	14.37	+45
1023	13.90	14.16	+26	13.02	13.07	+ 5
948	13.94	14.11	+17	13.04	13.20	+16
877	13.98	14.15	+17	13.06	13.08	+ 2
109	13.99	14.21	+22	13.14	13.38	+24
848	14.05	14.26	+21	13.10	13.18	+ 8
176	14.08	14.42	+34	13.14	13.42	+28
1043	14.09	14.24	+15	13.37	13.58	+21
201	14.10	14.31	+21	13.30	13.25	− 5
921	14.16	14.43	+27	13.16	13.45	+29
114	14.23	14.48	+25	13.36	13.54	+18
920	14.31	14.58	+27	13.58	13.84	+26
139	14.35	14.70	+35	13.93	14.09	+16
726	14.38	14.68	+30	13.57	13.72	+15
955	14.44	14.84	+40	13.80	13.98	+18
677	14.50	14.77	+27	13.66	13.94	+28
833	14.52	14.88	+36	13.99	14.24	+25
1114	14.63	14.84	+21	13.90	14.20	+30

* In units 0.01 mag. and taken in the sense (Brown − Shapley).

† Visual estimate. Star too bright for photometer.

TABLE 3—*Continued*

Star No. L	Magnitudes					
	Photographic			Photovisual		
	Shapley	Brown	Δm*	Shapley	Brown	Δm*
1001	14.65	15.01	+36	13.93	14.12	+19
946	14.71	14.97	+26	14.01	14.41	+40
985	14.74	15.12	+38	14.03	14.38	+35
943	14.80	15.28	+48	14.09	14.49	+40
140	14.80	14.96	+16	13.98	14.39	+41
1022	14.81	15.09	+28	14.70	15.13	+43
276	14.82	15.15	+33	14.90	15.21	+31
1053	14.85	15.10	+25	14.70	15.08	+38
141	14.88	15.11	+23	14.59	15.14	+55
796	14.93	15.16	+23	14.97	15.25	+28
528	14.96	15.33	+37	14.21	14.50	+29
933	15.01	15.23	+22	15.00	15.26	+26
230	15.04	15.43	+39	14.32	14.67	+35
1009	15.04	15.48	+44	14.35	14.73	+38
873	15.09	15.26	+17	15.13	15.31	+18
787	15.12	15.22	+10	14.27	14.30	+ 3
450	15.14	15.28	+14	15.18	15.28	+10
530	15.14	15.51	+37	14.40	14.68	+28
1079	15.14	15.33	+19	15.23	15.37	+14
621	15.20	15.42	+22	14.27	14.61	+34
130	15.21	15.50	+29	14.32	14.74	+42
1011	15.23	15.59	+36	14.56	14.78	+22
681	15.26	15.60	+34	14.46	14.81	+35
219	15.31	15.42	+11	14.32	14.58	+26
638	15.32	15.67	+35	14.56	14.94	+38
444	15.36	15.53	+17	14.56	14.82	+26
883	15.39	15.50	+11	14.46	14.76	+30
582	15.40	15.64	+24	14.59	14.87	+28
129	15.45	15.48	+ 3	14.65	14.91	+26
300	15.48	15.69	+21	14.59	14.92	+33
123	15.54	15.70	+16	14.70	14.97	+27
752	15.54	15.80	+26	14.75	15.13	+38
22	15.56	15.68	+12	14.54	14.98	+44
395	15.60	15.78	+18	14.72	15.06	+34
1018	15.64	15.83:‡	+19	15.00	15.08	+ 8
173	15.70	15.89:	+19	14.97	15.16	+19
146	15.71	15.91:	+20	15.03	15.12	+ 9
828	15.71	15.78	+ 7	14.75	15.05	+30
998	15.74	15.78	+ 4	14.97	15.09	+12
1085	15.80	15.88:	+ 8	14.95	15.12	+17
392	15.81	15.79	− 2	14.92	15.09	+17
1057	15.86	15.92:	+ 6	15.08	15.17	+ 9
596	15.90	15.84	− 6	14.85	15.14	+29
341	15.95	15.90:	− 5	15.18	15.19	+ 1
762	15.95	15.97:	+ 2	14.75	14.96	+21
619	15.96	15.85:	−11	14.80	15.15	+35

‡ Colons indicate observation of low weight.

Table 2 and Fig. 1). Outside this range, the colors are extrapolated and therefore less reliable. In particular, the values for very blue stars are liable to be in error (Paper I, p. 365).

There is also the risk of a systematic difference between the colors obtained from the photographic photometry and the photoelectric colors of the calibration sequence, if the effective wave lengths are not identical. To distinguish the two sets, colors obtained from the photographs are denoted by c'' in the subsequent tables, and c' is used for the colors obtained from the photoelectric observations. The relation between c'' and c' need not

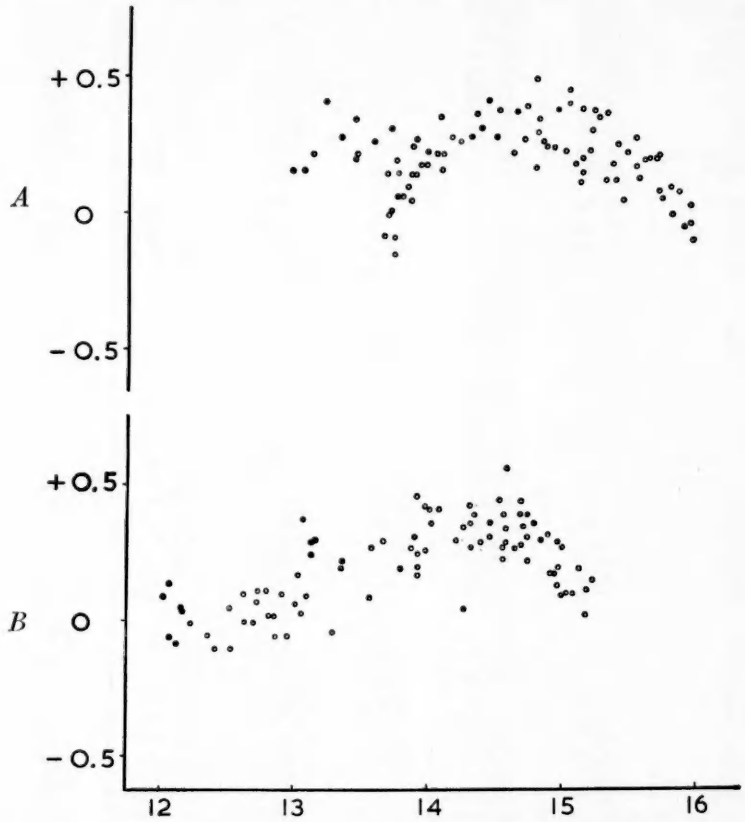

FIG. 1.—Comparison of magnitudes with Shapley's values. (Difference in magnitude, in the sense Brown−Shapley, plotted against apparent magnitude.) *A*, photographic magnitudes; *B*, photovisual magnitudes.

be linear, for the photographic photometry magnitudes were obtained by interpolation between the magnitudes of the photoelectric sequences and are thus affected by the wave length of the corresponding photoelectric sequence, as well as by any errors in the magnitude steps of the photoelectric sequence. In the present case, a comparison of c' and c'' for the stars of the calibration sequence (as far as this was possible) suggested that c' and c'' differ systematically, but the data were insufficient to establish this definitely.[1]

[1] The data suggested a linear relation $c' = 0.83c'' + 0.07$, over the range $-0.1 \leq c'' \leq +1.1$.

II. PROPER-MOTION OBSERVATIONS

Table 4 gives details of the plates used in the proper-motion measurements. The two 1901 plates were taken by G. W. Ritchey, the 1908 plate by E. E. Barnard, and the three second-epoch plates were taken by the author. Plate F 767 was taken on an Eastman II-G plate, Plates F 760 and F 768 on Eastman 103*a*-C plates. As in the work on M15, a yellow filter was used, and the aperture of the telescope was reduced from 40 to 24 inches. A single exposure was made on each plate, and the plates were measured separately, using the positions in Ludendorff's (1905) catalogue to orient the plates.

The measurement of the plates and the determination of the relative motions followed the same pattern as in Paper I, but some small differences were made in reducing

TABLE 4

PLATES USED IN PROPER-MOTION DETERMINATIONS
(Yerkes 40-Inch Refractor: Plate Scale = 10″.655 per Mm)

PAIR	PLATE NO.	EPOCH	EXPOSURE (MIN.)	INTERVAL (YEARS)	REFERENCE STARS	
					No.	m_{pv}
1.....	F Ry 28 F 767	1901.296 1949.461	180 100	48.165	48	14.8
2.....	F Ry 29 F 768	1901.315 1949.461	240 45	48.146	48	14.9
3.....	F 66 F 760	1908.554 1949.366	150 25	40.812	23	14.2

TABLE 5

MEAN PROPER MOTION OF REFERENCE STARS
(Unit 0″.0001 p.a.)

	Pair 1	Pair 2	Pair 3
R.A. (μ_x'').....	−15	−15	−18
Dec. (μ_y'').....	+ 3	+ 3	+ 4

the relative motions to absolute motions. As the galactic latitude of M13 is 40°, Binnendijk's (1943) formula[2] for the mean parallax becomes

$$\log p_m = -2.484 - 0.115\,(m_{pg} - 12)\,, \tag{1}$$

where p_m is the mean parallax for stars of photographic magnitude m_{pg} at galactic latitude 40°. (The constant −2.484 was obtained from Table 10 of Binnendijk's [1943] paper.) In the notation of Paper I, the mean proper motion of the reference stars is given by

$$\mu_x'' = \frac{P p_m V_0}{\kappa} \quad \text{and} \quad \mu_y'' = \frac{P' p_m V_0}{\kappa}. \tag{2}$$

In this case, $P = -0.29$ and $P' = +0.066$ (Van Rhijn and Bok 1931; interpolated from their Tables 11 and 12), and V_0, the speed of the solar motion relative to the reference stars, was again taken as 19.5 km/sec. The resulting values of μ_x'' and μ_y'' are shown in Table 5.

[2] Equation (1) corresponds to eq. (6) of Paper I.

It may be worth stressing again that allowing for the motion of the reference stars is one of the weakest links in the lengthy chain connecting the original measurements with the tabulated proper motions. The amount of the solar motion could be in error by 10 per cent or more, and the choice of the R.A. of the solar apex makes an appreciable difference to μ_x'' for a star at $\alpha = 250°$, $\delta = 36°.5$. Another difficulty is that the faintness of the reference stars for pairs 1 and 2 makes it necessary to extrapolate Binnendijk's formula to magnitudes fainter than those he considered in compiling his table of mean parallaxes. Errors in the magnitudes of the reference stars are unimportant compared with the uncertainty in the solar motion. In using equation (1), it was found that a change of 0.2 mag. in m_{pg} made no appreciable difference to μ_y'' and changed μ_x'' by one unit in the last place (Table 5).

The choice of reference stars could cause a difference between the results for different pairs of plates, since we have to assume that the mean motion of the sun relative to a limited group of reference stars is the same as the mean motion of the sun relative to all

TABLE 6*

MEAN MOTION FOR GROUPS OF CLUSTER STARS ON PAIR 1

Group	1	2	3	4	5	6	7	8	9	10	11
No. of stars	7	6	7	8	6	7	7	7	7	7	8
Mean m_{pv}	12.2	12.8	13.1	13.3	13.6	13.9	14.1	14.2	14.5	14.7	14.8
$\bar{\mu}_x$	−24	−20	−18	−12	− 7	− 3	−12	− 6	− 3	0	− 1
$\bar{\mu}_y$	+ 4	−11	+ 2	+ 3	− 3	+ 6	+10	+ 1	+10	+ 6	+ 1

* The mean motion $\bar{\mu}_x$ and $\bar{\mu}_y$ are in units 0".001 p.a.

stars of the given magnitude. However, a comparison of the mean motion of 40 stars measured in all three pairs of plates showed that this effect was small in the present case. This comparison also provided an estimate of the mean-square error of a single determination, and this came out as 0".0014 p.a.

Another by-product of this comparison was an indication of a magnitude effect, particularly in comparing pairs 1 and 2. Accordingly, a more extensive check was made. First of all, a comparison of 52 of the faintest stars common to pairs 1 and 2 showed that the mean motion of these faint stars was in agreement. As the mean magnitude of this group of stars was almost the same as that of the comparison stars, it seemed reasonable to use these faint stars as a control group and apply corrections to reduce the motion of the remaining stars to the same basis. For this purpose, a preliminary selection of cluster stars was made, and the mean motion of groups of different brightness was compared. For pair 2, the difference in the mean motion of these groups was not significant, and no corrections were applied. For pair 1, a similar subdivision of the material gave Table 6. An analysis of variance (within and between groups) showed that the $\bar{\mu}_x$ values varied significantly from group to group, but not the $\bar{\mu}_y$ values. Accordingly, no correction was made to the μ_y values, but a correction was applied to the μ_x values, as given in the accompanying table. (The corrections are in units of 0".0001 p.a.) This correction is

m_{pv}	≥14.45	14.00–14.45	13.55–14.00	13.10–13.55
Correction to μ_x	0	+4	+8	+12

m_{pv}	12.65–13.10	12.20–12.65	11.75–12.20
Correction to μ_x	+16	+20	+24

probably due to the quality of the images on Plate F Ry 28, where a slight elongation in R.A. is visible.

A similar analysis for pair 3 indicated that there was not a gradual change in this case but that a correction was required for the brightest stars on the plates. The corrections applied were $+0''.001$ p.a. to μ_x and $-0''.002$ p.a. to μ_y, and these corrections were applied to the stars brighter than 12.35 mag. (pv).

Table 7 shows a comparison of the results with those of Van Maanen (1927, Table 3;

TABLE 7

COMPARISON OF PROPER MOTIONS WITH VAN MAANEN'S (1927) RESULTS FOR STARS NEAR EDGE OF FIELD

(Unit: $0''.001$ p.a.)

Star	Proper Motion				Star	Proper Motion			
	Van Maanen (1927)		Brown			Van Maanen (1927)		Brown	
	μ_x	μ_y	μ_x	μ_y		μ_x	μ_y	μ_x	μ_y
L 1	+ 7	− 1	+ 3	+ 1	N 11 (f)	+ 3	0	− 2	− 1
15	−26	+ 19	−20	+ 16	13 (g)	− 7	0	− 6	+ 1
1019	+ 4	− 13	+ 8	− 16	23 (p)	−43	+ 31	−41	+ 38
1087	− 7	+ 16	− 4	+ 11	24 (o)	− 6	− 3	− 9	− 11
N 1 (a)	− 6	+ 9	−14	+ 4	26 (q)	+ 5	− 24	+ 2	− 26
4 (c)	+ 4	0	0	− 5	28 (s)	−16	−132	−20	−132
7 (e)	+ 4	0	− 1	− 1	30 (t)	− 3	+ 6	+ 2	− 2
8 (d)	+ 4	− 19	− 3	− 18					

the values here are those for the 80-foot focus plates, corrected by $-0''.001$ p.a. in μ_a to reduce them to absolute motions) for a number of stars toward the edge of the field. For the stars which are not in Ludendorff's (1905) catalogue, Van Maanen's (1927) identification letter is given in parentheses after the "N" number. It will be seen that the results agree moderately well.

III. ELIMINATION OF FIELD STARS; MEAN MOTION OF CLUSTER

The elimination of field stars was carried out in the same way as for M15. A preliminary sorting allowed the selection of 70 stars with well-determined proper motions which appeared to be members of the cluster. The motions of these stars gave the mean values:

$$\bar{\mu}_x = -0''.0022 \text{ p.a.}; \qquad \bar{\mu}_y = +0''.0007 \text{ p.a.} \tag{3}$$

with the standard deviations

$$\sigma_x = 0''.0007 \text{ p.a.}; \qquad \sigma_y = 0''.0008 \text{ p.a.}$$

for the two components. (These standard deviations correspond to determinations from three pairs of plates and are therefore consistent with the figure of $0''.0014$ p.a. previously mentioned, which referred to a determination from a single pair of plates.) Limiting values of μ_x and μ_y for inclusion as a cluster member were placed at $\bar{\mu}_x \pm 2.5\ \sigma_x$ and $\bar{\mu}_y \pm 2.5\ \sigma_y$, i.e., the criterion was

$$\begin{aligned} -0''.0039 \le \mu_x \le -0''.0004 \text{ p.a.}, \\ -0''.0013 \le \mu_y \le +0''.0027 \text{ p.a.} \end{aligned} \tag{4}$$

The mean motion of the cluster, as given by equation (3), has not been adjusted for the effect of galactic rotation. Hence it cannot be compared immediately with the mean motion given by Gamaley (1948) for this cluster. Indeed, even if we exclude Gamaley's correction for galactic rotation, the results are not directly comparable, because there is an appreciable difference in the correction for parallactic motion. It may be illuminating to show how large this difference can be. Gamaley (1948) used Deutsch's (1947) mean parallaxes and took the position of the solar apex at $\alpha = 285°$, $\delta = +36°$. His correction for the parallactic motion of the comparison stars was

$$\mu_x' = -0''.0038 \text{ p.a.}, \qquad \mu_y' = -0''.0006 \text{ p.a.} \tag{5}$$

If we take the mean photographic magnitude of his reference stars as 14.4 and use equations (1) and (2), with P and P' as given there, then

$$\mu_x' = -0''.0021 \text{ p.a.}, \qquad \mu_y' = +0''.0005 \text{ p.a.} \tag{6}$$

A change of 0.1 mag. in the mean magnitude of the reference stars would make hardly any difference. The important differences are that Binnendijk's (1943) mean parallaxes are smaller than Deutsch's (1947) by about 15 per cent for galactic latitude 40° and that

TABLE 8

ABSOLUTE PROPER MOTION OF CLUSTER M13

TELESCOPE	INTERVAL (YEARS)	FOCAL LENGTH (FT.)	PROPER MOTION		OBSERVER
			μ_x	μ_y	
60-inch reflector, Mount Wilson	9–14	{25 / 80}	+0".0005	+0".0008	Van Maanen*
24-inch reflector, Mill Hill	36	10.2	− .002	− .001	White†
13-inch refractor, Poulkovo	42	11.3	− .0058	+ .0030	Gamaley‡
13-inch refractor, Tashkent	40	11.3	− .0017	− .0002	Fatchikhin§
40-inch refractor, Yerkes	40–48	63	−0.0022	+0.0007	Brown

* *Ap. J.*, **66,** 93, 1927.
† *M.N.*, **94,** 783, 1934.
‡ *Poulkovo Bull.*, **17,** No. 6, 27, 1948. Gamaley's correction for galactic rotation has been omitted.
§ *Poulkovo Bull.*, **19,** No. 1, 150, 1952. The correction for galactic rotation has again been omitted.

the Van Rhijn and Bok (1931) tables are computed for a solar apex at $\alpha = 270°$, $\delta = +31°$. Roughly, the lower declination makes the μ_y' correction positive, and the change in R.A. reduces μ_x' by a factor of about 0.6. Table 8 shows the results of different determinations of the absolute proper motion of M13. The scatter in the results is a fair indication of the errors involved.

IV. TABULATION OF RESULTS FOR INDIVIDUAL STARS

The proper-motion criterion (eq. [4]) was used to pick out cluster members, and these are listed in the two parts of Table 9. Table 9, A, gives stars which satisfy the proper-motion criterion and are within 2.5 minutes of arc of the center of the cluster; Table 9, B, lists those whose distance from the center, r, is in the range $2'.5 < r < 7'$. The magnitudes for the latter group should, on the whole, be more reliable than those in the first group, where the congestion of images makes it difficult to separate the stars in the photometer field and more difficult still to get reliable control readings of the background intensity. In the area within 1′ of the center of the cluster, the majority of the stars had

TABLE 9

LIST OF CLUSTER MEMBERS
(Criteria: Proper Motion and Distance from Center)

STAR	MAGNITUDE		COLOR	PROPER MOTION (UNIT: 0".0001 p.a.)			NO. PAIRS OF PLATES
	m_{pg}	m_{pv}	c''	μ_x	μ_y		
				−	+	−	
	A. Stars within 2½′ of Center of Cluster						
L 123	15.70	14.97	+0.73	22	6	.....	2
140	14.96	14.39	+0.57	7	6	.....	2
160	14.63	13.81	+0.82	24	7	.....	3
166	15.82	15.08	+0.74	22	.....	8	1
174	14.93	14.22	+0.71	19	8	.....	3
176	14.42	13.42	+1.00	10	7	.....	3
178	14.87	14.04	+0.83	26	.....	4	3
180	15.65	14.94	+0.71	6	7	.....	2
181	14.95	14.12	+0.83	22	13	.....	3
193	14.67	13.76	+0.91	20	.....	4	3
194	13.83	12.20	+1.63	20	1	.....	3
198	14.02	12.96	+1.06	10	4	.....	2
201	14.31	13.25	+1.06	19	9	.....	3
206	.....	.....	*	14	.....	12	2
207	15.61	14.91	+0.70	12	26	.....	2
215	15.41	14.64	+0.77	18	8	.....	2
217	15.66	14.88	+0.78	36	17	.....	2
222†	(12.5)‡	13.43	(−0.9)	35	1	.....	3
225	15.51	14.74	+0.77	18	3	.....	2
227	15.15	14.60	+0.55	19	0	.....	2
230	15.43	14.67	+0.76	28	16	.....	2
231†	14.66:	13.88	+0.78	10	18	.....	3
235	15.66	14.90	+0.76	8	10	.....	2
245	15.10	15.06	+0.04	26	11	.....	2
249	14.19	13.22	+0.97	24	.....	6	3
250	13.67	12.38	+1.29	28	.....	1	3
256	14.97	14.11	+0.86	16	3	.....	3
261	13.58	12.22	+1.36	4	.....	8	3
262	13.61	12.27	+1.34	34	.....	6	1
267	13.64	14.17	−0.53	12	16	.....	3
268	14.56	13.61	+0.95	27	.....	3	3
269†	13.99:	13.18	+0.81	32	.....	4	3
273	15.52	14.77	+0.75	16	11	.....	2
274	14.98	14.20	+0.78	9	.....	2	3
278	15.14	14.32	+0.82	20	.....	11	3
281†	14.34:§	13.41	+0.93	13	4	.....	3
284	15.34	14.53	+0.81	28	.....	3	2
287	15.10	14.24	+0.86	22	14	.....	2
293	15.48	14.81	+0.67	20	4	.....	2
296†	13.81:§	12.57	+1.24	26	17	.....	1

* See notes at end of table.

† Not included in color-magnitude diagram; photometric data poor.

‡ Visual estimate; star too bright for photometer.

§ Multiple on photographic plates.

TABLE 9—*Continued*

Star	Magnitude m_{pg}	Magnitude m_{pv}	Color c''	Proper Motion (Unit: 0".0001 p.a.) μ_x −	μ_y +	μ_y −	No. Pairs of Plates
	A. Stars within 2½′ of Center of Cluster—*Continued*						
L 300	15.69	14.92	+0.77	27	.....	6	2
301	15.09	14.58	+0.51	4	.....	7	2
306	.....	.....	*	23	14	.....	3
309	15.37	14.67	+0.70	10	12	.....	2
318	14.93	14.15	+0.78	27	8	.....	3
324	14.0	12.2	+1.8*	29	0	.....	3
332	15.10	15.13	−0.03	25	10	.....	1
333	14.92	14.85	+0.07	9	18	.....	2
334	15.22	14.48	+0.74	19	10	.....	2
337	14.97	14.10	+0.87	24	7	.....	3
345	14.02	12.88	+1.14	25	2	.....	3
347†	14.84:	13.92	+0.92	22	6	.....	3
352	14.64	13.75	+0.89	21	8	.....	3
353	13.93	12.80	+1.13	20	7	.....	3
359	15.46	14.70	+0.76	21	4	.....	2
362	14.11	13.48	+0.63	18	12	.....	1
367†	13.75:	12.56	+1.19	23	20	.....	1
370	14.35	13.50	+0.85	13	5	.....	3
372	14.84	14.06	+0.78	27	13	.....	3
373	14.98	14.34	+0.64	16	3	.....	2
376†	13.62:	12.88	+0.74	7	22	.....	1
378	15.39	14.83	+0.56	36	.....	4	1
380	15.02	15.03	−0.01	16	27	.....	1
384†	13.72:	12.50	+1.22	15	20	.....	3
385	15.52	14.81	+0.71	28	.....	12	2
386	14.81	14.21	+0.60	32	.....	3	3
392	15.79	15.09	+0.70	17	.....	10	2
405†	15.61:	14.97	+0.64	25	11	.....	2
414	13.67	12.21	+1.46	18	.....	6	3
419†	14.97:	14.03	+0.94	33	14	.....	1
421	15.75	15.12	+0.63	18	5	.....	1
430†	15.50	14.81:	+0.69	29	.....	1	1
436‖	14.28	13.46	+0.82	22	10	.....	3
439	15.02	14.17	+0.85	15	12	.....	3
450	15.28	15.28	0.00	14	12	.....	2
457	15.36	14.64	+0.72	34	11	.....	2
460†	15.26:	14.48	+0.78	20	.....	4	2
462	15.30	14.66	+0.64	16	14	.....	2
465†	13.75:	12.50	+1.25	13	17	.....	1
476†	14.28:	13.16	+1.12	10	.....	6	1

‖ Double.

TABLE 9—*Continued*

Star	Magnitude m_{pg}	Magnitude m_{pv}	Color c''	Proper Motion (Unit: 0".0001 p.a.) μ_x	μ_y +	μ_y −	No. Pairs of Plates
	A. Stars within 2½′ of Center of Cluster—*Continued*						
L 484	15.07	14.27	+0.80	25	3	.....	3
487	13.8	12.6	+1.2*	18	25	.....	1
488	15.06	14.18	+0.88	13	6	.....	3
521	15.44	14.69	+0.75	38	.....	8	2
523†	15.56:	14.90:	+0.66	19	19	.....	1
524†	15.07:	14.87:	+0.20	10	.....	7	1
526	14.17	13.92	+0.25	27	.....	9	3
528	15.33	14.50	+0.83	20	18	.....	2
556	14.74	13.80	+0.94	17	12	.....	3
578†	14.76:	13.99	+0.77	39	.....	9	1
580	15.39	14.62	+0.77	6	10	.....	2
582	15.64	14.87	+0.77	7	8	.....	2
587†	15.67:	15.09	+0.58	14	.....	9	2
594†	14.01:	12.89	+1.12	19	12	.....	2
598†	13.64:	12.03:	+1.61	31	2	.....	1
602	15.76	15.13	+0.63	22	16	.....	1
605†	15.01:	14.02	+0.99	18	22	.....	1
609	14.94	14.04	+0.90	31	23	.....	3
616	15.05	15.12	−0.07	30	7	.....	2
618	15.26	14.41	+0.85	21	13	.....	3
621	15.42	14.61	+0.81	23	2	.....	2
625	15.46	14.71	+0.75	21	.....	11	2
629†	13.46:	12.00:	+1.46	37	.....	6	1
636	14.96	14.02	+0.94	26	3	.....	3
638	15.67	14.94	+0.73	20	14	.....	2
643	14.90	14.05	+0.85	16	19	.....	3
644	14.25	13.19	+1.06	15	16	.....	3
646	15.30	14.55	+0.75	16	.....	12	2
652	15.57	14.82	+0.75	16	3	.....	2
656	14.28	14.83	−0.55	17	4	.....	2
666†	14.00:	12.65	+1.35	36	25	.....	1
671†	15.88:	15.15	+0.73	17	.....	2	2
673#	.....	13.14	.....	28	.....	1	1
677	14.77	13.94	+0.83	28	19	.....	3
681	15.60	14.81	+0.79	12	20	.....	2
690	15.63	14.91	+0.72	16	.....	12	2
694†	15.63:	15.03	+0.60	32	6	.....	1
696	15.03	14.21	+0.82	34	27	.....	1
698†	15.70	15.04:	+0.66	24	.....	9	1
702	14.69	13.75	+0.94	32	0	.....	3

Close companion on photographic plates.

TABLE 9—*Continued*

Star	Magnitude m_{pg}	Magnitude m_{pv}	Color c''	Proper Motion (Unit: 0".0001 p.a.) μ_x −	μ_y +	μ_y −	No. Pairs of Plates
	A. Stars within 2½′ of Center of Cluster—*Continued*						
L 719	15.51	14.85	+0.66	18	1	.....	2
722	15.17	14.35	+0.82	24	12	.....	2
728	13.87	12.71	+1.16	33	17	.....	1
731	15.42	14.65	+0.77	16	22	.....	2
742	14.18	13.49	+0.69	5	.....	4	1
743	14.65	13.82	+0.83	20	2	.....	3
746	15.04	14.14	+0.90	21	1	.....	3
755	15.29	14.46	+0.83	25	7	.....	1
756	14.64	13.93	+0.71	33	13	.....	3
761	15.17	15.05	+0.12	29	.....	7	2
768	14.18	13.06	+1.12	24	15	.....	3
784	15.59	14.89	+0.70	21	.....	9	2
785	15.69	15.00	+0.69	29	0	.....	2
793	14.62	13.75	+0.87	11	3	.....	3
794†	14.73:	13.91	+0.82	26	2	.....	2
796	15.16	15.25	−0.09	16	10	.....	1
797†	15.31	14.76:	+0.55	25	8	.....	2
798	14.76	14.08	+0.68	28	5	.....	3
802	14.88	14.02	+0.86	13	17	.....	2
807	14.74	14.55	+0.19	26	.....	4	2
810	15.11	14.21	+0.90	17	15	.....	2
819	14.85	13.93	+0.92	15	15	.....	3
824	15.26	14.50	+0.76	10	8	.....	2
825	13.76	12.80	+0.96	18	3	.....	3
829	15.27	14.53	+0.74	21	18	.....	2
830	13.88	12.69	+1.19	30	15	.....	2
834	15.58	14.84	+0.74	20	7	.....	2
835	13.63	12.20	+1.43	22	9	.....	3
841	14.63	13.84	+0.79	20	21	.....	3
844	14.75	13.88	+0.87	17	12	.....	3
845	13.82	12.54	+1.28	32	13	.....	3
846	15.33	14.71	+0.62	36	22	.....	2
847	15.07	14.07	+1.00	8	.....	5	2
853	13.66	12.23	+1.43	29	9	.....	3
855†	15.72:	15.09	+0.63	11	.....	6	1
863	14.16	13.04	+1.12	26	2	.....	3
865	15.58	14.83	+0.75	36	12	.....	2
868	14.95	14.05	+0.90	20	1	.....	1
872	.....	14.0	*	14	.....	2	2
875	15.12	15.07	+0.05	16	15	.....	2

TABLE 9—*Continued*

Star	Magnitude m_{pg}	Magnitude m_{pv}	Color c''	Proper Motion (Unit: 0".0001 p.a.) μ_x −	μ_y +	μ_y −	No. Pairs of Plates
	A. Stars within 2½′ of Center of Cluster—*Continued*						
L 900	14.06	13.38	+0.68	25	9	.....	3
904	14.61	13.74	+0.87	26	14	.....	1
911	14.40	13.83	+0.57	18	8	.....	3
912	15.17	15.24	−0.07	11	14	.....	2
913	15.55	14.83	+0.72	26	.....	1	2
914	15.47	14.65	+0.82	7	8	.....	2
923	15.42	14.64	+0.78	19	6	.....	2
929	15.77	15.08	+0.69	31	.....	1	1
930	15.52	14.75	+0.77	14	21	.....	2
931	15.52	14.86	+0.66	11	14	.....	1
933	15.23	15.26	−0.03	5	.....	10	1
934	15.31	14.64	+0.67	33	6	.....	2
938	13.89	12.78	+1.11	19	14	.....	3
940†	13.53	12.13:	+1.40	24	12	.....	3
945	15.53	14.77	+0.76	15	1	.....	2
947	15.23	14.55	+0.68	31	15	.....	2
952	15.47	14.54	+0.93	19	.....	4	2
957	15.48	14.75	+0.73	36	20	.....	2
965	15.57	14.81	+0.76	24	14	.....	2
967	14.23	13.25	+0.98	29	12	.....	3
973†	13.62	12.01:	+1.61	17	18	.....	3
985	15.12	14.38	+0.74	5	.....	2	2
1125	14.79	14.04	+0.75	24	10	.....	3
N 15	15.69	14.90	+0.79	10	25	.....	2
	B. Stars More than 2½′ and Less than 7′ from Center of Cluster						
L 4	15.68	14.88	+0.80	20	16	.....	2
12	15.76	15.01	+0.75	8	3	.....	2
13	15.66	14.83	+0.83	4	.....	4	2
16	15.43	14.68	+0.75	20	3	.....	2
17	15.21	15.17	+0.04	34	.....	2	2
18	14.75	13.82	+0.93	19	.....	1	3
20	15.62	14.80	+0.82	22	.....	5	2
26	14.65	13.66	+0.99	29	9	.....	3
29	15.41	14.55	+0.86	15	.....	8	2
31	15.60	14.79	+0.81	9	13	.....	2

TABLE 9—*Continued*

Star	Magnitude m_{pg}	Magnitude m_{pv}	Color c''	Proper Motion (Unit: 0".0001 p.a.) μ_x −	μ_y +	μ_y −	No. Pairs of Plates
	B. Stars More than 2½′ and Less than 7′ from from Center of Cluster—*Continued*						
L 32†	15.89:	15.10	+0.79	24	11	.....	2
34	15.76	14.99	+0.77	11	4	.....	2
38	15.56	14.78	+0.78	32	6	.....	2
42†	15.84:	15.05	+0.79	33	14	.....	2
43	14.71	13.81	+0.90	33	1	.....	3
44	15.19	15.10	+0.09	38	3	.....	2
49	15.14	15.18	−0.04	24	.....	6	2
50	15.01	15.10	−0.09	4	3	.....	2
56	15.83	15.05	+0.78	24	15	.....	2
58	15.68	14.90	+0.78	36	.....	2	2
66	14.79	14.28	+0.51	19	10	.....	3
67†	15.85:	15.11	+0.74	10	17	.....	2
70†	13.78	12.12:	+1.66	30	7	.....	3
72	13.58	12.31	+1.27	27	1	.....	3
77	14.02	12.78	+1.24	24	.....	2	3
78	15.25	14.44	+0.81	28	1	.....	3
79	15.13	14.27	+0.86	14	.....	9	3
80	15.70	14.92	+0.78	19	.....	1	2
81	14.98	14.07	+0.91	33	.....	4	3
93	15.62	14.91	+0.71	16	.....	6	2
96	13.69	12.43	+1.26	33	16	.....	3
102	15.66	14.82	+0.84	32	6	.....	2
109	14.21	13.38	+0.83	18	12	.....	3
110	15.43	14.54	+0.89	24	22	.....	2
114	14.48	13.54	+0.94	16	1	.....	3
115	15.58	14.80	+0.78	29	.....	6	2
117	14.98	14.15	+0.83	39	.....	2	3
124	15.55	14.78	+0.77	34	13	.....	2
129	15.48	14.91	+0.57	7	2	.....	2
130	15.50	14.74	+0.76	26	7	.....	2
137	15.45	14.62	+0.83	34	8	.....	2
139	14.70	14.09	+0.61	19	13	.....	3
141	15.11	15.14	−0.03	16	1	.....	2
144	14.89	14.37	+0.52	29	6	.....	2
146†	15.91:	15.12	+0.79	24	6	.....	2
158	13.89	12.69	+1.20	27	.....	11	3
162	15.02	14.18	+0.84	38	6	.....	3
165	14.96	14.04	+0.92	19	4	.....	3
168	14.55	13.74	+0.81	24	9	.....	3
169	14.01	12.80	+1.21	22	5	.....	3

TABLE 9—*Continued*

Star	Magnitude m_{pg}	Magnitude m_{pv}	Color c''	Proper Motion (Unit: 0".0001 p.a.) μ_x −	μ_y +	μ_y −	No. Pairs of Plates
	B. Stars More than 2½′ and Less than 7′ from Center of Cluster—*Continued*						
L 172	14.63	13.65	+0.98	20	11	.....	3
199	13.57	12.22	+1.35	21	7	.....	3
205	15.58	14.85	+0.73	21	4	.....	2
219	15.42	14.58	+0.84	18	.....	8	2
239	15.60	14.82	+0.78	38	.....	4	2
240	13.71	12.31	+1.40	29	.....	6	3
243	14.41	13.39	+1.02	13	14	.....	3
244	13.85	12.63	+1.22	29	10	.....	3
252	13.91	12.62	+1.29	32	8	.....	3
258	14.60	13.59	+1.01	23	.....	5	3
260	15.57	14.85	+0.72	24	8	.....	2
271	15.64	14.86	+0.78	20	9	.....	2
276	15.15	15.21	−0.06	21	13	.....	2
316	13.82	12.56	+1.26	22	6	.....	3
326	13.81	14.14	−0.33	39	22	.....	1
348	15.15	14.20	+0.95	13	.....	1	3
403	14.28	13.20	+1.08	30	9	.....	3
423	15.29	14.33	+0.96	24	6	.....	2
444	15.53	14.82	+0.71	18	.....	2	2
469	15.49	14.67	+0.82	21	10	.....	2
512	15.52	14.67	+0.85	19	2	.....	2
517	15.77	14.99	+0.78	22	8	.....	2
530	15.51	14.68	+0.83	14	0	.....	2
557	15.08	14.15	+0.93	27	5	.....	3
558†	15.30	14.37:	+0.93	36	.....	12	2
637	15.59	14.80	+0.79	20	6	.....	2
648	15.27	14.80	+0.47	24	.....	5	2
687	13.90	12.89	+1.01	19	17	.....	3
691	15.70	14.94	+0.76	12	21	.....	2
726	14.68	13.72	+0.96	20	14	.....	3
745	13.89	12.49	+1.40	27	3	.....	3
763	15.04	14.14	+0.90	36	8	.....	3
766	14.60	13.56	+1.04	25	12	.....	3
773	14.12	13.16	+0.96	21	16	.....	3
783	14.91	13.97	+0.94	15	16	.....	3
787	15.22	14.30	+0.92	24	15	.....	2
789	15.12	14.24	+0.88	16	1	.....	3
817	15.10	15.18	−0.08	8	.....	4	2
828	15.78	15.05	+0.73	28	2	.....	2
848	14.26	13.18	+1.08	14	12	.....	3

TABLE 9—*Continued*

Star	Magnitude m_{pg}	Magnitude m_{pv}	Color c''	Proper Motion (Unit: 0".0001 p.a.) μ_x −	μ_y +	μ_y −	No. Pairs of Plates
	B. Stars More than 2½′ and Less than 7′ from Center of Cluster—*Continued*						
L 867	15.58	14.84	+0.74	26	18	.....	2
869	15.54	14.68	+0.86	18	1	.....	2
871	14.89	13.95	+0.94	14	0	.....	3
877	14.15	13.08	+1.07	20	.....	3	3
883	15.50	14.76	+0.74	14	1	.....	2
919	14.11	13.01	+1.10	19	23	.....	3
920	14.58	13.84	+0.74	21	13	.....	3
921	14.43	13.45	+0.98	19	17	.....	3
932	14.79	14.13	+0.66	28	13	.....	3
943	15.28	14.49	+0.79	10	5	.....	2
946	14.97	14.41	+0.56	16	.....	2	3
948	14.11	13.20	+0.91	4	11	.....	3
954†	13.64	12.05:	+1.59	28	.....	5	3
955	14.84	13.98	+0.86	14	12	.....	3
961	14.30	13.46	+0.84	21	.....	1	3
972	15.10	15.03	+0.07	5	18	.....	1
980	15.41	14.68	+0.73	17	14	.....	2
984	14.60	13.91	+0.69	22	14	.....	3
993	14.03	14.37	−0.34	15	.....	4	2
998	15.78	15.09	+0.69	9	8	.....	2
1001	15.01	14.12	+0.89	13	17	.....	3
1005	15.57	14.90	+0.67	34	.....	4	2
1009	15.48	14.73	+0.75	10	.....	2	2
1011	15.59	14.78	+0.81	14	3	.....	2
1016	15.08	14.21	+0.87	16	13	.....	2
1018†	15.83:	15.08	+0.75	25	1	.....	1
1021	15.65	14.97	+0.68	32	8	.....	2
1023	14.16	13.07	+1.09	24	4	.....	3
1024	15.62	14.91	+0.71	26	5	.....	2
1027	14.81	14.33	+0.48	19	.....	7	3
1030	14.33	13.28	+1.05	8	15	.....	3
1032	14.79	13.93	+0.86	15	7	.....	3
1043	14.30	13.59	+0.71	16	2	.....	3
1048	15.17	14.30	+0.87	16	8	.....	3
1051	15.07	14.21	+0.86	11	19	.....	3
1057†	15.92:	15.17	+0.75	7	12	.....	1
1060	15.05	14.20	+0.85	6	17	.....	3
1062	15.43	14.61	+0.82	19	10	.....	2
1065	15.46	14.69	+0.77	33	.....	4	2
1067	14.87	14.86	+0.01	24	10	.....	2

TABLE 9—*Continued*

Star	Magnitude m_{pg}	Magnitude m_{pv}	Color c''	Proper Motion (Unit: 0".0001 p.a.) μ_x	μ_y +	μ_y −	No. Pairs of Plates
	B. Stars More than 2½′ and Less than 7′ from Center of Cluster—*Continued*						
L 1072	15.29	14.44	+0.85	18	26	.....	3
1073	13.93	12.83	+1.10	22	18	.....	3
1080	15.62	14.82	+0.80	32	.....	4	2
1081	15.72	15.04	+0.68	12	12	.....	2
1085†	15.88:	15.12	+0.76	29	.....	1	1
1091	15.62	14.84	+0.78	20	.....	2	2
1095	15.65	14.96	+0.69	22	13	.....	2
1096	15.27	14.46	+0.81	27	14	.....	2
1109	15.13	15.13	0.00	31	8	.....	2
1112	15.79	15.06	+0.73	20	6	.....	2
1116	15.68	14.87	+0.81	14	3	.....	2
1118	15.64	14.86	+0.78	20	6	.....	2
N 10	14.39	13.32	+1.07	30	1	.....	3
18	15.68	14.92	+0.76	33	18	.....	2
19†	15.82:	15.10	+0.72	16	23	.....	2
20	15.12	15.19	−0.07	4	26	.....	2
21	14.12	13.02	+1.10	7	21	.....	3

NOTES TO TABLE 9

L 206—Variable No. 8. Observed m_{pg} 14.65–15.5, m_{pv} 15.0–15.2.
L 306—Variable No. 2. Observed m_{pg} 13.0–13.8, m_{pv} 12.8–13.7.
L 324—Variable No. 11. No appreciable variation observed.
L 487—Variable No. 10. No appreciable variation observed.
L 872—Variable No. 6. Observed m_{pg} 14.2–14.9. No appreciable variation in m_{pv}.

to be omitted because of the difficulty of measuring their position or their brightness. Apart from stars omitted because of difficulties of this kind, the measures should be complete down to $m_{pv} = 15.0$, the limit set by the proper-motion plates. The upper limit for r will exclude a few members of the cluster, but it does include the majority of the cluster members in the magnitude range considered.

Table 10 lists the field stars, as found from their proper motions. There are fewer than for M15, because a smaller area was examined. The only star with a large proper motion is N 28. From its color, it would appear to be a late-type dwarf. The star N 8 must be either a high-velocity star or unusually faint for its color. If we neglect absorption and assume an absolute magnitude of +1.9, then the transverse velocity would be 340 km/sec and the star would be 2560 parsecs above the galactic plane. To give a transverse velocity of 20–30 km/sec, the absolute magnitude would have to be about +7.5.

Table 11 gives a number of stars which do not satisfy the criteria for inclusion in Table 9 but which may be members of the cluster. Indeed, in the majority of cases they probably are members of the cluster. They are divided into two groups, (*a*) those satisfying the position criterion ($r < 7'$), but with proper motion slightly outside the limits

defined by equation (4), and (*b*) those more than 7′ from the center of the cluster and with proper motions either inside the permissible limits or slightly outside them. One of these stars, L 344, must certainly be considered a cluster member, for it is a cluster-type variable (Barnard 1914; Sawyer 1942). It was listed in Table 11 rather than in Table 9 because the proper motion in declination was slightly too large. However, this measurement is based on one pair of plates only, and the discrepancy can be considered as due to accidental errors.

Table 12 gives an identification list of the stars which were not in Ludendorff's (1905)

TABLE 10

MAGNITUDES AND PROPER MOTIONS OF FIELD STARS

	Star	m_{pg}	m_{pv}	c''	Proper Motion (Unit: 0.001 p.a.)		No. Pairs of Plates
					μ_x	μ_y	
L	15.....	13.13	12.90	+0.23	−20	+ 16	3
	37.....	15.63	14.69	+0.94	−20	− 22	2
	97.....	15.57	14.98	+0.59	+ 5	+ 5	1
	379.....	15.31	14.59	+0.72	+ 1	− 35	3
	833.....	14.88	14.24	+0.64	− 9	− 20	3
	991.....	14.51	13.56	+0.95	− 6	− 5	3
	1019.....	13.13	12.72	+0.41	+ 8	− 16	3
	1087.....	13.31	12.84	+0.47	− 4	+ 11	3
N	1.....	12.9:	12.46	+0.4:	−14	+ 4	3
	4*.....	13.28	12.34	+0.94	0	− 5	2
	8.....	14.83	14.93	−0.10	− 3	− 18	2
	9.....	15.76	14.82	+0.94	+ 5	+ 9	2
	12.....	15.48	14.93	+0.55	− 2	− 8	2
	13*.....	12.99	11.78	+1.21	− 6	+ 1	3
	23.....	13.30	12.58	+0.72	−41	+ 38	2
	24.....	14.78	14.19	+0.59	− 9	− 11	1
	26.....	14.30	14.07	+0.23	+ 2	− 26	3
	28.....	14.68	12.99	+1.69	−20	−132	3
	30.....	15.13	14.68	+0.45	+ 2	− 2	2
	31*.....	12.11	11.30	+0.81	−21	0	1

* The magnitudes for these stars are from photoelectric observations.

catalogue. The co-ordinates given in Table 12 are on the same system as the co-ordinates used by Ludendorff (1905). They measure positions relative to an arbitrary origin near the center of the cluster (Ludendorff 1905).

V. COLOR-MAGNITUDE ARRAY

A color-magnitude diagram (Fig. 2) was plotted from the data in Table 9. In the preliminary work, separate diagrams were drawn for the stars in Table 9, A and B, but, as they showed similar characteristics, they were combined into one diagram. (The stars nearer the center seemed to be slightly bluer than the stars farther out, probably because of the brighter background, but the effect was small.) Figure 2 shows a red giant sequence which seems to have a sharper boundary on the red side than on the blue side. There is a certain amount of spread due to the errors of measurement, but it is evident that the distribution of colors for a given photovisual magnitude would be strongly asymmetrical. As in the corresponding diagram for M15, a few blue stars lie well to the left of the red sequence. At $m_{pv} = 15$, there is a group of blue stars with color index zero, similar to

TABLE 11

LIST OF STARS WHICH MAY BE MEMBERS OF CLUSTER

	Star*	Magnitude		Color c''	Proper Motion (Unit: 0".001 p.a.)		No. Pairs of Plates
		m_{pg}	m_{pv}		μ_x	μ_y	
a) L	6.....	15.12	15.04	+0.08	0	+1	2
	28.....	15.85:	15.09	+0.76	0	0	2
	74.....	15.24	15.30	−0.06	+2	+4	1
	91.....	15.61	14.76	+0.85	−2	−2	2
	94.....	15.02	15.09	−0.07	−2	−1	2
	95.....	15.58	14.85	+0.73	−2	+4	2
	134.....	15.80	15.05	+0.75	0	+1	2
	173.....	15.89:	15.16	+0.73	−6	+4	1
	203.....	15.76	15.05	+0.71	−4	+2	2
	286.....	15.22	15.29	−0.07	−4	−2	1
	307.....	15.24	14.34	+0.90	−2	−3	3
	325.....	15.64	14.97	+0.67	−5	+3	2
	327.....	14.63	13.85	+0.78	−4	−1	1
	330.....	15.61	14.85	+0.76	0	0	2
	344.....	.....	15.0	†	−2	+4	1
	354.....	15.08	14.98:	+0.10	0	+1	2
	395.....	15.78	15.06	+0.72	0	−2	2
	404.....	13.92	12.81	+1.11	0	+4	1
	499.....	15.21	14.61	+0.60	+1	−1	2
	549.....	13.59:	12.60	+0.99	−3	+4	1
	592.....	14.11:	13.13	+0.98	0	+2	1
	595.....	14.96	15.10	−0.14	0	+1	2
	596.....	15.84	15.14	+0.70	−3	−3	1
	619.....	15.85:	15.15	+0.70	−3	−2	1
	682.....	15.73	15.02	+0.71	−1	−2	2
	712.....	15.66:	15.10	+0.56	0	+3	1
	736.....	14.86	13.91	+0.95	−4	−2	1
	737.....	15.50	14.77	+0.73	0	0	2
	752.....	15.80	15.13	+0.67	−3	+3	1
	754.....	13.99:	12.87	+1.12	−5	+3	1
	777.....	14.00	12.87	+1.13	−2	−2	3
	780.....	13.23:	13.54	−0.31	−1	−1	1
	782.....	14.25	13.15	+1.10	−5	+2	1
	795.....	15.39	14.68	+0.71	0	+1	2
	800.....	14.76	13.87	+0.89	−4	+2	3
	858.....	14.74	13.82	+0.92	0	0	1
	886.....	15.71	14.97	+0.74	0	0	2
	928.....	15.20	15.23	−0.03	−1	+3	1
	987.....	15.19	15.16	+0.03	−2	−4	2
	1022.....	15.09	15.13	−0.04	0	+1	2
	1050.....	15.24	14.36	+0.88	0	+1	3
	1055.....	15.09	15.12	−0.03	0	+1	1
	1105.....	15.63	15.20	+0.43	0	+2	1
	1123.....	15.62	14.95	+0.67	+1	+2	1
N	14.....	15.85:	15.04	+0.81	+1	+1	2
	22.....	14.51	14.12	+0.39	−1	−2	3

* Stars following *a*) are stars within 7′ of center of cluster, whose proper motion is slightly outside the acceptable limits. Stars following *b*) are stars more than 7′ from center of cluster, with proper motion within or just outside acceptable limits.

† L 344 = Variable No. 7. Observed m_{pg} 15.0–15.3. No appreciable variation in m_{pv}.

TABLE 11—*Continued*

Star*	Magnitude m_{pg}	Magnitude m_{pv}	Color c''	Proper Motion (Unit: 0".001 p.a.) μ_x	Proper Motion (Unit: 0".001 p.a.) μ_y	No. Pairs of Plates
b) L 1.....	15.05	14.34:	+0.71	+3	+1	3
7.....	15.30	15.29	+0.01	−2	+2	1
8.....	15.85:	15.10	+0.75	−2	−1	2
22.....	15.70	14.91	+0.79	−3	+1	2
1053.....	15.03	15.12	−0.09	−1	0	1
1114.....	14.84	14.20	+0.64	−2	0	3
1115.....	15.9:	15.09	+0.8	−1	−2	1
N 3.....	15.33	14.28:	+1.05	−1	0	2
5.....	15.76:	14.98	+0.78	−2	+2	1
6.....	15.64	14.79	+0.85	−2	0	2
7.....	15.44	14.59	+0.85	−1	−1	2
11.....	14.78	14.28:	+0.50	−2	−1	3
16.....	15.69:	14.86	+0.83	−3	−1	2
25.....	15.68	14.88	+0.80	0	+1	2
27.....	15.04	14.31	+0.73	−1	+2	3

TABLE 12

LIST OF ADDITIONAL STARS

Star	Position $\Delta\alpha$	Position $\Delta\delta$	m_{pv}	Star	Position $\Delta\alpha$	Position $\Delta\delta$	m_{pv}
N 1.....	−12′ 6″	−4′ 50″	12.5	N 17.....	+ 5′ 17″	+8′ 55″*	11.8
2.....	−11 31	−8 20*	10.6	18.....	+ 8 8	+1 25	14.9
3.....	−11 7	−5 28	14.3	19.....	+ 8 20	+0 40	15.1
4.....	−10 9	−6 42	12.3	20.....	+ 8 35	−0 10	15.2
5.....	− 9 30	−1 31	15.0	21.....	+ 8 37	−0 10	13.0
6.....	− 8 51	+0 34	14.8	22.....	+ 8 42	−0 36	14.1
7.....	− 8 37	−2 25	14.6	23.....	+ 9 9	−7 56	12.6
8.....	− 8 34	+5 43	14.9	24.....	+ 9 33	+1 20	14.2
9.....	− 8 30	−3 13	14.8	25.....	+ 9 40	+2 19	14.9
10.....	− 8 29	+0 26	13.3	26.....	+10 11	+6 14	14.1
11.....	− 7 31	−6 12	14.3	27.....	+10 18	+5 56	14.3
12.....	− 6 26	−6 10	14.9	28.....	+10 30	−6 38	13.0
13.....	− 5 18	−6 34	11.8	29.....	+10 36	−7 15*	10.8
14.....	− 3 2	−6 1	15.0	30.....	+11 26	+6 35	14.7
15.....	− 0 16	−1 14	14.9	31.....	+13 6	+2 40	11.3
16.....	+ 4 11	−7 58	14.9				

* Declination rounded off to nearest 5″.

that shown in the color-magnitude diagram for M92 given by Arp, Baum, and Sandage (1952 and 1953). If we assume that the brightest stars of this group have an absolute magnitude $M_{pv} = 0$, then the distance modulus of the cluster is about 15.0–15.05, and the brightest stars in the cluster are at $M_{pv} = -3.0$. The brightest blue star is L 222 at $M_{pv} = -1.6$. The gap between the blue stars and the yellow stars at $M_{pv} = 0$ is clearly marked. For M92, Arp, Baum, and Sandage (1953) give the position of the left-hand edge of this gap as at $P - V = +0.12$, which agrees with the c'' value in the present data.

If taken literally, this would indicate zero reddening for M13, but there are several considerations which could alter this estimate. To summarize these: (1) no allowance has been made for errors in the c'' values; (2) the "normal color" for the edge of the gap is not necessarily the same for all globular clusters. We can subdivide effect 1 into two parts.

a) A systematic error such as that mentioned at the end of Section I would alter the result. (The approximate relation between c' and c'' given in the footnote leads to $c' = 0.16$ for $c'' = 0.12$ and hence to a color excess of 0.04 mag.)

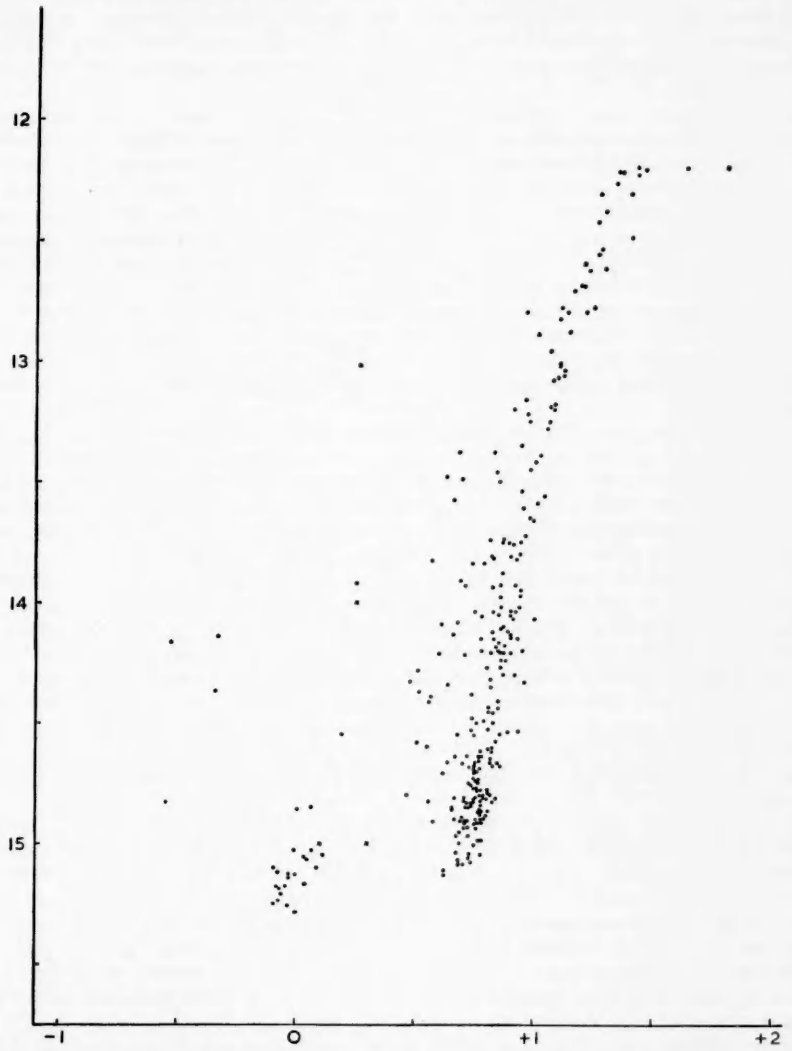

FIG. 2.—Color-magnitude diagram for cluster stars. (Apparent photovisual magnitude plotted against color index c'', from Table 9, *a* and *b*. The crosses correspond to variable stars. Distance modulus of cluster, $15^{m}0$.)

b) The mean-square error of a c'' value is 0.05–0.06 mag. As we are dealing with the extreme value of a frequency distribution, viz., the largest c'' for a group of stars of approximately the same intrinsic color, the fluctuations due to accidental errors could easily be of the order of 0.1 mag. (This effect would tend to exaggerate the observed color excess.)

As regards effect 2, Sandage (1953) gives $P - V = +0.05$ for the left-hand edge of the gap in the color-luminosity diagram for M3. The difference between this value and the value for M92 could easily arise from source 1*b*, but it could also represent, at least in part, an intrinsic difference between the clusters. As M13 resembles M92 rather than M3 in the number of variables, I have preferred the M92 value. However, it should be clear that there is no question here of evaluating the color excess to 0.01 mag. If taken at their face value, the data give zero reddening, but it could easily be as much as 0.1 mag.

As a comparison value, Stebbins and Whitford (1936) obtained a color excess $E = +0.08$ for M13, from photoelectric observations of the integrated light of the cluster. On the other hand, Baade[3] and Mayall (1946) both found that the number of extragalactic nebulae in the neighborhood of the cluster was normal. In obtaining their values of the color excess, Stebbins and Whitford (1936) assumed that all globular clusters have the same normal color, and, as a first approximation, this seems a reasonable assumption. However, it is evident from their results that the assumption is not strictly true. They call attention to two unusually blue clusters, and it seems probable that there will also be some clusters which are intrinsically redder than the average. Thus some of the clusters which they list as slightly reddened may be redder intrinsically rather than reddened by interstellar absorption. Another difficulty is to determine the "normal" color; Stebbins and Whitford (1936) appear to have done this from the results for two or three clusters.

The original program did not include a study of the variable stars in the cluster, and the observational material is obviously inadequate for this purpose. However, in view of the special place of the variable stars in any theory of evolution for stars in globular clusters, it seemed worth while to extract whatever information the observations gave and use it to indicate approximately where the variable stars fall in the color-luminosity diagram, especially as four of the variables observed are not RR Lyrae-type stars. As the color and luminosity of a variable star vary with phase, it would be best to follow each star through a complete cycle of its light-curve and plot the corresponding points. In default of such a series of observations, a representative point, such as the color and luminosity at median magnitude, would be a reasonable second-best.

The present material is not sufficient for even this modified degree of uniformity, so the observations for each star are discussed separately. The variables observed were Nos. 2, 6, 7, 8, 10, and 11 in Sawyer's (1940) list. (Notes on these stars are given at the end of Tables 9 and 11.) Sawyer (1942) gives some additional information about these stars in a later publication, and this proved of great value in co-ordinating the present observations.

Variables 10 and 11 are red stars which showed no appreciable variation. Sawyer (1942) mentions that they possibly belong to the bright irregular class and gives their photographic magnitude at minimum as 14.0 and 13.8, respectively. The observed photographic magnitudes and the absence of any variation suggest that the observations were made during a quiescent period at minimum light. In the color-magnitude diagram the point corresponding to variable 11 (L 324) falls at the top and slightly to the right of the red giant sequence, at $m_{pv} = 12.2$, $c'' = +1.8$, in a position reminiscent of that suggested by Baade (1951) for long-period Me variables of type II. As indicated earlier, the observations probably correspond to minimum light, and the color index would be smaller at median magnitude. Joy (1949) gives a range in spectral type from G2 to K0

[3] Quoted by Stebbins and Whitford 1936, Table 5.

for this star. An earlier observation by Popper (1947) gave the spectral type as K0 at maximum, with a color index of +1.8 at minimum.

Variable 10 (L 487) should be similar, for it has the same range in spectral type (Joy 1949) and almost the same range in magnitude (Sawyer 1940). However, the observed values, $m_{pv} = 12.6$ and $c'' = +1.2$, place it lower down on the red giant sequence. The readings on this star may be affected by its proximity to another bright star, L 470, which is bluish compared with the variable.

Variable 2 (L 306) has a period of 5 days, and the observations showed an appreciable variation in magnitude. Sawyer's (1942) values for the epoch and period were used to obtain the phase of the observations, and interpolation between the observed values gave $m_{pv} = 13.05$, $c'' = +0.25$, for the magnitude and color at median brightness. The corresponding point in Figure 2 is well to the left of the red giant sequence. Possibly it should be a little farther to the right in the diagram, though still distinct from the normal stars.

A similar procedure was used for variables 6 and 8. For variable 6 (L 872) the observations were inconveniently spaced for interpolation, and the results are rough. They gave $c'' = +0.25$, $m_{pv} = 14.0$ at median magnitude. This star has a period of 2 days and was observed spectroscopically by Joy (1949). His observations were made near median magnitude and gave a spectral type of F2–F5.

Variable 8 (L 206) is a cluster-type variable with a period of 0.75 day. It showed a pronounced variation, with values consistent with Sawyer's epoch and period. The color came out at $c'' = +0.3$ at median magnitude ($m_{pv} = 15.0$).

Variable 7 (L 344) is also a cluster-type variable, with a period less than $\frac{1}{2}$ day. Sawyer (1942) gives two possible periods which fitted her data. In the present work, the photovisual observations showed no appreciable change, while the photographic magnitudes ranged from 15.03 to 15.26. Averaging these values gave $c'' = +0.1$, with $m_{pv} = 15.0$, but it is uncertain what phase this corresponds to.

Comments on the observational technique involved in this work were included at the end of Paper I and can be omitted here. Similarly, Paper I includes a discussion of the effectiveness of the proper-motion criterion for separating foreground from cluster stars. One question that might be asked is whether the proper motions of the cluster stars could be used to look for systematic motions within the cluster, e.g., expansion or rotation of the cluster or motion of one group of stars relative to another. Some numerical work showed that such an investigation would be liable to give misleading results, for the results are strongly affected by any systematic errors in the proper motion. For example, a change of the order of 0".0005 p.a. in the mean motion of a group of stars could produce the appearance of a considerable rotational effect among the stars concerned.

I should like to acknowledge the co-operation of the staff of the Yerkes and McDonald Observatories, especially Dr. G. P. Kuiper and Dr. W. A. Hiltner, when I was engaged on the observational work for this paper. The work was carried out during my tenure of a Commonwealth Fund Fellowship at the University of Chicago. I should also like to thank Dr. R. v. d. R. Woolley for permission to work at the Mount Stromlo Observatory while preparing the data for publication.

REFERENCES

Arp, H. C., Baum, W. A., and Sandage, A. R. 1952, *A.J.*, **57**, 4–5.
———. 1953, *ibid.*, **58**, 4–10.
Baade, W. 1951, *Michigan Obs. Pub.*, **10**, 7–18.
Barnard, E. E. 1914, *Ap. J.*, **40**, 173–181.
Binnendijk, L. 1943, *B.A.N.*, **10**, No. 362, 9–18.
Brown, A. 1951, *Ap. J.*, **113**, 344–366.
Deutsch, A. N. 1947, *Puolkovo Bull.*, **17**, No. 3, 2–59.

Gamaley, N. V. 1948, *Poulkovo Bull.*, **17**, No. 6, 27–57.
Joy, Alfred H. 1949, *Ap. J.*, **110**, 105–116.
Ludendorff, H. 1905, *Potsdam Pub.*, **15**, No. 50, 1–56.
Maanen, Adriaan van. 1927, *Ap. J.*, **66**, 89–112.
Mayall, N. U. 1946, *Ap. J.*, **104**, 290–323.
Popper, D. 1947, *Ap. J.*, **105**, 204–211.
Rhijn, P. J. van, and Bok, B. J. 1931, *Groningen Pub.*, No. 45, pp. 1–24.
Sandage, A. R. 1953, *A.J.*, **58**, 61–75.
Sawyer, Helen B. 1940, *Pub. David Dunlap Obs.*, **1**, No. 5, 181–188.
———. 1942, *ibid.*, No. 11, pp. 231–239.
Shapley, H. 1915, *Mt. W. Contr.*, **6**, No. 116, 223–314.
Stebbins, J., and Whitford, A. E. 1936, *Ap. J.*, **84**, 132–157.

THE GLOBULAR CLUSTER, M13

H. C. ARP
Mount Wilson and Palomar Observatories
Carnegie Institution of Washington, California Institute of Technology
AND
H. L. JOHNSON
Lowell Observatory
Received January 31, 1955; revised February 28, 1955

ABSTRACT

A combination of photoelectric and photographic techniques has been used to obtain three-color photometric observations, on the U, B, V system, for the globular cluster M13 (NGC 6205). The ultraviolet excess, for the giant and subgiant stars, is about 0.05 mag. The blue horizontal sequence stars have considerable ultraviolet deficiency. The position and shape of the subgiant sequence in M13 differs significantly from that in M3.

I. INTRODUCTION

Three-color photometry on the Johnson-Morgan U, B, V system (Johnson and Morgan 1953) has been done on the globular cluster, M13 (NGC 6205). In order to make it possible to observe a relatively large number of stars, a combination of photoelectric and photographic methods was used. The photoelectric sequence given in Table 1 and Figure 4 was set up with the 82-inch telescope of the McDonald Observatory; the photographic observations were made with the 60-inch and 100-inch telescopes of the Mount Wilson Observatory.

II. THE OBSERVATIONS

The photoelectric observations were made in the same manner and with the same equipment as for Praesepe (Johnson 1952). They have been tied in to the U, B, V system with the estimated probable errors of zero points given in Table 1. The precision of the observations with respect to the two standard stars is similar to that for Praesepe down to $V = 15$, but becomes poorer below that point.

The photographic observations were made on 103*a*-O plates + UG2 filter in the ultraviolet, 103*a*-O plates + GG1 filter in the photographic, and 103*a*-D plates + GG11 filter in the photovisual wave lengths. These photographic measures were then transformed to magnitudes by the usual techniques of referring them to the photoelectric standards (Arp, Baum, and Sandage 1953). For U and V magnitudes the foregoing plate and filter combinations gave no detectable color equation. In photographic wave lengths, a 103*a*-O plate plus GG13 filter was also measured to check the empirically determined transformation from the m_{pg} system (with GG1 filter) to the B system (with GG13 filter) for these particular stars.

III. THE COLOR-MAGNITUDE AND TWO-COLOR INDEX DIAGRAMS

The observed color-magnitude diagram for M13 is shown in Figure 1, in which the usual globular-cluster giant, subgiant, and horizontal sequences are evident. The densities of points in the various regions of the diagram are not representative of the relative frequency of such stars in M13, especially below $V = 15.6$, where a much smaller sample of stars has been measured than for the brighter regions. The positions of the several sequences in M13 down to $V = 17.6$, however, are satisfactorily determined by our data.

TABLE 1

PHOTOELECTRIC STANDARDS

Star	V	$B-V$	$U-B$	n	Star	V	$B-V$	$U-B$	n
1.....	10.74	+0.57	+0.07	Std.	45.....	14.98	+0.76	+0.30	1
2.....	14.71	+0.85	+0.37	3	49.....	13.59	+0.99	+0.62	3
3.....	13.31	+1.06	+0.79	3	50.....	14.60	+0.88	+0.32	2
7.....	15.47	−0.04	−0.05	2	51.....	17.16	+0.60	+0.21	2
11.....	15.00	+0.17	+0.18	3	52.....	15.08	+0.10	+0.16	2
15.....	14.32	+0.68	+0.31	3	55.....	16.92	+0.66	0.00	1
21.....	16.10	+0.79	+0.22	1	56.....	10.87	+1.11	+1.12	Std.
24.....	15.30	+0.04	+0.10	3	59.....	12.03	+1.58	+1.81	2
34.....	14.82	+0.84	+0.15	2	62.....	15.49	+0.06	−0.10	1
37.....	14.52	+0.84	+0.40	1	62a.....	16.14	+0.87	+0.05	2
38.....	13.58	+1.01	+0.71	2	63.....	16.48	−0.19	−0.48	3
43.....	16.63	−0.16	−0.60	4	64.....	14.77	+0.85	+0.35	2
43a.....	15.41	+0.04	−0.01	2	81.....	15.39	−0.16	−0.50	1

PROBABLE ERRORS OF THE ZERO POINTS

	V	$B-V$	$U-B$
p.e. mag.....	±0.014	±0.007	±0.014

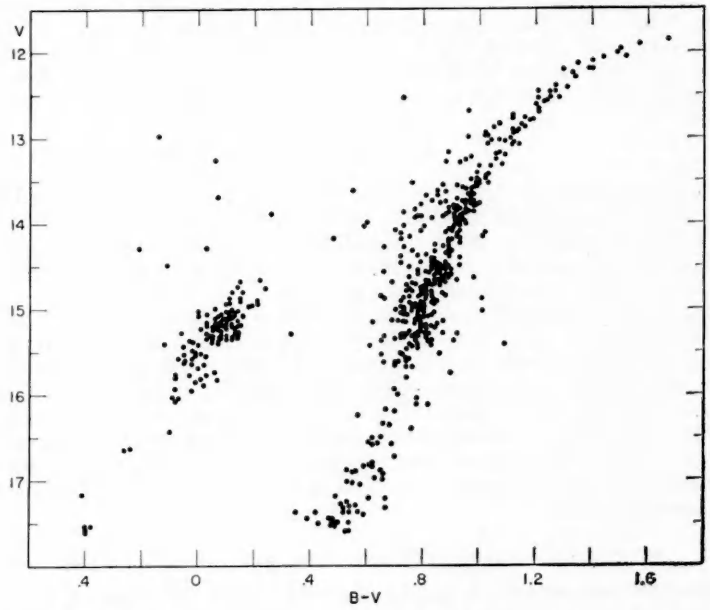

FIG. 1.—Two-color index diagram, $U - B$ versus $B - V$ for M13. Contains most of the stars plotted in Fig. 2. Solid line indicates relation for luminosity class V to $B - V = +1.0$ mag., luminosity class III redder than $B - V = +1.0$ mag., both with reddening of cluster. Star near main-sequence relation at $B - V = -0.14$ mag. is Barnard No. 29.

It should be noted that the horizontal sequence hardly exists to the red of the cluster-variable gap (it is, of course, well known that M13 has few RR Lyrae stars). Another part of the diagram that is of considerable interest is the extension of the horizontal branch to stars as blue as $B - V = -0.4$. These stars are the bluest that have yet been observed on the U, B, V system.

The two-color index diagram, $U - B$ versus $B - V$, is shown in Figure 2. The solid line represents, from $B - V = -0.2$ to $+1.0$, the standard relation determined from near-by bright stars of luminosity class V on the MK system and, from $B - V = +1.0$

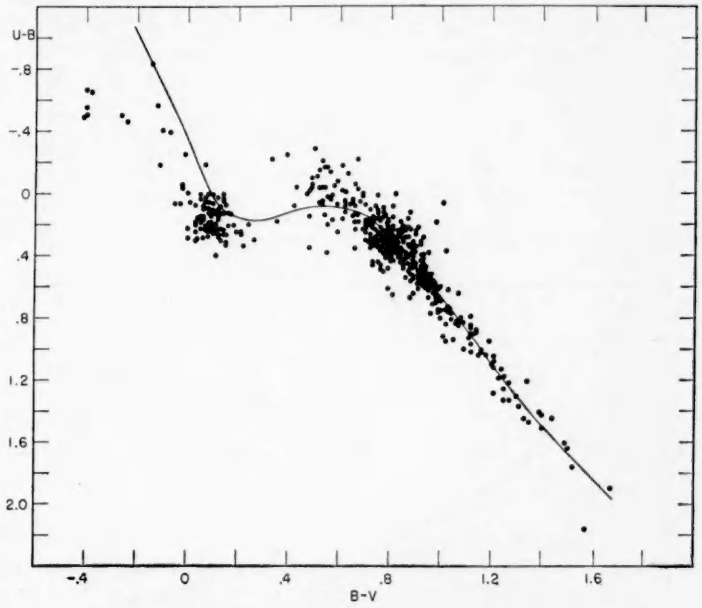

FIG. 2.—Color-magnitude diagram for M13. Sample from 100″ to 40″ (centered on cluster) to $V = 15.1$ mag. Plus sample from 300″ to 100″ to $V = 15.6$ mag. Below $V = 15.6$ stars are from area on west side of cluster, about 470″ from center.

on, the standard relation for stars of luminosity class III, both reddened by 0.12 mag. in $B - V$ and 0.09 mag. in $U - B$.

The cluster reddening has been determined in two ways: first, by comparison of two RR Lyrae variables in M13 with those of similar periods and light-curves in other globular clusters (Arp 1955), yielding $E_{(B-V)} = +0.13$ mag., and, second, by comparison of the two-color index diagram for M13 with that for near-by stars, yielding $E_{(B-V)} = +0.11$ mag. The procedure in the first method is obvious, but the second method requires more explanation.

Three-color photometry on two other globular clusters, M3 (Johnson and Sandage 1955) and NGC 4147 (Walker and Sandage 1954), has shown that the stars in some globular clusters have a considerable ultraviolet "excess" compared with stars in the solar neighborhood. For this reason we must be careful in determining the reddening of M13 from its two-color index diagram.

It is possible, however, to make a determination of the amount of ultraviolet excess in M13 by taking advantage of the fact that around $B - V = +0.6$ the slope of the

reddening line (Morgan, Harris, and Johnson 1953) is similar to the slope of the observed standard two-color index relationship for near-by stars. Therefore, the amount of ultraviolet excess found in the region of $B - V = +0.6$ will, for small amounts of reddening, be independent of the reddening. On this basis we find that, for stars for which $16 < V < 18$ and $+0.5 < B - V < +0.7$, the ultraviolet excess is 0.05 ± 0.025 (p.e.) mag. If we assume, on the basis of the M3 and NGC 4147 results, that the ultraviolet excess for giant stars is approximately the same as for the subgiants, we find that the reddening of M13 is $E_{(B-V)} = +0.11 \pm 0.04$ (p.e.) mag. We adopt the mean of our two determinations, $E_{(B-V)} = +0.12 \pm 0.03$ (p.e.) mag.

TABLE 2

MAGNITUDES AND COLORS OF THE FIVE BLUEST STARS

No.	V	$B-V$	$U-B$	No.	V	$B-V$	$U-B$
63	17.17	−0.41	−0.49	122	17.58	−0.40	−0.55
105*	17.54	− .38	− .65	127	17.60	−0.40	−0.50
110	17.54	−0.40	−0.66				

* One photoelectric measure gives $B-V=-0.42$, $U-B=-0.62$.

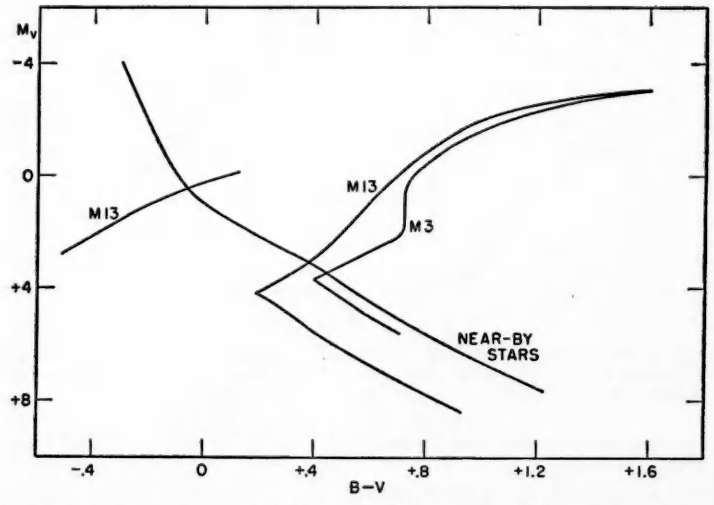

FIG. 3.—Color-luminosity diagram of M13 compared to that of M3 and near-by stars. The part of the M13 diagram below $M_v = +3$ is from data by Baum (1954).

One very interesting aspect of Figure 2 is the fact that the horizontal sequence stars bluer than $B - V = +0.2$ have very pronounced ultraviolet *deficiencies* compared with the near-by stars of population type I. Although there are possible systematic errors in the reductions for the bluest stars, this result seems to be fairly well established. The five bluest stars are listed in Table 2 and identified in Figure 4. Measures with both the GG1 and the GG13 filter gave accordant B magnitudes for these stars. In addition, No. 105 was sufficiently uncrowded to be measured photoelectrically on one night at the 100-inch telescope.

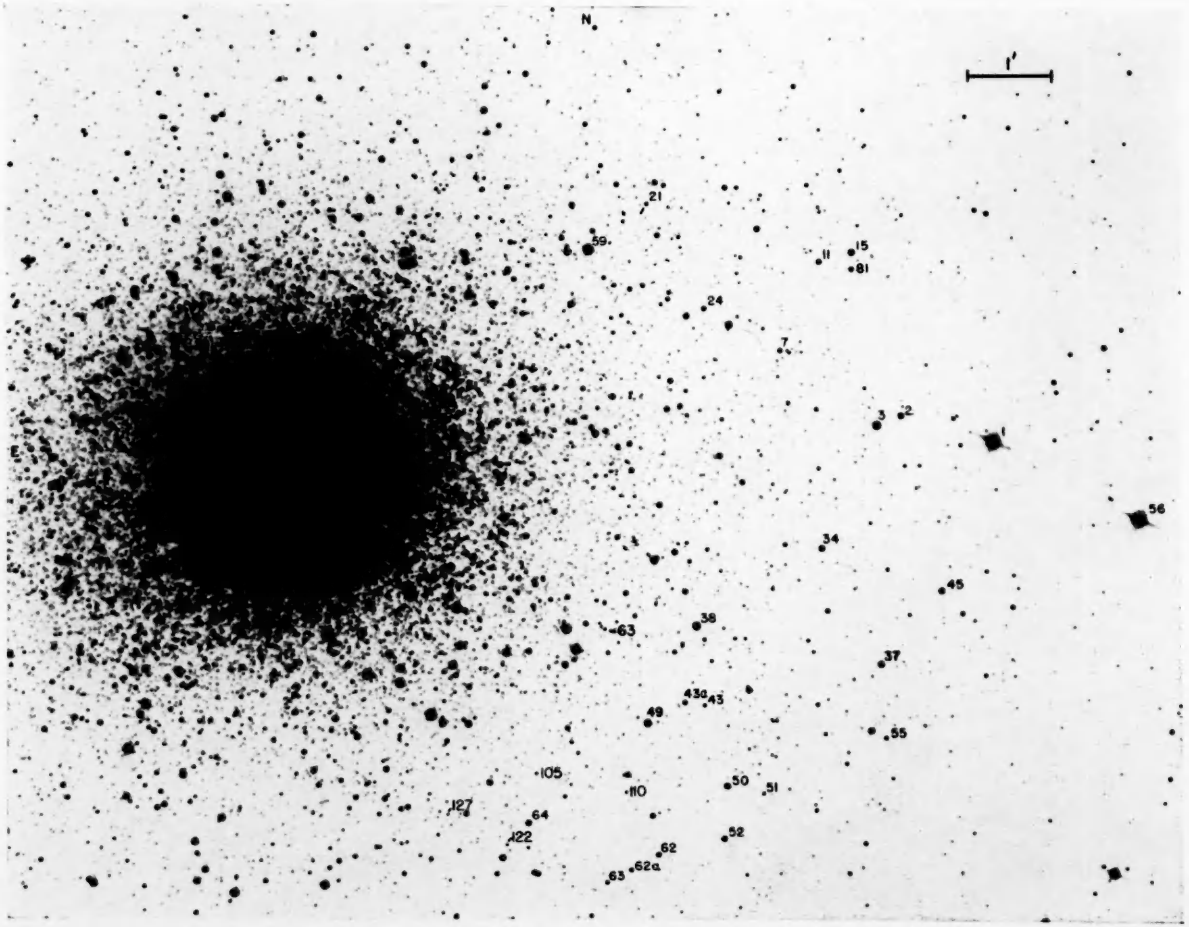

FIG. 4.—Photoelectrically measured stars in M13. Of the two stars designated No. 63, the lower one is listed in Table 1; the upper, in Table 2

There are no other stars known to have this characteristic; BD+28°4211, a subluminous O star (Greenstein 1952) which one might expect to be comparable with these stars in M13, has a normal ultraviolet intensity (BD+28°4211: $B - V = -0.34$; $U - B = -1.26$). In contrast, the bluest of the stars lying above the horizontal branch in Figure 1 is much stronger in the ultraviolet, having the same $U - B$ and $B - V$ as a main-sequence B2 V star. Greenstein and Münch identify this star, Barnard No. 29, as a cluster member from its radial velocity and classify it as having a B2 spectrum with strong, sharp helium lines. This would seem to point to the ultraviolet deficiency for the horizontal branch stars as a luminosity effect. In addition, if Barnard 29 is representative of the few other such stars found in almost every globular cluster recently investigated, the presence of such high-luminosity, main-sequence-like objects is puzzling on present ideas of evolution.

The ultraviolet excess found for M13, 0.05 mag., is considerably smaller than that for M3, ~0.25 mag., or that found by Miss Roman (1954) for high Z-velocity stars, 0.20 mag. As Miss Roman points out, this ultraviolet excess may be interpreted as a consequence of the weakened metallic lines in stars showing the excess. Further, we might interpret this weakness of metallic lines (and consequent ultraviolet excess) as a measure of the ratio of metals to hydrogen in the stellar atmospheres (Schwarzschild, Spitzer, and Wildt 1952). On this basis, the M13 subgiants and giants are more like the stars of population type I than are the stars of M3 or NGC 4147.

Figure 3 shows the color-luminosity diagram for M13, the near-by main sequence, and the main, subgiant, and giant sequences of M3 (Johnson and Sandage 1955). We make the conventional assumption that, for both M13 and M3, the cluster variables lie at $M_v = 0.0$. The lines for M13, $M_v < +3$, are drawn from the data of this paper; for $M_v > +3$, from data by Baum (1954). The very considerable dissimilarity between the sequences of the two globular clusters is evident. The difference in the main sequences has been pointed out by Baum; the differences in position and *shape* of the subgiant sequences are discussed here for the first time. In view of these discrepancies and the disparity in ultraviolet excess, it seems likely that the two clusters differ in a fundamental way. Also, of the seven globular clusters investigated to $M_v = +1$ (Arp 1955), M13 showed unique differences from the rest.

If in M13, as in M3, the ultraviolet excess for the main-sequence stars is approximately the same as for the subgiants, the M13 main sequence would correspond to near-by main-sequence stars in this respect. On the other hand, if the extrapolation of our magnitude scales in M13 is significant, an increasing ultraviolet excess toward the main sequence is indicated. Actual ultraviolet measures on main-sequence stars in M13 are needed to evaluate these possibilities.

It is interesting to note that the material that produces the reddening of M13 can be placed at some distance from the sun. One of the cluster standard stars, No. 56, falls in a region of the two-color index diagram, where it is possible under certain conditions to determine the reddening of individual stars. No. 56 falls right on the normal relation for unreddened stars, indicating that the star is not reddened. If No. 56 is a dwarf, its distance is about 60 parsecs, and the reddening material is at least this distance from the sun. Since the galactic latitude of M13 is +40°, it follows that the material producing the reddening of the cluster is at least 40 parsecs from the galactic plane.

IV. SUMMARY

A combination of photoelectric and photographic techniques has been used to obtain three-color photometric observations, on the U, B, V system, for the globular cluster M13. We find that, contrary to the results of three-color photometry on M3 and NGC 4147, the M13 stars do not have much ultraviolet excess compared with the near-by bright stars. Horizontal sequence stars bluer than $B - V = +0.2$ have a considerable

ultraviolet deficiency compared with O and B stars of population type I. On the other hand, there are some stars brighter than the horizontal branch, particularly Barnard No. 29, which is known to be a member of the cluster, which approach the intrinsic magnitudes and two-color indices of main-sequence stars. The position and shape of the subgiant sequence in M13 differ significantly from those found in M3. The disparities in the main sequences, the subgiant sequences, and the ultraviolet excesses suggest that the two globular clusters M3 and M13 differ fundamentally.

REFERENCES

Arp, H. C. 1955, *A.J.* (in press).
Arp, H. C., Baum, W. A., and Sandage, A. R. 1953, *A.J.*, **58**, 4.
Baum, W. A. 1954, *A.J.*, **59**, 422.
Greenstein, J. L. 1952, *Pub. A.S.P.*, **64**, 256.
Greenstein, J. L., and Münch, G. Unpublished results.
Johnson, H. L. 1952, *Ap. J.*, **116**, 640.
Johnson, H. L., and Morgan, W. W. 1953, *Ap. J.*, **117**, 313.
Johnson, H. L., and Sandage, A. R. 1955, unpublished results.
Morgan, W. W., Harris, D. L., and Johnson, H. L. 1953, *Ap. J.*, **118**, 92.
Roman, N. G. 1954, *A.J.*, **59**, 307.
Schwarzschild, M., Spitzer, L., and Wildt, R. 1952, *Ap.J.*, **114**, 398.
Walker, M., and Sandage, A. R. 1954, *A.J.*, **59**, 334.

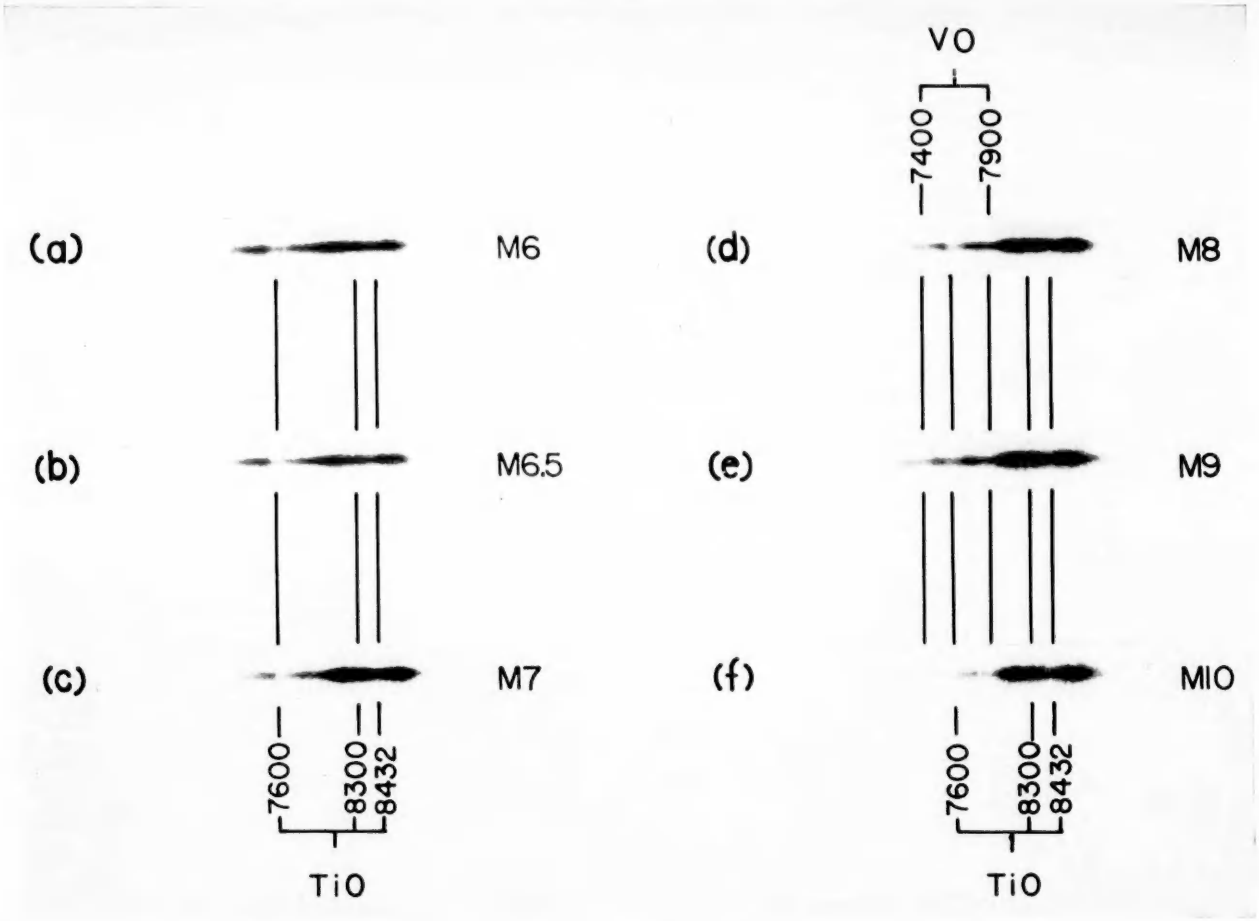

FIG. 1.—Late M-type spectra in the near infrared. *a*, Normal M6. *b*, M6.5; λ 8300 band appears as pinching of unwidened spectrum; no *VO* absorption. *c*, M7; *VO* absorption at λ 7400 and λ 7900 definitely present; *TiO* at λ 8300 increasingly strong. *d*, M8; all absorption features stronger. *e*, M9; strengthening absorption features produce fluted appearance shortward of λ 7900. *f*, M10; intense absorption shortward of λ 7900 produces appearance of a sharp break at λ 7900.

CLASSIFICATION OF LATE M-TYPE STARS FROM LOW-DISPERSION SPECTRA IN THE NEAR INFRARED

D. M. CAMERON AND J. J. NASSAU
Warner and Swasey Observatory, Case Institute of Technology
Received March 16, 1955

ABSTRACT

A system of classification of late M-type stars (M6–M10) from objective-prism spectra in the near infrared (λ 6800 to λ 8800) is proposed. It is based principally on strengthening *VO* absorption, starting at M7 in the λ 7400 and λ 7900 regions, and on the *TiO* absorption in the λ 8300 region, starting at M6.5. This system is a result of the study of the spectral variations of M-type variables in the near infrared, in which the spectral changes were correlated with the light-variations. Experience has shown that it is possible, by this means, to classify the great majority of the late M-type spectra observed. One interesting type of spectrum which does not fit into this system of classification is described in some detail.

The classification of M-type stars from infrared plates taken with the Burrell-Schmidt telescope at the Warner and Swasey Observatory, using the 2° or 4° objective prism is based on Mount Wilson (Adams *et al.* 1926) standards. These standards have proved satisfactory for the classification of stars from M0 through M6, utilizing the strengths of the *TiO* bands at λ 7054, λ 7589, and λ 8432 as criteria. However, the classification of the late M stars, from M7 and later, has been unsatisfactory for several reasons. First, nonvariable standards are not available for these very late-type stars, and the variables do not repeat exactly from cycle to cycle. Second, the principal *TiO* bands appear to be approaching their maximum strength and are no longer very useful as criteria for classification in this region. Third, the situation is further complicated by the appearance and rapid strengthening of other bands. These bands are the vanadium oxide bands at λ 7400 and λ 7900 and the double *TiO* band at about λ 8300. The present paper deals with the utilization of these bands for the classification of late M-type stars beginning with M6 and is a continuation of a previous investigation carried out by Nassau and Cameron (1954).

For the reasons given, no attempt is made to use standards later than M6 but rather to establish criteria for the classification of the late types, utilizing a well-defined sequence of spectral changes observed in M-type variables. The observational material for this is based on the examination of the spectra of 52 well-known red variables, taken over a period of about two years. It includes 26 Mira-type, 5 long-period, 11 irregular, and 10 semiregular variables. In all, some 140 spectra were examined for this purpose.

The basic sequence of spectral changes followed by M variables later than M6 has been given in a previous paper (Nassau and Cameron 1954), in which the arbitrary designation of types later than M6 is given by *b*, *c*, and *d*. These types were based upon strengthening *VO* absorption at λ 7400 and λ 7900. The *TiO* bands at λ 8300 were not utilized in the classification. However, these bands appear strong in the very late M-type stars (e.g., χ Cygni) when this spectral region is correctly exposed. In normally exposed spectra of late M stars, this region is usually overexposed, but the presence of the bands is easily detected by a "pinching" or narrowing of the unwidened spectrum at this wave length. A trace of this pinching effect is first noticed in some cases at M6 (Fig. 1, *a*). The pinching effect increases and becomes quite distinct (Fig. 1, *b*) *before* the first *VO* absorption appears at λ 7400 and λ 7900 (Fig. 1, *c*). Keenan and Schroeder (1952) call attention to the fact that *VO* bands appear to be present in the infrared in all M-type stars M7 and later.

The description of the criteria for the classification of the late M-type stars follows:

M6.—The *TiO* at the A band has reached its maximum strength. The λ 8432 band is moderately strong. In some cases the λ 8300 region shows a slight "pinching" in normally exposed spectra.

M6.5.—The λ 8432 band is quite strong, and the "pinching" at λ 8300 is quite distinct. Sometimes a trace of *VO* at λ 7400 or λ 7900 or both is evident.

M7.—The *VO* absorption at λ 7900 is moderately strong, and that at λ 7400 may or may not be apparent. The "pinching" at λ 8300 is increasingly distinct.

M8.—The *VO* absorption at λ 7900 and λ 7400 and the *TiO* absorption at λ 8300 are progressively stronger.

M9.—The *VO* absorption at λ 7400 and λ 7900 has increased in strength and is comparable to the *TiO* absorption at λ 7600, giving a fluted appearance to the spectrum shortward of λ 7900. The "pinching" at λ 8300 has strengthened and sometimes appears as two distinct absorption bands if this region of the spectrum is not too much overexposed.

M10.—The absorption shortward of λ 7900 has greatly increased, producing the effect of a sharp break at λ 7900. The fluted appearance shortward of λ 7900 is apparent only in greatly overexposed spectra.

Figure 1 shows representative examples of these types. In order to indicate the structure of the absorption shortward of λ 7900, the spectra selected are greatly overexposed in the λ 8300 region for the latest types (M9 and M10). Thus the λ 8300 bands do not appear to increase in strength in the M9 and M10 examples, as they would if this region were not so greatly overexposed. For an example of this see the spectrum of χ Cygni in five exposures in the previous paper (Nassau and Cameron 1954, Fig. 3).

Types M8, M9, and M10 are identical with types *b*, *c*, and *d* in the previous paper. It should be emphasized here that the symbols M8, M9, and M10 are not based on any standards. However, they do represent a sequence of advancing types, and experience has shown that the criteria listed are sufficiently sensitive to differentiate between integral subtypes.

These classifications, which were derived from the study of the progressive strengthening of the molecular bands, are well correlated with the change in light of the M variables. This may be illustrated by the following cases.

In 1953 the spectral changes of R Bootis were followed from 18 days after maximum to 66 days after maximum. The sequence of spectral changes, which was M5, M6, M6.5, and M7, shows clearly the appearance of the "pinching" effect in the λ 8300 region at M6.5 before any *VO* absorption had appeared. In both 1953 and 1954 a series of spectra of χ Cygni was obtained covering the period from about 120 days after maximum to about 15 days after minimum. The spectral changes were M7, M7, M9, M10. Many other stars for which only scattered spectral observations are available are in general agreement, in the sense that the stars near maximum have the earlier spectra, while those near minimum have the latest spectra. This is illustrated by Table 1, which contains representative stars for each of the spectral subclasses from M5 to M10. The table contains a few nonvariables from the Mount Wilson (Adams *et al.* 1926) list as examples of M5 and M6. From M7 through M10 the stars are nearly all Mira-type variables.

The spectral distribution of the 140 spectra of M variables utilized in the present study shows that, of the 23 semiregular variables, 15 are M6 or M6.5. Of the 15 irregular variables, 11 are M6 or M6.5. It is particularly noteworthy that only 3 were later than M6.5. In other words, very few of the irregular or semiregular variables showed appreciable *VO* absorption. The concentration of the irregular and semiregular variables around M6 is, of course, well known (Joy 1942).

It will be noted that for the late M stars the exclusive use of the *TiO* absorption has been abandoned as a basis for classification and the *VO* absorption is included. In addition, it is believed this system of classification represents a temperature sequence.

TABLE 1*

SPECTRAL CLASSIFICATION OF LATE M-TYPE STARS

Star	2	3	4	5	6	7
BD+27°887	M5	M5	.....	1-29-48	.....	.....
BD+66°878	M5	M5	.....	3-25-48	.....	.....
40 Com	M5	M5	.....	4-4-48	.....	.....
BD+8°2532	M6	M6	.....	3-26-48	.....	.....
V483 Aql	M6	.....	I	7-20-54	.....	.....
B0 Aur	M6	.....	SR	11-16-54	.....	.....
AF Cyg†	M6	M6	SR	7-22-54	.....	.....
AF Cyg†	M6	M6	SR	9-2-54	.....	.....
AI Cyg	M6	M5	I	7-22-54	.....	.....
PR Cyg	M6	M4	I	9-1-54	.....	.....
V417 Cyg	M6	.....	I	9-1-54	.....	.....
WY Oph	M6	M5	I	7-20-54	.....	.....
V670 Oph	M6	.....	I	7-20-54	.....	.....
U Per†	M6	M6e	M	1-9-55	0.02	0.57
W Tau	M6	M5	SR	1-12-55	.....	.....
UX And	M6.5	M6	SR	8-29-54	.....	.....
UX And	M6.5	M6	SR	11-1-54	.....	.....
UX And	M6.5	M6	SR	1-12-55	.....	.....
R Aqr†	M6.5	M7e	M	10-24-54	.90	.52
T Ari†	M6.5	M7e	LP	8-29-54	.26	.56
T Ari†	M6.5	M7e	LP	11-1-54	.46	.56
RY Ari	M6.5	M6	I	8-29-54	.....	.....
RY Ari	M6.5	M6	I	10-24-54	.....	.....
RY Ari	M6.5	M6	I	1-21-55	.....	.....
RR Cam	M6.5	M6	SR	2-3-55	.....	.....
GS Cas	M6.5	.....	I	8-29-54	.....	.....
GS Cas	M6.5	.....	I	11-1-54	.....	.....
SV Cas	M6.5	M5	LP	9-5-54	.29	.57
VY Cas	M6.5	M6	SR	8-29-54	.....	.....
TZ Cyg	M6.5	M7	I	8-20-53	.....	.....
W Cyg†	M6.5	M4e	SR	7-22-54	.....	.....
AI Cyg	M6.5	M5	I	9-5-54	.....	.....
V405 Cyg	M6.5	M6	I	10-24-54	.....	.....
V485 Cyg	M6.5	M7	I	10-24-54	.....	.....
BD Peg	M6.5	M6	I	9-5-54	.....	.....
TT Peg†	M6.5	M6e	LP	9-5-54	.0:	.5:
T Sge	M6.5	M4	I	8-20-53	.....	.....
W Tau	M6.5	M5	SR	11-1-54	.....	.....
T Ari†	M7	M7e	LP	1-12-55	.69	.56
T Cas†	M7	M8e	M	1-9-55	.82	.45
T Cep†	M7	M7e	M	9-5-54	.00	.47
T Cep†	M7	M7e	M	10-24-54	.13	.47
o Ceti†	M7	M6e	M	9-1-54	.53	.64
BG Cyg†	M7	M8e	LP	7-22-54	.08	.49
BG Cyg†	M7	M8e	LP	9-2-54	.23	.49
TW Cyg†	M7	M10e	M	9-5-54	.67	.55
U Per†	M7	M6e	M	8-29-54	.60	.57
U Per†	M7	M6e	M	10-24-54	.77	.57
R Leo†	M7	M8e	M	2-25-55	0.00	0.56

* Column 1 gives the name of the star. Column 2 gives the Case spectral class, based on the criteria given above. Column 3 contains the spectral class given in the *General Catalogue of Variable Stars* (Kukarkin and Parenago 1948). Column 4 gives the type of variability taken from the same catalogue. Column 5 gives the date on which the spectrum given in col. 2 was taken. Column 6 gives the fraction of a period after maximum on this date, calculated from the elements given in the *General Catalogue of Variable Stars*. Column 7 gives the fraction of a period from maximum to minimum, derived from the same catalogue.

† These stars are listed in the Bidelman (1954) *Catalogue and Bibliography of Emission-Line Stars of Types Later than B.*

TABLE 1—*Continued*

Star	2	3	4	5	6	7
R Aqr†	M8	M7e	M	8-29-54	0.76	0.52
X Cam†	M8	M3e	M	1-21-55	.58	.52
T Cas†	M8	M8e	M	10-24-54	.64	.45
BG Cyg†	M8	M8e	LP	10-24-54	.40	.49
χ Cyg†	M8	Mpe	M	6-19-54	.30	.58
χ Cyg†	M8	Mpe	M	7-22-54	.38	.58
R‡ L Mi†	M8	M8e	M	2-25-55	.22	.59
W And†	M9	M8e	M	8-29-54	.35	.58
W And†	M9	M8e	M	9-5-54	.37	.58
W And†	M9	M8e	M	10-24-54	.49	.58
T Cas†	M9	M8e	M	8-29-54	.52	.45
o Cet†	M9	M6e	M	11-1-54	.72	.64
χ Cyg†	M9	Mpe	M	9-2-54	.48	.58
R Tau†	M9	M5e	M	1-21-55	.53	.59
S Tau†	M9	M7e	M	11-1-54	.64	.57
U Aur†	M9	M7e	M	2-24-55	.50	.63
W And†	M10	M8e	M	1-21-55	.72	.58
R Aur†	M10	M7e	M	2-3-55	.44	.48
χ Cyg†	M10	Mpe	M	8-20-53	.56	.58
χ Cyg†	M10	Mpe	M	9-8-53	.58	.58
χ Cyg†	M10	Mpe	M	10-24-54	.61	.58
S§ Ori†	M10	M7e	M	2-3-55	0.53	0.48

‡ Merrill (1952) states that the absorption spectrum of this star is one of the most advanced M-type spectra yet observed."

§ The figure given in col. 6 for this star was computed from elements given in "Variable Star Notes" (Mayall 1954), because the period of this star varies so widely from cycle to cycle.

In the course of the Case infrared surveys many thousand spectra have been examined and classified, using the criteria given here. These have proved to be satisfactory for the classification of the greatest majority of the late M stars on a one-dimensional system. However, a few stars present anomalies. One such anomaly, which has been observed in several well-known red variables, deserves description here.

The over-all appearance of the spectrum is that of a very late M—about M9. The spectrum shortward of λ 7900 has the fluted appearance and is much weaker than longward, and there is a fairly sharp break at λ 7900. The λ 7400 and λ 7900 absorption bands are strong, and the absorption at the A band, while intense, is narrow for so late a type. No noticeable absorption appears at λ 8300, and the λ 8432 band is not as strong as should be expected for a very late M. It is suggested that the *TiO* absorption may be weakening and that this may represent the most advanced type of spectrum yet observed. Another possible explanation is difference in abundance.

This anomalous appearance has been observed in three spectra of W Hya taken in May and June, 1953. It is of interest to note here that Merrill (1930) has found peculiarities in the spectrum of W Hya. Also the star has been observed to have a gradually decreasing period (see Prager 1936), and the same in one spectrum of TW Cygni taken in July, 1954, near minimum. Another spectrum of TW Cygni taken in September, 1954, about 45 days after minimum does not show the anomalous appearance. It appears to be about M7, with an unusually strong λ 8300 band. A third star, not a known variable, showed the anomalous appearance on a plate taken on August 7, 1950. The 1855 co-ordinates of the star are R.A. = $18^h03^m.5$; dec. = $-18°.9$.

There are some indications that a two-dimensional system of spectral classification may be needed, where either abundance or luminosity is the second dimension. Slit spectra

and additional knowledge of the molecular bands involved should help to clarify the situation.

REFERENCES

Adams, W. S., Joy, A. H., and Humason, M. L. 1926, *Ap. J.*, **64**, 225.
Bidelman, W. P. 1954, *Ap. J., Supplement Series*, **1**, 175.
Joy, A. H. 1942, *Ap. J.*, **96**, 344.
Keenan, P. C., and Schroeder, L. W. 1952. *Ap.J.*, **115**, 82.
Kukarkin, B. V., and Parenago, P. P. 1948, *General Catalogue of Variable Stars* (Moscow: Academy of Sciences of the U.S.S.R.).
Mayall, M. W. 1954, *J.R.A.S. Canada*, **48**, 201.
Merrill, P. W. 1952, *Ap. J.*, **116**, 344.
Merrill, P. W., and Burwell, C. G. 1930, *Ap. J.*, **71**, 285.
Nassau, J. J., and Cameron, D. M. 1954, *Ap. J.*, **119**, 175.
Prager, R. 1936, *Geschichte und Literatur des Lichtwechsels der veränderlichen Sterne*, Vol. **2**.

MAGNITUDES AND COLORS OF BRIGHT F STARS*

PETER NAUR
McDonald Observatory
Received January 18, 1955

ABSTRACT

Three-color photoelectric observations on the (U, B, V) system have been made for 103 bright stars, mostly of spectral type F.

The magnitudes and colors given in the present paper were derived from measures made on 12 nights during February and March, 1953, with the aid of the 13-inch reflector of the McDonald Observatory. The photometer is of the type described by Johnson and Morgan (1951). The sensitivity settings of the amplifier were calibrated during the period of observation. The result of this calibration was quite close to others found earlier for the same amplifier. For each star ten deflections were generally taken, in the following order. Star: blue, yellow, ultraviolet. Sky: blue, yellow, ultraviolet. Star: ultraviolet, yellow, blue. Standard source.

TABLE 1

PROBABLE ERRORS OF THE PHOTOMETRY

	V	$B-V$	$U-B$
Single observation, at zenith....	$\pm 0^m.010$	$\pm 0^m.006$	$\pm 0^m.009$
Results given in Table 2.....	$\pm 0.0016\epsilon$	$\pm 0.0010\epsilon$	$\pm 0.0015\epsilon$

For the purpose of determining the extinction, selected standard stars were observed at both low and high altitudes. In addition, other standards of the (U, B, V) system were regularly observed. The average number of observations of extinction stars on one night was 8.9, while, on the average, 8.7 observations of standard stars were available. These latter refer to a selection of 24 stars from the list of Johnson and Harris (1954) and 15 from that of Johnson and Morgan (1953). The reduction for extinction and the transfer to the (U, B, V) system were carried out in a manner similar to that of Johnson and Morgan (1951). The final results are given in Table 2.

An estimate of the accuracy of the results was formed from the accordance of the single observations which had been made of the same star on different nights. Also, following Johnson and Morgan (1953), an estimate of the accuracy of the results given for each star has been expressed in terms of a factor $\epsilon = 6\,\overline{\sec z}\,n^{-1/2}$, $\overline{\sec z}$ being the mean of the values of the secants of the zenith distance and n the number of observations. The resulting probable errors are given in Table 1.

The eight columns of Table 2 give the following data: (1) the number of the star in the *Catalogue of Bright Stars* by Schlesinger and Jenkins; (2) and (3) the position, referred to the equinox of 1900.0; (4) the number of observations; (5) ϵ as defined above; and (6), (7), and (8) the magnitude and colors on the (U, B, V) system. The observations were made with the purpose of furnishing a color calibration of the narrow-band photometry which was performed during the same period of time by Dr. B. Strömgren, using the 82-inch reflector.

I am indebted to Dr. Strömgren for suggesting this program to me and to Dr. H. L. Johnson and Dr. D. L. Harris III for much helpful guidance and advice and for providing data on the standard stars in advance of publication.

* *Contributions from the McDonald Observatory, University of Texas*, No. 257.

TABLE 2

PHOTOMETRIC OBSERVATIONS

Star No.	(1900.0)		n	e	V	$B-V$	$U-B$
	α	δ					
BS							
740	$2^h27^m21^s$	−15j41′	1	11	4^m77	$+0^m46$	-0^m03
781	2 34 44	−12 18	1	10	4.86	+ .45	− .01
915	2 57 33	+53 7	1	8	2.91	+ .72	+ .44
937	3 1 51	+49 14	1	7	4.04	+ .61	+ .12
961	3 7 37	+77 22	1	9	5.45	+ .19	+ .11
1069	3 25 30	+45 43	2	5	5.30	+ .39	− .02
1129	3 37 17	+63 2	1	8	4.79	+ .80	+ .26
1135	3 38 24	+42 16	1	7	3.78	+ .42	+ .26
1210	3 49 10	+50 24	1	6	5.28	+ .41	.00
1412	4 22 57	+15 39	2	6	3.42	+ .17	+ .14
1430	4 25 0	+13 30	1	6	5.43	+ .26	+ .11
1547	4 45 31	+18 40	1	6	5.13	+ .21	+ .12
1560	4 47 59	− 5 37	1	8	4.39	+ .25	+ .18
1611	4 55 17	−12 41	1	8	4.78	+ .25	+ .18
1664	5 2 26	+ 8 22	1	7	5.34	+ .32	+ .11
1673	5 3 46	− 4 35	1	8	5.12	+ .44	− .03
1676	5 3 58	+15 28	1	6	4.83	+ .30	+ .19
1746	5 13 58	+ 2 30	1	7	5.34	+ .40	.....
1901	5 30 44	− 4 55	2	5	5.27	+ .23	+ .17
1935	5 33 50	−28 45	2	8	5.31	+ .46	+ .10
1983	5 40 18	−22 29	2	7	3.63	+ .47	+ .02
2047	5 48 28	+20 15	3	3	4.41	+ .59	+ .07
2085	5 51 51	−14 11	2	6	3.74	+ .32	+ .01
2220	6 8 58	+19 11	3	3	5.20	+ .44	.00
2241	6 10 50	+12 18	3	4	5.04	+ .42	− .02
2264	6 13 39	+53 30	4	4	5.36	+ .43	+ .12
2484	6 39 41	+13 0	2	5	3.38	+ .44	+ .06
2607	6 53 26	−24 30	2	5	5.46	+ .36	+ .03
2693	7 4 20	−26 14	2	8	1.86	+ .65	+ .57
2707	7 6 17	− 0 8	3	4	5.46	+ .29	+ .14
2777	7 14 9	+22 10	3	3	3.52	+ .34	+ .03
2849	7 22 21	+49 53	4	3	5.36	+ .45	− .06
2906	7 29 46	−22 5	4	5	4.44	+ .52	+ .06
2909–10	7 30 5	−23 15	1	10	5.09	+ .43	+ .03
2927	7 32 18	− 3 53	4	4	5.12	+ .44	+ .12
2930	7 32 38	+34 49	3	4	4.90	+ .41	+ .09
3015	7 41 1	−14 19	4	4	5.04	+ .33	+ .09
3102	7 52 34	−22 37	4	5	4.20	+ .72	+ .44
3262	8 13 59	+27 32	3	4	5.14	+ .47	− .05
3323	8 21 58	+61 3	1	7	3.34	+ .84	+ .51
3482	8 41 29	+ 6 47	3	4	3.36	+ .68	+ .34
3619	9 1 49	+52 0	3	4	4.47	+ .27	+ .11
3624	9 2 41	+63 55	4	4	4.66	+ .35	+ .14
3757	9 23 39	+63 30	2	5	3.66	+ .33	+ .10
3759	9 24 4	− 2 20	3	4	4.60	+ .45	.00
3775	9 26 10	+52 8	3	4	3.17	+ .46	.00
3852	9 35 49	+10 21	2	5	3.52	+ .48	+ .20
3871	9 39 45	−27 19	2	8	4.79	+ .49	+ .38
3873	9 40 11	+24 14	1	6	2.96	+ .81	+ .44
3888	9 43 53	+59 31	4	4	3.79	+0.29	+0.09

REFERENCES

Johnson, H. L., and Harris, D. L. 1954, *Ap. J.*, **120**, 196.
Johnson, H. L., and Morgan, W. W. 1951, *Ap. J.*, **114**, 522.
———. 1953, *ibid.*, **117**, 313.

TABLE 2—*Continued*

Star No.	(1900.0) α	(1900.0) δ	n	e	V	B−V	U−B
BS							
3928	9h51m34s	+41°32′	4	3	5m14	+0m46	0m00
3991	10 5 13	−12 19	3	5	5.31	+ .36	.00
3992	10 5 13	−35 22	1	15	6.12	+ .58	+ .16
4031	10 11 8	+23 55	1	7	3.44	+ .29	+ .21
4042	10 12 40	− 7 34	1	8	5.24	+ .29	+ .15
4054	10 14 18	+19 59	3	4	4.80	+ .46	+ .01
4084	10 18 55	+83 4	3	6	5.26	+ .37	− .05
4090	10 20 11	+34 18	2	5	4.74	+ .25	+ .17
4098	10 21 54	+49 19	2	5	6.48	+ .61	+ .04
4141	10 28 43	+57 36	3	4	5.15	+ .33	− .02
4191	10 37 40	+46 44	1	6	5.18	+ .33	+ .01
4251	10 48 36	−19 36	1	10	5.25	+ .46	+ .06
4277	10 53 52	+40 58	2	5	5.06	+ .60	+ .12
4288	10 55 14	+39 45	3	4	5.08	+ .24	+ .17
4310	10 59 52	+ 7 53	3	4	4.64	+ .33	+ .07
4314	11 0 31	−26 45	1	8	4.94	+ .35	+ .04
4395	11 18 24	−18 14	1	8	5.09	+ .42	− .06
4399	11 18 43	+11 5	4	3	3.94	+ .40	+ .07
4439	11 26 41	+61 38	5	3	5.48	+ .50	− .01
4525	11 42 16	−29 43	2	8	6.48	+ .68	+ .24
4527	11 42 50	+20 46	3	3	4.56	+ .53	+ .28
4587	11 55 36	− 9 53	2	6	5.54	+ .76	+ .43
4623	12 3 15	−24 10	1	11	4.04	+ .30	− .02
4707	12 17 29	+26 24	4	3	4.79	+ .49	+ .26
4753	12 24 27	+24 40	5	3	5.48	+ .43	+ .09
4775	12 26 55	−15 39	1	10	4.32	+ .35	+ .03
4803	12 32 24	−26 35	1	13	5.44	+ .31	+ .05
4821–22	12 36 4	−12 28	1	10	5.27	+ .42	+ .10
4825–26	12 36 36	− 0 54	1	8	2.76	+ .33	− .03
4845	12 40 16	+39 49	1	6	5.94	+ .55	− .04
4864	12 43 55	+25 23	3	4	6.31	+ .70	+ .25
4883	12 46 50	+28 5	3	3	4.93	+ .67	+ .19
4916	12 51 30	+65 59	4	3	5.24	+ .28	+ .02
4968–69	13 5 7	+18 3	2	5	4.32	+ .45	− .06
4981	13 6 44	−15 40	3	5	5.04	+ .46	+ .02
115043 HD	13 9 31	+57 14	4	4	6.83	+ .60	+ .09
5011	13 11 49	+ 9 57	2	5	5.22	+ .58	+ .09
5017	13 13 4	+41 6	3	4	4.72	+ .29	+ .21
5110	13 30 20	+37 42	5	4	4.96	+ .40	+ .06
5209	13 45 50	−23 53	3	6	6.45	+ .69	+ .27
5304	14 5 50	+25 34	3	3	4.83	+ .53	+ .07
5338	14 10 46	− 5 31	2	5	4.08	+ .50	+ .05
5365	14 14 26	+13 28	2	5	5.41	+ .38	− .04
5384	14 18 8	+ 1 43	3	4	6.27	+ .63	+ .08
5447	14 30 20	+30 11	2	4	4.46	+ .35	− .08
5487	14 37 47	− 5 13	2	6	3.88	+ .38	− .02
5530	14 45 9	−15 35	1	9	5.16	+ .38	+ .01
5570	14 51 58	− 3 56	4	4	4.49	+ .30	+ .04
5634	15 2 55	+25 16	3	3	4.94	+ .42	− .03
5691	15 13 29	+67 44	1	8	5.18	+ .52	+ .06
5747	15 23 42	+29 27	1	6	3.65	+ .26	+ .12
5936	15 52 9	+38 14	2	5	5.45	+ .33	+ .03
5968	15 57 13	+33 36	3	4	5.40	+0.60	+0.09

PHOTOMETRIC AND SPECTROSCOPIC STUDIES OF EARLY-TYPE STARS BETWEEN GALACTIC LONGITUDE $l = 338°$ AND $l = 33°$*

W. A. HILTNER AND BRAULIO IRIARTE
Yerkes and McDonald Observatories, Observatories of Tonantzintla and Tacubaya
Received February 25, 1955

ABSTRACT

Photometric observations on the (U, B, V) system and spectral classifications of 78 early-type stars between galactic longitudes $l = 338°$ and $l = 33°$ are given in Table 1. An analysis of the data suggests that the spiral arm discovered at 6.5 kpc from the galactic center by 21-cm observations (Kwee, Muller, and Westerhout 1954) is part of the Sagittarius arm. It is also suggested that earlier observations of a group of early-type stars at $l = 326°$ to $l = 331°$ (Hiltner 1954) form part of the arm at 5 kpc from the galactic center.

As part of a more extensive program of interstellar polarization studies, two lists of O- and B-type stars, then unpublished, were observed in part during September, 1953, and August, 1954. The stars are located between galactic longitudes $l = 337°$ and $l = 35°$. These lists, now published (Iriarte and Chavira 1954), comprise a total of 264 stars. Of this total number, 109 have been observed two or more times for color and magnitude, 28 additional stars have been observed once for color and magnitude, and spectrograms have been obtained for 85 stars. Of these 85 stars, 18 are of spectral type O9.5 or earlier, and 21 are of luminosity class *Ib* or brighter. The photographic magnitudes fall from 8.9 to 12.8.

Although we have both spectrograms and two or more observations of color and magnitude for only 30 per cent of the stars in the two lists, many of the objects are of sufficiently great interest for other studies of galactic structure to warrant publication of our limited data at this time. The observed data for 78 stars are recorded in Table 1. The first column gives the BD numbers. A few of the stars are also in the *Henry Draper Catalogue*. These are marked with an asterisk, and the HD numbers are recorded as footnotes at the end of the table. The second to fifth columns give the positions in equatorial (1900) and galactic co-ordinates. The latter are referred to the standard pole at 12^h40^m0, $+28°.0$. The sixth column gives the spectral type of each star. All stars were classified by W. W. Morgan from spectrograms taken at the McDonald Observatory by the authors. An average dispersion of 100 A/mm between $H\gamma$ and $H\delta$ was employed. Spectrogram width was 0.60 mm. The seventh to ninth columns give the results of the photometric observations on the (U, B, V) system (Johnson and Morgan 1953). At least two observations were obtained of each star. The means of the difference in the two observations for V, $B - V$, and $U - B$ of each star were 0.022, 0.010, and 0.013, respectively. The tenth column gives the color excess. The assumed normal colors were those published by Morgan, Harris, and Johnson (1953). It was further assumed that the intrinsic color for O5–O7 was $(B - V) = -0.32$ and that $B - V = -0.30$ for an O9.5 star. The total absorption is given in the next column on the accepted value of 3.0 for the ratio of total to selective absorption (Morgan *et al.* 1953). The twelfth column lists the assumed absolute magnitudes. No absolute magnitudes were assigned to stars of spectral type O8 or earlier because of lingering uncertainty as to their luminosity. The last column gives the corrected distance modulus. A colon after any entry in the table indicates an uncertainty in the entry. All observations were made with the 82-inch reflector of the McDonald Observatory.

The observations are shown graphically in Figure 1. In the lower section of the figure the stars are plotted in galactic co-ordinates. The closed circles refer to stars for which a distance modulus is given, and the crosses refer to stars of spectral type O8 or earlier. In

* *Contributions from the McDonald Observatory, University of Texas*, No. 258.

TABLE 1

Journal of Observations

Star	1900		l	b	Sp	V	B-V	U-B	E_{B-V}	$3(E_{B-V})$	Mo	m-M
	α	δ										
-15°4861	18h 6m6	-15°36'	342.4	-0.2	B1(V)ne	9.21	+0.24	-0.63	+0.50	1.50	-3.2	10.9:
-20 5043	18 8.1	-20 20	338.4	-2.3	O6	9.52	+0.35	-0.20	+1.17	3.51		
-12 4949	18 8.0	-12 55	344.9	+0.3	B9:IV:	10.78	+0.39	+0.13	+0.45	1.35	-1.0	10.4:
-14 4957	18 10.4	-14 39	343.6	-0.5	B0.5IV	9.81	+0.51	-0.49	+0.79	2.37	-4.0	11.4
-12 4979	18 12.4	-12 17	345.9	+0.2	O7(f)	10.44	+0.68	-0.32	+1.00	3.00		
-13 4928	18 13.0	-13 49	344.7	-0.6	B0.5:V:ne	10.12	+0.49	-0.56	+0.77	2.31	-3.6	11.4:
-13 4929	18 13.0	-13 48	344.7	-0.6	B0IV	9.85	+0.64	-0.44	+0.94	2.82	-4.2	11.2
-13 4930	18 13.2	-13 52	344.6	-0.7	O9.5V	9.44	+0.30	-0.70	+0.60	1.80	-4.1	11.7
-13 4936	18 13.4	-13 59	344.6	-0.8	B1:V:ne	9.71	+0.63	-0.59	+0.89	2.67	-3.2	10.2:
-13 4941	18 14.4	-13 05	345.4	-0.4	O9.5IV	9.75	+1.08	-0.07	+1.38	4.14	-4.5	10.1
-12 5008	18 14.5	-12 41	345.3	-0.4	B0.5III	9.81	+1.01	-0.08	+1.29	3.87	-4.4	10.3
-12 5009	18 14.7	-12 13	346.3	-0.2	O8	9.54	+0.68	-0.42	+0.99	2.97		
-14 5016	18 17.0	-14 42	344.4	-1.9	B1II	9.38	+0.64	-0.39	+0.90	2.70	-5.1	11.8
-11 4620	18 17.9	-11 58	346.9	-0.8	O5	10.17	+0.80	-0.31	+1.12	3.36		
-14 5029	18 18.1	-14 12	344.9	-1.9	B1.5Ib	9.61	+1.15	-0.02	+1.40	4.20	-5.8	11.2
-14 5030	18 18.6	-14 13	345.0	-2.0	B5Ia	9.52	+1.03	+0.03	+1.19	3.57	-7.0	13.0
-10 4682	18 18.8	-10 52	347.9	-0.5	O7	9.63	+0.56	-0.55	+0.88	2.64		
-13 4979	18 21.0	-13 43	345.7	-2.3	O7	9.28	+0.80	-0.36	+1.12	3.36		
-14 5050	18 21.0	-14 34	344.9	-2.7	B0V	9.26	+0.53	-0.50	+0.83	2.49	-3.9	10.7
-14 5062	18 22.2	-14 46	344.9	-3.1	B0.5:ne(V?)	9.30	+0.48	-0.61	+0.76	2.28	-3.6	10.6:
-13 4993	18 23.0	-13 34	346.0	-2.7	B0.5Ia	9.44	+0.80	-0.34	+1.08	3.24	-7.0	13.2
-13 5011	18 25.1	-13 42	346.2	-3.2	B1III	9.44	+0.44	-0.46	+0.70	2.10	-4.3	11.6
-15 4995	18 25.2	-14 59	345.0	-3.8	B3V	9.45	+0.19	-0.40	+0.39	1.17	-2.0	10.3
-12 5083	18 25.8	-12 25	347.4	-2.7	B1Ib	9.47	+0.42	-0.57	+0.68	2.04	-6.0	13.4
-13 5015	18 25.8	-13 38	346.3	-3.3	O7	10.02	+0.52	-0.54	+0.84	2.52		
-12 5095	18 27.1	-12 52	347.1	-3.2	B0IV	10.05	+0.46	-0.51	+0.76	2.28	-4.2	12.0
-14 5102	18 27.4	-13 58	346.2	-3.3	B1Vpe	9.01	+0.20	-0.70	+0.46	1.38	-3.2	10.3
-12 5104	18 28.3	-12 20	347.7	-3.2	O7	9.55	+0.58	-0.48	+0.90	2.70		
- 8 4634	18 28.9	- 8 10	351.5	-1.4	O9?V?p	9.44	+0.91	-0.18	+1.22	3.66	-4.2	10.0:
-13 5061	18 33.8	-13 57	346.9	-5.2	A3:Ia	9.36	+0.92	+0.13	+0.83	2.49	-7.0	14.4
-12 5132	18 34.1	-11 58	348.7	-4.3	B2:npe(V)	9.55	+0.67	-0.37	+0.91	2.73	-2.6	9.4:
-12 5133	18 34.4	-12 31	348.3	-4.6	B1V	10.78	+0.70	-0.23	+0.96	2.88	-3.2	11.1
-13 5065	18 34.7	-13 30	347.4	-5.2	B0:V:	9.69	+0.78	-0.19	+1.08	3.24	-3.9	10.4:
- 9 4790	18 34.9	- 9 14	351.2	-3.2	B9:Ib:	8.48	+0.80	+0.12	+0.86	2.58	-5.5	11.4:
-10 4749	18 35.0	-10 48	349.9	-4.0	B1IV	9.46	+0.48	-0.44	+0.74	2.22	-3.8	11.0
- 5 4718	18 34.9	- 5 36	354.4	-1.5	B2:II:p	9.92	+0.81	-0.10	+1.05	3.15	-5.0	11.8:
-13 5073	18 35.7	-13 57	347.2	-5.6	B1:(IV)pe	10.14	+0.86	-0.28	+1.12	3.36	-3.8	10.6:
- 1 3542	18 36.9	- 1 24	358.4	0.0	B8Ia:	9.22	+1.50	+0.45	+1.59	4.77	-7.0	11.4:
- 6 4849	18 37.5	- 6 35	353.9	-2.5	B1V	10.16	+0.23	-0.56	+0.49	1.47	-3.2	11.9
- 9 4805	18 38.0	- 9 26	351.4	-4.0	B0Ia(e?)	9.18	+0.33	-0.26	+1.13	3.39	-7.0	12.8
- 5 4737	18 38.1	- 5 53	354.6	-2.3	B0.5IV	10.07	+0.29	-0.58	+0.57	1.71	-4.0	12.4
-14 5172	18 39.2	-14 28	347.1	-6.6	B1II	9.09	+0.67	-0.28	+0.93	2.79	-5.1	11.4
- 4 4573	18 40.0	- 4 53	355.7	-2.3	B8Iab:	9.71	+1.08	+0.22	+1.17	3.51	-6.2	12.4:
- 8 4702	18 41.2	- 8 02	353.0	-4.0	B1V	9.35	+0.29	-0.66	+0.54	1.62	-3.2	10.9
-12 5163	18 41.3	-12 24	349.2	-6.1	B9:IV:	9.38	+0.57	+0.25	+0.63	1.89	-1.0	8.5:
-12 5166	18 41.5	-12 14	349.3	-6.0	B0.5I	9.91	+0.70	-0.37	+0.98	2.94	-6.5	13.4
- 6 4903	18 42.2	- 6 25	354.6	-3.5	O8	9.94	+0.31	-0.72	+0.62	1.86		
- 5 4769	18 43.2	- 5 37	354.5	-3.3	O8(I:)	10.40	+0.75	-0.35	+1.06	3.18		
- 6 4910	18 43.2	- 6 34	354.6	-3.8	B0.5Ia	8.92	+0.36	-0.64	+0.64	1.92	-7.0	14.0
- 4 4625	18 49.6	- 4 29	357.2	-4.2	B1II	10.20	+0.76	-0.28	+1.02	3.06	-5.1	12.2
- 5 4819	18 51.9	- 5 39	356.0	-5.3	B2pe(IV)	10.30	+0.40	-0.61	+0.64	1.92	-3.3	11.7:
-13 5166	18 52.9	-13 31	349.5	-9.1	B0II-III	10.34	+0.24	-0.70	+0.54	1.62	-4.8	13.5
- 7 4794	18 53.4	- 7 29	354.9	-6.4	B1Ia	9.55	+0.33	-0.67	+0.59	1.77	-7.0	14.8
+11 3707	18 57.9	+11 07	11.9	+1.3	B1Ia:	10.57	+1.04	-0.10	+1.30	3.90	-7.0	13.7:
+10 3774*	18 59.4	+10 58	11.9	+0.9	B1.5:IV:ne	9.13	+0.53	-0.41	+0.78	2.34	-3.6	10.4:

TABLE 1 (Concluded)

Star	1900 α	1900 δ	l	b	Sp	V	B-V	U-B	E_{B-V}	$3(E_{B-V})$	Mo	m-M
+11°3738*	19h 2m3	+11°17'	12.6	+0.4	B1Vnn	9.45	+0.41	-0.36	+0.67	2.01	-3.2	10.6
+14 3863*	19 14.3	+14 09	16.5	-0.7	B2III:	10.87	+0.62	-0.32	+0.86	2.58	-4.1	12.4:
+12 3927*	19 24.8	+12 22	16.2	-3.8	B1Ib	10.23	+0.79	+0.25	+1.05	3.15	-6.0	13.1
+ 8 4122	19 26.2	+ 8 18	12.8	-6.2	B1Ia	9.86	+0.25	-0.67	+0.51	1.53	-7.0	15.3
+23 3706*	19 31.7	+23 38	26.8	+0.4	B9Ib	8.20	+0.71	-0.06	+0.77	2.31	-5.5	11.4
+12 3981*	19 31.8	+12 45	17.4	-5.1	B2V	9.81	-0.01	-0.68	+0.23	0.69	-2.6	11.7
+25 3912	19 35.7	+25 11	28.6	+0.4	B2.5V	10.21	+0.70	-0.08	+0.92	2.76	-2.3	9.8
+23 3730	19 36.0	+23 47	27.4	-0.4	B8Ib	9.27	+0.99	+0.09	+1.08	3.24	-5.5	11.5
+11 3946	19 36.5	+11 50	17.2	-6.6	BOIb:n	9.36	+0.12	-0.78	+0.42	1.26	-6.0	14.1:
+24 3843	19 37.7	+24 06	27.9	-0.5	O8V	10.34	+0.99	-0.01	+1.30	3.90		
+22 3778	19 38.5	+22 19	26.4	-1.6	B2V:nne†	10.00	+0.37	-0.38	+0.61	1.83	-2.6	10.8:
+22 3781	19 38.8	+23 02	27.1	-1.3	BOIV	9.75	+0.43	-0.55	+0.73	2.19	-4.2	11.8
+25 3941	19 40.3	+25 59	29.8	0.0	B1.5V	10.41	+0.70	-0.19	+0.95	2.85	-2.9	10.5
+24 3866	19 41.5	+24 52	28.9	-0.9	O8f	9.57	+1.18	+0.02	+1.49	4.47		
+25 3952	19 41.5	+25 07	29.2	-0.7	O7	10.16	+0.63	-0.42	+0.95	2.85		
+28 3487	19 45.4	+28 42	32.6	+0.4	B2Ib:	10.10	+0.51	-0.40	+0.75	2.25	-5.7	13.6:
+25 3998	19 46.9	+25 42	30.3	-1.5	BO.5III:	9.96	+0.64	-0.38	+0.92	2.76	-4.4	11.6:
+23 3809‡	19 47.4	+23 38	28.6	-2.6	B1V:	10.68	+0.88	-0.12	+1.14	3.42	-3.2	10.5:
+21 3959	19 48.5	+21 59	27.4	-3.8	B2Vp(e)	9.85	+0.34	-0.36	+0.58	1.74	-2.6	10.7
+21 3963	19 49.1	+21 56	27.4	-3.9	B2V	10.06	+0.28	-0.44	+0.52	1.56	-2.6	11.1
+22 3847	19 49.4	+22 21	27.8	-3.7	B5III	9.58	+0.23	-0.45	+0.39	1.17	-3.2	11.6
+23 3834	19 50.6	+23 12	28.7	-3.5	B2V	9.66	+0.86	-0.24	+1.10	3.30	-2.6	9.0
+23 3835	19 50.7	+23 13	28.7	-3.5	B2V:	9.70	+0.41	-0.32	+0.65	1.95	-2.6	10.4:

* +10°3774 = HDE230579
* +11 3738 = HD178124
* +14 3863 = HDE231124
* +12 3927 = HDE231564
* +23 3706 = HD184943
* +12 3981 = HDE231970
† two-line binary (?)
‡ V = 10.68 is mean of: 1954, Aug. 13 V = 10.75
1954, Aug. 16 V = 10.62

TABLE 2

Journal of Observations

Star	1900 α	1900 δ	l	b	Sp	V	B-V	U-B	E_{B-V}	$3(E_{B-V})$	Mo	m-M
+2°3771	18h59m2	+2°58'	4.8	-2.9	BOIII	9.21	+0.63	-0.38	+0.83	2.79	-4.5	10.9
+3 3893*	19 1.1	+3 06	5.2	-3.2	B1Ib	8.60	+0.63	-0.36	+0.89	2.67	-6.0	11.9
+3 3902*	19 2.3	+3 17	5.5	-3.4	B3Ia	7.41	+0.50	-0.35	+0.70	2.10	-7.0	12.3

* +3°3893 = HD177812
* +3 3902 = HD178129

the upper section of the figure, we have plotted galactic longitude against distance modulus. The open circles refer to stars with uncertain distance modulus. Obviously, the stars fall within three distinct groups. However, this grouping should not be given much weight, for a variety of reasons, not the least important of which is an observational selection caused by an incompleteness of the survey.

An attempt has been made to arrive at distance estimates for the group at $l = 343°$ to $l = 357°$ and for the group at $l = 27°$ to $l = 30°$. The latter is clustered, with a distance modulus of 10.8, or 1450 parsecs. However, the former group offers more difficulty in selecting a mean distance modulus. If all stars with reliable distance moduli are averaged, the mean distance modulus is 12.0, or 2510 parsecs. However, three of the stars, BD−13°5061, BD−6°4910, and BD−7°4794, included in the mean, have distance moduli of 14.0 or greater. In order to place these stars at 12.0, the luminosity class must

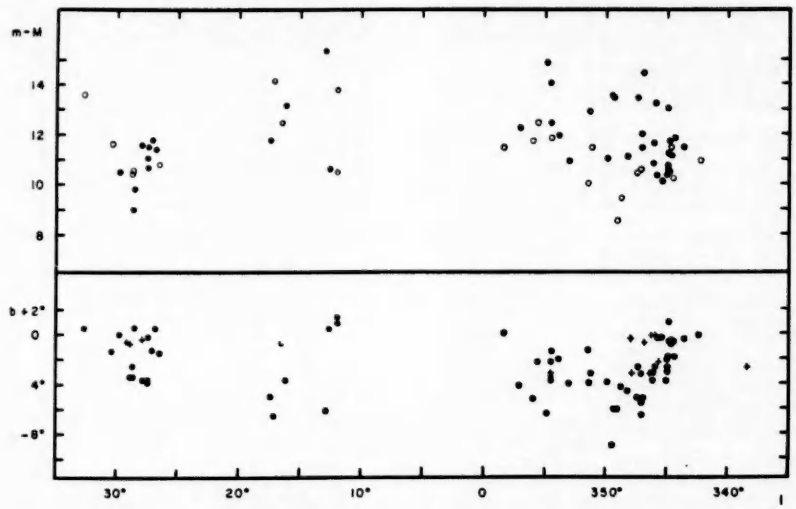

FIG. 1.—The lower section of the figure is a plot of the stars found in Table 1. The abscissa is galactic longitude and the ordinate galactic latitude. The filled circles represent stars for which a distance modulus is given. Crosses refer to stars O8 or earlier. In the upper section of the figure the stars are plotted on a galactic longitude–distance modulus diagram. The filled circles refer to stars with more reliable distance moduli; the open circles those with less reliable data.

be moved from I*a* to III, an intolerably large shift. Consequently, we prefer to exclude these stars from the mean. The distance modulus then becomes 11.7, or 2190 parsecs.

These two concentrations have been plotted on the sketch of the inner parts of the galactic system as published by Kwee, Muller, and Westerhout (1954). They are shown in Figure 2 as large closed circles. Also two other additions have been made to the diagram. First, the group of early-type stars in the direction of the galactic center, previously reported (Hiltner 1954), is designated by a large open circle. The second addition consists of three stars near $l = 5°$ recorded in an earlier list of OB stars (Nassau and Morgan 1951). Observational data regarding the three stars are recorded in Table 2. This group of three stars has a mean distance modulus of 11.7, or 2190 parsecs. These stars as a group are shown in Figure 2 as a second open circle.

The distances of early-type stars that we have observed here support the conclusion that the spiral arm discovered at 6.5 kpc from the galactic center by hydrogen emission

at 21 cm wave-length observations (Kwee *et al.* 1954) is indeed part of the Sagittarius arm (see Morgan, Sharpless, and Osterbrock 1952) and that a second arm at 5 kpc from the galactic center, reported by the same authors, is associated with a group of early-type stars, previously discussed (Hiltner 1954), in the direction of the galactic center.

Attention should be called to BD+8°4122, a B1 I*a* star with a distance modulus of 15.3. This star is located on Figure 2 as a cross. Its distance from the galactic plane is great, of the order of 1 kpc when the foregoing distance is accepted.

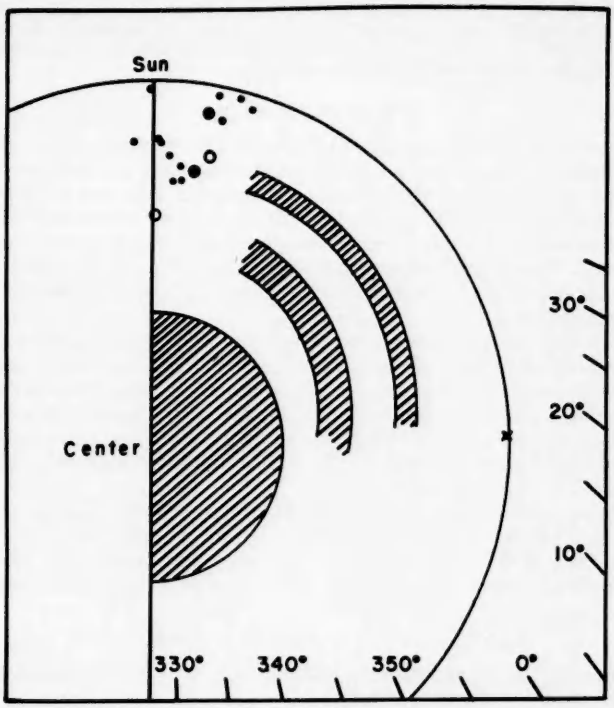

FIG. 2.—A sketch of the inner part of the galactic system as reported by Kwee, Muller, and Westerhout (1954). The small dots represent O associations (Morgan, Whitford, and Code 1953). The large closed and open circles are the results of the present series of investigations.

It is a pleasure to thank Dr. Morgan for the spectral classifications. One of us (W. A. H.) wishes to thank the National Science Foundation for financial support.

REFERENCES

Hiltner, W. A. 1954, *Ap. J.*, **120**, 40–47.
Iriarte, Braulio, and Chavira, Enrique. 1954, *Bol. Obs. Tonantzintla y Tacubaya*, No. 9, pp. 41–45, and No. 11, pp. 27–33.
Johnson, H. L., and Morgan, W. W. 1953, *Ap. J.*, **117**, 313–352.
Kwee, K. K., Muller, C. A., and Westerhout, G. 1954, *B.A.N.*, **12**, 220.
Morgan, W. W., Harris, D. L., and Johnson, H. L. 1953, *Ap. J.*, **118**, 92–105.
Morgan, W. W., Sharpless, Stewart, and Osterbrock, Donald. 1952, *A.J.*, **57**, 3.
Morgan, W. W., Whitford, A. E., and Code, A. D. 1953, *Ap. J.*, **118**, 318–322.

COMET OUTBURSTS

CHARLES WHITNEY
Harvard College Observatory
Received May 5, 1954; revised February 1, 1955

ABSTRACT

Several comet outbursts accompanied by the ejection of spherical halos are investigated. Special attention is paid to the mass and energy ejected in a typical halo. On the basis of the results, it is suggested that the energy of an outburst may be derived from normal insolation. The activity can possibly be explained in terms of the icy-conglomerate comet nucleus.

I. THE OBSERVATIONS

The purpose of the present investigation is to study the phenomenon of the ejection of spherical halos from cometary nuclei. A typical cometary outburst to be considered here consists in a brightening of the comet by 2–5 mag. and the expansion from the nucleus of a spherical halo with a velocity between 0.1 and 1.0 km/sec. The ejection of halos by comets is not an extremely rare occurrence, and certain comets appear particularly prone to it. The comet Schwassmann-Wachmann (1925 II), notable also for its orbit ($e = 0.14$, $q = 5.51$), is an extreme example. It shows an estimated two or three such outbursts per year.

Data concerning the adequately observed outbursts of three comets are compiled in Table 1. The first and second columns are self-explanatory. The third column shows the number of magnitudes by which the comet increased in brightness during the burst. The fourth column gives the magnitude of the comet at the height of the burst, reduced to the standard distances of 1 A from the sun and the earth and corrected for the phase angle at which the comet was observed. Table 2 contains the measured expansion velocities of the halos for these four outbursts.

The tabulated velocities are close to thermal velocities at the temperature of cometary nuclei (0.4 km/sec for molecular weight 20 at 6 A from the sun). N. Richter[1] has recently derived velocities of 0.1–0.5 km/sec for the halos associated with bursts of comet Schwassmann-Wachmann. Bobrovnikoff (1954) reached a similar conclusion from data on 57 halos.

II. THE MASS AND ENERGY OF A TYPICAL HALO

On the basis of the three following assumptions, certain conclusions will be drawn regarding the nature of the halo phenomena.

1. The material of a halo is primarily dust, each particle having an albedo similar to that of Ceres. The dusty nature of halos is suggested by the increased continuous background that has been observed at the time of the ejection of halos in the spectra of comets Pons-Brooks (1884 I) (Vogel 1884), Holmes (1892 III) (Keeler 1893), Schwassmann-Wachmann (1925 II) (Mayall 1941; Herbig 1946), and Sawerthal (1888 I) (Oort and Schmidt 1951).
2. At the time of maximum brightness, the light of the comet arises by direct reflection from the halo dust.
3. There are no shadowing effects other than self-shadowing.

If all halo particles were of the same radius, then the total number of particles, each of apparent magnitude m_s, contributing to the halo, of apparent magnitude m, is given by the equation

$$n = 10^{0.4(m_s - m)} . \quad (1)$$

[1] MS kindly communicated in advance of publication.

The total mass of the halo would be

$$M = \tfrac{4}{3}\pi n \rho s^3 , \tag{2}$$

where ρ is the density of the individual dust grains of radius s.

We have determined m_s as follows: The asteroid Ceres has a diameter of about 770 km and an absolute magnitude 3.7 (opposition at one astronomical unit distance from the sun and earth). If Ceres were moved off to the distances r and Δ from the sun and earth and its radius reduced to s, the new apparent magnitude would be

$$m = 3.7 + 5 \log \left[\frac{r\Delta 385 \times 10^5}{s\Phi^{1/2}(\alpha)} \right], \tag{3}$$

TABLE 1

COMETARY OUTBURST DATA

Comet	Date	Δm	Min. Abs. Mag.
Swift (1899 I)	June 4, 1899	2	6.3
Holmes (1892 III)	Jan. 16, 1893	4–5	4
Pons-Brooks (1884 I)	Sept. 23, 1883	5	4
Pons-Brooks (1884 I)	Jan. 1, 1884	1.3	6

TABLE 2

HALO RADIAL VELOCITIES

Comet	Velocities (Km/Sec)	Dates	Reference
Swift	0.96	June 4–5, 1899	Richter (1949)
	1.1	June 5–6, 1899	
Holmes		Jan. 16, 1893	Richter (1949); Barnard (1893)
	0.91	8:10– 9:45	
	7.25	9:45–10:29	
	7.4	10:29–10:43	
	0.27	Jan. 16–23, 1893	Bobrovnikoff (1943)
Pons-Brooks	0.84	Sept. 23–25, 1883	Richter (1949)
	0.54	Sept. 25–26, 1883	
	0.28	Sept. 23–27, 1883	Bobrovnikoff (1932)
Pons-Brooks		Jan. 1, 1884	Richter (1949)
	2.5:	8:20– 8:30	
	0.95	8:30– 9:03	

where $\Phi(\alpha)$ is the phase-angle dependence of the brightness of Ceres and gives the ratio of the brightness when observed at angle α to that when observed at zero phase angle (opposition). The phase-angle dependence of the moon (Russell 1916) is applied for the dust particles.

The m in equation (3) is just the m_s desired for equation (1). Combining equations (1), (2), and (3), we find the logarithm of the total mass of the halo:

$$\log_{10} M = \log_{10} \rho s + 2 \log_{10} \left[\frac{r\Delta 385 \times 10^5}{\Phi^{1/2}(\alpha)} \right] - 0.40 m_H + 2.10 . \tag{4}$$

In this equation,

m_H = Apparent magnitude of halo,
M = Total mass of halo (gm),
ρ = Density of individual dust grains (gm/cc),
r = Heliocentric distance of comet (A),
Δ = Geocentric distance of comet (A),
s = Radius of dust particles (cm), and
$\Phi(\alpha)$ = Fractional phase-angle dependence of brightness of dust particles.

Equation (4) may be written as

$$\log M = A + \log \rho s ,$$

where A depends only on the earth-comet-sun geometry and the observed brightness of the halo. The values of A for the outbursts in Table 1 are 14.8, 16.1, 15.7, and 14.9, respectively, in the c.g.s. system. The average antilog of A is 4.5×10^{15}. Adopting the

TABLE 3

CALCULATED HALO MASSES
(A = 15.7)

s (Cm)	M (Gm)	$M/4.2\times10^{15}$
10^{-3}	5×10^{12}	1.2×10^{-3}
10^{-4}	5×10^{11}	1.2×10^{-4}
10^{-5}	5×10^{10}	1.2×10^{-5}

TABLE 4

KINETIC ENERGIES OF HALOS (ERGS)

v (Km/Sec)	s (Cm)		
	10^{-3}	10^{-4}	10^{-5}
0.2	2×10^{21}	2×10^{20}	2×10^{19}
0.8	3×10^{22}	3×10^{21}	3×10^{20}
1.6	1×10^{23}	1×10^{22}	1×10^{21}

mean A of 15.7 and a density of 1 gm/cm^3, we may calculate the total mass, M, for various assumed values of s. In Table 3, the first column lists the assumed values of s, and the second column gives the resulting values of halo mass. The third column gives the ratio of the mass in the second column to the mass of a sphere of radius 1 km and density 1 gm/cm^3, the approximate dimensions of a comet (Whipple 1951).

The lower limit of 10^{-5} cm for s is necessary, since the particles must not be much smaller than 5000 A ($=5 \times 10^{-5}$ cm). No definite colors have been observed in the halos. An approximate upper limit on s is furnished by energy considerations. Since the ejection of halos produces no observed effect on the comet involved, we expect M to be several orders of magnitude less than the comet mass.

Table 4 contains values of the total kinetic energies of the halos, $\frac{1}{2} mv^2$, for the various

values of the velocities of expansion and total masses. The vertical columns correspond to the total mass but have been headed with the values of s from Table 3 rather than M. Note that $A = 15.7$ for these calculations.

An average halo apparently represents the ejection of 10^{12} gm with an energy of about 10^{21} ergs. This mass could be contained in a sphere of radius about 60 meters and density 1 gm/cm^3. To compute how long such a halo would be visible against the background of the light of the night sky, suppose that the halo were visible until its surface brightness fell below that of a 22-mag. star per square second (the brightness of the night sky). Its absolute magnitude at maximum light (4) indicates that, if it consisted of dust, the halo contained 10^{24} particles of assumed radius 10^{-4} cm. If the spherical halo expanded at the rate of 0.3 km/sec, as indicated by Bobrovnikoff's data, I calculate that it would take 30 days for the mean projected surface density of particles to fall below 10^{17} per square second, the limit of visibility assumed. The central regions would remain above the limit for a longer period. Comet Holmes was at an abnormal brightness for about two months following the outburst of January 16, 1893 (Bobrovnikoff 1943). This agreement is encouraging.

TABLE 5

OUTBURSTS OF COMET SCHWASSMANN-WACHMANN (1927–1939)

DATE	Δ	r	COMA		Δm	NO. DAYS SINCE PREVIOUS OBS.
			m (Obs.)	m (Abs.)		
Dec. 14, 1927	5.5	5.8	14	6.5	2	14
Dec. 2, 1929	5.4	6.4	13.5	6.0	3.5:	26
Nov. 23, 1930	5.8	6.8	15	7	1.5	32
Feb. 11, 1931	6.2	6.9	12.5	4.3	5	32
Jan. 22, 1932	6.1	7.1	14	5.8	2	48
Jan. 20, 1933	6.3	7.3	12.5	4.2	4.5	14
Apr. 22, 1933	7.0	7.3	12	3.5	2.5	28
Mar. 14, 1934	6.3	7.3	13	4.7	5	4
May 4, 1935	6.3	7.1	12.5	4.3	2.5	27
May 15, 1937	5.4	6.4	13.5	5.8	3	5
June 14, 1939	4.7	5.8	14.5	7.9	2.5	27

Comet Schwassmann-Wachmann (1925 II) has a planet-like orbit just beyond that of Jupiter, which makes it available for observation for a good fraction of every year. Table 5 (Richter 1940) lists the outbursts of this comet observed between 1927 and 1939. The second and third columns give the geocentric and heliocentric distances. The fourth and fifth columns give the observed magnitude of the coma and the magnitude reduced to the standard distances. In the sixth column are the changes in magnitude from the previous observation, and in the seventh column are the number of days since the previous observation. These bursts brought the comet to a mean brightness which corresponds to a magnitude of 5.8. Excluding the last tabulated burst, the mean is 5.2 mag. The bursts of comet Schwassmann-Wachmann thus fall into the same category as the four bursts in Table 1, for which the mean absolute magnitude was 5.

By estimating the radius of the nucleus of comet Schwassmann-Wachmann from comparisons with the brightness of Halley's comet at large heliocentric distances, we may conclude that comet Schwassmann-Wachmann has a radius about 5–10 times larger than that of comet Halley. This estimate puts the radius of comet Schwassmann-Wachmann at 70 ± 30 km. At a heliocentric distance of 6 A, about 6×10^{18} ergs of solar radiant energy are incident on the entire surface of the comet per second. Hence,

about 10^{18} ergs/sec will be absorbed by the nucleus, if of albedo 0.1. For the other comets listed in Table 1, the radii are probably nearer 1 km, and the mean distance at the times of bursts was about 2 A. For these we would expect the solar flux to be 10^{16} ergs/sec, leading to an absorption of about 10^{15} ergs/sec.

The entries in Table 6 are those of Table 4 divided by the solar flux of 10^{18} ergs/sec. They represent the time needed for the nucleus of comet Schwassmann-Wachmann to absorb the kinetic energy emitted in a typical halo. For the comets of Table 1 these times are about 10^3 times longer.

III. CONCLUSIONS

The occurrence of an outburst represents a drastic departure from thermal equilibrium between the comet and space. If the solar flux were suddenly doubled or the nuclear albedo dropped by a factor of 2, such a departure would take place. In a matter of hours the comet Schwassmann-Wachmann nucleus would then absorb enough energy to eject a halo.

TABLE 6

TIME TO ABSORB KINETIC ENERGY OF HALO (HOURS)
COMET SCHWASSMAN-WACHMANN

v (KM/SEC)	s (CM)			v (KM/SEC)	s (CM)		
	10^{-3}	10^{-4}	10^{-5}		10^{-3}	10^{-4}	10^{-5}
0.2.....	2	0.2	0.02	0.8.....	30	3	0.3
0.4.....	8	0.8	0.08	1.6.....	130	13	1.3

In a recent analysis, N. Richter (see n. 1) has demonstrated a strong correlation between the bursts of comet Schwassmann-Wachmann and terrestrial magnetic storms. In the period 1939–1950, the times of eight cometary bursts were established with an uncertainty less than several days. All of these could be associated with significant increases in the Potsdam terrestrial-magnetism characteristic numbers. The comet was within 35° of opposition in five of these cases, and Richter assumed that a single stream of solar particles caused both magnetic and cometary disturbances. From the time delays between the associated phenomena, he derived velocities of about 750–1000 km/sec for the particles. This value is in good agreement with velocities derived from time delays between solar flares and auroral storms (Meinel 1951).

However, these streams are inadequate to supply the energy involved in a cometary burst. The derived densities of these streams are about 10^2–10^3 particles/cm^3 at the earth. Such streams, if composed of protons, give a flux of only 50–500 ergs/cm^2 sec. This is about 1 per cent of the solar electromagnetic radiation. The correlations compiled by Richter suggest that these particle streams act as triggers for the cometary bursts. Some other energy source is still required to explain the violent departures from equilibrium and the ejection of halos.

The work of Oort and Schmidt (1951) indicates that older comets are more stable and less prone to the ejection of dust into the coma. This work and the icy-conglomerate comet model of F. L. Whipple (1950, 1951), combined with the peculiar frequency with which particular comets show the phenomena, suggest an *internal* cause for the outbursts.

Suppose comet Schwassmann-Wachmann were a relatively new comet. It would have

a high ratio of icy to meteoric material near its surface. The theoretical equilibrium temperature at its minimum distance of 5.5 A. is about 130° K. The only parent-molecule which would enter into the activity of the cometary nucleus at this temperature is CH_4.

Because of the low temperatures, segregation of the different species of molecules would be slight. The CH_4 immediately at the surface would vaporize and leave behind an irregular, porous layer of meteoric and inactive icy material. A large portion of the observed light from the comet at this time would be direct reflection from the surface. The inactive sheath would probably have low strength. Accidental concentrations of CH_4 might act as centers of stress in the surface regions and lead to explosive action. This type of phenomenon might cause the removal of large areas of the sheath and expose more volatile gases to the action of sunlight. The gases, expanding at thermal velocities, would then give outward momentum to the loosened meteoric material. The ejection of a layer of material 10^{-2} cm in thickness, distributed over the area of the nucleus of comet Schwassmann-Wachmann, would account for the mass of a typical halo.

It is also possible to explain the fact that the bursts of comets Holmes, Swift, and Pons-Brooks are relatively more violent than those of comet Schwassmann-Wachmann. When a comet's heliocentric distance approaches 2.3 A, CO_2 in addition to CH_4 will sublimate rapidly. In these bursts, then, two of the parent-molecules will be active, and greater violence would be expected. In this way it seems possible to account for the phenomena of cometary halos primarily in terms of the properties of the cometary nucleus.

I am grateful to Dr. F. L. Whipple for suggesting this investigation and for his advice during the preparation of this paper.

REFERENCES

Barnard, E. E. 1893, *Astronomy and Astrophysics*, **12**, 180.
Bobrovnikoff, N. 1932, *Pub. A.S.P.*, **44**, 296.
———. 1943, *Pop. Astr.*, **51**, 542.
———. 1954. *A.J.*, **59**, 357.
Herbig, G. 1946, *Pub. A.S.P.*, **58**, 61.
Keeler, J. E. 1893, *Astronomy and Astrophysics*, **12**, 272.
Mayall, N. U. 1941, *Pub. A.S.P.*, **53**, 340.
Meinel, A. B. 1951, *Ap. J.*, **113**, 50.
Oort, J. H., and Schmidt, M. 1951, *B.A.N.*, **419**, 259.
Richter, N. 1940, *A.N.*, **271**, 207.
———. 1949, *ibid.*, **277**, 12.
Russell, H. N. 1916, *Ap. J.*, **43**, 103.
Vogel, H. C. 1884, *A.N.*, **108**, 21.
Whipple, F. L. 1950, *Ap. J.*, **111**, 375.
———. 1951, *ibid.*, **113**, 464.

NOTES

IDENTIFICATION OF THE λ 3143 INTERSTELLAR LINE

In a recent paper Spitzer and Field (1955) reported having observed a weak, sharp interstellar line in the spectrum of ζ Persei at λ 3143.22. Their brief discussion of the line left its origin uncertain; they concluded that it "may perhaps be a molecular feature."

Their surmise is undoubtedly correct. The λ 3143.2 line is almost certainly the $Q_2(1) + {}^QR_{12}(1)$ line of the $^2\Sigma^+$, $^2\Pi$ transition of *CH*. In support of this identification we may cite the following facts: (1) The λ 4300 *CH* interstellar line is prominent in the spectrum of ζ Persei (Adams 1949), so the λ 3886 and λ 3143 groups of *CH* lines from the same normal state must be present; their detection is simply a matter of observation with sufficiently high resolving power. (2) λ 3143.2 is very close to the wave length of the strongest line to be expected from the lowest level of the ground state of *CH* in the λ 3143 band (cf. McKellar 1941; Herzberg 1954). The wave length given for the 3143.2 line (McKellar 1940) was 3143.15; but, since it was not a direct measurement, the discrepancy of 0.08 A is not considered outside the probable error of the laboratory value. The wave length 3143.22 from the stellar spectrum should be taken as the more reliable.[1]

The suggested identification with *CH* can be checked by observation of the two other lines expected from the $^2\Sigma^+$, $^2\Pi$ transition, namely, the $R_2(1)$ line at λ 3137.5 and the $^PQ_{12}(1)$ line at λ 3146.0. Since these lines are expected to be only one-half and one-third as intense, respectively, as λ 3143.2, which itself is near the limit of detectability of the coudé spectrograph of the 100-inch telescope at Mount Wilson, the check will require the highest available spectral resolution.

During the last few months we have secured spectrograms of a number of early-type stars in the ultraviolet with the new Victoria spectrograph, in a search for the interstellar lines of *CH* at λ 3143 and *OH* between λ 3072 and λ 3082. The dispersion employed was 3.8 A per millimeter, obtained by using a quartz-fluorite achromat of 41 inches in focal length in a Littrow mounting and the second order of a plane grating having 30,000 lines per inch. This form does not give as high resolving power as the Mount Wilson coudé spectrograph. Our search has not yet been very fruitful; the interstellar doublet of *Na* I at λ 3302 is clearly present for most stars observed, and the lines of *Ti* II (λλ 3384, etc.) were noted in the spectra of P Cygni and 55 Cygni. On a plate of ζ Persei obtained on October 25, 1954, there is a very faint suggestion of the narrow line at λ 3143. Our measurement of its wave length corrected to the scale of the interstellar *Na* I lines at λ 3302 is 2143.25, in good agreement with the value found by Spitzer and Field.

ANDREW MCKELLAR
E. H. RICHARDSON

DOMINION ASTROPHYSICAL OBSERVATORY
VICTORIA, B.C.

REFERENCES

Adams, W. S. 1949, *Ap. J.*, **109**, 254.
Herzberg, G. 1954, *Mem. Soc. r. des sci. de Liége*, 4th ser., Vol. **15**.
McKellar, A. 1940, *Pub. A.S.P.*, **52**, 312.
———. 1941, *Pub. Dom Ap. Obs. Victoria*, **7**, 251.
Spitzer, L., Jr., and Field, G. B. 1955, *Ap. J.*, **121**, 300.

[1] Dr. Spitzer has informed us that, according to advice from Dr. P. W. Merrill, the wave length from the stellar spectrogram probably requires a correction of −0.02 A, and so would be 3143.20 A. The correction results from the difference of 0.02 A between the best solar and laboratory values of the wave lengths of the H and K lines of ionized calcium.

A NOTE ON THE GALACTIC MICROWAVE SPECTRUM

In 1945 van de Hulst suggested that the hyperfine transition in interstellar hydrogen might be detected as a discrete spectral line in the galactic microwave spectrum. The line was found to be in emission by Ewen and Purcell (1951). Since its discovery, the 21-cm hydrogen line has been applied to a variety of astronomical problems by Dutch, Australian, British, and American radio astronomers.

The possibility of detecting other microwave spectral lines has been frequently discussed at symposia and stands as a challenge in radio astronomy. In particular, Purcell (1953), Shklovski (1952), and Townes (1954) have discussed the possibility of detecting other lines. Among the transitions suggested specifically are those of deuterium (hyperfine ~327 Mc/sec), the radical *OH* (lambda-type doubling ~1668 Mc/sec), and perhaps *CaH* (lowest rotational state $\sim 3 \times 10^5$ Mc/sec). Atoms such as helium, favorable in cosmic abundance, have even-even nuclei and no hyperfine structure.

When considering the possibility of detecting other lines, one needs to know something of the interstellar abundance of the element or radical in question, the type of transition, and the "temperature" that characterizes the population distribution over the states responsible for the transition. For the elements and radicals currently considered, very little is directly known about their cosmic abundances in the interstellar medium, and estimates of expected optical depths are difficult.

Interest is currently centered about the *OH* line at 1668 Mc/sec and the deuterium line at 327 Mc/sec, because these two lines have signals which may possibly be detected with the sensitivity of existing equipment. Equipment sensitivity is usually described in terms of "minimum detectable temperature." Various figures are quoted for the sensitivities of existing receivers, and about 1° K is currently approximately the limit for the particular case of hydrogen at a wave length of 21 cm.

Even with signals of the order of 1° K being detectable under favorable circumstances, the *OH* line, according to Townes (1954), may produce a signal which is of the same order as the minimum detectable signal. Although great strides have been made in improving receiver sensitivity (Ewen at Harvard, McClain at the Naval Research Laboratory, and Muller in Holland), it is unlikely that further improvements of 10^2–10^5 will be immediately forthcoming, i.e., minimum detectable signals of the order of 10^{-2}–10^{-5} ° K.

It is the purpose of this note to suggest an alternative method of observation which, with a large antenna, may prove to be the equivalent of an improvement of 10^2–10^5 in minimum detectable temperature.

Absorption lines due to interstellar *H* I clouds have been found in the microwave continuum spectrum of the radio source in Cassiopeia (Hagen, Lilley, and McClain 1954). These absorption lines in the microwave domain are comparable to optical interstellar absorption lines seen in stellar spectra.

The absorption produced in the continuum spectrum of a discrete source may be written as follows:

$$\left(T_{nn'} \frac{\Omega_i}{\Omega_B} - T_A \frac{\Omega_i}{\Omega_s}\right) [1 - e^{-\tau_i(\nu)}]\, G_i(\theta)\,,$$

where $T_{nn'}$ is the "temperature" which determines the population distribution over the two states responsible for the spectral line; Ω_i is the solid angle subtended by a "cloud" of the element or radical in question; $\tau_i(\nu)$ is the optical depth of the cloudy material between the observer and the discrete source; T_A is the apparent antenna temperature of the discrete source; Ω_B is the antenna beam width; and $G_i(\theta)$ is the antenna gain function normalized to unity on the main axis.

Let us consider the influence of a "large" antenna on the absorption equation, an antenna of 250–500 feet in diameter. With antennae of such sizes, the apparent antenna

temperature, T_A, will become large, 10^2–10^5 ° K, approaching or becoming equal to the true brightness temperature of the discrete source, T_B. However, we shall retain the apparent antenna temperature as T_A for the general case, although in some instances it will become T_B.

For the small beam widths which result from large antennae, the absorbing cloudy medium may reasonably be expected to "cover the source," and the absorption may be rewritten approximately as

$$(T_{nn'} - T_A)\,[1 - e^{-\tau_i(\nu)}]\,.$$

Interstellar atoms and radicals other than hydrogen probably have cosmic abundances that make the optical depths rather small. The population temperature, $T_{nn'}$, is unknown. For *H* I, $T_{nn'}$ is of the order of 10^2 ° K. Here $T_{nn'}$ may be small compared to T_A, which is the important consideration for the effect discussed. The apparent antenna temperature, T_A, for a large antenna and certain sources, will be considerable, 10^2–10^5 ° K (and perhaps greater), depending upon the wave length, discrete source, and the antenna used. Neglecting $T_{nn'}$ in comparison with T_A and for small optical depths, the absorption becomes

$$-T_A\,\tau_i\,(\nu)\,.$$

The transition in question and the discrete source used as a background temperature will determine the gain of the absorption, $-T_A\tau_i(\nu)$, over the emission, $T_{nn'}\tau(\nu)$, in each case.

The case of *H* I absorption in the Cassiopeia source is indicative of the expected improvement. For T_A of $\sim$100° K, an absorption of 80° K has been found in the Cassiopeia spectrum. Rough calculations show that, for an antenna 500 feet in diameter, the absorption would become approximately 8000° K. The emission in each case remains near 100° K. Under such conditions, the emission is negligible compared to the absorption. For the case of hydrogen observed in absorption with a large antenna, the possibility of using extremely narrow band widths presents itself, and thermal and turbulent detail may be resolved in the absorption profiles.

If we now set the expected absorption equal to the currently minimum detectable temperature, minimum observable optical depths are indicated. We may put

$$T_A\,\tau_i\,(\nu) = 1^\circ\,\mathrm{K}\,,$$

from which $\tau_i(\nu)$ may become of the order of $1/T_A$ and be detectable. Thus, for the more intense sources, values of optical depths running from 10^{-2} to 10^{-5} (depending on the wave length of the transition and the source used and assuming that $T_{nn'}$ may be neglected in comparison to T_A) may produce measurable absorptions with the sensitivity of existing equipment.

It appears that a large antenna, pointed toward intense discrete sources, would improve the chances of adding other lines to the galactic microwave spectrum.

A. E. Lilley

Naval Research Laboratory

REFERENCES

Ewen H. I., and Purcell, E. M. 1951, *Nature*, **168**, 256.
Hagen, J. P., Lilley, A. E., and McClain, E. F. 1954, *Naval Research Laboratory Report 4448*, Washington, D.C.
van de Hulst, H. C. 1945, *Nederl. Tydschr. Natuurk.*, **11**, 201.
Purcell, E. M. 1953, *Proc. Amer. Acad. Sci.*, **82**, 347.
Shklovski, I. S. 1948, *Astr. Zhur.*, **26**, 10.
———. 1952, *ibid.*, **29**, 144.
Townes, C. H., 1954 *J. Geophys. Research*, **59**, 191.

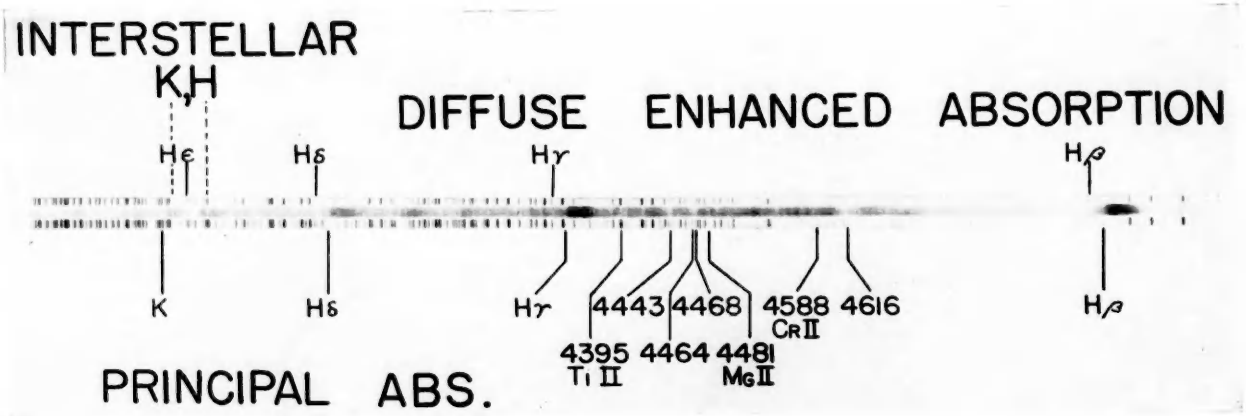

FIG. 1.—Spectrum of Nova Sagittarii 1954.1 on July 11.262

THE SPECTRUM OF NOVA SAGITTARII 1954.1*

Nova Sagittarii 1954.1[1] was discovered with a magnitude of 7.5 by G. Haro and L. Herraro on the night of July 4/5; on July 1/2 it had been fainter than 13. It was originally thought to be in Scorpius. Additional brightness estimates (*I.A.U. Circular*, Nos. 1461, 1467, 1469) indicate the moderately fast rate of decline of 2 mag. in about 8 days. Spectrograms marked "LS" and "Cg" in Table 1 were taken, respectively, with the 36-inch refractor of the Lick Observatory and the coudé grating spectrograph of the McDonald 82-inch reflector. The Lick spectrograms were taken by Dr. G. H. Herbig and loaned for the present study.

On July 7 the emission bands were very weak. Most of the stellar absorption lines belonged to the principal absorption system; only the hydrogen lines showed very weak diffuse enhanced absorption components. By July 9 the emission bands were strong. On July 11 the diffuse enhanced components, while stronger than the principal components of the hydrogen lines, still were not present for other lines in the photographic spectral region. On July 21 the principal absorption components were still prominent, and no [*O* III] emission was detected.

TABLE 1

Plate No.	Date (U.T.) 1954	Dispersion at $H\gamma$ (A/Mm)	Spectral Range	Quality
LS-37729	July 7.264	76	4100–5000	.....
Cg-629	9.239	18	3900–4900	Underexposed
LS-37736	9.365	76	4300–5000	.....
Cg-635	11.262	36	3800–5000	.....
Cg-639	12.211	36	3700–5000	Overexposed
LS-37778	21.212	76	4300–4900	Underexposed

On July 11 the principal absorption spectrum (Fig. 1) resembled that of an A5–F0 supergiant except for several notable exceptions discussed later. Sixty-seven unblended lines were identified as belonging to ionized metals, *H*, *Fe* I, *Mg* I, and *C* I. Measures of *Ti* II and *Fe* II line intensities led to a curve of growth of low precision—due to uncertainty in the location of the continuum for the absorption lines—but one which excludes the possibility of a Doppler velocity of more than 9 km/sec. The line λ 4481 *Mg* II was very weak relative to the *Ti* II and *Fe* II lines, indicating a marked effect of dilution of radiation. The lines whose positions coincide with λλ 4443, 4464, and 4468 of *Ti* II in the principal spectrum are much too strong in this nova, relative to other *Ti* II lines. For instance, λ 4443 originates from the same state (a^2D) as λ 4395 and has a transition probability that is smaller by a factor of 2; however, the line at this position has an equivalent width that is five times larger than that of λ 4395. The three strong lines are probably not members of the diffuse enhanced system, since they were strong on July 7, when the latter was still weak. The three *Ti* II lines originate from different lower states, so their strengths probably cannot be attributed to resonance effects. Furthermore, the strong line generally attributed to a blend of λ 4616.6 and λ 4618.8 of *Cr* II in other novae is probably also due primarily to other sources, because these *Cr* II lines should be weaker than the *Cr* II lines at λ 4558 and λ 4588, which are members of the same multiplet.

Four of the spectrograms were measured for radial velocities with the results given in

* *Contributions from the McDonald Observatory, University of Texas*, No. 254.

[1] $\alpha = 17^h55^m44^s$, $\delta = -36°18'.5$ (1950.0).

Table 2, where the numbers of lines measured are given in parentheses. The interstellar H and K lines are very strong. The duplicity of the diffuse enhanced lines is not well established. Weighted mean velocities for the principal and diffuse enhanced components are, respectively, −732 and −1665 km/sec. These velocities and the rate of decline of light are similar to those of Nova Cygni 1920 and Nova (EL) Aquilae 1927. For a decline

TABLE 2

Date (U.T.)	Velocities (Km/Sec)			
	Interstellar	Principal Abs.	Diffuse Enhanced Abs.	
July 7.264	.....	−687.9 (6)	−1769 (1)	−1532 (1)
11.262	−2.1 (2)	−736.0 (71)	−1707 (4)	−1595 (3)
12.211	−6.6 (2)	−728.7 (14)	−1688 (3)	.....
21.212	.....	−728.7 (5)	.....	.....

of 2 mag. in 8 days, McLaughlin's (1940) correlations predict velocities of −589 and −1202 km/sec for the principal and diffuse enhanced spectra, respectively. The discrepancy is well within the scatter of McLaughlin's correlations.

Helmut A. Abt

McDonald Observatory

REFERENCE

McLaughlin, D. B. 1940, *Ap. J.*, **91**, 369.

NOTE ON THE MASS OF M92

Recently Wilson and Coffeen (1954) published radial-velocity measurements of stars in the globular cluster M92 and derived an estimate of the mass of this cluster with the help of the virial theorem. For this purpose the virial theorem was used in a form given by Kurth (1951). Kurth's equation appears, however, unreliable for the following reasons. First, the potential energy is computed for a cluster model in which about half the mass is represented by a central point mass. The potential energy of this point mass, which is infinite, is left out of the computation. The resulting potential energy is rather low—somewhat lower than that of a homogeneous sphere of the same mass and radius as the cluster. Second, when the formula for the potential energy was introduced into the virial theorem, a factor 2 was missed. This second point partially compensates for the first point. Third, the cluster model used refers to the cluster radius, and, in consequence, the cluster radius appears in the final form for the virial theorem. But the cluster radius is a quantity which does not seem very well defined and seems to be used by observers as designating the distance beyond which the cluster cannot be traced with their respective techniques. Hence the cluster radii found in the literature are not easily related to the effective distance needed in the computation of the potential energy.

Instead of the foregoing procedure, one may perhaps more safely use the following form of the virial theorem (Schwarzschild 1954):

$$\overline{V^2} = \frac{GM}{\bar{r}} \qquad \text{with} \qquad \bar{r} = 2\,\frac{\left(\int_0^R S\,dq\right)^2}{\int_0^R S^2\,dq}. \tag{1}$$

Here the effective distance $\bar{r}$ is directly determined from the observed strip counts, S, which represent the number of stars in a strip of unit width, as a function of the perpendicular distance, q, of the strip from the cluster center. The main assumptions underlying equation (1) are that the cluster is spherically symmetrical and that the density of the counted stars is proportional to the density of all stars.

To apply equation (1) to M92, we have used the recent counts by Tayler (1955). By combining his counts down to apparent magnitude 14.64 for the inner part of the cluster with his counts down to apparent magnitude 19.25 for the outer portions of the cluster, we have obtained a smooth run of values for $n(I)$ which represents the number of stars brighter than apparent magnitude 19.25 in one square second of arc on the plate as a function of the distance on the plate, I, from the cluster center. These values are listed in the left half of Table 1. From them the strip counts may be computed by the relation

$$S(q) = 2\int_q^R n(I)\, d\sqrt{(I^2 - q^2)}\,. \tag{2}$$

TABLE 1

STAR COUNTS IN M92

I	$n(I)$	I	$n(I)$	q	$S(q)$	q	$S(q)$
15″	0.94	225″	0.0067	0″	83.0	210″	2.66
45	.234	255	.00465	30	37.6	240	1.880
75	.093	285	.00331	60	20.4	270	1.303
105	.0461	315	.00233	90	12.38	300	0.847
135	.0255	345	0.00168	120	8.00	330	0.484
165	.0157			150	5.46	360	0.000
195	0.0099			180	3.76		

The values of S—number of stars brighter than apparent magnitude 19.25 in a strip width of one second of arc—which were obtained with the help of equation (2) are listed in the right half of Table 1. These values introduced into equation (1) give, for the effective distance in M92,

$$\bar{r} = 201'' = 10.0 \text{ parsec}\,. \tag{3}$$

Here the transformation from seconds of arc to parsecs has been done with the help of Shapley's (1949) distance of 10.3 kiloparsecs for M92.

In addition to this value of $\bar{r}$, we need the mean-square total velocity $\overline{V^2}$, which follows from the mean-square radial velocity obtained by Wilson and Coffeen (1954):

$$\tfrac{1}{3}\overline{V^2} = 19.5 \pm 9\ (\text{km/sec})^2\,. \tag{4}$$

The probable error has here been derived as follows. Wilson and Coffeen find, from the measurements on 23 plates, 6.8 ± 0.7 km/sec for the observed velocity dispersion and, from 8 stars for which they have two plates, 5.1 ± 0.9 km/sec for the dispersion of the error on a single plate. The two probable errors have here been computed from the usual formula for the probable error of a dispersion. The sampling errors represented by these two probable errors are partially correlated. If one assumes that the two errors are largely correlated, one obtains for the probable error of the final true radial-velocity dispersion the estimate given in equation (4).

Introducing values (3) and (4) into the virial theorem (1), one obtains, for the mass of M92,

$$M = (1.4 \pm 0.7) \times 10^5 M\odot\,.$$

This value is 2.4 times smaller than the value based on the earlier form of the virial theorem. The probable error is still so large as not to permit the stating of a safe lower limit to the mass of M92. In particular, the new result is not longer in discrepancy with the low mass one obtains if one extrapolates the observed luminosity function of a globular cluster with the help of Van Rhijn's luminosity function of the solar neighborhood (Sandage 1954).

With the new mass value, one finds, for the mass-luminosity ratio for M92 in solar units,

$$\frac{M}{L} = 0.8 \pm 0.4 .$$

Thus the difference in mass-luminosity ratio between globular clusters and elliptical galaxies appears to be even larger than had been found earlier (Schwarzschild 1954).

M. SCHWARZSCHILD
S. BERNSTEIN

PRINCETON UNIVERSITY OBSERVATORY
Princeton, N.J.

REFERENCES

Kurth, R. 1951, *Zs. f. Ap.*, **29**, 26.
Sandage, A. R. 1953, *A.J.*, **58**, 61.
Schwarzschild, M. 1954, *A.J.*, **59**, 273.
Shapley, H. 1949, *Pop. Astr.*, **57**, 203.
Tayler, R. J., 1955, *A.J.*, **59**, 413.
Wilson, O. C., and Coffeen, M. F. 1954, *Ap. J.*, **119**, 197.

ON THE APSIDAL MOTION OF STARS WITH CONSTANT OPACITY

The point-convective model with constant opacity, homogeneous chemical composition, and negligible radiation pressure has been treated by Rudkjøbing (1941), Henrich (1943), the Bondis (1948, 1949), and Härm and Rogerson (1955). Henrich proceeded to construct models taking account of radiation pressure, and Tayler (1954) considered a progressive series of inhomogeneous models. Rudkjøbing (1953*a*, *b*) and Bosman-Crespin (1954) calculated models specifically for the mean of the two components of the eclipsing binary Y Cygni, the former assuming chemical homogeneity, the latter not. Since the orbit of Y Cygni exhibits perhaps the best-known example of apsidal motion, a direct observational check of these models consists of a comparison of the observed and the calculated apsidal motion constants k_2. In this note, results of approximate calculations of k_2 are given for all the models referred to.

The apsidal motion constant k_2 is related to $\eta_2(R)$, the solution of Radau's differential equation evaluated at $r = R$, by the formula $k_2 = [3 - \eta_2(R)]/[4 + 2\eta_2(R)]$. Kopal (1953) has shown that a series expansion for $\eta_2(R)$ exists, provided that the model's density distribution $\rho(r)$ is analytic at the surface, $r = R$. This condition is fulfilled for certain Cowling models, e.g., for the $\alpha = 0.375$ case of Williamson and Duff (1949). In particular, because the mass, luminosity, and ratio of radiation to total pressure are constants at and near the surface, the density in the neighborhood of the surface of a constant opacity model is expressible as

$$\rho(r) = A\left[\frac{R}{r} - 1\right]^3 ,$$

which is analytic around $r = R$.

The expression for $\eta_2(R)$ deduced by Kopal is

$$\eta_2(R) = 3 + \sum_{i=0}^{\infty} \frac{R u_i(R)}{6^{i+1}},$$

where

$$u_i(r) = -r\left[\frac{d}{dr} u_{i-1}(r) + \sum_{k=0}^{i-2} u_k(r)\, u_{i-2-k}(r)\right]$$

and

$$u_0(r) = \frac{3}{\bar{\rho}(r)} \frac{d}{dr} \rho(r),$$

in which $\bar{\rho}(r)$ is the mean density interior to r. By introducing $\epsilon = 1 - (r/R)$, with ϵ restricted to values less than a determinable number which itself is less than 1, u_0 can be written as an absolutely convergent power series in $A/\bar{\rho}$, where $\bar{\rho}$ is the model's average density, and the coefficients of the terms in the series are themselves convergent power series in ϵ. Expressions for the $u_i(R)$ were derived up to u_{15}, yielding

$$\begin{aligned}\eta_2(R) = 3 &- \frac{1}{12}\left[\frac{A}{\bar{\rho}}\right] \sum_{n=0}^{\infty} \left[\frac{1}{36}\right]^n - \frac{17}{432}\left[\frac{A}{\bar{\rho}}\right]^2 \left[1 - \frac{197}{204} + \frac{1061}{1224} - \frac{1655}{2448} + \frac{7399}{14688}\right. \\ &\left. - \frac{3985}{11016} + \frac{201713}{793152} - \frac{838063}{4758912} + \frac{1723091}{14276736} - \frac{28133079}{342641664} + \cdots\right] \\ &- \frac{3991}{31104}\left[\frac{A}{\bar{\rho}}\right]^3 \left[1 - \frac{81979}{23946} + \frac{93116}{11973} - \frac{6224581}{431028}\right. \\ &\left. + \frac{122971685}{5172336} - \frac{124580341}{3448224} + \cdots\right] - \cdots,\end{aligned} \tag{1}$$

in which

$$\log \frac{A}{\bar{\rho}} = 1.7265 + 4 \log \beta_0 - \log\left[\frac{\kappa}{\mu^4}\left(\frac{L}{L_\odot}\right)\left(\frac{M_\odot}{M}\right)^3\right], \tag{2}$$

where $1 - \beta_0$ is the ratio of radiation to total pressure at $r = R$, μ the mean molecular weight at $r = R$, κ the constant opacity, $L_\odot = 3.88 \times 10^{33}$, and $M_\odot = 1.9866 \times 10^{33}$. The apparent divergence of the coefficient of the term in $(A/\bar{\rho})^3$ is a serious difficulty; analyticity of $\rho(r)$ seems insufficient to insure convergence of the series expansion of $\eta_2(R)$. Nevertheless, by altogether neglecting the $(A/\bar{\rho})^2$ and higher terms, a formula is obtained,

$$\eta_2(R) \sim 3 - \frac{3}{35}\left[\frac{A}{\bar{\rho}}\right], \tag{3}$$

which, perhaps only fortuitously, gives an approximation to the correct k_2.

By numerical integration, Härm and Rogerson found $k_2 = 0.0284$, $A/\bar{\rho} = 2.5891$ for the homogeneous, $\beta_0 = 1$ model. Independently, Mr. R. A. Campbell and the author found $k_2 = 0.0282$, $A/\bar{\rho} = 2.5909$. Using Härm and Rogerson's value of $A/\bar{\rho}$, equation (3) leads to $k_2 \sim 0.023$. Even though the numerical value of k_2 is thus underestimated, it seems not unreasonable that equation (3) should show how radiation pressure and chemical inhomogeneities influence the apsidal motion of the constant opacity model.

Results are collected in Table 1. Most of the k_2's were calculated on the basis of

Thomson scattering opacity, for which $\kappa = 0.19\ (1 + X)$. The last three columns give values of the ratio of central to mean density, the effective polytropic index, and, for the three cases for which published data were available, the radius of gyration, H. This last quantity is of interest in view of the correlation found by Motz (1952) between $-\log k_2$ and $-\log H/R$. On Motz's diagram the homogeneous models lie almost exactly on the curve defined by the complete polytropes; the position of Bosman-Crespin's model is highly sensitive to the value of X_{CN}.

The observed k_2 for Y Cygni is 0.014 (Russell 1939). Results for the homogeneous models indicate that, if electron scattering is the major source of opacity, a k_2 of 0.014 or less can be obtained only if the model is chiefly supported by radiation pressure; but such a model cannot be constructed for a star whose mass is comparable to Y Cygni's

TABLE 1

	$1-\beta_0$	$\kappa/(1+X)$	$A/\bar{\rho}$	k_2	$\rho_c/\bar{\rho}$	n_{eff}	$(H/R)^2$
Härm and Rogerson	0	0.19	2.589	0.0284	19.7	2.62	0.1042
Approximate calculation	0	.19	2.589	.023	19.7	2.74	.1042
Henrich's models	0	.19	2.57	.023	20	2.74	.....
	0.033	.19	2.63	.024	20	2.72	.....
	0.093	.19	2.88	.026	19	2.67	.....
	0.200	.19	3.09	.028	20	2.62	.....
	0.385	.19	3.02	.027	23	2.64	.....
	0.594	.19	2.75	.025	28	2.70	.....
Rudkjøbing (1953*a*, *b*)	0.119	.231	2.938	.026	19.9	2.66	.1083
Limiting case	1.0	.....	0	0	∞	5.00	0
Bosman-Crespin							
$X_{CN}=0.0007$	0.147	.2555	1.726	.015	19.8	2.97	.0623
$X_{CN}=0.0019$	0.147	.2555	0.649	.0056	19.8	3.48	0.0623
Tayler's evolutionary sequence	0.009	.19	2.735	.025	21	2.70	.....
	0.010	.19	2.535	.023	23	2.75	.....
	0.011	.19	2.323	.021	27	2.80	.....
	0.012	.19	2.109	.019	33	2.85	.....
	0.013	.19	1.937	.017	42	2.90	.....
	0.014	.19	1.774	.016	53	2.95	.....
	0.015	.19	1.641	.0145	71	2.99	.....
	0.016	.19	1.503	.013	101	3.04	.....
	0.0175	.19	1.387	.012	157	3.08	.....
	0.019	0.19	1.282	0.011	288	3.13	.....

(Chandrasekhar 1939). On the other hand, Bosman-Crespin's inhomogeneous model results in significantly lower values of H and k_2, bringing the latter into agreement with observation for an appropriate choice of the carbon-nitrogen abundance X_{CN}. Tayler's evolutionary series of inhomogeneous electron-scattering models is also seen to lead to low values of k_2 as inhomogeneity becomes more pronounced.

The author wishes to thank both Dr. M. Schwarzschild for suggesting this work and Dr. M. P. Savedoff for many stimulating discussions throughout this investigation.

JOHN NAZARIAN PIKE

INSTITUTE OF OPTICS
UNIVERSITY OF ROCHESTER
February 9, 1955

REFERENCES

Bondi, C. M. 1948, *M.N.*, **108**, 324.
Bondi, C. M., and Bondi, H. 1949, *M.N.*, **109**, 62.
Bosman-Crespin, D. 1954, *Ann. d'ap.*, **17**, 263.
Chandrasekhar, S. 1939, *An Introduction to the Study of Stellar Structure* (Chicago: University of Chicago Press), p. 73.
Härm, R., and Rogerson, J. 1955, *Ap. J.*, **121**, 439.
Henrich, L. R. 1943, *Ap. J.*, **98**, 192.
Kopal, Z. 1953, *M.N.*, **113**, 769.
Motz, L. 1952, *Ap. J.*, **115**, 562.
Rudkjøbing, M. 1941, *Zs. f. Ap.*, **20**, 293.
———. 1953*a*, *Ann. d'ap.*, **16**, 65.
———. 1953*b*, *ibid.*, p. 414.
Russell, H. N. 1939, *Ap. J.*, **90**, 641
Tayler, R. J. 1954, *Ap. J.*, **120**, 332.
Williamson, R. E., and Duff, G. F. D. 1949, *M.N.*, **109**, 46.

EAST-WEST MOTIONS IN THE AURORA*

In view of the recent revival of interest in east-west auroral motions (Meinel and Schulte 1953; McLaughlin 1954; Meek 1954), it was felt that certain historical and recent data on the subject might be worth describing. Over a hundred years ago scores of visual aurora observations were published which described the east-west motion in its essentials. Since most older summary articles on aurorae do not discuss the east-west motion, a few descriptions are given below (Hough 1855).

November 14, 1837, St. Lawrence.—"At 8 o'clock it appeared in the greatest splendor when tall columns of silvery light were seen in the northern horizon, sometimes shooting up to the zenith, and again moving slowly from East to West."

June 21, 1831, Albany.—"About 10 P.M. appeared like a cloud in the north 10° high. At 10:30 it shot up into brilliant striated prismatic columns, which moved from West to East, preserving in this motion a parallel position. In one or two instances a sudden rapid motion in the opposite direction, towards the West."

In the first polar year (1882–1883) some 247 instances of auroral motion were recorded by the Swedish expedition at Cape Thordsen (Carlheim-Gyllenskiold 1886). Their analysis of these data showed practically no dependence of motion on local time, eastward or westward motions taking place at nearly any time.

Coming to more recent times, a study of the east-west auroral motion was undertaken as part of the Cornell–National Geographic Society aurora program begun in 1938. From visual observations made at Ithaca by C. W. Gartlein it became evident that, while active auroral forms generally move westward before midnight and eastward afterward, there are many exceptions and that this statement must be understood as indicating a trend rather than as a hard-and-fast rule.

This has been substantiated by a recently completed study of 40,000 frames of auroral movies taken at Ithaca since 1939.[1] Briefly, the data are as follows: of 120 displays recorded on the film, 57 showed definite motion to the east or west. Of these 57 aurorae, 45 showed a westward drift of rays, patches, and draperies and/or westward movement of bright patches and rays on arcs. Twenty-two displays showed similar motions to the east. In 39 displays, complex motions (mostly short periods of alternating east-west motion) were seen. In only 8 displays was there reversal of large-scale motion during the night. The time of reversal ranged from 10:00 P.M. to 2:00 A.M.

* Analysis supported in part by U.S. Signal Corps Project 26-182B. D. S. Kimball at Yale University Observatory.

[1] One of these films was shown and discussed at the Conference on Ionospheric Physics at State College, Pennsylvania, July, 1950.

From these data it was found that when steady motions are seen in the aurora, they will be westward early in the night, eastward late in the night, and may be either or both ways in the middle of the night. Random motions may occur at any hour and nearly always occur after an arc breaks into rays. This study indicates that the motions are not sharply controlled by local time.

Further details of this behavior will appear in a paper to be submitted for publication in the *Journal of Geophysical Research.*

R. C. Bless
C. W. Gartlein
D. S. Kimball

Physics Department
Cornell University
Ithaca, New York

REFERENCES

Carlheim-Gyllenskiold. 1886, "Observations faites au Cap Thordsen, Spitzberg par l'expédition Suédoise," Vol. **2.** Stockholm: Académie Royal des Sciences de Suède.
Hough, F. B. 1855, *Results of a Series of Meteorological Observations in New York State, 1826–1850.* 1st ser., 487–499 (Albany), pp. 487–499.
Loomis, Elias. 1862, *Am. J. Sci.*, II, **34,** 34–45.
McLaughlin, D. B. 1954, *Ap. J.*, **120,** 185.
Meek, J. H. 1954, *Ap. J.*, **120,** 602.
Meinel, A. B., and Schulte, D. H. 1953, *Ap. J.*, **117,** 454.

SYSTEMATIC AURORAL MOTIONS

The recent notes of McLaughlin (1954), Meek (1954), and Bless, Gartlein, and Kimball (1955) have apparently misinterpreted in varying degree the conclusions given by Meinel and Schulte (1953). The point of emphasis was not upon an *exact* or *detailed* relationship but with regard to a *systematic* relationship. Moreover, the motions that we refer to are so slow as to be hard to detect by the eye and have little in common with the spectacular motions of the aurora. Up to the time of our paper, the occasional remark of a west-to-east drift was often ascribed merely to a chance event and was neglected in the general picture of systematic auroral motions. The chief purpose of our paper was to point out that a *systematic* west-to-east drift did occur during the second half of the night. It was possible for us to point out that during our period of observations no examples of drift contrary to our general conclusions were observed either near dawn or near dusk.

The phenomenon that we noted has, as we said, a striking resemblance to the reversal of the ionospheric current near midnight and noon during magnetic storms. This, too, is also a systematic, but not an exact, relationship. In both phenomena the evening system is often stronger, as is amply shown by the illustrations given by Chapman (1927) and Vestine (1947). One such case as given by Vestine is reproduced in Figure 1. Yet the phenomenon, as a whole, is classified as symmetrical about the earth-sun line by Chapman (1927), and the cases illustrated by Vestine exhibit the extent of the asymmetry. While the local time at which reversal may occur differs from storm to storm, it must be relatively constant during any one storm because of the stability of such a large-scale current system. It is probable that the performance of the ionospheric currents and the systematic drifts are identical during a storm. The reversal is not an abrupt transition in either phenomenon. For the aurora we can only say that a reversal occurred because near morning the drift is opposite to that observed at dusk.

With regard to the question of mass motion versus motion of an excitation pattern, we find much violence of opinion. The fact that the velocities that we observed are up to ten times those found for upper atmospheric winds at low latitudes makes the interpre-

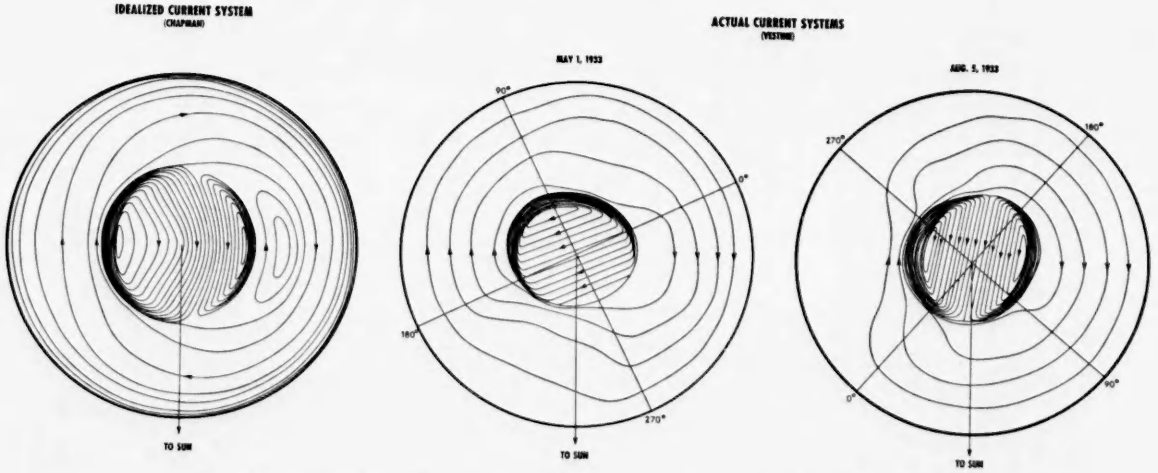

FIG. 1.—Illustrating reversal of ionospheric current near midnight and noon

tation unacceptable to many. An interesting fact is that the winds observed by ionospheric scintillation are also ten times faster during auroral activity. The low velocities are accepted as mass motion, yet the high velocities are not. When one attempts to build a physical theory bearing upon systematic motions, one finds evidence for mass motions (electrojet stream). It is surprising how a nebulous idea of motion of an excitation pattern is accepted more easily, even though—or perhaps because—it is impossible to pin down by analysis.

In the aurora the individual ray lasts for perhaps a few seconds. A new ray generally forms in the immediate vicinity, but with a random, detailed location. Statistically, however, the ensemble shows a displacement with time. In addition, each ensemble may last only a few minutes, with a new ensemble starting at some other place along the rayed feature. Again the location of the new ensemble is random with respect to the preceding one. The detailed ray structure therefore depends upon statistical fluctuations of the conditons producing the ray. The evidence for mass motion is that each ensemble appears to take part in a systematic displacement of the center of activity. We must therefore be absolutely certain that our velocity measurements are for the same ensemble, or the measurement is meaningless.

Ideally, we need the measurement of drift of a single ray event. Rays form as brilliant filaments, which gradually fuzz out while fading to invisibility. The motion of this single event could only be the result of the motion of the medium in which the event is located. As a consequence, significance can be attached only to the motion of a single ray event and to a lesser degree to a single ensemble event.

The one experiment crucial to the question of mass motions has not yet been accomplished. It is difficult technically and requires the full co-operation of the aurora. The procedure is to measure the relative Doppler shift of the λ 5577 auroral line between east and west. The aurora should be located nearly across the zenith, to avoid blending with λ 5577 emission from outside the electrojet and to give a maximum velocity component. Numerous techniques could be applied to measure this Doppler shift, and it would be a problem worth the effort to all interested persons.

The research reported in this letter has been supported in part by the Geophysics Research Directorate of the Air Force Cambridge Research Center, Air Research and Development Command, under Contract AF 19(122)-480 with the University of Chicago.

A. B. MEINEL

YERKES OBSERVATORY

REFERENCES

Bless, R. C., Gartlein, G. W., and Kimball, D. S. 1955, *Ap. J.*, **122**, 205.
Chapman, S. 1927, *Proc. R. Soc. London, A*, **115**, 242.
McLaughlin, D. B. 1954, *Ap. J.*, **120**, 185.
Meek, J. H. 1954, *Ap. J.*, **120**, 602.
Meinel, A. B., and Schulte, D. H. 1953, *Ap. J.*, **117**, 454.
Vestine, E. H. 1947, *The Geomagnetic Field* (Washington: Carnegie Institution of Washington), p. 366.

ERRATA

In *Ap. J.*, **118**, 137, 138, 1953, in equations (148) and (149) there should be minus signs in front of the first integral on the right-hand side of the equations in each case. The numerical factor 7/60 in equation (150) should be 1/60; and the numerical factors 9/20 in equations (151), (153), and (154) should be 7/20. Finally, the numerical factors 15/8 and 4.5 in equations (155) and (157) should be 35/24 and 3.5, respectively.

Beginning Volume II.

THE ASTROPHYSICAL JOURNAL SUPPLEMENT SERIES

These *Supplements* are intended to provide a medium for the publication of extensive investigations, such as wave-length lists of stars of special interest, photometric data, results of numerical integrations pertaining to stellar interiors, model stellar atmosphere calculations, and original memoirs.

Supplement No. 13

"On the Evolution of Type II Stars." F. HOYLE and M. SCHWARZSCHILD.

The evolution of stars in globular clusters has been followed theoretically from the main sequence to the top of the red giant branch. When account is taken of a growing isothermal helium core and a steadily deepening surface convection zone, the computed models agree with the observations. Differences between the red giants of population I and II are explained by differences in metal abundances.

(Published June, 1955. Price $1.25)

Supplement No. 14

"Studies in Galactic Structure. II. Luminosity Classification for 1270 Blue Giant Stars." W. W. MORGAN, A. D. CODE, and A. E. WHITFORD.

A catalogue of two-dimensional spectral types and colors for early-type stars of high luminosity. The work was carried out jointly by the University of Chicago and the University of Wisconsin. Some of the observations were obtained at the Mount Wilson, Radcliffe, and Cape Observatories.

(Ready July, 1955. Price $1.25)

An abstract of each supplement will be published in THE ASTROPHYSICAL JOURNAL. The Supplements will appear irregularly, and may be purchased separately or by subscription. Each volume of Supplements will consist of approximately 500 pages. Volume I has already been published.

Subscriptions

$8.00 per volume

Canada, $8.75. Foreign, $9.50.

To members of the American Astronomical Society, $6.00 per volume.

Orders now accepted.

THE UNIVERSITY OF CHICAGO PRESS

5750 ELLIS AVENUE CHICAGO 37, ILLINOIS

Princeton UNIVERSITY PRESS

FIRST ENGLISH TRANSLATION

Mathematical Foundations of Quantum Mechanics

By JOHN VON NEUMANN

Translated by ROBERT T. BEYER

A QUARTER-CENTURY of successful development was climaxed in 1925 with the first attempts at a systematic mathematical-physical approach to quantum theory. The resulting transformation theory brought the long-sought universal mechanical concept closer to hand.

In this important work, John von Neumann presents a comprehensive treatment of the mathematical bases of the theory, with emphasis on the general questions. *Investigations in Physics, No. 2*

410 pages $6.

Order from your bookstore. PRINCETON UNIVERSITY PRESS